ISSN 2710-1185 (Online)
ISSN 1813-1107 (Print)

ЕҢБЕК ҚЫЗЫЛ ТУ ОРДЕНДІ
«Ә. Б. БЕКТҰРОВ АТЫНДАҒЫ
ХИМИЯ ҒЫЛЫМДАРЫ ИНСТИТУТЫ»
АКЦИОНЕРЛІК ҚОҒАМЫ

ҚАЗАҚСТАННЫҢ ХИМИЯ ЖУРНАЛЫ

ХИМИЧЕСКИЙ ЖУРНАЛ КАЗАХСТАНА

CHEMICAL JOURNAL of KAZAKHSTAN

АКЦИОНЕРНОЕ ОБЩЕСТВО
ОРДЕНА ТРУДОВОГО КРАСНОГО ЗНАМЕНИ
«ИНСТИТУТ ХИМИЧЕСКИХ НАУК
им. А.Б. БЕКТУРОВА»

2(94)

АПРЕЛЬ – ИЮНЬ 2026 г.

ИЗДАЕТСЯ С ОКТЯБРЯ 2003 ГОДА

ВЫХОДИТ 4 РАЗА В ГОД

АЛМАТЫ
2026

«Қазақстанның химия журналы»
ISSN 2710-1185 (Online); ISSN 1813-1107 (Print)

Құрылтайшы:	Еңбек Қызыл Ту орденді Ә.Б. Бектұров атындағы Химия ғылымдары институты
Тіркеу:	Қазақстан Республикасының Мәдениет, ақпарат және қоғамдық келісім министрлігінде № 3995-Ж 2003 жылғы 25-маусымдағы
2003 жылы құрылған. Жылына 4 рет шығады.	
Редакцияның мекен-жайы:	050010 (А26F3Y1), Қазақстан Республикасы, Алматы қ., Ш.Уалиханов көшесі, 106. тел. 8 (727) 291-24-64, 8 (727) 291-59-31; ics_rk@mail.ru
Басылған баспахана:	ИП «Тойходжаев Н.О.», Алматы қаласы, Алмалы ауданы, Нұрмақов, көш. 26/195-49; iparuna@yandex.ru

---

«Қазпошта» АҚ-ның газет-журналдар каталогында немесе оның қосымшаларында жазылу индексі **75241**.

«Химический журнал Казахстана».
ISSN 2710-1185 (Online); ISSN 1813-1107 (Print)

Учредитель:	Ордена Трудового Красного Знамени Институт химических наук им. А.Б. Бектурова.
Регистрация:	Министерство культуры, информации и общественного согласия Республики Казахстан № 3995-Ж от 25 июня 2003 г.

Основан в 2003 г. Выходит 4 раза в год.

Адрес редакции	050010 (A26F3Y1), Республика Казахстан, г. Алматы, ул. Ш. Уалиханова, 106, тел. 8 (727) 291-24-64, 8 (727) 291-59-31; ics_rk@mail.ru
Отпечатано в типографии:	ИП «Тойходжаев Н.О.», г.Алматы, Алмалинский район, ул. Нурмакова, 26/195 кв. 49; iparuna@yandex.ru

---

Подписной индекс **75241** в Каталоге газет и журналов АО «Казпочта» или в дополнении к нему.

«Chemical Journal of Kazakhstan»
ISSN 2710-1185 (Online); ISSN 1813-1107 (Print)

Founder:	A.B. Bekturov Institute of chemical sciences awarded by the Order of Red Banner of Labor.
Registration:	Ministry of Culture, Information and Public Accord of the Republic of Kazakhstan No. 3995-Ж dated June 25, 2003 year.

«Chemical Journal of Kazakhstan» was founded in 2003 year, publishes four issues in a year.

Address of the Editorial board:	050010 (A26F3Y1), Republic of Kazakhstan, Almaty, Sh. Ualikhanov str., 106, A.B. Bekturov Institute of chemical sciences awarded by the Order of Red Banner of Labor, Fax: 8(727)291-24-64, ics_rk@mail.ru
Printed in the printing house:	IP " Toykhodzhaev N.O.", Almaty, Almainsky district, st. Nurmakova, 26/195 sq. 49, iparuna@yandex.ru

Chemical Journal of Kazakhstan
Volume 2, Number 94(2026), 5-28 https://doi.org/10.51580/2026-2.2710-1185.10

UDC 543.555:620.3

REVIEW OF ELECTROCHEMICAL BIOSENSORS BASED ON CARBON NANOMATERIALS FOR EARLY CANCER DIAGNOSIS

A.Yerezhepova*, Zh.Mukatayeva, Y.Bakytkarim , N. Shadin, Zh. Korganbayeva

Abai Kazakh National Pedagogical University, Almaty, Kazakhstan

**Corresponding author e-mail: yerezhepova.ainur@gmail.com*

Abstract. Cancer is one of the leading causes of mortality worldwide. Early diagnosis of tumors is considered a key and at the same time challenging task in the effective treatment of oncology patients. In recent years, nanomaterial-based biosensors have been rapidly developing as modern and highly sensitive tools for cancer diagnostics. In particular, carbon nanomaterials significantly enhance the analytical performance of electrochemical and optical sensing systems.

The aim of this review is to systematize the capabilities of electrochemical and optical biosensors based on carbon nanomaterials for early cancer detection. The main objectives include analyzing the properties of the applied carbon nanostructures (graphene, graphene oxide, carbon nanotubes, and carbon quantum dots) and evaluating their efficiency in the determination of tumor markers. A comprehensive analysis of the scientific literature was conducted, and methods such as voltammetry, amperometry, electrochemical impedance spectroscopy, electrochemiluminescence, and surface plasmon resonance were considered. Special attention is paid to strategies for bioreceptor immobilization and nanocomposite functionalization. Carbon nanomaterials exhibit high electrical conductivity, large specific surface area, and good biocompatibility. These properties enable the detection of tumor markers (CEA, AFP, miRNA, and proteins) at low concentrations. The sensors are characterized by portability, rapid response, and low limits of detection. Biosensors based on carbon nanomaterials have high practical significance in the field of early diagnosis and demonstrate strong potential for clinical application.

Keywords: biomarkers, cancer, electrochemical biosensors, carbon nanomaterials, graphene, carbon nanotubes, optical biosensors.

Yerezhepova Ainur	*1st year doctoral student; Email: yerezhepova.ainur@gmail.com*
Mukatayeva Zhazira Sagatbekovna	*Candidate of Chemical Sciences, Associate Professor; Email: zh.mukatayeva@abaiuniversity.edu.kz*
Bakytkarim Yrysgul	*PhD, Senior Lecturer; Email: Rysgul_01_88@mail.ru*
Shadin Nurgul Adyrbekkyzy	*PhD, Senior Lecturer; E-mail: nugen_87@mail.ru*
Korganbayeva Zhanar Kozhamberdievna	*Candidate of Chemical Sciences, Senior Lecturer; E-mail: korganbaeva.zhan@mail.ru*

Citation: Yerezhepova A., Mukatayeva Zh., Bakytkarim Y., Shadin N., Korganbayeva Zh. Review of electrochemical biosensors based on carbon nanomaterials for early cancer diagnosis. *Chem. J. Kaz.*, **2026**, 2*(94)*, 5-28. DOI: https://doi.org/10.51580/2026-2.2710-1185.10

1. Introduction

Globally, cancer remains one of the leading causes of human mortality. According to Siegel et al., approximately 2,001,140 new cancer cases and 611,720 cancer-related deaths were projected in the United States, corresponding to a mortality rate of about 30% [1].

In Kazakhstan, according to data reported in 2025, the number of patients diagnosed with cancer in 2024 increased by 5.9% compared to 2023 [2]. Cancer remains the second leading cause of death worldwide after cardiovascular diseases, and early detection significantly improves survival outcomes and reduces mortality [3].

Life expectancy largely depends on the stage at which cancer is diagnosed. If cancer biomarkers are detected at an early stage, the prognosis is more favorable, leading to improved therapeutic outcomes and reduced burden on patients [4]. However, conventional cancer diagnostic methods, including non-invasive imaging techniques such as Computed Tomography, Magnetic Resonance Imaging, Ultrasound Imaging, Positron Emission Tomography, And Single-Photon Emission Computed Tomography, as well as Invasive Biopsy and Histopathological Examinations used to identify cancer types and stages, are considered highly specific. Nevertheless, these methods are relatively expensive, require complex instrumentation, and may face limitations in point-of-care applications [5].

Molecular biomarkers such as proteins, nucleic acids, metabolites, and exosomes are considered promising indicators for the early diagnosis, prognosis, and monitoring of therapeutic response in cancer. The National Cancer Institute defines a biomarker as a biological molecule found in body fluids or tissues that indicates a normal or abnormal process, or a condition or disease [6]. Cancer biomarkers can generally be classified into two main groups:

1. Genetic biomarkers: BRCA1, BRCA2, COX2, EGFR, DAPK, KRAS, GSTP1, circulating tumor DNA (ctDNA), microRNA, tRNA, rRNA, miR-21, miR-122, miR-16, miR-155, P53, and others.

2. Protein biomarkers: AFP, CEA, PSA, VEGF, CA-15-3, CA-19-9, CA-125, CA-242, EPCAM, NSE, PAM-4, PAP, HER-2, Mucin-1, CYFRA-21-1, and others.

In many types of cancer, biomarkers such as Carcinoembryonic Antigen (CEA), Prostate-Specific Antigen (PSA), Interleukins (IL-6, IL-8), Circulating Tumor DNA (ctDNA), microRNA, and exosomes have been well established as indicators closely associated with tumor genesis and prognosis. However, the concentrations of these biomarkers may be extremely low during the early stages of the disease. Therefore, highly sensitive and selective detection methods, as well as efficient electrochemical biosensors, are required. Systems based on carbon nanomaterials fully meet these requirements. The high electrical conductivity and large specific surface area of graphene and carbon nanotubes enable the detection of cancer-related biomarkers at extremely low concentrations

[7]. In addition, their excellent capability for functionalization with biomolecules ensures accurate and rapid electrochemical signal transduction and detection.

Electrochemical Biosensors. An electrochemical sensor is an analytical device that converts chemical substances and their analytical properties into electrical signals [8]. The structure of an electrochemical sensor typically consists of three main components:

1) Electrode system or analyzer (Transducer) – the core component that converts a chemical or biochemical signal into an electrical signal (current, potential, or impedance). Most commonly, a three-electrode system is used:

a) Working electrode (WE): The primary surface where the electrochemical reaction of the analyte occurs and where the signal is measured. Common materials include gold (Au), carbon (C), glassy carbon, and modified electrodes.

b) Reference electrode (RE): Maintains a stable and well-defined potential for accurate measurement of the working electrode potential. Common examples include Ag/AgCl and saturated calomel electrodes (SCE).

c) Counter electrode (CE): Completes the electrical circuit and allows current to flow. The electrochemical reaction occurs at this electrode, but it is not used for signal measurement. Typical materials include platinum wire and carbon.

2) Recognition layer (Biorecognition layer) – the selective component responsible for recognizing the target analyte and facilitating its interaction with or binding to the electrode surface. This layer determines the selectivity of the sensor. Its composition includes:

a) For chemical sensors: simple chemical compounds, ionophores, and polymer membranes.

b) For biosensors: biological materials (bioreceptors), such as enzymes, antibodies, DNA, or cells, which are immobilized on the electrode surface.

3) Electrode (Electrode platform) – a solid conductive material that supports the biorecognition layer and enables the measurement of electrical signals. Common types include:

a) Screen-printed electrodes (SPE): Widely used in modern portable sensor systems.

b) Glassy carbon electrodes (GCE)

c) Gold and platinum electrodes

The fundamental components and operating principle of the proposed electrochemical biosensor are illustrated in Figure 1, comprising three sequential stages: biological recognition, signal transduction, and data processing. Initially, the electrode surface is functionalized with specific biorecognition elements, such as antibodies, which selectively bind target cancer biomarkers through high-affinity interactions. This binding event is subsequently converted by the transducer into a measurable electrical or optical signal using electrochemical (e.g., potentiostatic) or optical (e.g., SPR or fluorescence) techniques. The resulting signal is then processed by the signal processing unit, where it undergoes amplification, filtering, and analysis to yield a precise quantitative output. Such an integrated system enables real-time monitoring and accurate

determination of biomarker concentrations, supporting its potential application in clinical diagnostics [5, 9].

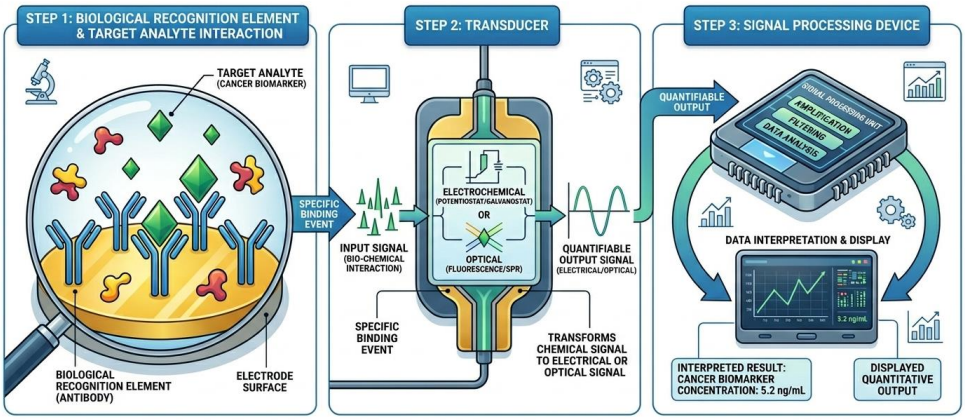

Figure 1 - Fundamental components and workflow of a biosensor

Early cancer detection remains a critical challenge that requires highly sensitive, selective, and rapid analytical tools, as conventional diagnostic methods are often limited by cost, complexity, and restricted applicability in point-of-care settings [1,3]. In this context, this review critically examines recent advances in carbon nanomaterial-based biosensors, with particular emphasis on electrochemical and optical platforms, and evaluates how key nanostructures such as graphene, carbon nanotubes and carbon quantum dots enhance sensivity, selectivity and detection limits. By comparatively analyzing different sensing strategies and biomarker types, including proteins and nucleic acids. This work highlights the relationships between nanomaterial properties, sensor design and analytical performance, while identifying current limitations and promising future directions for the development of next-generation biosensing systems suitable for early cancer diagnostics and clinical applications.

2. Discussion and Analysis

The analytical performance characteristics of sensors, such as sensitivity, selectivity, and limit of detection, primarily depend on the material of the working electrode and its surface structure [10]. Therefore, the electrode material plays a crucial role in the development and improvement of electrochemical sensors. In recent years, carbon based nanomaterials (CNMs), such as graphene, carbon nanotubes, carbon quantum dots, and graphitic nanostructures, have been increasingly explored to improve the performance of electrochemical sensors.

The incorporation of CNMs onto the surface of the working electrode accelerates the electron transfer process at the electrode-analyte interface. As a result, the kinetics of electrochemical reactions are improved, and the current

response of the sensor is enhanced. This increases the sensitivity of the sensor and enables the detection of analytes at very low concentrations. Since the surface of CNMs can be easily modified with various functional groups, they provide an ideal platform for the immobilization of biomolecules, enzymes, or selective recognition elements. This property makes CNMs particularly effective for the fabrication of electrochemical biosensors and significantly improves sensor selectivity [11]. The main nanomaterials commonly used for the modification and enhancement of electrochemical sensors, as well as their functional roles, are presented in Table 1.

Table 1 - Types of nanomaterials and their roles in electrochemical sensors

Type of Nanomaterial	Material	Structural Features and Properties	Effect on Sensor
Carbon based nanomaterials	Graphene	A single-atom-thick, two-dimensional (2D) sp^2-hybridized carbon lattice with exceptional electrical conductivity and high surface area [12]	Enhances electron transfer and provides a large interface for bioreceptor immobilization, improving sensitivity and signal amplification
	Carbon nanotubes (SWCNTs, MWCNTs)	One-dimensional (1D) cylindrical nanostructures formed by rolled graphene sheets with high conductivity and mechanical strength [13]	Increases active surface area and facilitates efficient electron transport pathways
Metal-based nanomaterials	Gold nanoparticles (AuNPs)	Nanoscale metallic particles with high surface-to-volume ratio, excellent conductivity, and strong affinity to biomolecules [14]	Enable efficient biomolecule immobilization and accelerate electron transfer, enhancing ECL/SERS signals
Other nanomaterials	MXenes	Two-dimensional transition metal carbides/nitrides with metallic conductivity and hydrophilic functional groups (-OH, -O, -F) [15]	Improve charge transfer kinetics and enable stable immobilization of biomolecules
	Metal–organic frameworks (MOFs)	Three-dimensional porous crystalline materials composed of metal nodes and organic ligands with tunable pore size and large surface area [16]	Improve selectivity via selective adsorption and increase sensitivity through analyte preconcentration
	Nanostructured polymers (e.g., chitosan, polyaniline)	Three-dimensional crosslinked or network-like polymer structures composed of repeating monomer units, often forming porous and flexible architectures [17]	Provide a biocompatible matrix for immobilization, enhance stability, and improve adhesion to electrode surfaces

Carbon Nanomaterial-Based Electrochemical Biosensors for Cancer Diagnosis. Among the various types of biosensors, electrochemical biosensors are widely used in disease diagnosis, environmental monitoring and food safety control [18]. These sensors consist of a biological recognition element and an electronic detection system. The operating principle of a biosensor is based on specific electrochemical interactions between the surface of the working electrode

and the target analyte. When the analyte interacts with the electrode surface, electrochemical responses such as current, impedance, or potential are generated and recorded. For practical applications, it is essential to maintain a linear relationship between the analyte concentration and the sensor signal. Various approaches are employed for the detection of target molecules. For example, electroactive analytes such as dopamine and glucose can be directly detected at the electrode surface, either in the presence or absence of a catalyst. In contrast, the detection of non-electroactive compounds requires the use of additional electroactive species, such as hexacyanoferrate or hydrogen peroxide. In sandwich-type structures, the binding of the analyte triggers redox reactions of electroactive species, thereby enhancing the sensitivity of the electrode.

Two key performance characteristics of biosensor electrodes are selectivity and sensitivity. Selectivity refers to the ability of the electrode to specifically recognize a particular analyte, while sensitivity depends on the efficiency of electron transfer between the analyte and the electrode. The signal amplitude can be increased by enlarging the electrode surface area, modifying it with highly conductive materials, or promoting redox reactions. Generally, electrodes with larger surface areas provide more active sites for electrochemical reactions, resulting in higher current responses [19].

One of the important quantitative parameters of a sensor is the limit of detection (LOD), which represents the lowest concentration of the analyte that can be reliably detected by the sensor. This is typically defined by a signal-to-noise ratio greater than 3 [20]. The LOD is a critical parameter for evaluating sensor performance. Selectivity also plays a decisive role in biosensors; therefore, biorecognition elements specific to the target analyte are immobilized on the electrode surface. In cancer biosensors, the primary objective is the proper selection of the target antigen and the accurate determination of its concentration in the human body. Once the antigen is selected, the corresponding antibodies are immobilized on the electrode surface. DNA biosensors are typically fabricated by immobilizing single-stranded oligonucleotides on the sensing surface, which hybridize with complementary DNA sequences [21]. This hybridization process is converted into a measurable electrical signal by the transducer. After immobilization, it is necessary to block the remaining free binding sites on the electrode surface to prevent nonspecific interactions. For this purpose, bovine serum albumin (BSA) or thiol-containing molecules on gold surfaces are commonly used [22].

Carbon nanoparticles are highly suitable materials for biosensor platforms due to their excellent electrical conductivity and large specific surface area. Currently, electrochemical techniques such as amperometry, voltammetric methods including Cyclic Voltammetry (CV), Stripping Voltammetry, Square-Wave Voltammetry (SWV), Differential Pulse Voltammetry (DPV), And Linear Sweep Voltammetry (LSV), as well as impedimetric methods, are widely used for the detection of cancer biomarkers. Voltammetric methods typically employ an electrochemical cell consisting of two or three electrodes and a potentiostat. This system operates by applying a controlled potential and measuring the resulting

current. In contrast, the working principle of amperometric biosensors is based on the use of antibodies conjugated with electroactive nanoparticles or enzymes to capture the target analyte, and determining its concentration by measuring the current generated under an applied potential. The performance of such biosensors is directly influenced by the properties of the electrode, as the signal is generated in close proximity to the electrode surface [22, 23].

Biomarkers are important indicators for the diagnosis of various diseases. Biomarkers found in biological fluids include DNA, RNA, proteins, polysaccharides, and small molecules such as dopamine, uric acid, and glucose. In cancer biosensors, the accurate determination of antigen concentration is of critical importance. Carbon nanomaterials are used in sensors as biorecognition elements for biomarker binding, as transducers that convert molecular interactions into electrochemical signals such as current or impedance, and as labeling elements for signal amplification. Functionalization of carbon nanomaterials with organic polymers or metal oxide nanoparticles increases the electrode surface area and facilitates the immobilization of biorecognition elements. The development of functionalized carbon nanomaterials has significantly improved the analytical performance of electrochemical sensors [22,23].

In recent years, there has been growing in the development of carbon nanomaterial based biosensors for the detection of cancer biomarkers. This interest is driven by the potential of these biosensors to enable rapid, simple, and reliable detection of biomarkers, with strong prospects for clinical application. Carbon nanomaterial-based biosensors offer advantages such as high sensitivity, rapid response time, and ease of use, making them promising tools for early cancer diagnosis. In this field, the recent achievements of international researchers in detecting cancer biomarkers are summarized in Table 2, which presents selected cancer biomarkers, the carbon nanomaterials and composite materials used, the detection methods employed, the associated cancer types, the analytical performance (including detection limits and linear ranges), and references to the corresponding scientific publications.

Table 2 - Various carbon-based nanomaterials used for biomarker detection

Biomarker	Carbon material	Detection method	Detection level	Associated cancer type	Reference
TP53	rGO-CMC	Amperometry	2.9-3.4 nM	All types of cancer	[25]
miR-21	GME	DPV and EIS	2.09 μg mL^{-1}	Breast, lung, prostate cancers	[26]
VEGFR2	Chitosan-functionalized rGO	CV, DPV	0.28 pM	Leukemia, breast and ovarian cancers	[27]
LRG1	rGO nanosheets	CV, EIS, SWV	75 pg mL	Colorectal cancer	[28]
PSMA	Magnetic graphene oxide-$PSMA_{ab}$	DPV	10 pg mL^{-1}	Prostate cancer	[29]
CYFRA-21-1	APTES-modified rGO-ZrO_2 nanocomposite	DPV	0.122 ng mL^{-1}	Oral cancer	[30]
p53 protein	GO@CdS NCs/Au NPs	ECL	4fg mL^{-1}	p53 related cancers	[31]
miR-223	GO@Au-NS	CV, DPV and EIS	0.012 aM	colorectal cancer	[32]

Biomarker	Carbon material	Detection method	Detection level	Associated cancer type	Reference
CEA	Pb^{2+}@Au@MWCNTs-Fe_3O_4)	Amperometry and CV	1.7 fg mL^{-1}	Colon cancer	[38]
CEA	GO/MWCNT-COOH/Au@CeO_2 nanocomposite	ECL	0.02 ng mL^{-1}	Breast tumor, Ovarian and cervical carcinomas	[38]
CEA	Ag NPs-MWCNTs/MnO_2	Amperometry	0.03 pg mL^{-1}	Ovarian carcinoma, colon cancer, breast and lung cancers	[39]
PSA	rGO-MWCNT/AuNPs	Rct and DPV	1 pg mL^{-1}	Prostate cancer	[40]
AFP	PLL-functionalized SWCNTs	DPV and EIS	0.011 ng mL^{-1}	Liver and ovarian cancers, hepatic carcinoma, nasopharyn geal cancer	[41]
miRNA-24	MWCNT-modified GCE	DPV	1 pM mL^{-1}	Multiple cancer types (miR-24-associated, not specified in this study)	[42]
miR-21	FTO-SWCNTs-denAu	DPV	0.01 fmol L^{-1}	Prostate cancer	[43]
CEA	SWCNTs@GQDs / rGO-AuNPs	CV and EIS	5.3 pg mL^{-1}	Ovarian, colon, breast, pancreatic and lung cancers	[44]
CEACAM 5	VA-MWCNTs	CV and EIS	0.92 μM	Gastric, colorectal, lung, breast, and pancreatic cancers	[45]
MALAT1	AuNCs/MWCNT-NH_2	DPV	42.8 fM	lung cancer (NSCLC)	[46]
PSA	Au/Ag-rGO/aminated-GQDs/carboxyl-GQDs	ECL	0.29 pg mL^{-1}	Prostate cancer	[48]
CEA	GQDs/Au@Pt	ECL	0.6 pg mL^{-1}	Colon cancer	[49]
CA-19-9	GQD-functionalized pPtPd nanochains	ECL	0.96 mU mL^{-1}	Pancreatic cancer	[50]
miRNA-155	GQDs	Amperometry	0.14 fM	Not specified (miR-155 is a cancer-related biomarker)	[51]
IL-13Rα2	GQD-functionalized MWCNTs	Amperometry	0.8 ng mL^{-1}	Colorectal cancer, glioma, squamous cell carcinoma of head and neck	[52]
α-L-Fucosidase (AFU)	Au-functionalized carbon dots	Fluorescence emission spectroscopy	3.4 nM	Hepatocellular carcinoma	[53]
ANXA2	CNDs derived from Aloe vera	CV	1 fg mL^{-1}	Liver cancer	[54]
PSA	rGO/g-C3N4/Au NPs	CV, SWV, EIS	0.44 fM	Prostate cancer	[55]
miRNA-141	GO-AuNPs	SPR	1 fM	Prostate cancer	[58]
BRCA1	GCOF	SPR	1-100 nM	Breast and ovarian cancers	[59]
BRCA2	GCOF	SPR	1-100 nM	Breast and ovarian cancers	[59]
CK-19	GO-COOH	SPR	1fg mL^{-1}	Lung cancer	[60]
FAP	Au/rGO	SPR	5 fM	Early detection of cancer	[61]
PPi	PDI-HIS-Cu-GO nanocomposite	Fluorescence spectroscopy	$0.60 \cdot 10^{-7}$ M	Although not a direct cancer biomarker, (monitored as a byproduct of enzymatic reactions)	[63]
uPA	ssDNA-SWCNTs	Fluorescence spectroscopy	50 nM	Prostate cancer	[64]
CA-125	3DNCNTs	Fluorescence spectroscopy	20 μg mL^{-1}	Ovarian cancer	[65]
miR-19 and miR-23 RNA	SWCNTs	Photoluminescence	0.02 mg mL^{-1}	Breast cancer, lung cancer, lymphoma	[66]

Biomarker	Carbon material	Detection method	Detection level	Associated cancer type	Reference
Leukemia K562 cells	CNTs functionalized with GPMS	Photoconductivity	27 cell/ml	Leukemia	[67]
PSMA	Functionalized MWCNTs	ECL	0.88 ng mL^{-1}	Prostate cancer	[68]
CD63	sSWCNTs	UV-Vis spectroscopy	$5.2 \cdot 10^5$ particles/μL	breast cancer	[69]
uPA	Peptide-MWCNT nanoprobes	Fluorescence spectroscopy	500 pg mL^{-1}	general cancer-related proteases	[70]
MMP-7	Peptide-functionalized MWCNT nanoprobes	Fluorescence spectroscopy	0.5 pg mL^{-1}	general cancer-related proteases	[70]
MMP-2	Peptide-functionalized MWCNT nanoprobes	Fluorescence spectroscopy	4.8 pg mL^{-1}	general cancer-related proteases	[70]
miRNA-155	C-dot-MnO_2 nanosheets	FRET	0.1×10^{-18} M	Cancer cells	[71]
CA-15-3	GO-PEI-CQD-Au nanohybrid	ECL	0.0017 U mL^{-1}	Specific to breast cancer (for metastasis monitoring)	[72]
β-Glucuronidase (GLU)	Nitrogen-doped carbon quantum dots (N-CQDs)	Photoluminescence	0.3 U L^{-1}	Colorectal, pancreatic, breast, bladder, liver cancers	[73]
AFP	CNF/AuNPs	CV, SWV and EIS	0.50 pg mL^{-1} (SWV) 0.48 pg mL^{-1} (EIS)	Liver cancer	[74]
miR-31	PEI-Ru@Ti_3C_2@AuNPs	ECL	1.67 aM	Lung cancer	[75]

Graphene-Based Electrochemical Biosensors. Two-dimensional (2D) nanomaterials such as graphene, graphene oxide (GO), and reduced graphene oxide (rGO) have been extensively studied to improve the analytical performance of electrochemical biosensors for the early detection of cancer biomarkers. Graphene-based biosensors exhibit high affinity toward biomarkers such as microRNAs (miRNAs), p53 gene mutations, carcinoembryonic antigen (CEA), alpha-fetoprotein (AFP), and cancer antigens (CA-125, CA15-3), enabling their efficient capture and detection. Electrochemical sensors based on graphene and graphene-like nanomaterials are characterized by rapid response times and high selectivity for the detection of nucleic acid biomarkers. Wu et al. developed a paper-based microfluidic electrochemical platform incorporating rGO for the quantitative analysis of cancer biomarkers [24]. Esteban et al. fabricated a screen-printed carbon electrode functionalized with o-carboxymethylcellulose and rGO for the detection of the tumor suppressor gene TP53, and covalently immobilized two different selective hairpin-forming capture probes onto its surface [25].

In addition, graphene-modified electrodes were used for the voltammetric detection of miR-21 in lysates obtained from breast cancer cells. First, an inosine-substituted anti-miR-21 probe was passively adsorbed onto the surface of a graphene-modified pencil graphite electrode (GME). Subsequently, solid-phase hybridization occurred between the inosine substituted probe and the target miR-21. This process was monitored using DPV and electrochemical impedance spectroscopy (EIS), achieving a detection limit of 2.09 mg mL^{-1}. The proposed method successfully distinguished miR-21-positive breast cancer cells (MCF-7)

from miR-21-negative hepatoma cells (HUH-7) [26]. To detect vascular endothelial growth factor receptor 2 (VEGFR2), the surface of a glassy carbon electrode was modified with chitosan-functionalized rGO to fabricate an electrochemical biosensor. The hybridization process was monitored using voltammetric techniques, and an increase in peak current was observed as the protein concentration increased from 0.4 to 86 pM. This biosensor demonstrated a detection limit of 0.28 pM for VEGFR2 and was described as a simple and effective method for detecting small changes in protein concentration at the electrode surface [27].

Yu et al. developed an advanced electrochemical biosensor for the detection of the colorectal cancer (CRC) biomarker leucine-rich alpha-2 glycoprotein-1 (LRG1), based on graphene-peptide conjugates integrating rationally designed synthetic peptides with rGO nanosheets. The peptides were engineered with dual graphene-anchoring motifs to ensure optimal orientation and high binding affinity toward LRG1 when immobilized on rGO-modified gold electrodes. Benefiting from the high conductivity, large surface area, and stability of rGO, together with the specificity, small size, and facile modification of synthetic peptides compared to conventional antibodies, the sensor exhibited enhanced analytical performance. Electrochemical detection using SWV demonstrated high sensitivity (22.3 $\mu A/(ng/mL \cdot cm^2)$), a low limit of detection of 75 pg/mL in serum, and a wide linear range from 100 pg/mL to 100 ng/mL. The biosensor also showed excellent selectivity, precision (RSD<6-7%), and high accuracy (recovery ~97-104%). Importantly, analysis of colonoscopy-classified patient serum samples enabled clear discrimination between normal, precancerous adenomatous polyps, and malignant CRC stages, with LRG1 levels increasing by approximately 24% in adenomas and 103% in CRC cases. Compared to traditional antibody-based assays, the proposed platform demonstrated superior sensitivity, broader linear range, improved reproducibility, and faster response time. This work highlights the significant potential of combining computational peptide design with graphene-based nanomaterials to develop highly efficient electrochemical biosensors for quantitative detection and staging of colorectal cancer biomarkers [28].

Graphene-based electrochemical immunosensors have also been applied for the detection of tumor-associated biomarkers such as prostate-specific antigen (PSA), carcinoembryonic antigen (CEA), and squamous cell carcinoma antigen (SCCA). Yang et al. proposed an immunomagnetic sensor composed of magnetic GO and anti-PSMA antibodies for the efficient capture and rapid detection of prostate-specific membrane antigen (PSMA) and PSMA-positive prostate cancer cells in blood samples [29]. To detect the CYFRA-21-1 biomarker associated with oral cancer, indium tin oxide (ITO) electrodes were modified with an rGO-zirconium dioxide (ZrO_2) nanocomposite functionalized with APTES (aminopropyltriethoxysilane) [30]. Furthermore, Heidari et al. developed an immunosensor for the detection of the p53 biomarker using a sandwich-type configuration based on GCE/CdS/p53-Ab1 and p53-Ab2-tGO-AuNP. The

incorporation of graphene oxide and gold nanoparticles significantly enhanced the electrochemiluminescence (ECL) signal. This immunosensor exhibited a linear detection range of 20-1000 fg mL^{-1} and an ultralow detection limit of 4 fg mL^{-1} [31].

Akbari et al. developed a novel label-free electrochemical biosensor based on a nanostructured platform composed of graphene oxide (GO) nanosheets decorated with gold nanoflowers (GO@Au-NS) for the sensitive detection of miR-223, a microRNA biomarker associated with colorectal cancer. The sensor utilizes a thiolated single-stranded DNA probe (Cap-223) immobilized covalently on the GO@Au-NS surface through thiol-gold interactions to capture the target miR-223 via hybridization. The biosensor demonstrated excellent electrochemical activity and a remarkably low detection limit of 0.012 aM, with high selectivity against mismatched sequences. Importantly, it showed reliable performance in detecting miR-223 in human serum samples, indicating its clinical applicability. This nanostructured electrochemical immunosensor exhibits high sensitivity, specificity, and antifouling properties due to the hydrophilic nature of the platform, making it a promising tool for early, non-invasive diagnosis of colorectal cancer [32].

Carbon Nanotube (CNT)-Based Electrochemical Biosensors. CEA is a highly glycosylated complex macromolecule belonging to the family of cell surface glycoproteins [33]. These glycoproteins are produced in gastrointestinal tract cells during embryonic development. In healthy adults, the normal concentration of CEA in blood should be below 2.5 μg mL^{-1} [34]. Elevated CEA levels are closely associated with ovarian, lung, and breast cancers [35], and particularly with colorectal carcinoma [36].

Li et al. proposed a label-free electrochemical immunosensor for CEA detection based on the catalytic reduction of hydrogen peroxide. In this system, a glassy carbon electrode modified with magnetic multi-walled carbon nanotubes functionalized with gold nanoparticles (AuNPs) and Pb(II) ions was used to immobilize primary antibodies (Ab1). The sensor exhibited a linear relationship between analyte concentration and catalytic hydrogen peroxide reduction, achieving a detection limit of 1.7 fg mL^{-1} [37]. Pang and et al. developed a notable label-free immunosensor for CEA detection based on ECL characteristics. They proposed a bioanalytical GCE modified with GO, carboxylated MWCNTs, and AuNPs that were functionalized with CeO_2NPs, all dispersed within a chitosan matrix. The biorecognition event was monitored through a decrease in ECL intensity upon interaction with CEA, achieving a detection limit of approximately 0.02 ng mL^{-1}. The proposed immunosensor demonstrated excellent stability and selectivity, showing negligible interference from other biomarkers such as PSA, BSA and AFP. Furthermore, it exhibited reliable performance in serum samples, with recovery values ranging from 98.9% to 102.6% [38].

In an enzyme-free sandwich-type electrochemical biosensor, primary antibodies (Ab1) specific to CEA were immobilized on β-cyclodextrin/multi-walled carbon nanotubes (β-CD/MWCNTs), which enhanced the electrode

surface area and electrical conductivity. Further signal amplification was achieved by immobilizing secondary antibodies (Ab2) on an AgNPs-MWCNTs/MnO_2 nanocomposite, enabling catalytic hydrogen peroxide reduction. This sensor achieved a detection limit of 0.03 pg mL^{-1} for CEA [39]. Heydari-Bafrooei and Shemszadeh prepared an ultrasensitive label-free electrochemical aptasensor based on a modified rGO-MWCNT with densely packed gold nanoparticle (rGO-MWCNT/AuNP) platform to detect the biomarker PSA in serum. The detection was carried out on the variation of electron transfer resistance (Rct) and DPV. As compared to other platforms, the rGO-MWCNT/AuNP nanocomposite modified electrode is the most sensitive aptasensing proposal for the determination of PSA with a detection limit of 1 pg mL^{-1} [40]. The detection of alpha-fetoprotein (AFP) is important for liver cancer diagnosis. Wang et al. fabricated a glassy carbon electrode modified with a Prussian blue (PB) layer and coated with poly-L-lysine-functionalized single-walled carbon nanotubes (PLL-SWCNTs), onto which HRP-labeled anti-AFP antibodies were immobilized. Voltammetric and impedimetric measurements demonstrated a detection limit of 0.011 ng mL^{-1} for AFP [41]. Li et al. developed a biosensor for miRNA-24 detection by covalently immobilizing synthetic DNA probes onto an MWCNT-modified glassy carbon electrode. Hybridization with complementary miRNA-24 was evaluated based on changes in guanine oxidation signals using DPV [42].

Sabahi et al. developed an Fluorine-doped Tin Oxide-based biosensor for detecting the miR-21 biomarker associated with prostate cancer. The fluorine-doped tin oxide (FTO) electrode was functionalized with dendritic gold nanostructures (den-Au) and thiolated receptor probes immobilized on a single-walled carbon nanotube platform. The detection limit obtained using DPV was 0.01 fmol L^{-1} [43]. Luo et al. developed an enzyme-free electrochemical CEA immunosensor using an SWCNT@GQD composite platform modified with an rGO-AuNP system. This immunosensor exhibited a dual signal amplification effect, providing a linear detection range of 50-650 pg mL^{-1} and a low detection limit of 5.3 pg mL^{-1} [44]. Genosensors have demonstrated high cost-effectiveness in detecting the colorectal cancer biomarker CEACAM5. In this system, vertically aligned multi-walled carbon nanotubes were fabricated on a flexible PET substrate using a hot-pressing method and used as a sensing electrode. Target DNA was captured through immobilized DNA probes and characterized using EIS and CV. The hybridization process was studied within the concentration range of 50-250 μM, and the detection limit was determined to be 0.92 μM [45].

Currently, non-small cell lung cancer (NSCLC) is recognized as the most common type of lung cancer. Mei et al. developed an ultrasensitive electrochemical biosensor for detecting the MALAT1 biomarker for NSCLC diagnosis. The biosensor was based on a screen-printed electrode modified with gold nanocages and aminated MWCNTs (AuNC/MWCNT-NH_2). DPV measurements demonstrated an ultralow detection limit of 42.8 fM [46].

Carbon Quantum Dot-Based Electrochemical Biosensors. Carbon quantum dots (QDs) are currently in the early stages of development for the fabrication of

biosensors aimed at biomarker detection [47]. In general, graphene quantum dots (GQDs) have emerged as promising candidates for the construction of ECL and fluorescent biosensors. Wu and co-workers designed a label-free electrochemiluminescent (ECL) immunosensor for PSA detection. The sensor was fabricated by coating a glassy carbon electrode (GCE) with Au/Ag-rGO modified using aminated GR-QDs and GO-QDs, followed by immobilization of anti-PSA on the electrode surface. The developed immunosensor exhibited a detection limit of 0.29 pg·mL^{-1} [48]. Li et al. developed a highly sensitive paper-based ECL immunobiosensor for CEA detection using nanoporous gold-chitosan hybrids and Au@Pt functionalized with graphene quantum dots. In addition, a simple one-pot synthesis strategy for graphene quantum dots was shown to enhance their quantum yield and biocompatibility [49].

The one-pot synthesis of graphene quantum dots provides high quantum yield and excellent biocompatibility. Owing to their good electrical conductivity, Yang et al. developed an ECL-based immunosensor for the detection of carbohydrate antigen 19-9 (CA19-9). In this system, a GCE was modified with a hybrid nanomaterial composed of reduced rGO doped with Au and Ag nanoparticles (GN-Ag-Au) to increase the electrode surface area and improve electron transfer, enabling immobilization of primary antibodies (Ab1). After the specific binding of CA19-9, signal amplification was performed using a secondary antibodies (Ab2) labeled with GQDs functionalized porous PtPd nanochainstructures (pPtPd@GQDs). Under optimal conditions, the immunosensor exhibited a wide detection range of 0.002-70 U mL^{-1} and a low detection limit of 0.96 mU mL^{-1} [50]. A sensitive and accurate method for detecting miRNA-155 was developed based on an electrochemical biosensor fabricated by immobilizing activated carboxyl groups of graphene quantum dots onto aminated DNA structures on the electrode surface. A specific amount of horseradish peroxidase (HRP) immobilized on graphene quantum dots effectively catalyzed the oxidation of 3,3′,5,5′-tetramethylbenzidine (TMB) in the presence of hydrogen peroxide (H_2O_2), resulting in enhanced electrochemical signals. The proposed sensor operated over a concentration range from 1 fM to 100 pM and achieved a detection limit of 0.14 fM [51].

Serafin et al. developed the first integrated electrochemical immunosensor for detecting interleukin-13 receptor alpha-2 (IL-13Rα2). The operating principle of this sensor was based on two main components: 1) MWCNTs functionalized with graphene quantum dots, serving as carriers for multiple detector antibodies and HRP molecules, and 2) biotinylated capture antibodies specific to IL-13Rα2 immobilized on streptavidin-modified screen-printed electrodes. The calibration curve obtained using the amperometric H_2O_2/hydroquinone (HQ) system showed a linear concentration range from 2.7 to 100 ng mL^{-1} and a detection limit of 0.8 ng·mL^{-1} [52].

Mintz and co-workers designed an assay combining AuNPs and CDs for the detection of the α-L-fucosidase (AFU) biomarker, aimed at monitoring hepatocellular carcinoma (HCC). The approach is based on the selective binding

between AFU and its specific antibody (IgG anti-FUCA2). In the presence of AFU, the close proximity of these components enables energy transfer to the surface plasmon band of the AuNPs, leading to fluorescence quenching of the CDs. This method achieved a detection limit of 3.4 nM and exhibited a wide linear detection range from 11.3 to 200 nM [53].

Kulkarni et al. reported a highly efficient electrochemical biosensing platform for the detection of the liver cancer biomarker Annexin A2 (ANXA2), employing CNDs derived from Aloe vera. In this system, anti-ANXA2 antibodies were immobilized onto a thin CND layer electrophoretically deposited on ITO electrodes, while BSA was used to block nonspecific adsorption sites. The sensing mechanism relies on the specific antigen-antibody interaction between ANXA2 and its corresponding antibody, enabling highly sensitive detection using CV. The developed platform exhibited an ultralow detection limit of 1 fg mL^{-1} and a broad linear range from 1 fg mL^{-1} to 500 ng mL^{-1}, along with a rapid response time of 20 minutes, high selectivity, and good reproducibility. This biosensor demonstrates a cost-effective, environmentally benign, and highly sensitive electrochemical immunosensing approach for early-stage liver cancer diagnosis [54].

Saeidi Tabar et al. developed a highly sensitive electrochemical aptasensor for the detection of PSA) a biomarker for prostate cancer diagnosis, based on a novel two-dimensional (2D):2D rGO/graphitic carbon nitride (g-C_3N_4) nanocomposite decorated with AuNPs. The sensing platform was constructed by modifying a GCE with the rGO/g-C_3N_4/AuNPs composite, followed by immobilization of PSA-specific aptamer strands. The successful synthesis of the nanocomposite and electrode modification were confirmed using XRD, FTIR, and TEM. Electrochemical characterization using CV, SWV, and EIS demonstrated enhanced electron transfer properties and effective surface functionalization. The aptasensor exhibited excellent selectivity toward PSA over potential interfering species, including CA 15-3, BSA, fetal bovine serum (FBS), and glucose. Under optimized conditions, the sensor achieved rapid detection within 30 minutes, with an ultralow LOD of 0.44 fM and a limit of quantification of 2.5 fM using methylene blue as a redox mediator. Furthermore, the practical applicability of the developed platform was validated through analysis of real serum samples, highlighting its strong potential for clinical diagnostics [55].

Optical Biosensors. The operating mechanism of optical biosensors is based on changes in light emission resulting from interactions between the target analyte and the recognition element. The generated optical signal is proportional to the concentration of the target analyte in the solution. Carbon nanomaterials, particularly graphene derivatives, are known to be highly efficient fluorescence quenchers. In GO- or rGO-based fluorescent sensors, fluorophores are typically covalently linked to probes designed to capture target analytes. These probe-fluorophore complexes are non-covalently adsorbed onto the GO surface, resulting in fluorescence quenching. Upon binding of the target analyte to the probe, the fluorophore detaches from the GO surface, restoring fluorescence. Due

to their high sensitivity, signal enhancement capability, simplicity of operation, and potential for multiplex detection, optical biosensors based on surface-enhanced Raman scattering (SERS) and localized surface plasmon resonance (LSPR) have attracted significant attention in modern analytical applications [56].

Graphene-Based Optical Biosensors. In SPR-based sensors, biorecognition elements are immobilized on a metal surface, and molecular interactions with the target analyte or biomarker result in changes in the surface mass and refractive index. These changes are converted by the transducer into an SPR signal proportional to the analyte concentration [57]. A highly sensitive and simple SPR biosensor for the detection of miRNA-141 was developed using GO-AuNP hybrids. In this system, a thiolated complementary DNA probe was first immobilized on the gold film surface, and subsequently, the second segment of miRNA-141 was captured using GO-AuNP hybrids conjugated with auxiliary DNA. As a result, an ultralow detection limit of 1 fM was achieved [58]. In addition, quantitative analysis using a graphene-coated fiber-optic SPR biosensor was performed to detect BRCA1 and BRCA2 gene mutations for early breast cancer diagnosis. The 916delTT and 6174delT mutations in the BRCA1 and BRCA2 genes were monitored using the attenuated total reflection (ATR) method [59]. When carboxyl-functionalized graphene oxide (GO-COOH) was incorporated onto a gold film surface, the sensitivity of the SPR sensor for detecting CK19 protein, a biomarker associated with NSCLC, was significantly enhanced, achieving a detection limit of 1 fg mL^{-1} [60]. Li et al. also developed a selective and sensitive label-free graphene-based SPR biosensor for detecting folic acid protein (FAP) in human serum at fM concentrations [61]. By exploiting the polarization and absorption properties of graphene under attenuated total reflection conditions, Fei et al. developed a high-resolution optical sensor capable of detecting refractive index changes with a precision of $1.7 \cdot 10^{-8}$ and a sensitivity of $4.3 \cdot 10^{7}$ mV/RIU. This sensor enables label-free detection of living cells at the single-cell level [62].

Another important optical approach related to cancer detection involves the measurement of pyrophosphate (PPi). A sensor platform based on a self-assembled nanocomposite composed of perylene diimide-histidine (PDI-HIS), Cu^{2+} ions, and graphene oxide demonstrated a detection limit of $0.60 \cdot 10^{-7}$ M for PPi detection [63].

Carbon Nanotube-Based Optical Biosensors. Single-walled carbon nanotubes exhibit near-infrared (NIR) photoluminescence properties in the wavelength range of 900-1600 nm, making them highly suitable for optical biosensing applications. Ryan M. Williams et al. developed a sensitive fluorescent biosensor for detecting urokinase plasminogen activator (uPA), a biomarker associated with metastatic prostate cancer, by utilizing the optical properties of SWCNTs [64]. The DNA/aptamer-CNT platform demonstrated enhanced performance in detecting the cancer biomarker CA125. A fluorescence-based biosensor has also been developed for CA125 detection, employing anti-CA125 antibodies immobilized on three-dimensional carbon nanotubes (3D CNTs) [65].

The near-infrared emission, photostability, and high sensitivity of SWCNTs enable real-time monitoring of the hybridization of microRNAs and other oligonucleotides. A DNA - nanotube-based photoluminescent sensor employing a $(GT)_{15}$ single-stranded oligonucleotide demonstrated a detection range of 10-100 pM for miR-19 and miR-23 RNA targets [66]. For the early diagnosis of chronic myeloid leukemia (CML), a light-induced optoelectronic sensor based on CNTs functionalized with GPMS molecules was developed, achieving a detection limit of 27 cells mL^{-1} for K562 leukemia cells [67].

An ECL-based ELISA-type immunosensor using carbon nanotubes was developed for detecting prostate-specific membrane antigen (PSMA), achieving a detection limit of 0.88 ng mL^{-1} in complex biological samples [68]. To detect exosomes, a visible and colorimetric aptasensor based on DNA-functionalized SWCNTs was proposed. Exosomes bound to the transmembrane protein CD63 catalyzed the oxidation of tetramethylbenzidine (TMB), resulting in a measurable color change. This system demonstrated a detection limit of $5.2 \cdot 10^2$ particles μL^{-1} [69]. Yong et al. developed multicolor fluorescent peptide-CNT nanoprobes capable of simultaneously detecting three cancer-related proteases, including MMP-7, uPA, and MMP-2. Based on fluorescence quenching and recovery mechanisms, protease activity was quantitatively evaluated, achieving detection limits in the range of 0.5-500 $pg \cdot mL^{-1}$ [70]. Mohammadi and co-workers developed a FRET-based sensing platform for the quantification of miRNA-155 using carbon dots (CDs) and MnO_2 nanosheets as donor-acceptor pairs. The system exhibited high specificity, enabling clear discrimination between perfectly complementary miRNA-155 and sequences with a single-base mismatch. Moreover, this approach was successfully applied to the detection of miRNA-155 in spiked serum samples as well as in breast cancer cells, such as MCF-7 [71]. Under the synergistic action of polydopamine, AuNPs, PEI-GO and AgNPs, the ECL signal of CQDs was significantly enhanced and considered as an excellent conductive material to speed up the electron transfer rate and electrochemical detection capability as well. Under optimal conditions, the constructed immunosensor presented a linear concentration in the range from 0.005 to 500 U mL^{-1}, with a detection limit of 0.0017 U mL^{-1} [72]. Early diagnosis is of great practical importance for improving the survival rate and effectiveness of cancer treatment. Shuaimin Lu and colleagues developed a highly sensitive fluorescent biosensor based on the inner-filter effect (IFE) for detecting the tumor-related biomarker β-glucuronidase (GLU). N-CQDs were used as fluorophores, while p-nitrophenol (pNP), generated from the GLU-catalyzed reaction of PNPG, acted as an absorber that quenched fluorescence due to spectral overlap. The sensor enabled monitoring of GLU activity with a low detection limit of 0.3 U L^{-1} [73]. Olorundare et al. developed a highly sensitive electrochemical immunosensor for the detection of AFP, a key cancer biomarker, using a hybrid nanomaterial platform composed of functionalized CNFs and electrodeposited AuNPs on a GCE. The CNF/AuNPs composite significantly enhanced the electrochemical

response, enabling AFP detection over a wide linear range of 0.005 to 500 ng mL^{-1} with a low limit of detection of 0.50 pg mL^{-1} from SWV and 0.48 pg mL^{-1} from EIS measurements. The immunosensor demonstrated excellent sensitivity, selectivity, repeatability, and stability, and was successfully applied to AFP detection in human serum samples, highlighting its potential for clinical cancer diagnostics [74]. Ji et al. developed an ultrasensitive signal-on electrochemiluminescence (ECL) biosensor based on CRISPR/Cas12a and MXene nanocomposites for the detection of miR-31. The platform combined a PEI-Ru@Ti_3C_2@AuNPs-modified electrode with a ferrocene-labeled DNA probe and employed a cascade amplification mechanism involving isothermal strand displacement amplification and Cas12a-mediated trans-cleavage, leading to efficient ECL signal restoration. The biosensor exhibited a wide linear range from 10 aM to 100 pM with an ultralow detection limit of 1.67 aM, along with high specificity and good performance in serum samples, demonstrating its potential for early cancer diagnosis [75].

Overall, the comparative analysis of the reviewed studies clearly demonstrates that hybrid nanocomposite platforms, particularly those combining carbon nanomaterials with metal nanoparticles (e.g., rGO/AuNPs, CNT/AuNPs, CNF/AuNPs), provide the highest analytical performance in electrochemical biosensing of cancer biomarkers. These systems exhibit significantly lower limits of detection (down to fg-aM levels) compared to single-component materials, due to synergistic effects such as enhanced electron transfer kinetics, increased surface area, and improved immobilization efficiency of biorecognition elements. Among detection techniques, electrochemical methods such as DPV, SWV, and EIS demonstrate superior sensitivity and reliability, particularly for nucleic acid biomarkers (e.g., miRNAs), while ECL-based systems show excellent performance for protein biomarkers due to their low background signal and high amplification capability. In contrast, purely optical or single-material systems generally exhibit higher detection limits and lower stability. Therefore, the most effective strategy for the detection of cancer biomarkers involves the use of multifunctional nanocomposite platforms combined with highly sensitive electrochemical techniques, enabling ultrasensitive, selective, and reproducible detection.

3. Conclusion

The theoretical foundations of electrochemical sensors are closely related to the properties of CNMs. The use of CNMs as electrode materials represents a promising approach for improving the analytical performance of electrochemical sensors, thereby making a significant contribution to the advancement of modern sensing technologies.

Nanomaterials are commonly used to modify the surface of working electrodes. In addition to increasing the effective surface area of the electrode, they significantly enhance its analytical performance. Surface modification with

nanomaterials accelerates electron transfer at the electrode/electrolyte interface, resulting in amplified output signals from biosensors. The unique properties of CNMs have contributed substantially to the development and evolution of biosensors for cancer diagnosis. Compared with conventional sensing methods, next-generation biosensors based on CNMs demonstrate superior analytical performance. The distinctive characteristics of graphene, CNTs, and carbon quantum dots have facilitated the development of various nanostructured biosensors and promoted diverse scientific approaches in biosensor design.

In recent years, considerable research efforts have been devoted to improving immunosensors and DNA-based biosensors for the detection of major cancer biomarkers. Considering their cost-effectiveness, high sensitivity, stability, simplicity, and selectivity, biosensors based on carbon nanostructures represent promising tools for the development of advanced diagnostic technologies. With the rapid progress of nanotechnology, particularly in the synthesis and fabrication of carbon nanomaterials, their contribution to biosensing applications continues to expand. Biosensor electrodes modified with nanostructures not only enhance electrochemical and optical properties but also provide a favorable and biocompatible environment for the immobilization of recognition elements. This represents a critical step in the development of immunosensors and DNA biosensors.

In this review, various types of carbon nanomaterial-based biosensors developed for clinical cancer diagnosis over recent decades were analyzed, highlighting the advantages of incorporating carbon nanostructures at different stages of biosensor fabrication. The biosensors discussed in this article enable highly selective, sensitive, and cost-effective detection of cancer biomarkers through the use of carbon nanomaterials as functional components. Therefore, such biosensors have strong potential for widespread application in automated diagnostic systems. However, further improvements in key parameters such as reproducibility, long-term stability, and biocompatibility are required to facilitate their practical implementation. These advancements will enable the use of CNM-based biosensors as affordable and efficient diagnostic tools in clinical laboratories and healthcare settings.

Despite the significant progress achieved in the development of carbon nanomaterial-based biosensors, several critical challenges remain that limit their widespread clinical application. One of the major issues is the lack of reproducibility and standardization in nanomaterial synthesis and electrode fabrication, which leads to variability in sensor performance. In addition, long-term stability and biofouling effects in complex biological samples remain insufficiently addressed. Another important limitation is the gap between laboratory-scale studies and real clinical validation, as many reported sensors are tested only in controlled conditions or spiked samples. Current research trends indicate a shift toward the development of multifunctional, miniaturized, and portable sensing platforms, including lab-on-a-chip and wearable biosensors, as

well as the integration of artificial intelligence for signal processing and data analysis. Future research should focus on improving the scalability, stability, and real-sample applicability of these systems, as well as developing multiplexed biosensors capable of simultaneous detection of multiple biomarkers. Addressing these challenges will be essential for translating carbon nanomaterial-based biosensors from laboratory research into practical clinical diagnostic tools.

Acknowledgments: The authors declare that this research received no external funding.
Conflict of Interest: The authors declare no conflict of interest.

ОБЗОР ЭЛЕКТРОХИМИЧЕСКИХ БИОСЕНСОРОВ НА ОСНОВЕ УГЛЕРОДНЫХ НАНОМАТЕРИАЛОВ ДЛЯ РАННЕЙ ДИАГНОСТИКИ РАКА

А. Ережепова*, Ж. Мукатаева, Ы. Бакыткарим, Н. Шадин, Ж. Қорганбаева

Казахский национальный педагогический университет имени Абая, Алматы, Казахстан

Резюме. Рак является одной из основных причин смертности во всём мире. Ранняя диагностика опухолей рассматривается как ключевая и одновременно сложная задача в эффективном лечении онкологических пациентов. В последние годы биосенсоры на основе наноматериалов активно развиваются как современные и высокочувствительные инструменты диагностики рака. В частности, углеродные наноматериалы значительно улучшают аналитические характеристики электрохимических и оптических сенсорных систем. Целью данного обзора является систематизация возможностей электрохимических и оптических биосенсоров на основе углеродных наноматериалов для раннего выявления рака. К основным задачам относится анализ свойств применяемых углеродных наноструктур (графен, оксид графена, углеродные нанотрубки, углеродные квантовые точки) и оценка их эффективности при определении опухолевых маркеров. Проведён анализ научной литературы, рассмотрены методы вольтамперометрии, амперометрии, электрохимической импедансной спектроскопии, электрохемилюминесценции и поверхностного плазмонного резонанса. Особое внимание уделено стратегиям иммобилизации биорецепторов и функционализации нанокомпозитов. Углеродные наноматериалы обладают высокой электропроводностью, большой удельной поверхностью и биосовместимостью. Эти свойства обеспечивают возможность определения опухолевых маркеров (CEA, AFP, miRNA и белков) в низких концентрациях. Сенсоры характеризуются портативностью, быстрым откликом и низким пределом обнаружения. Биосенсоры на основе углеродных наноматериалов имеют высокую практическую значимость в области ранней диагностики и демонстрируют большой потенциал для клинического применения.

Ключевые слова: биомаркеры, рак, электрохимические биосенсоры, углеродные наноматериалы, графен, углеродные нанотрубки, оптические биосенсоры.

Ережепова Айнур Шамаханкызы	*докторант 1 курса*
Мукатаева Жазира Сагатбековна	*кандидат химических наук, ассоциированный профессор*
Бакыткарим Ырысгул	*PhD, старший преподаватель*
Шадин Нургуль Адырбеккызы	*PhD, старший преподаватель*
Корганбаева Жанар Кожамбердиевна	*кандидат химических наук, старший преподаватель*

ҚАТЕРЛІ ІСІКТІ ЕРТЕ ДИАГНОСТИКАЛАУҒА АРНАЛҒАН КӨМІРТЕКТІ НАНОМАТЕРИАЛДАР НЕГІЗІНДЕГІ ЭЛЕКТРОХИМИЯЛЫҚ БИОСЕНСОРЛАРҒА ШОЛУ

А.Ережепова*, Ж.Мукатаева , Ы.Бақытқәрім , Н. Шадин, Ж. Қорғанбаева

Абай атындағы Қазақ Ұлттық Педагогикалық Университеті, Алматы, Қазақстан

Түйіндеме. Қатерлі ісік әлем бойынша адам өлімінің негізгі себептерінің бірі болып табылады. Ісіктерді ерте кезеңде анықтау онкологиялық науқастарды тиімді емдеудің шешуші әрі күрделі міндеті саналады. Соңғы жылдары наноматериалдарға негізделген биосенсорлар қатерлі ісікті диагностикалаудың заманауи әрі жоғары сезімтал құралы ретінде қарқынды дамып келеді. Әсіресе көміртекті наноматериалдар электрохимиялық және оптикалық сенсорлық жүйелердің аналитикалық сипаттамаларын едәуір жақсартады. Бұл шолудың мақсаты – көміртекті наноматериалдарға негізделген электрохимиялық және оптикалық биосенсорлардың қатерлі ісікті ерте анықтаудағы мүмкіндіктерін жүйелеу. Негізгі міндеттерге қолданылатын көміртекті нанокұрылымдардың (графен, графен оксиді, көміртекті нанотүтіктер, көміртекті кванттық нүктелер) қасиеттерін талдау және олардың ісік маркерлерін анықтаудағы тиімділігін бағалау жатады. Ғылыми әдебиеттерге талдау жүргізіліп, вольтамперометрия, амперометрия, электрохимиялық импеданстық спектроскопия, электрохемилюминесценция және беттік плазмондық резонанс сияқты әдістер қарастырылды. Биорецепторларды иммобилизациялау және нанокомпозиттерді функционализациялау стратегияларына ерекше назар аударылды. Көміртекті наноматериалдар жоғары электрөткізгіштікке, үлкен меншікті бетке және биосәйкестілікке ие. Бұл қасиеттер ісік маркерлерін (CEA, AFP, miRNA және ақуыздар) төмен концентрацияларда анықтауға мүмкіндік береді. Сенсорлар портативтілігімен, жылдам жауап беруімен және төмен анықтау шегімен ерекшеленеді. Көміртекті наноматериалдарға негізделген биосенсорлар ерте диагностика саласында жоғары практикалық маңызға ие және клиникалық қолдануға үлкен әлеует көрсетеді.

Түйін сөздер: биомаркерлер, қатерлі ісік, электрохимиялық биосенсорлар, көміртекті наноматериалдар, графен, көміртекті нанотүтікшелер, оптикалық биосенсорлар

Ережепова Айнұр Шамаханқызы	*1 курс докторанты*
Мукатаева Жазира Сагатбековна	*химия ғылымдарының кандидаты, қауымдастырылған профессор*
Бақытқәрім Ырысгүл	*PhD, аға оқытушы*
Шадин Нұргүл Адырбекқызы	*PhD, аға оқытушы*
Қорғанбаева Жанар Қожамбердіқызы	*химия ғылымдарының кандидаты, аға оқытушы*

References

1. Siegel R.L., Giaquinto A.N., Jemal A. Cancer statistics, 2024. *CA Cancer J. Clin.* **2024,** 74, No.1, 12-49. DOI:10.3322/caac.21820

2. Ministry of Health of the Republic of Kazakhstan. More than one third of new oncological cases detected at early stage. Official Website of the Ministry of Health of the Republic of Kazakhstan, **2025**. https://www.gov.kz/memleket/entities/dsm/press/news/details/930604?lang=kk

3. Crosby D., Bhatia S., Brindle K.M., Coussens L.M., Dive C., Emberton M., Esener S., Fitzgerald R.C., Gambhir S.S., Kuhn P., Rebbeck T.R., Balasubramanian S. Early detection of cancer. *Science.* **2022,** Vol.375, No.6586.Art.aay9040. DOI:10.1126/science.aay9040

4. World Health Organization. Cancer. WHO Fact Sheet, **2025.** https://www.who.int/news-room/fact-sheets/detail/cancer

5. Saasa V., Chibagidi R., Ipileng K., Feleni U. Advances in cancer detection: A review on electrochemical biosensor technologies. *Sens. Bio-Sens. Res.* **2025**. Vol. 49. Article 100826. DOI:10.1016/j.sbsr.2025.100826

6. Khan H., Shah M.R., Barek J., Malik M.I. Cancer biomarkers and their biosensors: A comprehensive review. *TrAC Trends Anal. Chem.* **2022**, 157, 116813. DOI:10.1016/j.trac.2022.116813

7. Shao Y., Wang J., Wu H., Liu J., Aksay I.A., Lin Y. Graphene based electrochemical sensors and biosensors: A review. *Electroanalysis.* **2010**, 22, № 10, 1027-1036. DOI:10.1002/elan.200900571

8. Saputra H.A. Electrochemical sensors: basic principles, engineering, and state of the art. *Monatsh. Chem.* **2023**, 154, № 8, 1083-1100. DOI:10.1007/s00706-023-03113-z

9. Turner A.P.F. Biosensors: sense and sensibility. *Chem. Soc. Rev.* **2013**. Vol. 42. 3184-3196. DOI:10.1039/C3CS35528D

10. Estrela P., Hammond J.L., Formisano N., Carrara S., Tkac J. Electrochemical biosensors and nanobiosensors. *Essays Biochem.* **2016**, 60, № 1, 69-80. DOI:10.1042/EBC20150008

11. Scida K., Stege P.W., Haby G., Messina G.A., Garcia C.D. Recent applications of carbon-based nanomaterials in analytical chemistry: critical review. *Anal. Chim. Acta*. **2011**, 691, № 1-2, 6-17. DOI:10.1016/j.aca.2011.02.025

12. Pumera M. Graphene-based nanomaterials for energy storage. *Chem. Soc. Rev.* **2010**. Vol. 39, No. 11. 4146-4157. DOI:10.1039/C002690P

13. Dresselhaus M.S., Dresselhaus G., Avouris P. Carbon Nanotubes: Synthesis, Structure, Properties, and Applications. *Springer*, Berlin. **2001**. 454. (1-9, 59-92, 273-300)

14. Dykman L.A., Khlebtsov N.G. Gold nanoparticles in biomedical applications: recent advances and perspectives**.** *Chem. Soc. Rev.* **2012**, Vol. 41, No. 6, 2256-2282**.** DOI:10.1039/C1CS15166E

15. Ali A., Ali, A., Majhi, S. M., Siddig, L. A., Deshmukh, A. H., Wen, H., Qamhieh, N. N., Greish, Y. E., & Mahmoud, S. T. Recent advancements in MXene-based biosensors for analytical applications. *Biosensors*. **2024**, Vol. 14, No. 10, Article 497, **1-32**. DOI:10.3390/bios14100497

16. Furukawa H., Cordova K.E., O'Keeffe M., Yaghi O.M. The chemistry and applications of metal-organic frameworks. *Science*. **2013**, Vol. 341, No. 6149, 1230444-1-1230444-12**.** DOI:10.1126/science.1230444

17. Sassolas A., Leca-Bouvier B.D., Blum L.J. Immobilization strategies to develop enzymatic biosensors. *Biotechnol. Adv.* **2012**, Vol. 30, No. 3, 489-**511.** DOI:10.1016/j.biotechadv.2011.09.003

18. Mei, Y., He, C., Zeng, W. et al. Electrochemical Biosensors for Foodborne Pathogens Detection Based on Carbon Nanomaterials: Recent Advances and Challenges. *Food Bioprocess Technol*. **2022**. 15, 498-513. DOI:10.1007/s11947-022-02759-7

19. Ambrosi A., Chua C.K., Bonanni A., Pumera M. Electrochemistry of graphene and related materials. *Chem. Rev.* **2014**, 114, № 14, 7150-7188. DOI:10.1021/cr500023c

20. Tiwari J.N., Vij V., Kemp K.C., Kim K.S. Engineered carbon-nanomaterial-based electrochemical sensors for biomolecules. *ACS Nano*. **2016**, 10, № 1, 46-80. DOI:10.1021/acsnano.5b05690

21. Wang L., Xiong Q., Xiao F., Duan H. 2D nanomaterials based electrochemical biosensors for cancer diagnosis. *Biosens. Bioelectron.* **2017**, 89, No.1, 136-151. DOI:10.1016/j.bios.2016.06.011

22. Pasinszki T., Krebsz M., Tung T.T., Losic D. Carbon nanomaterial based biosensors for non-invasive detection of cancer and disease biomarkers for clinical diagnosis. *Sens.* **2017**, 17, № 8, 1919. DOI:10.3390/s17081919

23. Chikkaveeraiah B.V., Bhirde A.A., Morgan N.Y., Eden H.S., Chen X. Electrochemical immunosensors for detection of cancer protein biomarkers. *ACS Nano.* **2012**, 6, No.8, 6546-6561. DOI:10.1021/nn3023969

24. Wu Y., Xue P., Kang Y., Hui K.M. Paper-based microfluidic electrochemical immunodevice integrated with nanobioprobes onto graphene film for ultrasensitive multiplexed detection of cancer biomarkers. *Anal. Chem.* **2013**, 85, No.18, 8661-8668. DOI:10.1021/ac401445a

25. Esteban-Fernández de Ávila B., Araque E., Campuzano S., Pedrero M., Dalkiran B., Barderas R., Villalonga R., Kiliç E., Pingarrón J.M. Dual functional graphene derivative-based electrochemical platforms for detection of the TP53 gene with single nucleotide polymorphism selectivity in biological samples. *Anal. Chem.* **2015**, 87, No.4, 2290-2298. DOI:10.1021/ac504032d

26. Kilic T., Erdem A., Erac Y., Seydibeyoglu M.O., Okur S., Ozsoz M. Electrochemical detection of a cancer biomarker mir-21 in cell lysates using graphene modified sensors. *Electroanalysis*. **2014**, 27, № 2, 367-374. DOI:10.1002/elan.201400518

27. Wei T., Tu W., Zhao B., et al. Electrochemical monitoring of an important biomarker and target protein: VEGFR2 in cell lysates. *Sci. Rep.* **2014**, 4, № 1, 3982. DOI:10.1038/srep03982

28. Yu M., Li Q., Yu H. Graphene-based synthetic peptide electrochemical sensor for colorectal cancer diagnosis. *Alex. Eng. J.* **2024.** Vol. 101. 90-97. DOI: 10.1016/j.aej.2024.05.048

29. Yang H.W., Lin C.W., Hua M.Y., Liao S.S., Chen Y.T., Chen H.C., Weng W.H., Chuang C.K., Pang S.T., Ma C.C. Combined detection of cancer cells and a tumor biomarker using an immunomagnetic sensor for the improvement of prostate-cancer diagnosis. *Adv. Mater.* **2014**, 26, № 22, 3662-3666. DOI:10.1002/adma.201305842

30. Kumar S., Sharma J.G., Maji S., Malhotra B.D. Nanostructured zirconia decorated reduced graphene oxide based efficient biosensing platform for non-invasive oral cancer detection. *Biosens. Bioelectron.* **2016**, 78, No.1, 497-504. DOI:10.1016/j.bios.2015.11.084

31. Heidari R., Rashidiani J., Abkar M., Taheri R.A., Moghaddam M.M., Mirhosseini S.A., Seidmoradi R., Nourani M.R., Mahboobi M., Keihan A.H., Kooshki H. CdS nanocrystals/graphene oxide-AuNPs based electrochemiluminescence immunosensor in sensitive quantification of a cancer biomarker: p53. *Biosens. Bioelectron.* **2019**, 126, 7-14. DOI:10.1016/j.bios.2018.10.031

32. Akbari A., Hashemzadeh H., Shokati Eshkiki Z., Masoodi M., Tabaeian S.P., Naderi-Manesh H., Zare A.A., Agah S. Detection of plasma miR-223 by a novel label-free graphene oxide/gold nanocomposite immunosensor in colorectal cancer patients: An electrochemical biosensor approach. *Biosens. Bioelectron. X*. **2023.** Vol. 14. Article No.100331. DOI: 10.1016/j.biosx.2023.100331

33. Wang Y., Li X., Cao W., Li Y., Li H., Du B., Wei Q. Ultrasensitive sandwich-type electrochemical immunosensor based on a novel signal amplification strategy using highly loaded toluidine blue/gold nanoparticles decorated KIT-6/carboxymethyl chitosan/ionic liquids as signal labels. *Biosens. Bioelectron.* **2014**, 61, 618-624. DOI:10.1016/j.bios.2014.05.059

34. Farzin L., Shamsipur M. Recent advances in design of electrochemical affinity biosensors for low level detection of cancer protein biomarkers using nanomaterial-assisted signal enhancement strategies. *J. Pharm. Biomed. Anal.* **2018**. 6 Vol.147. 185-210. DOI:10.1016/j.jpba.2017.07.042

35. Ballesta A.M., Molina R., Filella X., Jo J., Giménez N. Carcinoembryonic antigen in staging and follow-up of patients with solid tumors. *Tumour Biol.* 1995, 16, №1, 32-41. https://doi.org/10.1159/000217926

36. Naghibalhossaini F., Ebadi P. Evidence for CEA release from human colon cancer cells by an endogenous GPI-PLD enzyme. *Cancer Lett.* **2006**, 234, No 2, 158-167. DOI:10.1016/j.canlet.2005.03.028

37. Li F., Jiang L., Han J., Liu Q., Dong Y., Li Y., Wei Q. A label-free amperometric immunosensor for the detection of carcinoembryonic antigen based on novel magnetic carbon and gold nanocomposites. *RSC Adv.* **2015**, 5, No. 26, 19961-19969. DOI:10.1039/C4RA16569A

38. Pang X., Li J., Zhao Y., Wu D., Zhang Y., Du B., Ma H., Wei Q. Label-free electrochemiluminescent immunosensor for detection of carcinoembryonic antigen based on nanocomposites of GO/MWCNTs-COOH/Au@CeO_2. *ACS Appl. Mater. Interfaces*. **2015**, 7, № 34, 19260-19267. DOI:10.1021/acsami.5b05185

39. Han J., Li Y., Feng J., Li M., Wang P., Chen Z., Dong Y. A novel sandwich-type immunosensor for detection of carcinoembryonic antigen using silver hybrid multiwalled carbon nanotubes/manganese dioxide. *J. Electroanal. Chem.* **2017**, 786, 112-119. DOI:10.1016/j.jelechem.2017.01.021

40. Heydari-Bafrooei E., Shamszadeh **N.S.** Electrochemical bioassay development for ultrasensitive aptasensing of prostate specific antigen. *Biosens. Bioelectron.* **2017**, 91, 284-292. DOI:10.1016/j.bios.2016.12.048

41. Wang Y., Qu Y., Ye X., Wu K., Li Ch. Fabrication of an electrochemical immunosensor for α-fetoprotein based on a poly-L-lysine-single-walled carbon nanotubes/Prussian blue composite film interface. *J. Solid State Electrochem.* **2016**, 20, № 8, 2217-2222. DOI:10.1007/s10008-016-3229-0

42. Li F., Peng J., Wang J., Tang H., Tan L., Xie Q., Yao S. Carbon nanotube-based label-free electrochemical biosensor for sensitive detection of miRNA-24. *Biosens. Bioelectron.* **2014**, 54, № 1, 158-164. DOI:10.1016/j.bios.2013.10.061

43. Sabahi A., Salahandish R., Ghaffarinejad A., Omidinia E. Electrochemical nano-genosensor for highly sensitive detection of miR-21 biomarker based on SWCNT-grafted dendritic Au nanostructure for early detection of prostate cancer. *Talanta*. **2020**, 209, 120595. DOI:10.1016/j.talanta.2019.120595

44. Luo Y., Wang Y., Yan H., Wu Y., Zhu C., Du D., Lin Y. SWCNTs@GQDs composites as nanocarriers for enzyme-free dual-signal amplification electrochemical immunoassay of cancer biomarker. *Anal. Chim. Acta*. **2018**, 1042, 44-51. DOI:10.1016/j.aca.2018.08.023

45. Gulati P., Mishra P., Khanuja M., Narang J., Islam S.S. Nano-moles detection of tumor specific biomarker DNA for colorectal cancer detection using vertically aligned multi-wall carbon nanotubes based flexible electrodes. *Process Biochem.* **2020**, 90, 184-192. DOI:10.1016/j.procbio.2019.11.021

46. Chen M., Wu D., Tu S., et al. A novel biosensor for the ultrasensitive detection of the lncRNA biomarker MALAT1 in non-small cell lung cancer. *Sci. Rep.* **2021**, 11, No.1, 3666. DOI:10.1038/s41598-021-83244-7

47. Hasanzadeh M., Shadjou N. What are the reasons for low use of graphene quantum dots in immunosensing of cancer biomarkers? *Mater. Sci. Eng. C.* **2017**, No.71, 1313-1326. DOI:10.1016/j.msec.2016.11.068

48. Wu D., Liu Y., Wang Y., Hu L., Ma H., Wang G., Wei Q. Label-free electrochemiluminescent immunosensor for prostate-specific antigen detection based on graphene quantum dots and Au/Ag-rGO composite. *Sci.Rep.* **2016**. Vol. 6. 1-7. DOI:10.1038/srep20511

49. Li L., Li W., Ma C., Yang H., Ge S., Yu J. Paper-based electrochemiluminescence immunodevice for carcinoembryonic antigen using nanoporous gold-chitosan hybrids and graphene quantum dots functionalized Au@Pt. *Sens. Actuators B Chem.* **2014**, 202, 314-322. DOI:10.1016/j.snb.2014.05.087

50. Yang H., Liu W., Ma C., Zhang Y., Wang X., Yu J., Song X. Gold-silver nanocomposite-functionalized graphene based electrochemiluminescence immunosensor using graphene quantum dots coated porous PtPd nanochains as labels. *Electrochim. Acta*. **2014**, 123, 470-476. DOI:10.1016/j.electacta.2014.01.014

51. Hu T., Zhang L., Wen W., Zhang X., Wang S. Enzyme catalytic amplification of miRNA-155 detection with graphene quantum dot-based electrochemical biosensor. *Biosens. Bioelectron.* **2016**, 77, 451-456. DOI:10.1016/j.bios.2015.09.068

52. Serafin V., Valverde A., Martinez-Garcia G., Martinez-Periñán E., Comba F., Garranzo-Asensio M., Barderas R., Yáñez-Sedeño P., Campuzano S., Pingarrón J.M. Graphene quantum dots-functionalized multi-walled carbon nanotubes as nanocarriers in electrochemical immunosensing. *Sens. Actuators B Chem.* **2019**, 284, 711-722. DOI:10.1016/j.snb.2019.01.012

53. Mintz K., Waidely E., Zhou Y., Peng Z., Al-Youbi A.O., Bashammakh A.S., El-Shahawi M.S., Leblanc R.M. Carbon dots and gold nanoparticles-based immunoassay for detection of alpha-L-fucosidase. *Anal. Chim. Acta*. **2018**, 1041, 114-121. DOI:10.1016/j.aca.2018.08.055

54. Kulkarni U.S., Gawali C.R., Pankaj, Kumar S. Ultraefficient electrochemical biosensing platform utilizing aloe vera-derived carbon nanodots for ANXA2 liver cancer biomarker diagnosis. *Ind. Crops Prod.* **2025.** Vol. 229. Article No.120996. DOI: 10.1016/j.indcrop.2025.120996.

55. Saedi Tabar F., Pourmadadi M., Yazdian F., Rashedi H., Rahdar A., Fathi-karkan S., Romanholo Ferreira L.F. Ultrasensitive aptamer-based electrochemical nanobiosensor in diagnosis of prostate cancer using 2D:2D reduced graphene oxide/graphitic carbon nitride decorated with Au nanoparticles. *Eur. J. Med. Chem. Rep.* **2024.** Vol. 12. Article No.100192. DOI: 10.1016/j.ejmcr.2024.100192.

56. Nanda B.P., Rani P., Paul P., Aman, Ganti S.S., Bhatia R. Recent trends and impact of localized surface plasmon resonance (LSPR) and surface-enhanced Raman spectroscopy (SERS) in modern analysis. *J. Pharm. Anal.* **2024.** Vol. 14, No. 11. Article No.100959. DOI: 10.1016/j.jpha.2024.02.013

57. Guo X. Surface plasmon resonance-based biosensor technique: a review. *J.Biophotonics*. **2012**, 5, № 7, 483-501. DOI:10.1002/jbio.201200015

58. Wang Q., Li Q., Yang X., Wang K., Du S., Zhang H., Nie Y. Graphene oxide-gold nanoparticles hybrids-based surface plasmon resonance for sensitive detection of microRNA. *Biosens. Bioelectron.* **2016**, 77, 1001-1007. DOI:10.1016/j.bios.2015.10.091

59. Hossain M.B., Islam M.M., Abdulrazak L.F., et al. Graphene-coated optical fiber SPR biosensor for BRCA1 and BRCA2 breast cancer biomarker detection: A numerical design-based analysis. *Photonic Sens.* **2020**, 10, № 1, 67-79. DOI:10.1007/s13320-019-0556-7

60. Chiu N.F., Lin T.L., Kuo C.T. Highly sensitive carboxyl-graphene oxide-based surface plasmon resonance immunosensor for the detection of lung cancer cytokeratin 19 biomarker in human plasma. *Sens. Actuators B Chem.* **2018**, 265, 264-272. DOI:10.1016/j.snb.2018.03.070

61. He L., Pagneux Q., Larroulet I., Serrano A.Y., Pesquera A., Zurutuza A., Mandler D., Boukherroub R., Szunerits S. Label-free femtomolar cancer biomarker detection in human serum using graphene-coated surface plasmon resonance chips. *Biosens. Bioelectron.* **2017**, 89, № 1, 606-611. DOI:10.1016/j.bios.2016.01.076

62. Xing F., Meng G.X., Zhang Q., Pan L.T., Wang P., Liu Z.B., Jiang W.S., Chen Y., Tian J.-G. Ultrasensitive flow sensing of a single cell using graphene-based optical sensors. *Nano Lett.* **2014**. Vol. 14, No. 6. 3563-3569. DOI:10.1021/nl5012036

63. Muthuraj B., Mukherjee S., Chowdhury S.R., Patra C.R., Iyer P.K. An efficient strategy to assemble water soluble histidine-perylene diimide and graphene oxide for the detection of PPi in physiological conditions and in vitro. *Biosens. Bioelectron.* **2017**, 89, No.1, 636-644. DOI:10.1016/j.bios.2015.12.036

64. Williams R.M., Lee C., Heller D.A. A fluorescent carbon nanotube sensor detects the metastatic prostate cancer biomarker uPA. *ACS Sens.* **2018**, 3, No.9, 1838-1845. DOI:10.1021/acssensors.8b00631

65. Gedi V., Song C.K., Kim G.B., Lee J.O., Oh E., Shin B.S., Jung M., Shim J., Lee H., Kim Y.P. Sensitive on-chip detection of cancer antigen 125 using a DNA aptamer/carbon nanotube network platform. *Sens. Actuators B Chem.* **2018**, 256, 89-97. DOI:10.1016/j.snb.2017.10.049

66. Harvey J.D., Jena P.V., Baker H.A., Zerze G.H., Williams R.M., Galassi T.V., Roxbury D., Mittal J., Heller D.A. A carbon nanotube reporter of miRNA hybridization events in vivo. *Nat. Biomed. Eng.* **2017**, 1, № 1, 0041. DOI:10.1038/s41551-017-0041

67. Gulati P., Kaur P., Rajam M.V., Srivastava T., Ali M.A., Mishra P., Islam S.S. Leukemia biomarker detection by using photoconductive response of CNT electrode: Analysis of sensing mechanism based on charge transfer induced Fermi level fluctuation. *Sens. Actuators B Chem.* **2018**, 270, 45-55. DOI:10.1016/j.snb.2018.05.019

68. Juzgado A., Soldà A., Ostric A., Criado A., Valenti G., Rapino S., Conti G., Fracasso G., Paolucci F., Prato M. Highly sensitive electrochemiluminescence detection of a prostate cancer biomarker. *J. Mater. Chem. B.* **2017**, 5, No. 32, 6681-6687. DOI:10.1039/c7tb01557g

69. Xia Y., Liu M., Wang L., Yan A., He W., Chen M., Lan J., Xu J., Guan L., Chen J. A visible and colorimetric aptasensor based on DNA-capped single-walled carbon nanotubes for detection of exosomes. *Biosens. Bioelectron.* **2017**, 92, 8-15. DOI:10.1016/j.bios.2017.01.063

70. Huang Y., Shi M., Hu K., Zhao S., Lu X., Chen Z.F., Chen J., Liang H. Carbon nanotube-based multicolor fluorescent peptide probes for highly sensitive multiplex detection of cancer-related proteases. *J. Mater. Chem. B.* **2013**, 1, No. 28, 3470-3476. DOI:10.1039/c3tb20408a

71. Mohammadi S., Salimi A. Fluorometric determination of microRNA-155 in cancer cells based on carbon dots and MnO_2 nanosheets as a donor-acceptor pair. *Mikrochim. Acta*. **2018**, 185, No.8, 372. 1-10. DOI:10.1007/s00604-018-2868-5

72. Qin D., Jiang X., Mo G., Feng J., Yu C., Deng B. A novel carbon quantum dots signal amplification strategy coupled with sandwich electrochemiluminescence immunosensor for the detection of CA15-3 in human serum. *ACS Sens.* **2019**, 4, No.2, 504-512. DOI:10.1021/acssensors.8b01607

73. Lu S., Li G., Lv Z., Qiu N., Kong W., Gong P., Chen G., Xia L., Guo X., You J., Wu Y. Facile and ultrasensitive fluorescence sensor platform for tumor invasive biomarker β-glucuronidase detection and inhibitor evaluation with carbon quantum dots based on inner-filter effect. *Biosens. Bioelectron.* **2016,** Vol. 85. 358-362. DOI: 10.1016/j.bios.2016.05.021

74. Olorundare F.O.G., Sipuka D.S., Sebokolodi T.I., Makaluza S., Midzi N., Kodama T., Arotiba O.A., Nkosi D. An electrochemical immunosensor on a carbon nanofiber/gold nanoparticles platform for the detection of alpha-fetoprotein cancer biomarker. *Sens. Bio-Sens. Res.* **2023**, Vol. 41. 100574. DOI: 10.1016/j.sbsr.2023.100574

75. Ji Z., Cheng S., Li W., Xing Y., Tang Z., Zhu X., Wang D., Hao C., Wang B., Shi M. Ultrasensitive detection of miR-31 using a signal-on electrochemiluminescence biosensor based on CRISPR/Cas12a and MXene nanocomposites. *Bioelectrochemistry.* **2026,** Vol. 167. 109059. DOI: 10.1016/j.bioelechem.2025.109059.

Chemical Journal of Kazakhstan
Volume 2, Number 94(2026), 29-39 https://doi.org/10.51580/2026-2.2710-1185.11

UDC 546.7:620.3

STABILIZATION OF IRON NANOPARTICLES BY BIOPOLYMERS DURING CHEMICAL REDUCTION WITH SODIUM BOROHYDRIDE

Zh.Zh. Nurtazina[1], Zh.S. Kassymova[1*], L.K. Orazzhanova[1], Łęska Bogusława[2]

[1]Shakarim University, Semey, Kazakhstan
[2]Adam Mickiewicz University in Poznań, Poznań, Poland

[*]Corresponding author e-mail: kasymova-z@mail.ru

Abstract. *Introduction.* One of the effective ways to regulate the processes of formation and agglomeration of FeNPs is the use of biopolymer stabilizers. *The goal* is to investigate the influence of biopolymer stabilization on the size, morphological and crystalline characteristics of FeNPs obtained by chemical reduction of $NaBH_4$. *Methods.* FeNPs were synthesized by reduction of Fe^{3+} with $NaBH_4$, stabilized with chitosan and sodium carboxymethylcellulose. The optical properties were studied using UV-Visible spectrophotometry, FTIR to identify functional groups, SEM-EDS and TEM to examine morphology and elemental composition, XRD to determine crystalline phases, and DLS-ELS to evaluate hydrodynamic diameter and ζ-potential. *Results and discussion.* UV-Vis spectra showed a characteristic 260-300 nm absorption band of iron-containing nanostructures. FTIR spectra indicated Fe-O bonds and interactions between FeNPs and biopolymer functional groups. SEM analysis showed reduced aggregation in FeNPs/Na-CMC and FeNPs/CS compared with unstabilized FeNPs. EDS analysis confirmed the presence of Fe and O elements and the formation of an oxide/hydroxide phase. XRD analysis revealed the formation of crystalline iron oxide phases. The average-sized crystallites are approximately 18 nm for FeNPs, 14 nm for FeNPs/Na-CMC, and 10 nm for FeNPs/CS. TEM and DLS/ELS confirmed the formation of spherical FeNP/CS nanoparticles with a size range of 20.03 ± 3.62 nm and a zeta-potential of -30.6 mV.*Conclusion.* Biopolymer stabilizers were found to reduce the growth and aggregation of FeNPs. CS effectively limits crystallite growth and suppresses agglomeration, while Na-CMC forms structurally organized composite particles. The results demonstrate the potential of using biopolymers to stabilize iron-containing nanomaterials.

Key words: iron nanoparticles, biopolymers, sodium carboxymethylcellulose, chitosan, sodium borohydride reduction

Nurtazina Zhanar Zhursinovna	*Master of Ecology; E-mail:nurtazina830912@gmail.com*
Kassymova Zhanar Sailaubekovna	*Candidate of Biological Sciences;* *E-mail: kasymova-z@mail.ru*
Orazzhanova Lazzyat Kametaevna	*Candidate of Chemical Sciences;* *E-mail: lazzyat.orazzhanova.70@mail.ru*
Łęska Bogusława	*Doctor of Chemical Sciences;* *E-mail: boguslawa.leska@amu.edu.pl*

Citation: Nurtazina Zh.Zh., Kassymova Zh.S., Orazzhanova L.K., Łęska B. Stabilization of iron nanoparticles by biopolymers during chemical reduction with sodium borohydride. *Chem. J. Kaz.*, **2026**, 2*(94)*, 29-39. DOI: https://doi.org/10.51580/2026-2.2710-1185.11

1. Introduction

Iron nanopacticles (FeNPs) have attracted scientific interest and are widely used in medicine, biotechnology and agriculture due to their redox activity, catalytic ability, magnetic properties and environmental compatibility [1-2].

Among the chemical methods for the synthesis of FeNPs [3], the most optimal is the reduction of Fe^{3+} with sodium borohydride:

$$4Fe^{3+} + 3BH_4^- + 9H_2O \rightarrow 4Fe^0 + 6H_2 \uparrow + 3H_2BO_3^- + 12H^+$$

The advantages of this synthesis method include the availability of reagents and equipment, as well as the ability to control nanoscale sizes [4]. Despite the efficiency of reduction, in an aqueous environment, Fe^o nanoparticles oxidize to form oxide phases with a core-oxide shell structure and are prone to agglomeration due to insufficient stabilization [5]. Stabilization of FeNPs during synthesis is a key factor determining particle size distribution, morphology, and colloidal stability. The use of sodium carboxymethylcellulose (Na-CMC) and chitosan (CS) biopolymers as effective FeNPs stabilizers is relevant due to their non-toxicity, biocompatibility, and complexing ability with metals. The stabilization mechanism includes the complexation of Fe^{3+} ions with nitrogen (-NH_2) and oxygen (-OH, -COO^-) atoms, which act as electron pair donors and form Fe-N, Fe-O donor-acceptor bonds [6,7]. In the chemical synthesis of FeNPs using the CS stabilizer, a distinctive condition is maintaining pH≈5.5-6.5 for protonation of -NH_2 and obtaining a polycation. Further, the interaction of Fe^{3+} with the cationic center of NH_3^+ through the "bridges" of anions and water molecules causes deprotonation of NH_3^+ due to the high affinity of Fe^{3+} for the electron pair of nitrogen. As a result, chelation of Fe^{3+} ions with the NH_2 group and the formation of the Fe-N donor-acceptor bond [8]. The aim of the study is to investigate the effect of biopolymer stabilization on the size, morphological and crystalline characteristics of FeNPs obtained by chemical reduction of $NaBH_4$.

2. Experimental part

2.1 Synthesis of FeNPs without stabilizers

To a 150 mL mixture of isopropanol and deionized water (1:1) added 0.5 g $FeCl_3 \times 6H_2O$ and stirred on a JOANLAB Lab 6 magnetic stirrer (China) at 50°C and 1000 rpm for 30 minutes. The beaker with the reaction mixture was covered with aluminum foil to limit contact with air, and 50 mL of cooled 0.5 M $NaBH_4$ solution was added dropwise until a black suspension appeared. The resulting suspension was cooled to room temperature with stirring, then left at rest for 15-20 minutes. The suspension was separated on an OPN-8 centrifuge (Kyrgyzstan) at 3000 rpm. The supernatant was decanted, and the black precipitate was frozen and dried in a Scientz-12 freeze dryer (China) at -60°C and reduced pressure <5 Pa. This yielded a dry powdered FeNPs product for further study.

2.2 Preparation of FeNPs stabilized by Na-CMC and CS

To synthesize FeNPs stabilized with Na-CMC (FeNPs/Na-CMC) and CS (FeNPs/CS), a solution of 0.5 g $FeCl_3 \times 6H_2O$ in 50 mL of deionized water was added to 120 mL of 1% biopolymer solutions. The resulting reaction mixture was stirred with a magnetic stirrer at 80°C and 1500 rpm for 2 hours to ensure uniform distribution of Fe^{3+} iron ions in the biopolymer matrix. After completion of the thermal treatment, the mixture was cooled to room temperature. Next, 10 mL of a cooled 1 M $NaBH_4$ solution was added dropwise to the reaction mixture. To limit contact with the environment, the reaction beakers were pre-wrapped in aluminum foil. The resulting suspension was centrifuged to separate the solid nanoparticles. The resulting precipitates were frozen and dried in a Scientz-12 freeze dryer (China) at a temperature of -60°C and reduced pressure <5 Pa. The physicochemical characteristics of the biopolymers used were studied earlier in our study [9].

2.3 UV-Vis analysis

The optical absorption spectrum was measured using a PE-5400UV spectrophotometer (Russia) at a scan rate of 40 nm/min in the wavelength range of 200-600 nm. Measurements were performed in a quartz cuvette with an optical layer thickness of 10 mm.

2.4 FTIR analysis

IR spectra were obtained using a Simex FTIR-801 IR spectrometer (Russia) with Fourier transform in transmission mode, scanning was carried out with a resolution of 4 cm^{-1} in the range from 500 to 4000 cm^{-1}.

2.5 SEM/EDS analysis

The surface morphology and microstructure of the coatings were examined using scanning electron microscopy (SEM) on an SEM3200 (China) instrument with a tungsten cathode and an XFlash Detector 730M-300 (Bruker) energy-dispersive X-ray microanalysis (EDS) system. The studies were performed at an accelerating voltage of 15 kV in low vacuum mode. Micrographs were obtained at magnifications of 35×, 250×, and 500×.

2.6 TEM analysis

The shape and size distribution of the nanoparticles were studied using a JEOL JEM-1400 Plus transmission electron microscope (Japan). The study was conducted at an accelerating voltage of 120 keV. Aliquots of 10 μl were taken from the samples, applied to 200-mesh copper grids coated with Formvar, and dried at room temperature.

2.7 XRD analysis

The crystal structure of the samples was studied by X-ray diffraction using an X'Pert PRO diffractometer (Netherlands) equipped with monochromatic CuKα radiation (λ = 0.1542 Å). The diffractometer was operated at an accelerating voltage of 40 kV and an X-ray tube current of 30-45 mÅ. Diffraction intensity was recorded over a range of 10^o to 80^o at an angle of 2θ. The average nanoparticle size was calculated using the Debye-Scherrer equation:

$$d = \frac{K\lambda}{\beta cos\theta}$$

where d - the average crystallite diameter in nm, K - the shape factor (0.9 for spherical particles), λ - the X-ray wavelength (0.15 nm), β is the width of the diffraction peak in radians, θ is the Bragg angle, 2θ [4].

2.8 DLS-ELS analysis

The hydrodynamic diameter and particle size distribution were determined by dynamic light scattering (DLS) on a Zetasizer NanoZS 90 instrument (Malvern, UK) using Zetasizer Software v.7.01. The surface charge of the particles was characterized by zeta potential values measured by electrophoretic light scattering (ELS) on the same instrument.

3. Results and discussion

3.1 Characterization of FeNPs, FeNPs/Na-CMC, FeNPs/CS

The synthesized FeNPs samples differ in appearance depending on the biopolymer stabilizers (Figure 1). The FeNPs sample (Figure 1a), obtained without stabilizers, is a dense black powder. FeNPs/Na-CMC (Figure 1b) has a looser, light gray appearance with a fibrous texture. The FeNPs/CS sample (Figure 1c) is also characterized by a non-uniform, loose, gray-black mass.

The synthesized FeNPs were characterized by ultraviolet-visible spectroscopy (UV-Vis), Fourier transform infrared spectroscopy (FTIR), scanning and transmission electron microscopy (SEM and TEM), energy dispersive analysis (EDS), X-ray diffraction (XRD), dynamic and electrophoretic light scattering (DLS and ELS).

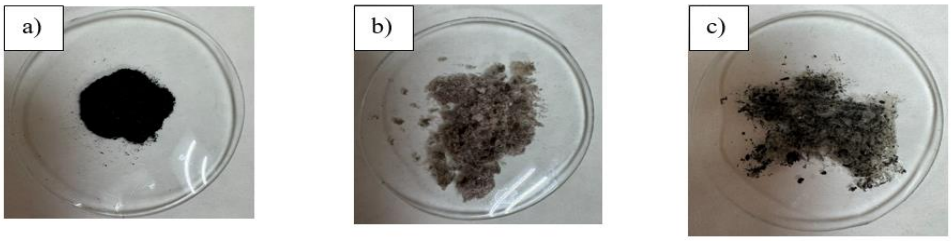

Figure 1 – Synthesized FeNPs (a), FeNPs/ Na-CMC (b), FeNPs/CS (c)

3.2 UV-Vis analysis results

UV-Vis spectra of all three samples were studied in the range from 200 to 600 nm (Figure 2a). In the region of 260-300 nm, a broad absorption band characteristic of iron-based nanoparticles is observed in all cases. The broadening of the absorption band is likely due to various electronic transitions in the iron/iron oxide system, in contrast to noble metal nanoparticles (Au, Ag), which are characterized by a clearly defined surface plasmon resonance. For the FeNPs sample, the most intense band is located at 270 nm, for FeNPs/Na-CMC it shifts

to 260 nm, and for FeNPs/CS to 280 nm. Such shifts and changes in intensity indicate that biopolymer stabilizers alter the electronic environment and optical properties of nanoparticles, affecting the surface oxide layer and the degree of aggregation [10].

3.3 FTIR analysis results

Analysis of the FTIR spectra (Figure 2b) revealed the presence of peaks at 534, 557, and 562 cm^{-1}, characteristic of the Fe-O bond. The presence of the Fe-O bond demonstrates partial oxidation of reduced iron upon exposure to air [2].

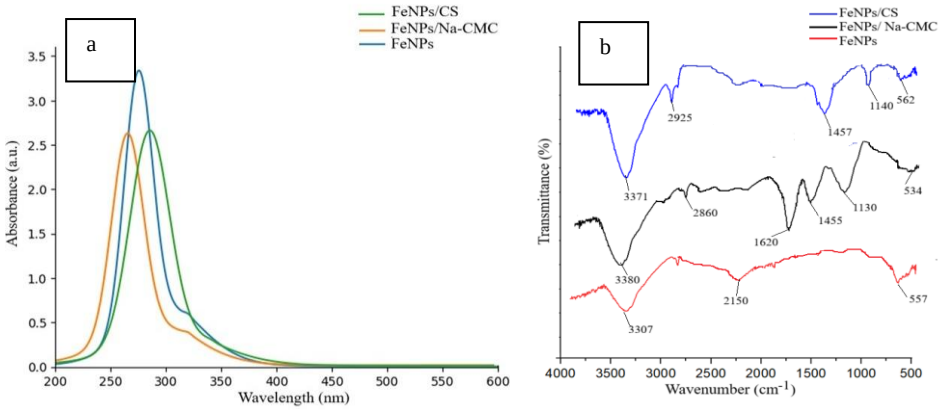

Figure 2 – Spectral characteristics (a) UV-visible spectra, (b) FTIR spectra

The FTIR spectrum of the FeNPs sample has a peak at 3307 cm^{-1} for the hydroxyl group -OH. Literature data confirm that the presence of the -OH group is associated with the formation of an oxide-hydroxide shell from the compounds $Fe(OH)_2$, FeOOH, Fe_2O_3 and Fe_3O_4 [10]. The spectra of the FeNPs/Na-CMC and FeNPs/CS samples show absorption peaks characteristic of the -OH, $-COO^-$, $-NH_2$ functional groups. The peaks at 3371 and 3380 cm^{-1} correspond to the stretching vibrations of the -OH and $-COO^-$ groups. The peaks at 2860 and 2925 cm^{-1} are due to the symmetric stretching vibrations of the -C-H bond. In the FeNPs/CMC sample, the peak at 1620 cm^{-1} is due to the asymmetric vibrations of $-COO^-$ and 1455 cm^{-1} to the symmetric vibrations of COO^-. Glycosidic bonds C-O-C show characteristic peaks at wavenumbers of 1130 cm^{-1}. In the FeNPs/CS sample, the peak at 1457 cm^{-1} corresponds to the amino group $-NH_2$ of chitosan CS, and 1140 cm^{-1} is related to the stretching vibrations of the glycosidic bond C-O-C [9]. Comparison of FTIR spectra of the studied samples shows the presence of biopolymer stabilizers in the obtained nanocomposites.

3.4 SEM/EDS analysis results

The obtained SEM images show the morphology of the synthesized FeNPs (Figure 3).

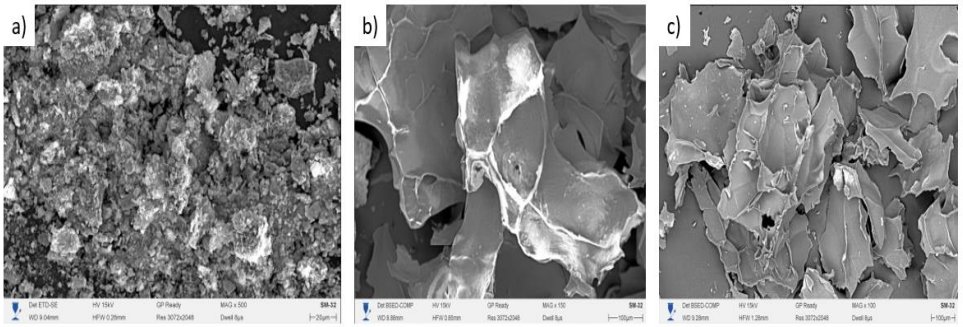

Figure 3 – SEM images of synthesized
FeNPs (a), FeNPs/Na-CMC (b), FeNPs/CS (c)

The FeNPs sample without stabilizers consists of flaky aggregates 20-100 μm in size (Figure 3a). This morphology is typical of FeNPs obtained by borohydride reduction followed by partial oxidation [3]. Individual FeNPs are not clearly visible due to pronounced aggregation. The morphology of FeNPs/Na-CMC and FeNPs/CS is characterized by a large, lamellar-film structure with a smooth polymer coating relief. FeNPs/Na-CMC aggregates appear less dense compared to the FeNPs sample. FeNPs/Na-CMC have sizes up to 500 μm (Figure 3b). The ability of Na-CMC to adsorb on the surface of nanoparticles via carboxyl groups, forming steric and electrostatic repulsive interactions that lead to increased colloidal stability, has been widely discussed in the literature [6]. FeNPs/Na-CMC particle aggregates have a loose, porous surface compared to FeNPs/Na-CMC. The fine-grained structure within the aggregates is poorly visible due to complete coverage by the CS polymer matrix. Due to more effective suppression of agglomeration by the CS stabilizer, FeNPs/CS particles have sizes up to 306 μm (Figure 3c).

EDS results show the elemental composition of the resulting nanoparticles (Figure 4).

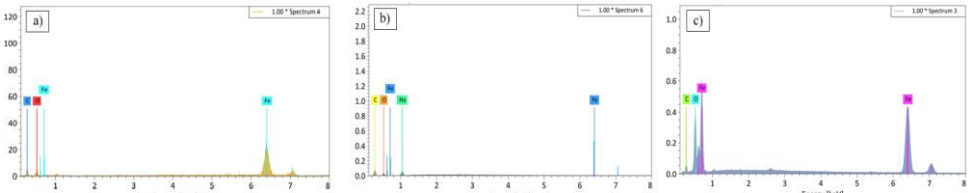

Element	Atomic number	Line series	Net counts	Mass Concentration /%	Norm. mass concentration /%	Norm. atomic concentration /%	1σ uncertainty /mass%
C	6	K	187	15.66	9.40	30.79	1.30
O	8	K	163	5.13	3.08	7.57	0.47
Fe	26	K	2959	145.78	87.52	61.64	22.75
			Sum	166.57	100.00	100.00	

Element	Atomic number	Line series	Net counts	Mass Concentration /%	Norm. mass concentration /%	Norm. atomic concentration /%	1σ uncertainty /mass%
C	6	K	31126	32.61	27.83	37.85	0.63
O	8	K	81892	60.53	51.65	52.75	1.00
Na	11	K	29216	9.53	8.13	5.78	0.61
Fe	26	K	11601	14.52	12.39	3.62	0.65
			Sum	117.18	100.00	100.00	

Element	Atomic number	Line series	Net counts	Mass Concentration /%	Norm. mass concentration /%	Norm. atomic concentration /%	1σ uncertainty /mass%
C	6	K	1488	2.97	3.23	10.41	0.14
O	8	K	18465	12.00	13.04	31.56	0.20
Fe	26	K	65264	77.03	83.72	58.03	2.50
			Sum	92.01	100.00	100.00	

Figure 4 – EDS data of FeNPs (a), FeNPs/Na-CMC (b), FeNPs/CS (c)

Quantitative analysis of FeNPs shows that the mass fractions are 87.52% for Fe and 3.08% for O, thereby confirming the presence of Fe and O elements and the formation of an oxide/hydroxide phase. The absence of foreign elements in the EDS spectrum (Figure 4a) indicates the purity of the obtained FeNPs and confirms the effectiveness of the synthesis method using $NaBH_4$ [3, 5]. In the FeNPs/Na-CMC sample, in addition to Fe, O, and C, a Na peak is observed, characteristic of the Na-CMC structure. However, the mass fraction of Fe is lower (12.39%), and O is higher (51.65%) compared to other samples (Figure 4b). The lower Fe content and higher O concentration are possibly associated with an increase in the proportion of the organic phase due to stabilization by the dense polymer film of Na-CMC [10]. In the FeNPs/CS sample (Figure 4c), the Fe content is 83.72% and O content is 13.04%, indicating partial surface oxidation and the formation of an oxide shell. CS adsorbed on the nanoparticle surface also more effectively stabilizes and prevents agglomeration. The obtained SEM/EDS results confirm that biopolymers alter the surface morphology and limit the aggregation of FeNPs.

3.5 XRD analysis results

The X-ray diffraction patterns of FeNPs, FeNPs/Na-CMC and FeNPs/CS are shown in Figure 5.

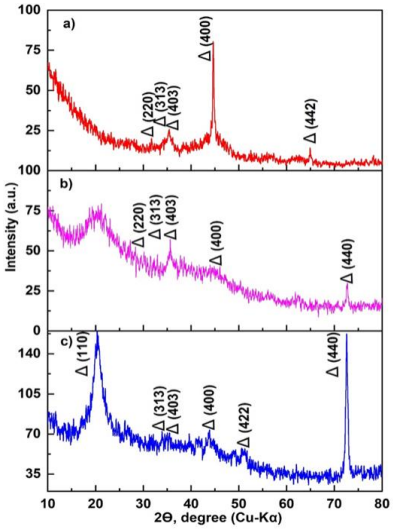

Figure 5 – Diffraction patterns of synthesized FeNPs (a), FeNPs/Na-CMC (b), FeNPs/CS (c)

The diffraction pattern of the FeNPs sample (Figure 5a) shows an intense and relatively narrow peak at 44°(400), which, along with peaks at 30.1°(220), 33.1°(313) and 35.2°(403), can be attributed to spinel-type iron oxides, thereby confirming the oxidation of zero-valent iron in the isopropanol-water system [4]. In the FeNPs/Na-CMC and FeNPs/CS samples (Figures 5b and 5c), the diffraction peaks exhibit lower intensity and a broader shape. This can be

explained by the presence of biopolymers, which reduce the degree of crystallinity and lead to a decrease in crystallite size by stabilizing the nanoparticles and preventing their aggregation [7, 8]. In the case of the FeNPs/CS sample (Figure 5c), a pronounced diffraction feature is observed near 20°(110), which is associated with the amorphous-semicrystalline structure of CS, while an intense peak near 72°(440) corresponds to the spinel phase of FeNPs on the CS matrix. The average crystallite size calculated using the Debye–Scherrer equation is 18 nm for FeNPs, 14 nm for FeNPs/NaCMC, and 10 nm for FeNPs/CS. Overall, X-ray diffraction analysis shows that biopolymers significantly influence the size and structure of FeNPs crystallites, facilitating the formation of stable nanocomposites. CS, in particular, has the strongest effect on the formation of the smallest crystallites. This is explained by the stronger electrostatic interaction of the polycation's -NH_2 groups with Fe^{3+} and the rigid and ordered conformation of the biopolymer chain.

3.6 TEM, DLS-ELS analysis results of FeNPs/CS

To confirm the X-ray diffraction data and refine the FeNPs/CS morphology, the sample was also examined using TEM and DLS-ELS. TEM analysis revealed that the FeNPs were predominantly spherical in shape and had a fairly uniform size distribution. The average nanoparticle core size was 20.03±3.62 nm. The average hydrodynamic diameter of the FeNPs/CS in the dispersed medium was 127±3 nm. The ζ-potential was -30.6 mV. The negative ζ-potential is due to the deprotonation of the -NH_3^+ groups of CS and the formation of a surface Fe-O^- oxide-hydrate shell. These parameters ensure the stability of the colloidal suspension.

4. Conclusion

FeNPs, FeNPs/Na-CMC and FeNPs/CS were synthesized using chemical reduction of Fe^{3+} ions with $NaBH_4$ and stabilization with biopolymers. UV-Vis, FTIR, SEM/EDS, XRD, TEM, and DLS-ELS analyses showed that large nanoparticle aggregates form in the absence of stabilizers, while the introduction of biopolymers leads to the formation of less agglomerated composite structures. When stabilized with CS, the nanocomposites have an average size of 10 nm and an ordered crystal structure (XRD), 20.03 nm (TEM), and 127 nm (DLS), indicating its effectiveness compared to Na-CMC. The resulting iron-based nanocomposites with biopolymers hold promise for practical applications in environmental monitoring and cleanup, biomedical technologies (diagnostics, delivery of biologically active substances), and agriculture (targeted delivery of microelements and increasing the bioavailability of iron for plants and microorganisms).

Funding: This research was funded by the Science Committee of the Ministry of Science and Higher Education of the Republic of Kazakhstan (Grant No. AP23488216).

Conflict of Interest: All authors declare that they have no conflict of interest.

НАТРИЙ БОРОГИДРИДІМЕН ХИМИЯЛЫҚ ТОТЫҚСЫЗДАНУ ПРОЦЕСІНДЕ БИОПОЛИМЕРЛЕРДІҢ КӨМЕГІМЕН ТЕМІР НАНОБӨЛШЕКТЕРІН ТҰРАҚТАНДЫРУ

Ж.Ж. Нуртазина [1], Ж.С. Касымова [1*], Л.К. Оразжанова [1], Б. Леска [2]

[1]Шәкәрім университеті, Семей, Қазақстан
[2]Адам Мицкевич атындағы университет, Познань, Польша

Түйіндеме. *Кіріспе*. FeNPs түзілуі және агломерациясы процестерін реттеудің тиімді тәсілдерінің бірі - биополимер тұрақтандырғыштарын қолдану. *Зерттеудің мақсаты мен міндеттері*. $NaBH_4$ химиялық тотықсыздануымен алынған FeNPs морфологиялық, құрылымдық және кристалдық сипаттамаларына биополимерлерімен тұрақтандырудың әсерін анықтау болды. *Зерттеу әдістері*. Fe^{3+} иондарын натрий борогидридімен химиялық тотықсыздандыру және кейіннен хитозан және натрийкарбоксиметилцеллюлоза биополимерлерімен тұрақтандыру арқылы FeNPs синтезделді. Оптикалық қасиеттер УК-көрінетін спектрофотометрия арқылы зерттелді, функционалды топтарды анықтау үшін FTIR спектроскопиясы, морфология мен элементтік құрамын зерттеу үшін SEM/EDS және TEM, кристалдық фазаларды анықтау үшін рентгендік талдау және гидродинамикалық диаметр мен ζ-потенциалды бағалау үшін DLS/ELS қолданылды. *Нәтижелер мен талқылау.* UV-Vis спектрлері құрамында темір бар наноқұрылымдарға сәйкес келетін 260-300 нм аймақта тән сіңіру жолағын анықтады. FTIR талдауы нанобөлшектердің бетімен әрекеттесуге қатысатын Fe-O байланыстары мен биополимерлердің функционалдық топтарының болуын растады. SEM талдауы тұрақтандырғышсыз FeNPs ірі агломераттар түзетінін көрсетті, ал биополимерлерді енгізу аз айқын агрегациясы бар нанокомпозиттік құрылымдардың пайда болуына әкеледі. EDS талдау Fe және O элементтерінің болуын, сондай-ақ оксид/гидроксид фазасының түзілуін растады. XRD мәліметтері бойынша темір оксидтерінің кристалдық фазаларының түзілуі анықталды. Кристаллиттердің орташа мөлшері тұрақтандырғышсыз үлгі үшін шамамен 18 нм, FeNPs/Na-CMC үшін 14 нм және FeNPs/CS үшін 10 нм болды. TEM және DLS/ELS әдістері өлшемі 20,03±3,62 нм және ζ-потенциалы -30,6 мВ болатын сфералық FeNPs /CS нанобөлшектерінің түзілуін растады. *Қорытынды*. Биополимер тұрақтандырғыштары борогидридті тотықсыздандыру кезінде FeNPs өсуін және агрегациясын төмендететіні анықталды. CS кристаллиттің өсуін шектеудің және агломерацияны басудың ең тиімді әдісін қамтамасыз етеді, ал Na-CMC құрылымдық тұрғыдан ұйымдастырылған композиттік бөлшектердің түзілуіне ықпал етеді. Алынған нәтижелер темір бар наноматериалдарды тұрақтандыру үшін биополимерлерді қолданудың перспективтілігін көрсетеді.

Түйін сөздер: темір нанобөлшектері, биополимерлер, натрий карбоксиметилцеллюлоза, хитозан, натрий борогидридінің тотықсыздануы

Нуртазина Жанар Журсиновна	*Экология магистрі*
Касымова Жанар Сайлаубековна	*Биология ғылымдарының кандидаты*
Оразжанова Лаззят Каметаевна	*Химия ғылымдарының кандидаты*
Леска Богуслава	*Химия ғылымдарының докторы*

СТАБИЛИЗАЦИЯ НАНОЧАСТИЦ ЖЕЛЕЗА БИОПОЛИМЕРАМИ В ПРОЦЕССЕ ХИМИЧЕСКОГО ВОССТАНОВЛЕНИЯ БОРОГИДРИДОМ НАТРИЯ

Ж.Ж. Нуртазина[1], Ж.С. Касымова[1*], Л.К. Оразжанова[1], Б. Леска[2]

[1]Университет Шакарима, Семей, Казахстан
[2]Университет имени Адама Мицкевича, Познань, Польша

Резюме. *Введение*. Одним из эффективных способов регулирования процессами формирования и агломерации FeNPs является использование биополимерных стабилизаторов. *Цель работы*. Исследование влияния биополимерной стабилизации на размер, морфологические и кристаллические характеристики FeNPs, полученных методом химического восстановления $NaBH_4$. *Методы исследования*. FeNPs синтезировали методом химического восстановления Fe^{3+} ионов $NaBH_4$ с последующей стабилизацией хитозаном и натрийкарбоксиметилцеллюлозой. Оптические свойства изучались с помощью УФ-видимой спектрофотометрии, использовались FTIR-спектроскопия для идентификации функциональных групп, SEM/EDS и TEM для исследования морфологии и элементного состава, рентгенодифракционного анализа для определения кристаллических фаз и DLS/ELS для оценки гидродинамического диаметра и ζ-потенциала. *Результаты и обсуждение*. UV-Vis спектры выявили характерную полосу поглощения в области 260-300 нм, соответствующую железосодержащим наноструктурам. FTIR-анализ подтвердил наличие связей Fe-O и функциональных групп биополимеров, участвующих во взаимодействии с поверхностью наночастиц. SEM-анализ показал, что FeNPs без стабилизаторов образуют крупные агломераты, тогда как введение биополимеров приводит к формированию нанокомпозитных структур с менее выраженной агрегацией. EDS анализ подтвердил наличие элементов Fe и O, а также образование оксидной/гидроксидной фазы. По данным XRD установлено образование кристаллических фаз оксидов железа. Средний размер кристаллитов составил около 18 нм для образца без стабилизаторов, 14 нм для FeNPs/Na-CMC и 10 нм для FeNPs/CS. Методы TEM и DLS/ELS подтвердили образование сферических наночастиц FeNP/CS размером 20,03±3,62 нм и дзета-потенциалом -30,6 мВ. *Заключение*. Установлено, что биополимерные стабилизаторы уменьшают рост и агрегацию FeNPs при боргидридном восстановлении. CS обеспечивает наиболее эффективное ограничение роста кристаллитов и подавление агломерации, тогда как Na-CMC способствует формированию более структурно организованных композитных частиц. Полученные результаты демонстрируют перспективность применения биополимеров для стабилизации железосодержащих наноматериалов.

Ключевые слова: наночастицы железа, биополимеры, натрийкарбоксиметилцеллюлоза, хитозан, восстановление борогидридом натрия

Нуртазина Жанар Журсиновна	*Магистр экологии*
Касымова Жанар Сайлаубековна	*Кандидат биологических наук*
Оразжанова Лаззят Каметаевна	*Кандидат химических наук*
Леска Богуслава	*Доктор химических наук*

References

1. Bibi M., Zhu X., Munir M., Angelidaki I. Bioavailability and effect of α-Fe_2O_3 nanoparticles on growth, fatty acid composition and morphological indices of Chlorella vulgaris. *Chemosphere*. **2021**, 282, 131044. DOI: 10.1016/j.chemosphere.2021.131044

2. Vargas-Estrada, L., Domínguez-Espíndola, R.B., Sebastian, P.J. The Influence of Fe_2O_3 Nanoparticles on Chlorella spp. Growth and Biochemicals Accumulation. *Waste Biomass Valor*. **2024**, 15, 3281-3295. DOI: 10.1007/s12649-023-02378-z

3. Sudirman, Lubis, W.Z., Mujamilah, Sulungbudi, G.Tj., Rahmayani, N. Synthesis and characterization of magnetic nanoparticles Fe/Fe oxide of sodium borohydride reduction results within chitosan hydrogel. *Presented at the 4TH International Seminar on Chemistry, Surabaya, Indonesia*, 2021, 020005. DOI: 10.1063/5.0051848

4. Nkosi N.C., Basson A.K., Ntombela Z.G., Dlamini N.G., Pullabhotla R.V.S.R. Green synthesis and characterization of iron nanoparticles synthesized from bioflocculant for wastewater treatment: A review. *Biotechnology Reports*. **2024**. DOI: 10.1016/j.biotno.2024.12.001

5. Huyen N.T.T., Nhung N.H., Thanh L., Khanh P.D., Lam T.D., Son H.A. Preparation and characterization of zerovalent iron nanoparticles. *Vietnam Journal of Chemistry*. **2018**, 56, 2, 226-230. DOI: 10.1002/vjch.201800018

6. Dong H., Zhao F., Zeng G., Tang L., Fan C., Zhang L., Zeng Y., He Q., Xie Y., Wu Y. Aging study on carboxymethyl cellulose-coated zero-valent iron nanoparticles in water: Chemical transformation and structural evolution. *Journal of Hazardous Materials*. **2016**, 312, 234–242. DOI: 10.1016/j.jhazmat.2016.03.069

7. Huang D., Ren Z., Li X., Jing Q. Mechanism of Stability and Transport of Chitosan-Stabilized Nano Zero-Valent Iron in Saturated Porous Media. *International Journal of Environmental Research and Public Health*. **2021**, 18, 10, 5115. DOI: 10.3390/ijerph18105115

8. Jin X., Zhuang Z., Yu B., Chen Zhengxian, Chen Zuliang. Functional chitosan-stabilized nanoscale zero-valent iron used to remove acid fuchsine with the assistance of ultrasound. *Carbohydrate Polymers*. **2016**, 136, 1085-1090. DOI: 10.1016/j.carbpol.2015.10.002

9. Klivenko A., Orazzhanova L., Mussabayeva B., Yelemessova G., Kassymova Z. Soil structuring using interpolyelectrolyte complexes of water-soluble polysaccharides. *Polymers for Advanced Technologies*. **2020**, 31, 3292–3301. DOI: 10.1002/pat.5053

10. Eljamal R., Eljamal O., Maamoun I., Yilmaz G., Sugihara Y. Enhancing the characteristics and reactivity of nZVI: Polymers effect and mechanisms. *Journal of Molecular Liquids.* **2020**, 315,113714. DOI: /10.1016/j.molliq.2020.113714

Chemical Journal of Kazakhstan
Volume 2, Number 94(2026), 40-50 https://doi.org/10.51580/2026-2.2710-1185.12

UDC 665.668

REGENERATION AND CATALYTIC PERFORMANCE OF NI-MO-AL-HMS-H-BENTONITE CATALYST IN HYDROGENATION OF AROMATIC HYDROCARBONS

A. Abdrassilova[1,2*], G. Vassilina[3], K. Abdildina[4]

[1]Institute of Combustion Problems, Almaty, Kazakhstan
[2]Kazakh-British Technical University, Almaty, Kazakhstan
[3]Almaty Technological University, Almaty, Kazakhstan
[4]Al-Farabi Kazakh National University, Almaty, Kazakhstan

[*]Corresponding author e-mail: albina06.07@mail.ru

Abstract. *Introduction.* The physico-chemical and catalytic properties of the bifunctional catalyst Ni-Mo-Al-HMS-H-bentonite were investigated in the hydrogenation of a model mixture of 2-methylnaphthalene and dibenzothiophene. *This study aimed to* compare the properties of fresh and regenerated catalysts and evaluate their efficiency in this reaction. *Results and discussion.* Catalyst physico-chemical parameters were analyzed by X-ray photoelectron spectroscopy, temperature-programmed hydrogen reduction, nitrogen adsorption-desorption analysis and thermogravimetric analysis. It was established that nickel and molybdenum are mainly present on the catalyst surface in oxide and sulfide forms that determine its catalytic activity. Textural analysis showed that the catalyst possesses a well-developed mesoporous structure with a monomodal distribution of pore sizes. After the catalytic reaction and regeneration, a decline in the textural characteristics were evaluated. Catalytic tests were carried out at 260°C, hydrogen pressure of 6 MPa and reaction time of 5 hours. The fresh catalyst maintained stable activity for four reaction cycles, while the regenerated catalyst demonstrated high efficiency for three subsequent cycles. *Conclusion.* The obtained results confirm the potential application of the Ni-Mo-Al-HMS-H-bentonite catalyst in hydrogenation processes of aromatic and sulfur-containing compounds.

Key words: mesoporous aluminosilicate, activated bentonite, bifunctional catalyst, Ni-Mo, model mixture

Albina Abdrassilova	*PhD; E-mail: albina06.07@mail.ru*
Gulzira Vassilina	*Candidate of Chemical Sciences; E-mail: vasilina.g@atu.edu.kz*
Kamilla Abdildina	*PhD; E-mail: kamilla.u.m21@mail.ru*

Citation: Abdrassilova A., Vassilina G., Abdildina K. Regeneration and catalytic performance of Ni-Mo-Al-HMS-H-Bentonite catalyst in hydrogenation of aromatic hydrocarbons. *Chem. J. Kaz.*, **2026**, 2*(94)*, 40-50. DOI: https://doi.org/10.51580/2026-2.2710-1185.12

1. Introduction

A substantial reduction in sulfur and aromatic compounds in petroleum products has become necessary due to the tightening of environmental standards for motor fuel quality. Sulfur-containing compounds, such as dibenzothiophene and its derivatives, produce sulfur oxides during combustion and must be removed from petroleum fuels. Therefore, the removal of these compounds is of considerable importance in contemporary petroleum refining [1]. Nowadays hydrodesulfurization is the most widely employed and effective industrial method for sulfur removal from petroleum fractions. This process is based on the catalytic hydrogenation of sulfur-containing compounds, followed by cleavage of the C-S bond [2,3].

The most widely used hydrodesulfurization catalysts are Ni-Mo and Co-Mo systems supported on oxide or aluminosilicate carriers. The high catalytic activity of these systems is attributed to the formation of an active Ni-Mo-S sulfide phase. This phase promotes both the hydrogenation of aromatic compounds and the cleavage of C-S bonds in sulfur-containing molecules [4]. Activity and selectivity of such catalysts strongly depend on the structure of the active phase, the metal particle dispersion and the characteristics of metal-support interactions [5,6].

The use of mesoporous aluminosilicate materials as supports for hydrotreating catalysts has generated particular interest. Such materials are notable for their large surface area, highly developed porosity, and the ability to tune surface acidity. These properties enable high dispersion of active metal components and facilitate reactant access to the catalytic sites [7].

Despite extensive studies on Ni-Mo catalysts, their stability and regeneration under hydrogenation and hydrodesulfurization conditions remain relevant. During operation, catalysts may undergo deactivation due to coke formation, agglomeration of active particles, and changes in the textural characteristics of the support [8]. In this regard, the comparative study of fresh and regenerated catalysts remains of considerable interest. It provides insight into the effect of the catalytic process on catalyst structure.

This work focuses on investigating the physico-chemical and catalytic properties of fresh and regenerated Ni-Mo-Al-HMS-H-bentonite catalysts in the hydrogenation of a model mixture of 2-methylnaphthalene and dibenzothiophene. Dibenzothiophene was selected as a representative sulfur compound, since middle distillates mainly contain its alkylated derivatives [9]. The novelty of this work lies in the use of a combined Al-HMS-H-bentonite support containing activated bentonite from the Tagan deposit. This approach contributes to the development of catalytic materials based on Kazakhstan's significant bentonite resources. Particular attention is devoted to the state of active metal sites, the textural characteristics of the catalysts, and the evaluation of their catalytic activity, as well as to the effect of the regeneration process on the performance of the catalytic system.

2. Experimental part

Al-HMS mesoporous aluminosilicate with a Si/Al = 10 was obtained by a templating method using hexadecylamine. Tetraethyl orthosilicate and aluminum sec-butoxide were used as the sources of Si and Al, respectively. The resulting precipitate was separated by centrifugation, dried, and subjected to thermal treatment.

The catalysts synthesized by incipient wetness impregnation of the Al-HMS-H-bentonite support with aqueous solutions of $Ni(NO_3)_2 \cdot 6H_2O$ and $(NH_4)_6Mo_7O_{24} \cdot 4H_2O$, where activated bentonite was used as a secondary support. The obtained catalysts contained 5 wt.% Ni and 5 wt.% Mo. After mixing the solutions with the support, the samples were dried and subjected to thermal treatment.

The state of the metal centers in the catalysts was investigated by X-ray photoelectron spectroscopy (XPS) using a Nexsa G2 spectrometer (Thermo Scientific) and by hydrogen temperature-programmed reduction (H_2-TPR) by a Micromeritics AutoChem 2910 system. The textural characteristics of the synthesized samples were determined from nitrogen adsorption-desorption isotherms at 77 K using a Micromeritics TriStar 3000 analyzer. The specific surface area was calculated by the Brunauer-Emmett-Teller (BET) method, while the total pore volume and pore size distribution were determined using the Barrett-Joyner-Halenda (BJH) method. Thermogravimetric analysis (TGA) of the bifunctional catalysts was carried out using a Mettler Toledo TGA/SDTA 851e instrument in an air atmosphere over a temperature range of 30-1000°C with a heating rate of 10°C/min.

The hydrogenation of aromatic compounds was studied using a model mixture. The mixture contained 9 wt.% 2-methylnaphthalene, 300 ppm dibenzothiophene (DBT), and 91 wt.% n-hexadecane. Before the experiments, the catalysts were activated in a flow reactor at 400°C in a H_2S/H_2 stream (10 vol %) for 5 hours with a heating rate of 4°C/min. After the hydrogenation reaction, the catalyst was regenerated in a muffle furnace in an air flow at 500°C for 5 hours with a heating rate of 3°C /min. The reaction was carried out in a high-pressure reactor at 260°C for 5 hours under a hydrogen pressure of 6 MPa. After the reaction, the products were examined using gas chromatography-mass spectrometry.

3. Results and discussion

The state of the active metal centers in the Ni-Mo-Al-HMS-H-bentonite catalyst was analyzed by XPS (Figure 1).

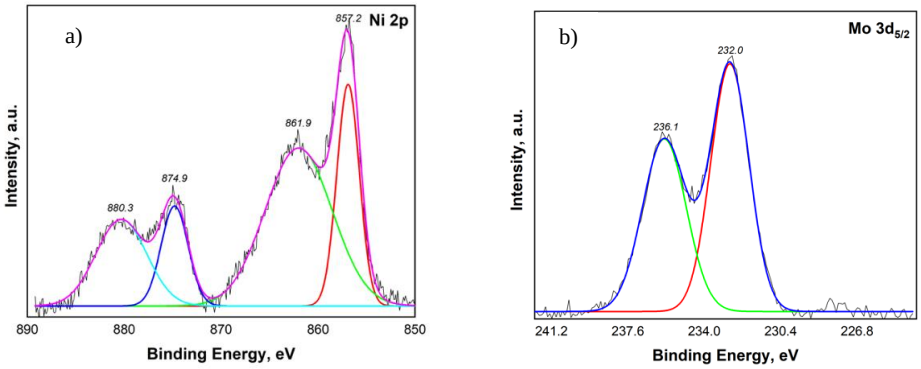

Figure 1 – XPS profiles corresponding to Ni 2p (a) and Mo 3d (b) for the bifunctional Ni-Mo-Al-HMS-H-bentonite catalyst

Analysis of the Ni 2p spectrum reveals the presence of two spin–orbit doublets (Figure 1a). The main Ni $2p_3/_2$ peak is observed at 857.2 eV with a satellite peak at 861.9 eV, while the Ni $2p_1/_2$ peak is located at 874.9 eV with a satellite signal at approximately 880.3 eV. The Ni $2p_3/_2$ peak corresponds to nickel oxide (NiO), indicating the presence of nickel in the oxidized Ni^{2+} state [10]. The presence of characteristic satellite peaks further confirms the oxide form of nickel.

The Mo 3d signals are displayed in Figure 1b. The obtained spectra exhibit two main peaks corresponding to the Mo^{4+} and Mo^{6+} oxidation states. The signals observed at binding energies around 232.0 eV and 236.1 eV are identified as MoS_2 and MoO_3 species, respectively [11]. This indicates the presence of molybdenum in both sulfide and oxide forms in the catalyst.

Metal-support interactions were investigated by H_2-TPR. The H_2-TPR curve of the Ni-Mo-Al-HMS-H-bentonite catalyst illustrates three peaks associated with different stages of reduction of the metal phases (Figure 2).

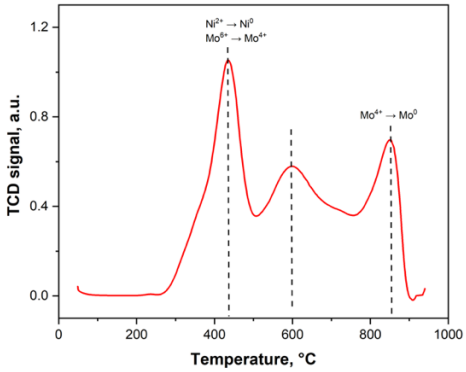

Figure 2 – H_2-TPR curve of the Ni-Mo-Al-HMS-H-bentonite catalyst

In Figure 2, the peak around 435°C is attributed with the reduction of NiO and MoO_3 oxides exhibiting high reducibility, corresponding to the transformation of Ni^{2+} to Ni^0 and Mo^{6+} to Mo^{4+} [12]. The peak at 600°C is associated with stronger metal-support interactions, indicating enhanced stability of the metal phases. A high-temperature peak at around 852°C is associated with the reduction of hardly reducible molybdenum species. It may correspond to the transformation of Mo^{4+} to Mo^0. The presence of this peak indicates the high thermal stability of the catalyst. Further, to evaluate the effect of the hydrogenation of aromatic compounds on the physico-chemical properties of the catalyst, a comparison of fresh and regenerated Ni-Mo-Al-HMS-H-bentonite samples was performed.

The catalyst's textural characteristics were studied by analyzing the BET surface area, pore volume, and average pore diameter. These parameters play an important role in the formation of active sites and the accessibility of reactants to the catalyst surface. The obtained results are presented in Figures 3 and 4.

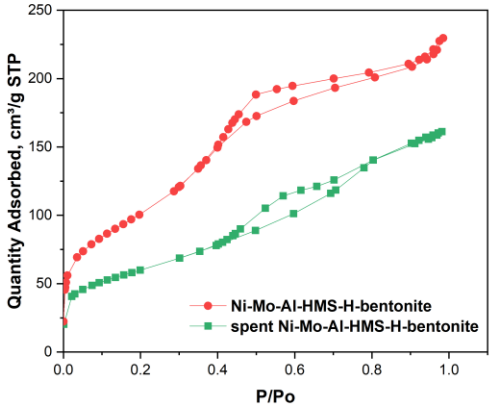

Figure 3 – N_2 physisorption isotherms of fresh and regenerated catalysts

An analysis of the textural characteristics of the Ni-Mo-Al-HMS-H-bentonite system was conducted using nitrogen physisorption. As shown in Figure 3, both fresh and regenerated samples exhibit type IV adsorption-desorption isotherms according to the IUPAC classification. The distinct H4 hysteresis loop observed for these materials serves as evidence of their mesoporous nature. The steep rise in adsorption within the 0.4-0.8 P/P_0 region can be attributed to the filling of mesopores via capillary condensation [13]. A comparative analysis reveals that the regenerated catalyst shows a significant decline in nitrogen uptake relative to its fresh counterpart. This reduction points to a partial degradation of the porous structure or a loss of surface area, likely resulting from the harsh conditions of the catalytic reaction.

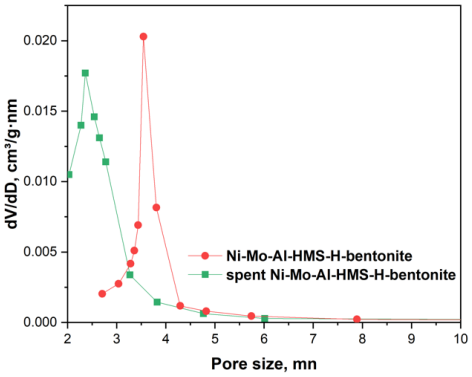

Figure 4 – Pore size profiles of fresh and regenerated catalytic materials

Figure 4 shows the pore size profiles of fresh and regenerated Ni-Mo-Al-HMS-H-bentonite catalysts. The distribution is monomodal and lies within the mesopore region (Figure 4). The fresh catalyst is characterized by a maximum at 3.46 nm, whereas the regenerated sample exhibits a shift of the maximum toward smaller pore sizes, 2.36 nm, along with a decrease in peak intensity (Table 1).

Table 1 – Textural characteristics of fresh and regenerated Ni-Mo-Al-HMS-H-bentonite catalyst

Ni-Mo-Al-HMS-H-bentonite	Specific surface area (BET), m^2/g	Pore volume, cm^3/g	Average pore diameter, nm
Fresh	805	0.74	3.46
Regenerated	675	0.67	2.36

After regeneration, the BET of the catalyst decreases from 805 to 675 m^2/g, while the pore volume decreases from 0.74 to 0.67 cm^3/g (Table 1). The reduction in textural characteristics after regeneration is likely associated with partial pore clogging by carbonaceous deposits formed during the catalytic reaction [2].

The TGA curves of fresh and regenerated Ni-Mo-Al-HMS-H-bentonite catalysts show a decomposition of the sample with rising temperature. The primary decomposition step is observed from 200 to 600°C and is associated with the removal of adsorbed moisture, residual organic compounds, and the decomposition of surface functional groups (Figure 5).

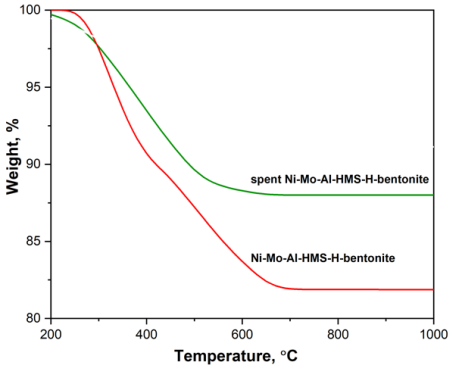

Figure 5 – TGA curves of fresh and regenerated Ni-Mo-Al-HMS-H-bentonite catalysts

As shown in Figure 5, the fresh catalyst demonstrates a more weight loss compared to the regenerated sample. This may be attributed to the presence of a larger amount of surface species and residual organic compounds, whereas the regenerated catalyst demonstrates higher thermal stability [14].

The results of the study on the effect of sulfur-containing compounds on catalyst performance are presented in Figure 6 and Table 2. The catalytic performance was evaluated in the hydrogenation of a model mixture of 2-methylnaphthalene and dibenzothiophene at T = 260°C, $P(H_2)$ = 6 MPa, and a reaction time of 5 hours. The catalyst stability was examined over four consecutive cycles. It was found that after regeneration, the catalyst retains high activity for up to three cycles.

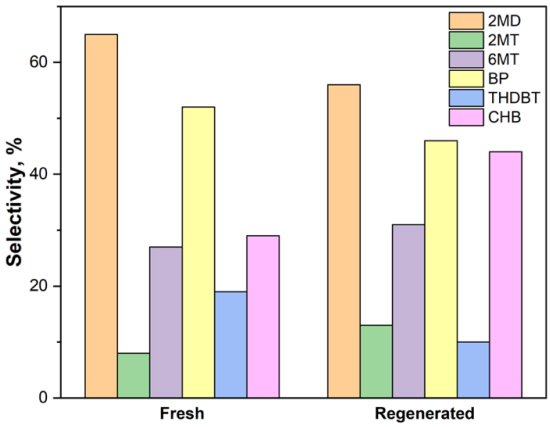

Figure 6 – Selectivity of hydrogenation products of a sulfur-containing model compound over fresh and regenerated Ni-Mo-Al-HMS-H-bentonite catalyst

Table 2 – Comparison of the performance of fresh and regenerated Ni-Mo-Al-HMS-H-bentonite catalysts in the hydrogenation of a model mixture of 2MD and DBT

Ni-Mo-Al-HMS-H-bentonite	Conversion, %		Selectivity, %					
	2MN	DBT	**2MD**	2MT	6MT	**BP**	THDBT	CHB
Fresh	92	76	**68**	8	27	**52**	19	29
Regenerated	86	61	**56**	13	31	**46**	10	44

*Note:
2MN: 2-methylnaphthalene;
DBT: dibenzothiophene;
2MD: 2-methyldecalin;
2MT and 6MT are 2-methyltetralin and 6-methyltetralin, respectively;
BP: biphenyl;
THDBT: tetrahydrodibenzothiophene;
CHB: cyclohexylbenzene.

The target products of hydrogenation are 2-methyldecalins and biphenyl. A comparison of fresh and regenerated catalysts revealed a decrease in both conversion and selectivity toward the target products after regeneration. The conversion of 2-methylnaphthalene decreases from 92 to 86%, while the conversion of dibenzothiophene decreases from 76 to 61%. At the same time, the selectivity toward 2-methyldecalins decreases from 65 to 56%, and the selectivity toward biphenyl in the hydrodesulfurization of dibenzothiophene decreases from 52 to 46%. Furthermore, the fresh catalyst yielded 63% 2-methyldecalin and 40% biphenyl. The corresponding values for the regenerated catalyst were 48% and 28%, respectively. The reduction in conversion and selectivity after regeneration may be attributed to partial changes in the state of active metal centers and a decrease in the catalyst textural characteristics. In addition, interaction of sulfur-containing compounds with active metal sites may lead to a decrease in their accessibility [15].

4. Conclusion

The physico-chemical and catalytic properties of fresh and regenerated Ni-Mo-Al-HMS-H-bentonite catalysts were investigated. Their performance was evaluated in the hydrogenation of a model mixture of 2-methylnaphthalene and dibenzothiophene. It was shown that the catalyst possesses a well-developed mesoporous structure and high catalytic activity. It was established that the catalyst maintains stability over four reaction cycles and, after regeneration, demonstrates high performance over three subsequent cycles. The obtained results confirm the potential of this catalyst for application in the hydrogenation of aromatic and sulfur-containing compounds.

Funding: This research was funded by the Science Committee of the Ministry of Science and Higher Education of the Republic of Kazakhstan (Grant No. AP32724827).

Conflict of Interest: The authors declare no conflict of interest.

РЕГЕНЕРАЦИЯ И КАТАЛИТИЧЕСКАЯ АКТИВНОСТЬ NI-MO-AL-HMS-H-БЕНТОНИТ КАТАЛИЗАТОРА В ПРОЦЕССЕ ГИДРИРОВАНИЯ АРОМАТИЧЕСКИХ УГЛЕВОДОРОДОВ

А.К. Абдрасилова[1,2*], Г.К. Василина[3], К.М. Абдильдина[4]

[1]Институт проблем горения, Алматы, Казахстан
[2]Казахстанско-Британский технический университет, Алматы, Казахстан
[3]Алматинский технологический университет, Алматы, Казахстан
[4]Казахский национальный университет им. аль-Фараби, Алматы, Казахстан

Резюме: *Введение.* Физико-химические и каталитические свойства бифункционального катализатора Ni-Mo-Al-HMS-H-бентонит были исследованы в реакции гидрирования модельной смеси 2-метилнафталина и дибензотиофена. *Целью данного исследования* являлось сравнение свойств свежего и регенерированного катализаторов, а также оценка их эффективности в данной реакции. *Результаты и обсуждение.* Физико-химические характеристики катализаторов были изучены с использованием рентгенофотоэлектронной спектроскопии, температурно-программированного восстановления водородом, анализа адсорбции-десорбции азота и термогравиметрического анализа. Установлено, что никель и молибден преимущественно присутствуют на поверхности катализатора в оксидной и сульфидной формах, которые определяют его каталитическую активность. Текстурный анализ показал, что катализатор обладает хорошо развитой мезопористой структурой с мономодальным распределением пор. После каталитической реакции и регенерации было отмечено снижение текстурных свойств. Каталитические испытания проводились при температуре 260°C, давлении водорода 6 МПа и времени реакции 5 часов. Свежий катализатор сохранял стабильную активность в течение четырех реакционных циклов, тогда как регенерированный катализатор демонстрировал высокую эффективность в течение трех последующих циклов. *Заключение.* Полученные результаты подтверждают перспективность применения катализатора Ni-Mo-Al-HMS-H-бентонит в процессах гидрирования ароматических и серосодержащих соединений.

Ключевые слова: мезопористый алюмосиликат, активированный бентонит, бифункциональный катализатор, Ni-Mo, модельная смесь

Абдрасилова Альбина Канатовна	*PhD*
Василина Гулзира Кажмуратовна	*Кандидат химических наук*
Абдильдина Камилла Манапқызы	*PhD*

NI-MO-AL-HMS–H-БЕНТОНИТ НЕГІЗІНДЕГІ КАТАЛИЗАТОРДЫҢ АРОМАТТЫ КӨМІРСУТЕКТЕРДІ ГИДРЛЕУ ПРОЦЕСІНДЕГІ РЕГЕНЕРАЦИЯСЫ ЖӘНЕ КАТАЛИТИКАЛЫҚ БЕЛСЕНДІЛІГІ

А.К. Абдрасилова[1,2*], Г.К. Василина[3], К.М. Абдильдина[4]

[1]Жану проблемалары институты, Алматы, Қазақстан
[2]Қазақстан-Британ техникалық университеті, Алматы, Қазақстан
[3]Алматы технологиялық университеті, Алматы, Қазақстан
[4]әл-Фараби ат. Қазақ ұлттық университеті, Алматы, Қазақстан

Түйіндеме. *Кіріспе.* Ni-Mo-Al-HMS-H-бентонит бифункционалды катализаторының физика-химиялық және каталитикалық қасиеттері 2-метилнафталин мен дибензотиофеннің модельді қоспасын гидрлеу реакциясында зерттелді. *Зерттеудің мақсаты* жаңа және регенерацияланған катализаторлардың қасиеттерін салыстыру, сондай-ақ олардың осы реакциядағы эффективтілігін бағалау болды. *Нәтижелер және талқылау.* Катализаторлардың физика-химиялық сипаттамалары

рентгенофотоэлектрондық спектроскопия, сутек температуралық бағдарламаланған сутегімен тотықсыздану, азоттың адсорбция-десорбция әдісі және термогравиметриялық талдау арқылы зерттелді. Зерттеу нәтижесінде катализатордың активтілігін анықтайтын никель мен молибден оның бетінде негізінен оксидті және сульфидті күйде болатыны анықталды. Текстуралық талдау катализатордың жақсы дамыған мезокеуекті құрылымға ие екенін және кеуектердің мономодальды таралуымен сипатталатынын көрсетті. Каталитикалық реакция мен регенерациядан кейін текстуралық қасиеттердің төмендеуі байқалды. Каталитикалық сынақтар 260°C температурада, 6 МПа сутек қысымында және 5 сағат реакция уақыты жағдайында жүргізілді. Жаңа катализатор төрт реакциялық цикл бойы тұрақтығын сақтаса, регенерацияланған катализатор кейінгі үш циклде жоғары тұрақтылық көрсетті. *Қорытынды*. Алынған нәтижелер Ni-Mo-Al-HMS-H-бентонит катализаторының ароматты және күкіртқұрамды қосылыстарды гидрлеу процестерінде қолдану мүмкіндігінің жоғары екенін дәлелдейді.

Түйін сөздер: мезокеуекті алюмосиликат, активтендірілген бентонит, бифункционалды катализатор, Ni-Mo, модельді қоспа

Абдрасилова Альбина Канатовна	*PhD*
Василина Гулзира Кажмуратовна	*Химия ғылымдарының кандидаты*
Абдильдина Камилла Манапқызы	*PhD*

References

1. Shi Y., Wang G., Mei J., Xiao C., Hu D., Wang A., Song Y., Ni Y., Jiang G., Duan A. The Influence of Pore Structure and Acidity on the Hydrodesulfurization of Dibenzothiophene over NiMo-Supported Catalysts. *ACS Omega*. **2020**, 5, 15576-15585. DOI: 10.1021/acsomega.0c01783

2. Li M., Ihli J., Verheijen M.A., Holler M., Guizar-Sicairos M., van Bokhoven J.A., Hensen E.J.M., Weber T. Alumina-Supported NiMo Hydrotreating Catalysts – Aspects of 3D Structure, Synthesis, and Activity. *J. Phys. Chem. C*. **2022**, 126, 18536-18549. DOI: 10.1021/acs.jpcc.2c05927

3. Yang C., Hu A., Dai Q., Yang Q., Hou R., Liu Z. Study on the Performance of Ni–MoS_2 Catalysts with Different MoS_2 Structures for Dibenzothiophene Hydrodesulfurization. *ACS Omega*. **2023**, 8, 41182-41193. DOI: 10.1021/acsomega.3c04059

4. Arora S., Sivakumar S. Unblocking of NiMo Active Sites for Hydrodesulfurization Catalysts: A Study Focused on Inactive Ni_xS_y Segregation. *Energy & Fuels*. **2023**, 37, 8539-8551. DOI: 10.1021/acs.energyfuels.3c00893

5. He W., Xiang Y., Xin M., Zhai W., Qiao S., Zhang N., Qiu L., Yan S., Liu F., Wang J., Xu G., Liu J., Li M. Insight into metal-support interactions of NiMo hydrodesulfurization catalysts and their variations during application. *J. Chem. Eng*. **2025**, 525, 170627. DOI: 10.1016/j.cej.2025.170627

6. Yuan M., Zheng Zh., Yu Y., Wang Y., Wang W., Li Q., Li X., Zhao D., Topology-enhanced oil adsorption by flower-like mesoporous silica nanoparticles for advanced cosmetic oil control. *RSC Adv*. **2026**, 16, 6865-6875. DOI: 10.1039/D5RA08525J

7. Contreras J.R., Cuevas García R., Fabila Bustos D.A., Puente Lee I., Hernández Chávez M. Solvothermal Synthesis of Unsupported NiMo Catalyst with High Activity in Hydrodesulfurization of 4,6-Dimethyldibenzothiophene. *Crystals*. **2025**, 15, 245. DOI: 10.3390/cryst15030245

8. Puello-Polo E., Betancourt P., Méndez F.J. Enhanced hydrotreating performance of hierarchical NiMo-S/Al_2O_3 catalysts through ZrO_2 incorporation and template-driven structural modulation. *Catal. Today*. **2025**, 443, 114973. DOI: 10.1016/j.cattod.2024.114973

9. Méndez F.J., Franco-López O.E., Díaz G., Gómez-Cortés A., Bokhimi X., Klimova T.E. On the role of niobium in nanostructured Mo/Nb-MCM-41 and NiMo/Nb-MCM-41 catalysts for hydrodesulfurization of dibenzothiophene. *Fuel*. **2020**, 280, 118550. DOI: 10.1016/j.fuel.2020.118550

10. Al-Kuhaili M.F., Ahmad S.H.A., Durrani S.M.A., Faiz M.M., Ul-Hamid A. Application of nickel oxide thin films in NiO/Ag multilayer energy-efficient coatings. *Mater. Sci. Semicond. Process*. **2015**, 39, 84-89. DOI: 10.1016/j.mssp.2015.04.049

11. Pan P., Zeng Q., Li X., Liu C., Zeng J., Liang T., Qi X. A Low-Cost Ni–Mo Electrocatalyst for Highly Efficient Hydrogen and Oxygen Evolution Reaction. *Energy Technol.* **2023**, 11, 2300118. DOI: 10.1002/ente.202300118

12. Jiang S., Ding S., Jiang Q., Zhou Y., Yuan S., Geng X., Yang G., Zhang C. Effects of Al introduction methods for Al-SBA-15 on NiMoS active phase morphology and hydrodesulfurization reaction selectivities. *Fuel*. **2022**, 330, 125493. DOI: 10.1016/j.fuel.2022.125493

13. Yoshimoto Y., Hori T., Kinefuchi I., Takagi S. Effect of capillary condensation on gas transport properties in porous media. *PRE*. **2017**, 96, 043112. DOI: 10.1103/PhysRevE.96.043112.

14. Chiranjeevi T., Kumaran G.M., Gupta J.K., Dhar G.M. Synthesis and characterization of acidic properties of Al-HMS materials of varying Si/Al ratios. *Thermochim. Acta*. **2006**, 443, 87-92. DOI: 10.1016/j.tca.2006.01.004

15. Huber P.P., Studt F., Plessow P.N. Reactivity of surface Lewis and Brønsted acid sites in zeolite catalysis: A computational case study of DME synthesis using H-SSZ-13. *JACS*. **2022**, 126, 5896-5905. DOI: 10.1021/acs.jpcc.2c00668

Chemical Journal of Kazakhstan
Volume 2, Number 94(2026), 51-63 https://doi.org/10.51580/2026-2.2710-1185.13

UDC 544.7

INFLUENCE OF CEFAZOLIN LOADING ON THE STRUCTURE AND INTERFACIAL ACTIVITY OF CHITOSAN-BASED NANOGELS

A.A. Sharipova[1]. A.B. Issayeva[1*], S.B. Aidarova[1,2], M. Lofti[3], A.B. Akbotin[1,2], U.B. Issayeva[4]

[1] Satbayev University, Almaty, Kazakhstan
[2] Kazakh-British Technical University, Almaty, Kazakhstan
[3]Jundi-Shapur university of Technology, Dezful, Iran
[4]A.B.Bekturov Institute of Chemical Sciences JSC, Almaty, Kazakhstan

[*]Corresponding author e-mail: isa-asem@mail.ru

Abstract: Chitosan-based nanogels are promising colloidal carriers for hydrophilic drugs de too their biocompatibility, adjustable physicochemical properties, and mild preparation conditions. In this study, cefazolin-loaded chitosan nanogels were prepared by ionic gelation using sodium tripolyphosphate (TPP) as a crosslinker. The effect of drug incorporation on the colloidal characteristics and interfacial behavior of the system was systematically evaluated. Freshly prepared blank and cefazolin-loaded nanogels showed hydrodynamic diameters of about 210 nm and 285 nm, respectively. Both systems exhibited positive zeta potential values above +25mV, indicating good electrostatic stability under acidic conditions. The encapsulation efficiency of cefazolin, determined by an indirect UV-Vis method, was 48 ± 6%, confirming effective drug entrapment within the crosslinked polymer network. After dialysis to remove low-weight impurities, purified dispersions were analyzed by dynamic surface tension measurements using the pendant drop method. Blank nanogels gradually adsorbed at the air-water interface, reducing surface tension from 71.8 to 67.4 mN/m ver time. In contrast, cefazoli-loaded nanogels exhibited slower adsorption kinetics and a smaller decrease in surface tension, reahing equilibrium values around 68.9mN/m.These differences are attributed to increased hydration and reduced mobility of chitosan chains after drug incorporation. Overall, cefazolin encapsulation significantly modified the interfacial adsorption behavior of chitosan nanogels while maintaining their colloidal stability. The results provide insight into structure-property relationships relevant to aqueous and topical drug delivery applications.

Kew words: chitosan nanogels, ionic gelation, cefazolin encapsulation, dynamic surface tension, interfacial adsorption, colloidal stability

Sharipova Altynay Azigarovna	*PhD, Research professor; E-mail: a_sharipova85@mail.ru*
Issayeva Assem Bakhytzhanovna	*PhD, Scientific researcher; E-mail: isa-asem@mail.ru,*
Aidarova Saule Baylyarovna	*Doctor of chemical sciences, professor; E-mail: ainano9999@gmail.com*
Lotfi Marzieh	*Assistant professor; E-mail: marzyeh.lotfi@gmail.com*
Akbotin Asylzhan Bolatbekovich	*PhD doctoral student; E-mail:asylzhan.akbotin@yahoo.com*
Issayeva Ulzhalgas Bakhytzhankyzy	*PhD, Scientific Researcher; E-mail: ulyano.iss@gmail.com*

Citation: Sharipova A.A., Issayeva A.B., Aidarova S.B., Lofti M., Akbotin A.B., Issayeva U.B. Influence of cefazolin loading on the structure and interfacial activity of chitosan-based nanogels. *Chem. J. Kaz.*, **2026**, 2*(94)*, 51-63. DOI: https://doi.org/10.51580/2026-2.2710-1185.13

1. Introduction

In recent years, chitosan-based nanostructured systems have attracted considerable attention as promising carriers for drug delivery applications due to their biodegradability, biocompatibility, mucoadhesive properties, and the presence of reactive amino groups capable of electrostatic interactions. Chitosan, a cationic polysaccharide derived from chitin, can readily form nanoscale gel networks via physical or ionic crosslinking mechanisms, enabling efficient encapsulation of hydrophilic therapeutic agents. [1]

Among various preparation techniques, ionic gelation has emerged as one of the most widely used methods for the fabrication of chitosan nanogels owing to its mild processing conditions and avoidance of toxic organic solvents [2,3]. This method relies on electrostatic interactions between protonated amino groups of chitosan and multivalent anions such as sodium tripolyphosphate (TPP), leading to spontaneous formation of three-dimensional hydrogel networks at the nanoscale. The resulting nanogels exhibit tunable physicochemical characteristics, including particle size, surface charge, and swelling behavior, which can be adjusted through formulation parameters such as polymer concentration, crosslinker ratio, and pH [4,5].

Encapsulation of hydrophilic drugs within polymeric nanogels remains challenging due to their tendency to partition into the aqueous phase during nanoparticle formation [6]. However, chitosan – TPP nanogels providea suitable matrix for physical entrapment of antibiotic molecules through a combination of electrostatic interactions, hydrogen bonding, and steric confinement within the crosslinked network [7].

Previous studies have demonstrated that loading of β – lactam antibiotics, including cefazolin, into chitosan-based carriers can influence both structural organization and colloidal stability of the resulting nanosystems. Drug incorporation may induce partial rearrangement of polymer chains, leading to increased hydrodynamic diameter and modification of surface charge due to screening of protonated amino groups. These structural changes are particularly important for applications involving aqueous or topical formulations, where interfacial properties strongly affect spreading behavior, adhesion and drug release kinetics [8].

Colloidal Stability and Electrostatic Interactions in Chitosan Nanogels

The colloidal stability of chitosan nanogels is governed primarily by electrostatic repulsion arising from positively charged amino groups on the polymer backbone. Zeta potential values exceeding +25 mV are generally considered sufficient to maintain nanoscale dispersion stability under acidic conditions. Nevertheless, incorporation of drug molecules or removal of low-melecular-weight species may significantly alter the ionic environment of the system and affect nanoparticle size distribution and surface charge [9].

Purification techniques such as dialysis are therefore frequently employed to eliminate residual acetic acid, unreacted crosslinker or non-encapsulated drug molecules. However, changes in ionic strength during purification may potentially

induce structural rearrangements or aggregation in weakly crosslinked hydrogel systems. For this reason, evaluation of nanogel properties before and after purification is essential for assessing preservation of native colloidal structure [10].

Interfacial Behavior of Polymeric Nanogels

Beyond bulk physicochemical properties, the interfacial behavior of polymeric nanogels plays a critical role in determining their performance in biomedical formulations. Unlike conventional molecular surfactants, nanogel systems exhibit time-dependent adsorption at fluid interfaces, governed by diffusion of nanoscale entities followed by conformational rearrangement of polymer segments [11].

Recent studies have shown that chitosan-based nanoparticles and nanogels may display moderate surface activity arising from partial exposure of hydrophobic polymer domains at the air-water interface. This interfacial adsorption can result in gradual reduction of surface tension over time, reflecting slow structural relaxation processes rather than instantaneous interfacial coverage [12].

Drug loading may further influence adsorption kinetics by increasing hydration of the polymer network and restricting chain mobility through intermolecular interactions. As a consequence, drug-loaded nonogels often exhibit reduced interfacial responsiveness compared to blank systems. Understanding these effects is particularly important for the rational design of aqueous and topical drug delivery platforms, where predictable spreading and formulation stability are required [13].

Based on the literature analysis presented above, it is evident that although chitosan-based nanogels have been extensively investigated as drug delivery systems, considerably less attention has been devoted to understanding how drug incorporation affects their interfacial behavior and adsorption kinetics. In particular, the relationship between drug loading, nanogel structural organization and dynamic surface activity remains insufficiently elucidated.

Therefore, the present study aims to systematically investigate the influence of cefazolin incorporation on the colloidal characteristics and interfacial properties of chitosan – TPP nanogels prepared by ionic gelation. Special emphasis is placed on correlating particle size, surface charge, encapsulation efficiency and adsorption kinetics at the air – water interface in order to clarify structure – property relationships relevant to aqueous and topical pharmaceutical formulations.

2. Materials and Methods

2.1 Materials

Chitosan (medium molecular weight, average molecular weight ≈ 310 – 375 kDa, degree of deacetylation ≥ 75%) was purchased from Sigma – Aldrich and used as the polymeric matrix for nanogel preparation. Sodium tripolyphosphate (TPP, ≥ 98% purity) was obtained from Sigma – Aldrich and employed as the

ionic crosslinking agent. Cefazolin sodium (assay 89.1 – 110.1%) was purchased from Sigma – Aldrich and used as a model hydrophilic antibiotic. Acetic acid (glacial, ≥ 99.7% purity) was obtained from Sigma – Aldrich and used for the preparation of chitosan solutions. Sodium hydroxide (NaOH, pellets, ≥ 98% purity) was purchased from Sigma – Aldrich and used for pH adjustment. All chemicals were of analytical grade and used as received without further purification. Deionized water was used throughout the experiments for the preparation of all solutions and dispersions.

Dialysis membranes (using cellulose – based dialysis tubing membranes (regenerated cellulose)) purchased from Sigma – Aldrich. The dialysis membranes had a molecular weight cut – off (MWCO) of 10 – 14 kDa, allowing efficient removal of low – molecular – weight species such as residual acetic acid, free TPP and non – encapsulated cefazolin, while retaining the chitosan nanogels.

2.2 Preparation of chitosan nanogels

Blank chitosan nanogels (CS) were prepared using the ionic gelation method with sodium tripolyphosphate (TPP) as the crosslinking agent. Briefly, chitosan was dissolved in an aqueous acetic acid solution (1% v/v) to obtain a final polymer concentration of 0.1% (w/v). the solution was magnetically stirred at room temperature until a clear and homogeneous solution was obtained. The pH of the chitosan solution was adjusted to approximately 5.0 using dilute NaOH solution when necessary.

Separately, an aqueous solution of sodium tripolyphosphate (TPP) was prepared at a concentration of 0.05% (w/v). the TPP solution was added dropwise to the chitosan solution under continuous magnetic stirring at a constant stirring rate, while maintaining the volume ratio of chitosan solution to TPP solution 5:1. During the addition process, chitosan nanogels formed spontaneously due to electrostatic interactions between the protonated amino groups of chitosan and the negatively charged phosphate groups of TPP. After complete addition of TPP, the resulting suspension was further stirred for 20 – 30 min at room temperature to ensure stabilization of the nanogels. The obtained blank chitosan nanogels exhibited a slightly opalescent appearance, indicating successful formation of nanosized gel particles.

Cefazolin – loaded chitosan nanogels (CS – Cef) were prepared using the same ionic gelation approach. Cefazolin sodium was dissolved separately in deionized water to prepare a concentrated stock solution. An appropriate volume of this stock solution was added to the chitosan solution under gentle stirring to achieve the desired drug concentration, followed by stirring for 10 min to ensure homogeneous distribution of the antibiotic within the polymer solution. Subsequently, the aqueous TPP solution (0.05% w/v) was added dropwise to the chitosan – to – TPP volume ratio of 5:1. Drug – loaded nanogels formed spontaneously due to electrostatic interactions between chitosan and TPP, leading to physical entrapment of cefazolin within the nanogel network. After complete

addition of TPP, the suspension was stirred for an additional 20 – 30 min at room temperature to allow stabilization of the nanogels.

Unless otherwise stated, freshly prepared CS and CS – Cef nanogels were used directly for subsequent characterization and analysis.

2.3 Encapsulation efficiency of cefazolin

The encapsulation efficiency (EE%) of cefazolin in chitosan nanogels was determined using an indirect UV – Vis spectrophotometric method. The CS – Cef nanogel suspension was subjected to centrifugation to separate the nanogels from the aqueous phase containing free (non – encapsulated) cefazolin. The supernatant was carefully collected for analysis.

The concenteration of free cefazolin in the supernatant was quantified using a UV – Vis spectrophotometer at the maximum absorption wavelength of cefazolin, which was determined by scanning in the range of 200 – 400 nm. A calibration curve was constructed using standard cefazolin solutions of known concentrations prepared in deionized water.

To eliminate background interference from formulation components, the supernatant obtained from blank chitosan nanogels (CS) processed under identical conditions was used as the blank reference. The encapsulation efficiency was calculated using the following equation:

$$100 \times \frac{({}_{\text{free}}W_{\text{total}} - W)}{{}_{\text{total}}W} = \%EE$$

where W_{total} – is the total amount of cefazolin initially added to the formulation and W_{free} – is the amount of free cefazolin detected in the supernatant.

2.4 Purification of nanogels for interfacial analysis

To minimize the influence of unreacted low – molecular – weight species on interfacial measurements, freshly prepared blank chitosan nanogels (CS) and cefazolin – loaded chitosan nanogels (CS – Cef) were subjected to a mild purification step prior to surface tension analysis. Purification was performed using dialysis to remove residual acetic acid, free sodium tripolyphosphate (TPP) and non – encapsulated cefazolin while preserving the native nanogel structure.

Briefly, nanogel dispersions were transferred into dialysis membranes with an appropriate molecular weight cut – off (MWCO) and dialyzed against deionized water at room temperature. The external dialysis medium was replaced several times to ensure efficient removal of diffusible components. After dialysis, the purified nanogels were directly used for surface tension measurements and complementary characterization.

Drying or powder formation of the nanogels was intentionally avoided. Drying processes such as freeze – drying or spray – drying can induce irreversible structural changes in chitosan – based nanogels, including aggregation, collapse of the gel network and altered polymer chain conformation. Subsequent

redispersion of dried nanogels may therefore not accurately reproduce the original colloidal and interfacial properties of the freshly prepared system. Since the primary objective of this study was to investigate the interfacial behavior of chitosan nanogels in aqueous environments, purified nanogel dispersions were used to preserve their intrinsic adsorption kinetics and surface activity.

2.5 Particle size and zeta potential measurements

The hydrodynamic diameter, polydispersity index (PDI) and zeta potential of blank chitosan nanogels (CS) and cefazolin – loaded chitosan nanogels (CS – Cef) were measured using dynamic light scattering (DLS) and electrophoretic light scattering techniques.

To accurately reflect the native colloidal properties of the nanogels under synthesis conditions, all particle size and zeta potential measurements were performed on freshly prepared nanogel dispersions prior to any purification or dialysis steps. This approach was adopted because changes in ionic strength, pH or removal of counterions during purification can significantly alter the electrostatic environment of chitosan – based nanogels and may lead to artificial variations in particle size or surface charge.

Fresh nanogel dispersions were appropriately diluted with deionized water to avoid multiple scattering effects prior to measurement. All measurement were carried out at room temperature and each sample was analyzed in triplicate. The reported values are presented as mean ± standard deviation.

To verify that the purification procedure did not induce significant structural alterations, selected samples were additionally characterized after dialysis and compared with their freshly prepared counterparts. This comparison was performed as a methodological validation step to confirm that the mild purification process preserved the overall nanogel structure.

Dynamic light scattering (DLS) measurement were performed using a Malvern Zetasizer Nano – ZS instrument (UK) equipped with a 4 mW He – Ne laser (λ = 633 nm) at a fixed backscattering angle of 173°, to determine the hydrodynamic diameter of the nanogels.

Zeta potential measurement were carried out independently using a Nano – flex analyzer (Particle Metrix, Germany) based on electrophoretic mobility measurements, providing complementary assessment of surface charge characteristics.

2.6 Dynamic surface tension measurements

Surface tension measurements were conducted at room temperature using a tensiometry technique under controlled conditions. Prior to measurement, all samples were gently mixed to ensure homogeneity while avoiding air bubble formation. Dynamic surface tension was recorded as a function of time immediately after formation of the air – liquid interface. Each measurement was performed at least in triplicate and average values were reported.

Surface tension measurements were performed using the conventional pendant drop technique employing a tensiometer manufactured by KRUSS (Hambrg, Germany). A stainless – steel needle with an internal diameter of 0.5 mm was used to form pendant droplets of the investigated liquids. The analysis involved continuous image acquisition of the droplet profile, followed by digital image processing and numerical fitting of the Young – Laplace equation to the experimental drop shape, as described elsewhere [1].

3. Results and Discussi

3.1 Formation and visual characteristics of chitosan nanogels

The formation of chitosan nanogels was initially confirmed through visual observation immediately after ionic gelation. Upon dropwise addition of sodium tripolyphosphate (TPP) to the chitosan solution, the system gradually transitioned from a clear solution to a slightly opalescent and homogeneous dispersion, indicating the formation of nanoscale gel particles. No visible precipitation, phase separation or macroscopic aggregation was observed, suggesting effective electrostatic crosslinking between chitosan chains.

All observations were conducted at room temperature (25 ± 1 °C) anf pH ≈ 5.0, corresponding to the synthesis conditions of the chitosan – TPP system. Both blank chitosan nanogels (CS) and cefazolin – loaded nanogels (CS – Cef) remained visually stable without sedimentation for at least 24 h, demonstrating adequate short – term colloidal stability for subsequent analyses. The slightly increased turbidity observed for CS – Cef dispersions is attributed to drug incorporation and associated polymer – drug interactions during gel formation.

The polymer concentration was fixed at 0.1 % (w/v) chitosan for all formulations to ensure consistent and comparable preparation conditions.

3.2. Colloidal properties and effect of cefazolin loading

The hydrodynamic diameter, polydispersity index (PDI) and zeta potential of freshly prepared nanogels were measured by dynamic light scattering a 25 °C and pH ≈ 5.0 (Table 1). Blank CS nanogels exhibited an average hydrodynamic diameter of approximately 210 nm with a narrow size distribution (PDI < 0.30), confirming successful formation of uniformly dispersed nanoscale particles.

Incorporation of cefazolin resulted in an increase in average particle size to approximately 285 nm, accompanied by a moderate increase in PDI. This size enlargement reflects drug incorporation within the chitosan – TPP network and suggests partial swelling and rearrangement of polymer chains during ionic gelation. Similar trends have been reported for hydrophilic drug – loaded chitosan nanogels.

Both CS and CS – Cef nanogels exhibited positive zeta potentials exceeding +25 mV, indicative of sufficient electrostatic stabilization under acidic conditions. The reducted zeta potential observed for CS – Cef nanogels likely arises from partial charge screening and specific interactions between cefazolin molecules

and protonated amino groups of chitosan. Nevertheless, the surface charge remained within a range suitable for maintaining colloidal stability.

Table 1 – Particle size, polydispersity index (PDI), and zeta potential of freshly prepared blank chitosan nanogels (CS) and cefazolin-loaded chitosan nanogels (CS–Cef)

Sample	Size (nm)	PDI	Zeta potential (mV)
CS	210 ± 25	0.22 ± 0.04	+33 ± 5
CS–Cef	285 ± 35	0.30 ± 0.05	+26 ± 4

3.3 Encapsulation efficiency of cefazolin in chitosan nanogels

The encapsulation efficiency (EE %) of cefazolin was determined using an indirect UV – Vis method by quantifying free drug in the supernatant at $\lambda = 270$ nm. Measurements were conducted at 25 °C and pH ≈ 5+.0. The encapsulation efficiency was found to be approximately 48 ± 6%, confirming effective corporation of cefazolin into the nanogel matrix.

The moderate EE% is attributed to the hydrophilic nature of cefazolin and its partial partitioning into the aqueous phase during gelation. Drug entrapment is governed by a combination of electrostatic interactions and physical confinement within the crosslinked polymer network. The obtained encapsulation efficiency is sufficient for evaluating interfacial and colloidal behavior without excessive polymer or crosslinker loading.

3.4 Influence of dialysis on nanogel colloidal stability

To assess whether the dialysis purification step affected the colloidal characteristics of the nanogels, selected samples of blank chitosan nanogels (CS) and cefazolin – loaded nanogels (CS – Cef) were characterized before and after dialysis. Dialysis and subsequent measurements were conducted at room temperature (25 **°C**) using agueous media at neutral pH, while preserving the initial nanogel concentration. The hydrodynamic diameter and polydispersity index were measured to evaluate potential changes in particle size distribution induced by the purification process. A comparison of particle size before and after dialysis is summarized in Table 2.

Following dialysis, both CS and CS – Cef nanogels retained their nanoscale dimensions, with only minor variations in average particle size and PDI compared to the freshly prepared dispersions. No evidence of severe aggregation or macroscopic instability was observed after purification, indicating that the dialysis procedure did not compromise that overall colloidal integrity of the nanogels.

The slight changes observed in particle size and size distribution after dialysis can be attributed to the removal of low – molecular – weight species, such as residual acetic acid, free sodium tripolyphophate and non – encapsulated cafazolin, which may influence the ionic environment or broadening of the size distribution suggests that the chitosan – TPP network remained structurally intact during dialysis.

These findings confirm that dialysis represents a mild and suitable purification strategy for chitosan – based nanogels when the objective is to eliminate small – molecule contaminants while preserving the native colloidal structure. This validation step supports the use of dialyzed nanogel dispersions for subsequent interfacial characterization, particularly dynamic surface tension measurements, where the presence of residual low – molecular – weight species could otherwise interfere with the interpretation of results.

Table 2 – Effect of dialysis on the hydrodynamic size and PDI of chitosan nanogels

Sample	Size before dialysis (nm)	Size after dialysis (nm)	PDI after dialysis
CS	210 ± 25	230 ± 30	0.24 ± 0.05
CS–Cef	285 ± 35	305 ± 40	0.32 ± 0.06

3.5 Dynamic surface tension and adsorption kinetics at pH 5 and 25 °C

The dynamic surface tension behavior of deionized water, an aqueous cefazolin solution (0.5 mg mL^{-1}), blank chitosan nanogels (CS) and cefazolin – loaded chitosan nanogels (CS – Cef) was investigated at pH 5 and 25 °C to elucidate adsorption kinetics at the air – water interface. The dynamic surface tension profiles of the investigated systems are shown in Figure 1.

Deionized water exhibited a constant surface tension value of approximately 72 mN m^{-1} throughout the measurement period, confirming the absence of surface – active impurities. Similarly, the aqueous cefazolin solution (0.5 mg mL^{-1}) showed negligible time – dependent variation in surface tension, indicating that free cefazolin does not exhibit significant surface activity under the investigated conditions.

In contrast, chitosan nanogel dispersions (prepared at a polymer concentration of 0.1% w/v chitosan) displayed a gradual decrease in surface tension with time, reflecting adsorption and interfacial rearrangement of nanogel – associated polymer segments. Blank CS nanogels showed a reduction in surface tension from approximately 71.8 mN m^{-1} to a plateau value of approximately 67.4 mN m^{-1} ($\Delta\gamma \approx 4.4$ mN m^{-1}), with interfacial equilibrium reached after approximately 25 – 30 min.

Cefazolin – loaded nanogels, containing cefazolin at an equivalent initial concentration of 0.5 mg mL^{-1}, exhibited a similar qualitative trend but with reduced magnitude and slower kinetics. The surface tension decreased from approximately 72.0 mN m^{-1} to a plateau value of approximately 68.9 mN m^{-1} ($\Delta\gamma \approx 3.1$ mN m^{-1}), with equilibrium reached after approximately 30-35 min.

The lower extent and slower rate of surface tension reduction observed for CS – Cef nanogels can be attributed to increased hydration and reduced interfacial mobility of chitosan segments following cefazolin incorporation. Importantly, the negligible surface activity of free cefazolin at 0.5 mg mL^{-1} confirms that the observed changes originate from modifications in nanogel architecture rather than direct adsorption of the antibiotic at the interface.

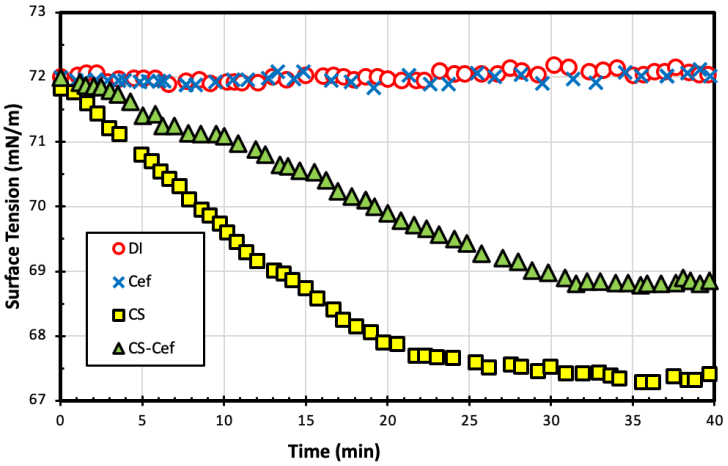

Figure 1 – Dynamic surface tension profiles (γ vs time) of deionized water (DI), free cefazolin solution (Cef), blank chitosan nanogels (CS), and cefazolin-loaded chitosan nanogels (CS–Cef)

3.6 Interfacial adsorption and structural rearrangement mechanisms

The time – dependent surface tension profiles reveal that interfacial activity of chitosan nanogels is governed by slow adsorption and structural rearrangement rather than instantaneous surface coverage. For blank CS nanogels, gradual surface tension reduction reflects diffusion of nanogel entities to the interface followed by partial rearrangement of chitosan segments.

Cefazolin incorporation increases nanogel hydration and restricts polymer segment mobility through electrostatic and hydrogen – bonding interactions, resulting in reduced interfacial responsiveness. The negligible surface activity of free cefazolin confirms that observed effects originate from drug – induced changes in nanogel architecture rather than direct adsorption of the antibiotic.

3.7 Implications for aqueous and topical formulations

The controlled interfacial activity and preserved colloidal stability observed for chitosan nanogels are advantageous for aqueous and topical formulations. Moderate surface tension reduction avoids surfactant – like behavior that could destabilize formulations, while gradual interfacial adsorption may facilitate uniform spreading on hydrated surfaces.

For drug – loaded systems, reduced interfacial activity and enhanced hydration contribute to formulation robustness during storage and application. Collectively, these properties support the suitability of chitosan nanogels as carriers for aqueous and topical delivery systems where predictable interfacial behavior and colloidal stability are required.

4. Conclusion

In this work, cefazolin – loaded chitosan nanogels were successfully prepared via ionic gelation using sodium tripolyphosphate as a crosslinking agent.

The incorporation of cefazolin resulted in a measurable increase in hydrodynamic diameter and a moderate reduction in zeta potential, while maintaining sufficient electrostatic stabilization of the colloidal system under acidic conditions.

The encapsulation efficiency of approximately 48% confirmed effective physical entrapment of the hydrophilic antibiotic within the crosslinked chitosan network. Importantly, dialysis purification did not induce significant structural destabilization, demonstrating that the nanogels retained their nanoscale dimensions and colloidal integrity after removal of low – molecular – weight species.

Dynamic surface tension measurements revealed that chitosan nanogels exhibit time – dependent interfacial adsorption behavior characteristic of soft polymeric colloids. Cefazolin incorporation led to blank nanogels. These finding indicate that drug loading modifies polymer chain mobility and hydration within the nanogel architecture, thereby altering interfacial responsiveness without compromising dispersion stability.

Overall, the results demonstrate that drug incorporation behavior. The established correlations between nanogel structure, drug loading and adsorption kinetics provide valuable insight for the rational design of chitosan – based nanosystems intended for agueous and topical drug delivery applications where controlled interfacial activity and predictable spreading behavior are required.

Funding: The work was carried out within the framework of the project of the Committee of Science of the Ministry of Science and Higher Education of the Republic of Kazakhstan under the project AP26199303.

Conflict of Interest: The authors declare that there is no conflict of interest regarding the publication of this article.

ВЛИЯНИЕ ЗАГРУЗКИ ЦЕФАЗОЛИНА НА СТРУКТУРУ И МЕЖФАЗНУЮ АКТИВНОСТЬ НАНОГЕЛЕЙ НА ОСНОВЕ ХИТОЗАНА

А.А. Шарипова[1], А.Б. Исаева[1]*, С.Б. Айдарова[12], М. Лофти[3], А.Б. Акботин[12], У.Б. Исаева[4]

[1] Satbayev University, Алматы, Казахстан
[2] Казахстанско-Британский технический университет, Алматы, Казахстан
[3] Технологический университет Джунди-Шапур, Дезфул, Иран
[4] АО Институт химических наук им. А.Б. Бектурова, Алматы, Казахстан

Резюме. Наногели на основе хитозана представляют собой перспективные коллоидные носители для гидрофильных лекарственных средств благодаря их биосовместимости, регулируемым физико-химическим свойствам и мягким условиям получения. В данной работе наногели хитозана с включённым цефазолином были получены методом ионной геляции с использованием триполифосфата натрия (ТРР) в качестве сшивающего агента. Влияние включения лекарственного препарата на коллоидные характеристики и межфазное поведение системы было систематически изучено. Свежеприготовленные пустые и нагруженные цефазолином наногели имели гидродинамические диаметры около 210 нм и 285 нм соответственно. Обе системы характеризовались положительными значениями дзета-потенциала выше +25 мВ, что свидетельствует о хорошей электростатической стабильности в кислой среде. Эффективность инкапсуляции цефазолина, определённая косвенным методом УФ–видимой спектроскопии, составила 48 ± 6 %, что подтверждает эффективное включение препарата в сшитую полимерную сеть. После диализа для удаления низкомолекулярных примесей очищенные дисперсии были исследованы методом динамического измерения поверхностного натяжения с использованием

метода висячей капли. Пустые наногели постепенно адсорбировались на границе раздела воздух–вода, снижая поверхностное натяжение с 71,8 до 67,4 мН/м со временем. В отличие от них, наногели с цефазолином демонстрировали более медленную кинетику адсорбции и менее выраженное снижение поверхностного натяжения, достигая равновесных значений около 68,9 мН/м. Выявленные различия объясняются повышенной гидратацией и сниженной подвижностью цепей хитозана после включения препарата. В целом инкапсуляция цефазолина существенно изменяет межфазное адсорбционное поведение наногелей хитозана, сохраняя их коллоидную стабильность. Полученные результаты расширяют представления о взаимосвязи структуры и свойств полимерных наногелей, применяемых в водных и топических системах доставки лекарств.

Ключевые слова: наногели хитозана, ионная геляция, инкапсуляция цефазолина, динамическое поверхностное натяжение, межфазная адсорбция, коллоидная стабильность.

Шарипова Алтынай Азигаровна	*PhD, профессор-исследователь*
Исаева Асем Бахытжановна	*PhD, научный сотрудник*
Айдарова Сауле Байляровна	*Доктор химических наук, профессор*
Лотфи Марзи	*Ассистент-профессор*
Акботин Асылжан Болатбекович	*PhD-докторант*
Исаева Улжалгас Бакытжановна	*PhD, научный сотрудник*

ЦЕФАЗОЛИНДІ ЖҮКТЕУДІҢ ХИТОЗАН НЕГІЗІНДЕГІ НАНОГЕЛЬДЕРДІҢ ҚҰРЫЛЫМЫ МЕН ФАЗААРАЛЫҚ БЕЛСЕНДІЛІГІНЕ ӘСЕРІ

А.А. Шарипова[1], А.Б. Исаева[1]*, С.Б. Айдарова[1,2], М. Лофти[3], А.Б. Ақботин[1,2], У.Б. Исаева[4]

[1] Satbayev University, Алматы, Қазақстан
[2] Қазақ-Британ техникалық университеті, Алматы, Қазақстан
[3] Джунди-Шапур технологиялық университеті, Дезфул, Иран
[4] Ә.Б. Бектұров атындағы Химия ғылымдары институты АҚ, Алматы, Қазақстан

Түйіндеме. Хитозан негізіндегі наногельдер биосәйкестілігі, реттелетін физика-химиялық қасиеттері және жұмсақ алу шарттарының арқасында гидрофильді дәрілік заттар үшін перспективалы коллоидтық тасымалдаушылар болып табылады. Осы жұмыста цефазолинмен жүктелген хитозан наногельдері натрий триполифосфатын (TPP) айқаспалы байланыстырушы агент ретінде қолдана отырып, иондық геляция әдісімен алынды. Дәрілік затты енгізудің жүйенің коллоидтық сипаттамалары мен фазааралық мінез-құлқына әсері жүйелі түрде зерттелді. Жаңадан дайындалған бос және цефазолинмен жүктелген наногельдердің гидродинамикалық диаметрлері сәйкесінше шамамен 210 нм және 285 нм болды. Екі жүйе де +25 мВ-тан жоғары оң дзета-потенциал мәндерін көрсетті, бұл қышқыл ортада жақсы электростатикалық тұрақтылықты білдіреді. УФ–көрінетін спектроскопияның жанама әдісімен анықталған цефазолиннің инкапсуляция тиімділігі 48 ± 6 % құрап, препараттың айқаспалы байланысқан полимерлік тор ішінде тиімді бекітілгенін растады. Төмен молекулалы қоспаларды жою үшін диализ жүргізілгеннен кейін тазартылған дисперсиялар ілінген тамшы әдісі арқылы динамикалық беттік керілуді өлшеу әдісімен зерттелді. Бос наногельдер ауа–су шекарасында біртіндеп адсорбцияланып, уақыт өте келе беттік керілуді 71,8-ден 67,4 мН/м-ге дейін төмендетті. Ал цефазолинмен жүктелген наногельдер адсорбция кинетикасының баяулауын және беттік керілудің аздау төмендеуін көрсетті, тепе-теңдік мәні шамамен 68,9 мН/м болды. Анықталған айырмашылықтар препарат енгізілгеннен кейін хитозан тізбектерінің гидратациясының артуымен және қозғалғыштығының төмендеуімен түсіндіріледі. Жалпы алғанда, цефазолинді инкапсуляциялау хитозан наногельдерінің фазааралық адсорбциясын едәуір өзгертеді, бірақ олардың коллоидтық тұрақтылығын сақтайды. Алынған нәтижелер су және жергілікті дәрі жеткізу жүйелерінде қолданылатын полимерлік наногельдердің құрылым–қасиет байланыстарын тереңірек түсінуге мүмкіндік береді.

Түйінді сөздер: хитозан наногельдері, иондық геляция, цефазолин инкапсуляциясы, динамикалық беттік керілу, фазааралық адсорбция, коллоидтық тұрақтылық.

Шарипова Алтынай Азигаровна	*PhD, зерттеуші-профессор*
Исаева Асем Бахытжановна	*PhD, ғылыми қызметкер*
Айдарова Сауле Байляровна	*химия ғылымдарының докторы, профессор*
Лотфи Марзи	*ассистент-профессор*
Ақботин Асылжан Болатбекович	*PhD докторанты*
Исаева Ұлжалғас Бақытжанқызы	*PhD, ғылыми қызметкер*

References

1. Ul-Islam M., Alabbosh K.F., Manan S., Khan S., Ahmad F., Ullah M.W. Chitosan-based nanostructured biomaterials: Synthesis, properties, and biomedical applications. *Advanced Industrial and Engineering Polymer Research*. **2024**. Vol. 7, Issue 1, p. 79-99. DOI: https://doi.org/10.1016/j.aiepr.2023.07.002
2. Fard A.S., Sabouri Z., Darroudi M., Arezumand R. Application of chitosan-based nanogels for dermal and transdermal delivery systems. *Journal of Materials Science: Materials in Medicine*. **2026**. Vol. 37, 10. DOI: https://doi.org/10.1007/s10856-025-06965-5
3. Arpa, M.D., and Akbuğa F.J. Chitosan-Based Nanogels in Modern Drug Delivery: Focus on Protein and Gene Applications. *Gels*. **2025**, vol. 11, p. 735. DOI: https://doi.org/10.3390/gels11090735
4. Khorasani M.A., Naghib S.M., Jafari T., and Takdehghan G. Recent advances in engineering chitosan-based nanoplatforms in biotherapeutic multi-delivery for multi-targeted disease treatments: Promises and outlooks. *Colloid and Interface Science Communications.* **2025**, vol. 69, p. 100861. DOI: https://doi.org/10.1016/j.colcom.2025.100861
5. Sacco, P., Furlani F., De Marzo G., Marsich E., Paoletti S., and Donati I. Concepts for Developing Physical Gels of Chitosan and of Chitosan Derivatives. *Gels*. **2018**, vol. 4, p. 67. DOI: https://doi.org/10.3390/gels4030067
6. Detsi, A., Kavetsou E., Kostopoulou I., Pitterou I., Pontillo A.R.N., Tzani A., Christodoulou P., Siliachli A., and Zoumpoulakis P. Nanosystems for the Encapsulation of Natural Products: The Case of Chitosan Biopolymer as a Matrix. *Pharmaceutics*. **2020**, vol. 12, p. 669. DOI: https://doi.org/10.3390/pharmaceutics12070669
7. Liu, B., and Chen K. Advances in Hydrogel-Based Drug Delivery Systems. *Gels*. **2024**, vol. 10, p. 262. DOI: https://doi.org/10.3390/gels10040262
8. Jamil, B., Habib H., Abbasi S., Nasir H., Rahman A., Rehman A., Bokhari H., and Imran M. Cefazolin loaded chitosan nanoparticles to cure multi drug resistant Gram-negative pathogens. *Carbohydrate polymers*. **2016**, vol. 136, p. 682-691. DOI: https://doi.org/10.1016/j.carbpol.2015.09.078
9. Akdaşçi, E., Duman H., Eker F., Bechelany M., and Karav S. Chitosan and Its Nanoparticles: A Multifaceted Approach to Antibacterial Applications. *Nanomaterials*. **2025**, vol. 15, p. 126. DOI: https://doi.org/10.3390/nano15020126
10. Priya, A.S., Premanand R., Ragupathi I., Bhaviripudi V.R., Aepuru R., Kannan K., Shanmugaraj K. Comprehensive Review of Hydrogel Synthesis, Characterization, and Emerging Applications. *J. Compos. Sci.* **2024**, vol. 8, p. 457. DOI: https://doi.org/10.3390/jcs8110457
11. Soni, K.S., Desale S.S., Bronich T.K. Nanogels: An overview of properties, biomedical applications and obstacles to clinical translation. Journal of Controlled *Release*. **2016**, vol. 240, p. 109-126. DOI: https://doi.org/10.1016/j.jconrel.2015.11.009
12. Ahmed, J., Mulla M., Maniruzzaman M. Rheological and Dielectric Behavior of 3D-Printable Chitosan/Graphene Oxide Hydrogels. *ACS Biomaterials Science & Engineering.* **2019**, vol. 6. DOI: https://doi.org/10.1021/acsbiomaterials.9b00201
13. Kubeil, M., Suzuki Y., Casulli M.A., Kamal R., Hashimoto T., Bachmann M., Hayashita T., Stephan H. Exploring the Potential of Nanogels: From Drug Carriers to Radiopharmaceutical Agents. *Advanced healthcare materials*. **2024**, vol. 13, no. 1, e2301404. DOI: https://doi.org/10.1002/adhm.202301404

Chemical Journal of Kazakhstan
Volume 2, Number 94(2026), 64-72 https://doi.org/10.51580/2026-2.2710-1185.14

UDC 541.183

STUDY OF THE SORPTION OF NI^{2+}, CO^{2+}, AND V^{4+} CATIONS IN A THREE-COMPONENT SYSTEM USING MODIFIED ZEOLITE

R.A. Kaiynbaeva, G.Sh.Sultanbaeva, R.M Chernyakova.*, U.Zh.Dzhusipbekov

A.B. Bekturov Institute of Chemical Sciences JSC, Almaty, Kazakhstan

**Corresponding author e-mail: *E-mail: chernyakova1947@mail.ru*

Abstract. *Introduction.* Cobalt, nickel, and vanadium are toxic heavy metals that can concentrate and accumulate in soil, wastewater, groundwater, and even in the human body. One of the effective ways to address these problems is the use of accessible adsorbents capable of purifying various types of water. According to the analysis of literature data, the most suitable sorbents are natural and modified forms of zeolites. *The aim of the study* was to investigate the sorption properties of nickel(II), cobalt(II), and vanadium(IV) ions using the saturation method from aqueous solutions with zeolites modified by guar gum. *Results and discussion*. The sorption efficiency of the modified zeolite in multimetal systems was investigated, and it was established that the obtained sorbent simultaneously absorbs all cations. It was shown that, unlike natural zeolite, a high degree of sorption by the modified zeolite is achieved both for a cation with a fixed concentration and for one with a variable concentration. The degree of uptake of the sorbed cations is determined by the combination of two cations with constant and equal contents and the concentration of the variable cation. In all the studied systems, a high degree of cation sorption (from 75.0 to 99.5%, depending on the process conditions) occurs in the region with a low concentration of the variable cation (0.5–10 mg/L). ***Conclusion.*** It was revealed that in multimetal systems competitive adsorption of cations occurs. Series of sorption efficiency for the cations were obtained, as well as data on the initiating influence of the variable cation—under conditions of its increased concentration—on the sorption of other ions present in the system. In the system "Ni^{2+} – Co^{2+} – V^{4+} – MPC – H_2O" with variable C(Co^{2+}) and saturated solutions, the Co^{2+} cation initiates the sorption efficiency of the modified sorbent toward V^{4+} and Ni^{2+} cations: RV (66.6%) > RCo (42.4%) > RNi (13.4%). With variable C(Ni^{2+}), the Ni^{2+} cation increases the sorption efficiency of V^{4+} and Co^{2+} ions: RV (63.6%) > RCo (1.8%) > RNi (3.8%).

Keywords: modified zeolite, saturation method, sorption, cobalt, nickel, and vanadium cations.

Kaiynbaeva Raushan Alibekovna	*Candidate of Technical Sciences; E-mail: raushan_1972@mail.ru*
Sultanbayeva Gita Shamilyevna	*Candidate of technical sciences; E-mail: sultanbaeva@mail.ru*
Chernyakova Raissa Michailovna	*Doctor of Technical Sciences, Professor; E-mail: chernyakova1947@mail.ru*
Jussipbekov Umirzak Zhumasilovich	*Academician of the National Academy of Sciences of the Republic of Kazakhstan; E-mail: jussipbekov@mail.ru*

Citation: Kaiynbayeva R.A., Sultanbayeva G.Sh., Chernyakova R.M., Jussipbekov U.Zh. Study of the sorption of Ni^{2+}, Co^{2+}, and V^{4+} cations in a three-component system using modified zeolite. *Chem. J. Kaz.*, **2026**, 2*(94)*, 64-72. DOI: https://doi.org/10.51580/2026-2.2710-1185.14

1. Introduction

At present, under conditions of increasing environmental pollution caused by industrial waste, including drilling waste, the removal of heavy metal ions (Ni^{2+}, Co^{2+}, and V^{4+}) from drilling fluids has become particularly important. Environmental contamination by heavy metals is recognized as one of the major problems of ecology and public health.

Recent studies have shown that sorption purification not only provides competitive removal efficiency compared with traditional chemical methods, but also minimizes the environmental impact of the treatment process. The use of advanced sorbents, often chemically modified, has further improved the removal capacity for heavy metals such as lead, cadmium, and mercury. These advances highlight the potential of sorption methods as a cornerstone of modern drilling fluid treatment systems [1].

The choice of a purification method depends on specific operational and environmental conditions. The integration of sorption processes offers a promising approach to more sustainable and efficient management of drilling fluids contaminated with heavy metals.

Each method for the removal of heavy metals has its own unique advantages and disadvantages, which requires careful selection based on the specific characteristics of wastewater and operational constraints. Chemical treatment methods, including precipitation and oxidation, provide a high degree of purification but often produce hazardous sludge that requires further treatment.

Cobalt, nickel, and vanadium are toxic heavy metals that can concentrate and accumulate in soil, wastewater, groundwater, and even in the human body.

The sorption removal of heavy metals from drilling fluids is based on the interaction of physicochemical mechanisms, including adsorption, absorption, ion exchange, surface complexation, and precipitation. Adsorption, the predominant mechanism, occurs through electrostatic interactions, van der Waals forces, or chemical bonding between metal ions and functional groups on the sorbent surface (e.g., hydroxyl, carboxyl, or amino groups) [2]. Absorption, although less common in solid sorbents, is important for polymeric materials where metals diffuse into the sorbent matrix.

Ion exchange plays a crucial role for aluminosilicate sorbents such as zeolites, where metal cations replace exchangeable ions (e.g., Na^{+}, Ca^{2+}) within their porous structures. Surface complexation predominates in oxide-based sorbents (e.g., iron oxides), where metals form coordination bonds with surface hydroxyl groups [3]. Studies of adsorption toward metal cations on zeolites with deposited organic layers have suggested [4,5] that the movement of molecules in the inner sphere is coordinated by the zeolite's own pore system.

In study [6], the adsorption of Cu(II), Cd(II), and Pb(II) from aqueous solution onto a methyl methacrylate–Na-Y zeolite composite (MMA–Na-Y zeolite) was analyzed depending on pH, contact time, initial concentration of metal cations, adsorbent dosage, and temperature.

The removal of copper, nickel, cobalt, and iron ions from water resources in the concentration range of 0.5–3.5 mg-eq/dm³ using natural zeolite from the Yagodninskoye deposit in the Kamchatka region was experimentally studied [7]. The results show that natural zeolite can be used as an effective sorbent for the extraction of Cu(II), Ni(II), Co(II), and Fe(II) ions from contaminated water.

The adsorption activity of zeolites from the Kholinskoye deposit toward copper, zinc, and chromium ions was investigated [8], demonstrating the potential of such materials for wastewater treatment from these ions.

One of the effective ways to solve these problems is the use of accessible adsorbents capable of providing the required degree of wastewater purification. These include adsorption technologies based on synthetic, natural, and modified zeolites [9, 10]. According to the analysis of literature data, the application of sorption methods for the treatment of drilling fluids using natural and readily available sorbents capable of reducing the concentration of heavy metals is the most suitable approach. Natural zeolite, significant reserves of which are available in Kazakhstan, largely meets these requirements.

As is known, natural zeolite is characterized by less effective sorption properties compared with synthetic ion-exchange resins. This disadvantage is compensated by the good response of natural zeolite to modification processes. There are various methods for modifying natural aluminosilicates: mechanical, thermal, and chemical modification, which includes acid and alkaline activation, modification with inorganic and organic compounds, and combined activation methods.

Currently, promising modifiers include accessible, inexpensive, natural, and non-toxic organic compounds that possess functional hydroxyl and amino groups active in sorption processes, such as guar gum. This modifier is an inexpensive natural biopolymer with functional hydroxyl and CH_2 groups that participate in the sorption processes of cations.

It should be noted that the scientific literature provides insufficient information on sorption processes for the removal of common pollutants such as Ni(II), Co(II), and V(IV) cations using natural zeolite and its modified polysaccharide forms, especially for environmental purification processes under conditions of their simultaneous presence.

The necessity to improve the sorption characteristics of natural zeolite was experimentally substantiated, since the degree of sorption even in systems containing one metal cation does not exceed 75%, and in multi-metal systems Rsorb. of a competing cation is no more than (60-65)%.

The sorption of heavy metals (Ni^{2+}, Co^{2+}, V^{4+}) by a guar gum-modified zeolite in single- and multi-metal systems is studied for the first time. The modified zeolite is shown to be an effective sorbent, and sorption efficiency series for cations in multi-metal systems are obtained.

The aim of this study was to investigate the sorption properties of nickel(II), cobalt(II), and vanadium(IV) ions using the saturation method from aqueous solutions with zeolites modified by guar gum.

2. Experimental part

Experiments to determine the sorption characteristics were carried out at room temperature. The preparation of the modified zeolite was performed as follows: natural zeolite was mixed with a guar gum solution at a solid-to-liquid ratio of 1:100 for 10 hours. The precipitate was then separated and dried at 50 °C. The dried samples of the modified zeolite were placed in conical flasks, and model solutions with various concentrations were added. Each test was repeated twice.The margin of error of experimental data is 0.1-1%.

For the preparation of model solutions, the following salts were used: nickel sulfate $NiSO_4 \cdot 7H_2O$, cobalt sulfate $CoSO_4 \cdot 7H_2O$, and vanadium sulfate $VOSO_4 \cdot 3H_2O$ dissolved in H_2O. To eliminate the influence of impurities, the sorption of divalent and tetravalent cations of nickel, cobalt, and vanadium was studied in the model system "Ni^{2+}, Co^{2+}, V^{4+} – H_2O – modified zeolite."

Sorption of nickel(II), cobalt(II), and vanadium(IV) cations was carried out at a constant zeolite-to-solution ratio (solid-to-liquid, 10:100) and equal concentrations of the sorbed cations. The concentrations of nickel, cobalt, and vanadium cations in the solutions were determined using atomic emission spectroscopy.

3. Results and Discussion

The table presents the main sorption characteristics of the resulting sorbent compared to the natural zeolite. The results show that all sorption characteristics of the modified zeolite are higher than those of the PC. For the modified zeolite, SEC cat is 15 times higher, SECan is 85.6 times higher, TSC is 9.7 times higher, and TPV is 77 times higher than those of the natural zeolite.

Table - Sorption Characteristics of Modified and Natural Zeolites

TPV, *g*/cm^3	TSC, *g*/cm^3	SEC_{cat}, mg-eq/g	SEC_{an}, mg-eq/g
Modified zeolite			
1.814	35.44	14.896	42.658
Natural zeolite			
0.0235	3.67	0.997	0.4985

The sorption properties of natural zeolite modified with guar gum were studied in the system "Ni^{2+} – Co^{2+} – V^{4+} – modified zeolite – H_2O" under conditions similar to those for sorption of these cations by natural zeolite, where the concentrations of two cations were equal and constant, and the concentration of the third component varied from 0.5 to 500 mg/L.

The sorption curves in all studied systems exhibit a wavelike pattern (Figures 1–3), in contrast to those observed for natural zeolite [12]. Furthermore, the highest degree of sorption by the modified zeolite was observed for all sorbed cations in low-concentration solutions, from 0.5 to 1.0 mg/L for the cation with variable concentration.

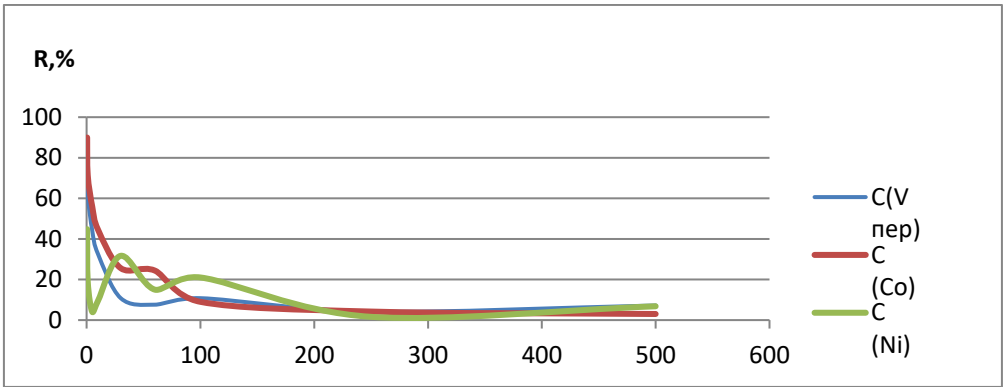

C (Ni, Co) = 5 mg/L

Figure 1 – Influence of vanadium (IV) cation concentration on the extraction efficiency of cations by the modified zeolite in the system "Ni^{2+} – Co^{2+} – V^{4+} – modified zeolite – H_2O"

Regardless of the sorption conditions, as the concentration of the variable cation increases, the sorption degree ($R_{sor}b$) of all sorbed cations decreases. Moreover, unlike natural zeolite, its modified form exhibits high sorption capacity for cations with both constant and variable concentrations, simultaneously absorbing both cations.

In the first scenario, where C(Ni, Co) = 0.5 mg/L (constant) and C(V) is the variable factor, the modified zeolite shows preferential sorption toward Co^{2+} ($R_{sor}b$ = 90.0%) and V^{4+} ($R_{sor}b$ = 85.16%), while the sorption degree of Ni^{2+} is 44.8% (Figure 1).

The appearance of a weak maximum on the Co(II) sorption curve at C(V) = 50 mg/L (RCo = 25%), as well as more pronounced maxima at C(V) = 30 and 100 mg/L on the Ni^{2+} sorption curve (RNi = 31.7% and 21.0%), is associated with partial desorption processes. From 200 mg/L onward, the dependence of R for Co^{2+} and V^{4+} on the concentration of V^{4+} becomes approximately linear, and $R_{sor}b$ fluctuates slightly (3.0–7.2%).

The sorption degrees of the cations can be ranked as: RCo > RV > RNi.

In the second scenario, where CNi = CV and the concentration of Co^{2+} is variable (Figure 2), the shape of the sorption curves is somewhat simplified compared to the system described above (Figure 1).

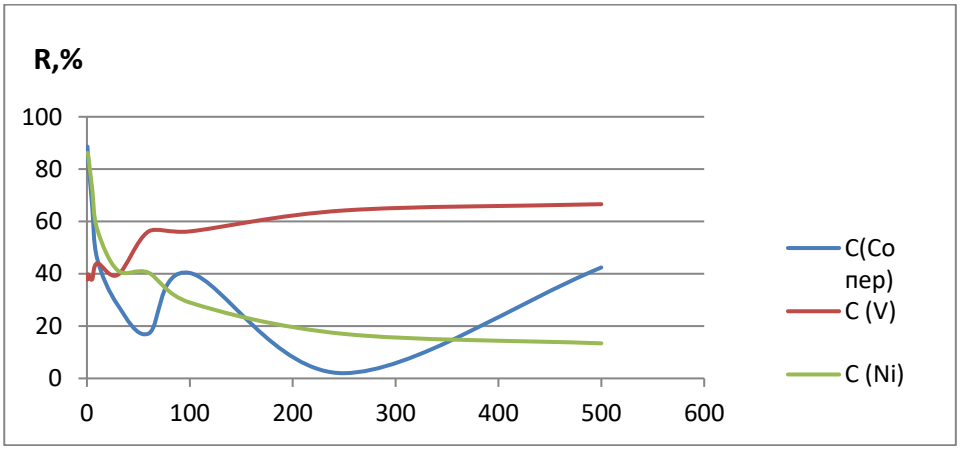

C (Ni, V) = 5 mg/L

Figure 2 – Influence of cobalt (II) cation concentration on the extraction efficiency of cations by the modified zeolite in the system "Ni^{2+} – Co^{2+} – V^{4+} – modified zeolite – H_2O"

In the sorption curves, no maxima are observed for nickel(II) and vanadium(IV) cations, while the cobalt(II) sorption curve exhibits a single pronounced maximum at C_{Co} = 100 mg/L. The modified zeolite demonstrates preferential sorption toward Ni^{2+} at constant nickel concentration (R_{Ni} = 86.24%) and for variable Co^{2+} concentration (RCo = 88.6%) in the cobalt(II) concentration range of 0.5–1.0 mg/L, while RV ranges from 37.8 to 39.8%.

Starting from C_{Co} = 30 mg/L, the sorption degree of vanadium(IV) cations increases, reaching 66.6% at C_{Co} = 500 mg/L, which is 26.8–28.8% higher than in the low-concentration range of Co^{2+}. For the Co^{2+} sorption curve (variable), starting from 100 mg/L, R_{sorb} also increases with increasing C_{Co}, reaching 42.4% at 500 mg/L. Meanwhile, the sorption curve of Ni^{2+} decreases, and R_{Ni} drops to 13.4% at 500 mg/L cobalt(II). In this case, cobalt cations initiate the sorption process of vanadium cations, while a decrease in vanadium concentration, in turn, stimulates the sorption of cobalt cations.

The amount of sorbed Co^{2+} at its concentrations of 400 and 500 mg/L is 105 and 212 mg/L, respectively, whereas for natural zeolite under the same conditions it is 99 and 95 mg/L (Figure 1). In this system, at low cobalt concentrations, the sorption ranking is $R_{Co} > R_{Ni} > R_V$, whereas in saturated solutions it changes to RV > RCo > RNi.

In the third scenario, according to the data shown in Figure 3, in the system "Ni^{2+} – Co^{2+} – V^{4+} – modified zeolite – H_2O" with $C_{Co} = C_V$ = const and variable C_{Ni}, the curves are further simplified compared to the previous scenario (Figure 2). As C_{Ni} increases from 0.5 to 30 mg/L, the sorption degree of Co^{2+} and V^{4+} sharply decreases; with further increase in C_{Ni}, its sorption gradually decreases, while Co^{2+} sorption slightly increases and then decreases again at 300 mg/L Ni^{2+}. The V^{4+} sorption curve, in contrast, rises with increasing C_{Ni}.

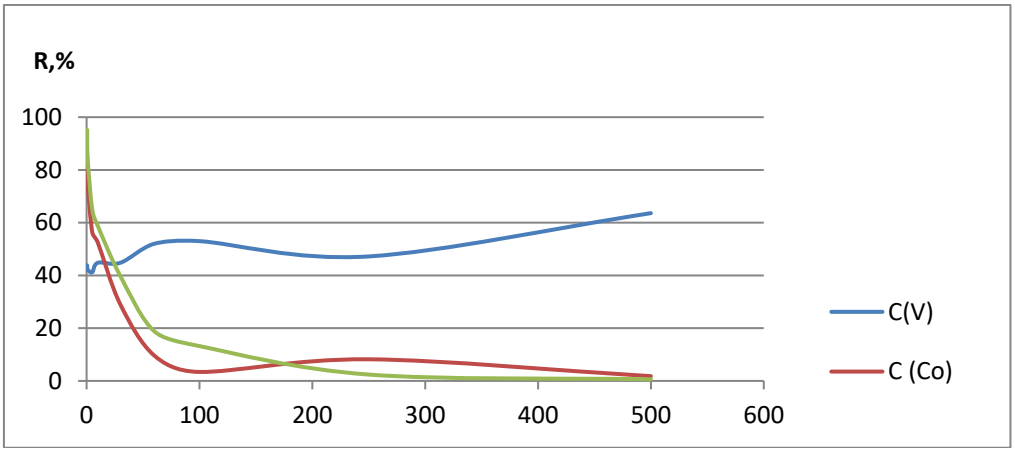

C (V, Co) = 5 mg/L

Figure 3 – Influence of nickel (II) cation concentration on the extraction efficiency of cations by the modified zeolite in the system "Ni^{2+} – Co^{2+} – V^{4+} – modified zeolite – H_2O"

In the low Ni^{2+} concentration range, the modified zeolite demonstrates preferential sorption for Ni^{2+} ($R_{sor}b$ = 95.2%) and Co^{2+} (RCo = 84.5%), while RV under these conditions does not exceed 42.2–43.8%. Starting from 10–30 mg/L Ni^{2+}, the sorption degree of vanadium(IV) increases from 44.8% to 63.6%, whereas RCo and RNi sharply decrease and continue to decline with further increases in CNi.

Thus, the modified zeolite acts as an effective sorbent for Ni^{2+} and Co^{2+} cations (RNi > RCo > RV) in solutions with low nickel(II) concentrations, while in nickel-saturated solutions it is more effective for V^{4+} cations, where RV > RCo > RNi.

4. Conclusion

The sorption efficiency of a modified guar gum zeolite on multiple metal components was studied. It was found that the resulting sorbent consistently controls all cations (Ni^{2+}, Co^{2+}, V^{4+}). The degree of cation distribution is determined by the combination of two cations with constant and equal concentrations and the concentration of a variable cation.

In all experimental studies, high cation sorption (75.0–99.5%) was observed, depending on low concentrations of the variable cation (0.5–10 mg/L).

Competitive adsorption of cations was revealed, cation sorption efficiency series were obtained, and data were provided on the onset of the variable cation's existence under conditions of its high concentration on the sorption of other ions present in the system. With variable C(Ni^{2+}), the Ni^{2+} cation increases the efficiency of sorption of V^{4+} and Co^{2+} ions: RV (63.6%) > RCo (1.8%) > RNi (3.8%). The results of the studies using the modified sorbent showed the possibility of using the modified zeolite to purify wastewater from metallurgical production from heavy metal ions, including nickel, cobalt and vanadium.

Acknowledgments: This work was funded by the Committee of Science of the Ministry of Science and Higher Education of the Republic of Kazakhstan (Targeted Scientific Research Program BR 27101179 "Fundamental Principles for Obtaining Innovative, Environmentally Safe, Multifunctional Chemical Products and Materials").

Conflict of Interest: The authors declare no conflict of interest.

МОДИФИКАЦИЯЛАНҒАН ЦЕОЛИТ АРҚЫЛЫ ҮШ КОМПОНЕНТТІ ЖҮЙЕДЕ N_I^{2+}, C_O^{2+}, V^{4+} КАТИОНДАРЫНЫҢ СОРБЦИЯСЫН ЗЕРТТЕУ

Р.Ә. Қайыңбаева, Г.Ш. Сұлтанбаева, Р.М. Чернякова*, Ө.Ж. Жүсіпбеков

Ә.Б. Бектұров атындағы химия ғылымдары институты, Алматы, Қазақстан

Түйіндеме. *Кіріспе.* Кобальт, никель және ванадий - улы ауыр металдар, олар топырақта, ағынды суларда, жер асты суларында және тіпті адам ағзасында шоғырланып, жиналуы мүмкін. Бұл мәселелерді шешудің бір тиімді жолы - әртүрлі су түрлерін тазартуға қабілетті оңай қолжетімді адсорбенттерді пайдалану. Әдеби шолуға сәйкес, ең қолайлы сорбенттер - табиғи және модификацияланған цеолиттер. *Жұмыстың мақсаты* гуар шайырымен түрлендірілген цеолиттермен сулы ерітінділерден қанығу әдісімен никель (II), кобальт (II) және ванадий (IV) иондарының сорбциялық қасиеттерін зерттеу. *Нәтижелер мен пікірталас.* Модификацияланған цеолиттің көпметалды жүйелеріндегі сорбциялық тиімділігі зерттелді және алынған сорбент бір мезгілде барлық катиондарды адсорбциялайтыны анықталды. Табиғи цеолиттен айырмашылығы, модификацияланған цеолиттің жоғары дәрежедегі сорбциясына тұрақты және айнымалы концентрациялы катиондар үшін қолжетімділігі көрсетілген. Адсорбцияланған катиондардың сорбция дәрежесі айнымалы катионның тұрақты және тең мөлшерлі концентрациясы бар екі катионның тіркесімімен анықталады. Зерттелген барлық жүйелерде катион сорбциясының жоғары дәрежесі, процесс жағдайларына байланысты 75.0-ден 99.5%-ға дейін, төмен айнымалы катион концентрациясы аймағында (0.5-10 мг/л) орын алады. *Қорытынды.* Көпметаллды жүйелерде катиондардың бәсекеге қабілетті адсорбциясы анықталды және катиондар үшін сорбциялық тиімділік қатарлары, сондай-ақ жоғары концентрациядағы айнымалы катиондар жүйесінде басқа иондардың сорбциясына бастамашылық әсері туралы деректер алынды. Айнымалы $C(Co^{2+})$ және қаныққан ерітінділері бар Ni^{2+} – Co^{2+} – V^{4+}–МТЦ–H_2O жүйесінде Co^{2+} катионы модификацияланған сорбенттің тиімділігін V^{4+} және Ni^{2+} катиондарына қарай басымдылық көрсетеді: R_V (66.6%)>R_{Co} (42.4%)>RNi (13.4%). Ni^{2+} катионының $C(Ni^{2+})$ айнымалысымен V^{4+} және Co^{2+} иондарының сорбция тиімділігі артады: RV (63.6%) > RCo (1.8%) > RNi (3.8%).

Түйін сөздер: табиғи цеолит, қанықтыру әдісі, сорбция, кобальт, никель және ванадий катиондары

Сұлтанбаева Гита Шамилқызы	*Техника ғылымдары кандидаты*
Қайыңбаева Раушан Әлібекқызы	*Техника ғылымдары кандидаты*
Чернякова Раиса Михайловна	*Техника ғылымдары докторы*
Жүсіпбеков Өмірзақ Жұмасылұлы	*Техника ғылымдары докторы*

ИЗУЧЕНИЕ СОРБЦИИ КАТИОНОВ Ni^{2+}, Co^{2+}, V^{4+} В ТРЕХКОМПОНЕНТНОЙ СИСТЕМЕ МОДИФИЦИРОВАННЫМ ЦЕОЛИТОМ

Р.А.Кайынбаева, Г.Ш.Султанбаева, Р.М. Чернякова, У.Ж. Джусипбеков

АО Институт химических наук им.А.Б.Бектурова, Алматы, Казахстан

Резюме. *Введение.* Кобальт, никель и ванадий — токсичные тяжелые металлы, которые могут концентрироваться и накапливаться в почве, сточных водах, грунтовых водах и даже в организме человека. Одним из эффективных способов решения этих проблем является использование доступных адсорбентов, способных обеспечить очистку различных вод. Согласно анализу литературных данных наиболее подходящими сорбентами являются природные и модифицированные формы цеолитов. *Целью работы* являлось изучение сорбционных свойств ионов никеля(II), кобальта(II) и ванадия (IV) методом насыщения из водных растворов цеолитами,

модифицированными гуаровой камедью. *Результаты и обсуждение.* Исследована сорбционная эффективность модифицированного цеолита в многометальных системах и установлено, что полученный сорбент одновременно поглощает все катионы. Показано, что в отличие от природного цеолита, высокая степень сорбции модифицированным цеолитом достигаться как для катиона с фиксированной, так и с переменной концентрацией. Степень поглощения сорбируемых катионов определяется комбинацией двух катионов с постоянным и равным содержанием и концентрацией переменного катиона. Во всех исследуемых системах высокая степень сорбции катионов от 75.0 до 99.5 %в зависимости от условий процесса приходится на низкоконцентрированную по переменному катиону область (0.5-10 мг/л). *Заключение.* Выявлено, что в многометальных системах протекает конкурентная адсорбция катионов и получены ряды сорбционной эффективности катионов, а также данные об инициирующем влиянии переменного катиона в условиях его повышенной концентрации на сорбцию других присутствующих в системе ионов. В системе «Ni^{2+} – Co^{2+} – V^{4+}– МПЦ–H_2O» с переменной С(Co^{2+}) и насыщенных растворах катион Co^{2+} инициируется эффективность модифицированного сорбента к катионам V^{4+} и Ni^{2+}: R_V (66.6 %)>R_{Co} (42.4 %)>R_{Ni} (13.4 %). При переменной С(Ni^{2+}) катион Ni^{2+} повышается эффективность сорбции ионов V^{4+} и Co^{2+}: R_V (63.6 %) > R_{Co} (1.8 %)> R_{Ni} (3.8 %).

Ключевые слова: модифицированный цеолит, метод насыщения, сорбция, катионы кобальта , никеля и ванадия

Кайынбаева Раушан Алибековна	*Кандидат технических наук*
Султанбаева Гита Шамильевна	*Кандидат технических наук*
Чернякова Раиса Михайловна	*Доктор технических наук, профессор*
Джусипбеков Умирзак Жумасилович	*Академик Национальной академии наук Республики Казахстан, профессор, доктор технических наук*

References

1. Hazrat Ali, Ezzat Khan, Muhammad Anwar Sajjad. Phytoremediation of heavy metals: concepts and applications. *Chemosphere*. **2016,** PMID: 23466085, DOI: 10.1016/j.chemosphere.2016.01.075.

2. K.G. Bhattacharyya and S.S. Gupta. Adsorption of Cu(II), Ni(II), Zn(II), Cd(II) and Pb(II) onto Kaolin/Zeolite Based Geopolymers. *Advances in Materials Physics and Chemistry*, Vol. 2, No. 4B, January 16, **2013**, pp. 114–131.

3. Crini, G., Lichtfouse, E. (). Advantages and Disadvantages of Techniques Used for Wastewater Treatment. *Environmental Chemistry Letters*, **2019**, 17, 145–155. https://doi.org/10.1007/s10311-018-0785-9

4. Meng B., Ren S., Zhang X. et al. Enhancement of the strong Brønsted acidity and mesoporosity: Zr promoted framework modification of Zeolite Y^{4+}. *Microporous and Mesoporous Materials*, **2022**, Vol. 335, p. 111849. DOI: 10.1016/j.micromeso.2022.111849

5. Loganina V., Zhegera K., Fediuk R, Timokhin R, Liseitsev T, Zayakhanov M. Amorphous aluminosilicates as a structure-forming additive in cementitious systems. *Journal of materials in civil engineering*,**2020**, Vol 32, No 5, DOI: 10.1061/(ASCE)MT.1943-5533.0002995

6. Hasanizadeh, M., Aroujalian, A., et al. Retention of copper, cadmium and lead from water by Na-Y zeolite confined in methyl methacrylate shell. *Journal of Environmental Chemical Engineering*, **2017,** Vol. 5, No. 4, pp. 3698–3710. DOI 10.1016/j.jece.2017.06.049

7. Belova, T.P. Adsorption of heavy metal ions (Cu^{2+}, Ni^{2+}, Co^{2+}, and Fe^{2+}) from aqueous solutions by natural zeolite. *Heliyon*, **2019**, Vol. 5, No. 9, e02320. DOI:10.1016/j.heliyon.2019.e02320

8. Filatova, E.G., Pozhidaev, Yu.N., Pomazkina, O.I. Physicochemical processes at interphase boundaries: adsorption of zinc(II) and chromium(III) ions by modified zeolites. *Surface Physics and Materials Protection*, 2020, Vol. 56, No. 5, pp. 479–484. ISBN: 978-5-4465-3448-7 https://www.elibrary.ru/item.asp?id=50244828

9. Pomazkina, O.I., Filatova, E.G., Lebedeva, O.V., Pozhidaev, Yu.N. *Surface Physics and Protective Materials*, **2018**, Vol. 54, No. 4, pp. 393. https://doi.org/10.15217/ISSN1998984-9.2018.43

10. Filatova, E.G., Pozhidaev, Yu.N., Pomazkina, O.I. *Surface Physics and Protective Materials*, **2019**, Vol. 55, No. 5, pp. 507. URL: https://journals.rcsi.science/2070-2051/issue/view/12761

Chemical Journal of Kazakhstan
Volume 2, Number 94(2026), 73-80 https://doi.org/10.51580/2026-2.2710-1185.15

UDC 541.183

STUDY OF THE SORPTION CHARACTERISTICS OF MODIFIED ZEOLITE

G.Sh. Sultanbaeva, R.A. Kaiynbaeva, R.M.Chernyakova*, U.Zh. Dzhusipbekov

JSC Institute of Chemical Sciences named after A.B. Bekturov, Almaty, Kazakhstan

**Corresponding author e-mail: chernyakova1947@mail.ru*

Abstract. *Introduction.*Contaminated industrial wastewater contains carcinogenic metals that negatively affect human health. Research in the field of purification of liquid media polluted with heavy metals focuses on the use of efficient, accessible, inexpensive, and environmentally friendly sorbents and sorption materials based on natural raw materials, in particular zeolite. Natural zeolites from different deposits vary in their mineralogical composition andare characterized by less effective sorption properties compared to synthetic sorbents. To improve the sorption characteristics, an inexpensive modifier guar gum has been selected. *The aim of the work.* Modification of natural zeolite with guar gum by the precipitation method and determination of the optimal conditions under which the highest sorption characteristics are achieved. *Results and discussion.* Study of the effect of guar gum consumption on the properties of modified zeolite showed that with an increase in the amount of modifier, the static exchange capacity (SEC) of the cation exchanger sharply decreases. The optimal stirring time for obtaining the modified sorbent was found to be 10 hours, at which the maximum SEC value of the cation exchanger reaches 1398 mg-eq/g. Investigation of the effect of stirring temperature showed that in the range from 25°C to 75°C, the sorption characteristics of the composite sorbent change insignificantly. An increase in the drying temperature to 100°C leads to an improvement in the sorption characteristics of the sorbent, especially with respect to the sorption of cations. ***Conclusion.*** The conditions for modifying natural zeolite with a natural polysaccharide (guar gum) by the precipitation method have been studied. Optimal conditions for the modification process have been determined, and a new sorbent has been obtained in which the cation exchange capacity, anion exchange capacity, overall exchange capacity, and total sorption capacity are 15 times, 85.6 times, 9.7 times, and 77 times higher, respectively, compared to natural zeolite.

Keywords: natural zeolite, zeolite modification, guar gum, static exchange capacity, total pore volume, overall sorption capacity

Gita Shamilyevna Sultanbayeva	*Candidate of technical sciences; E-mail: sultanbaeva@mail.ru*
Raushan Alibekovna Kaiynbaeva	*Candidate of Technical Sciences; E-mail: raushan_1972@mail.ru*
Raissa Michailovna Chernyakova	*Doctor of Technical Sciences, Professor; E-mail: chernyakova1947@mail.ru*
Umirzak Zhumasilovich Jussipbekov	*Academician of the National Academy of Sciences of the Republic of Kazakhstan; E-mail: jussipbekov@mail.ru*

Citation: Sultanbayeva G.Sh., Kaiynbayeva R.A., Chernyakova R.M., Jussipbekov U.Zh. Study of the sorption characteristics of modified zeolite. *Chem. J. Kaz.*, **2026**, *2(94)*, 73-80. DOI: https://doi.org/10.51580/2026-2.2710-1185.15

1. Introduction

The main sources of heavy metals are liquid wastes from the chemical, metallurgical, oil extraction and refining, pharmaceutical, and other industries [1,2].

At present, research in the field of purification of liquid media contaminated with heavy metals is highly relevant, particularly using efficient, accessible, inexpensive, and environmentally friendly sorbents and sorption materials based on natural raw materials. Natural zeolite meets these requirements to a considerable extent, and significant reserves of it are available in Kazakhstan. It should be noted that natural zeolites from different deposits vary in their mineralogical composition, as well as in the content of the main component–clinoptilolite,which determines their sorption characteristics. Natural zeolite is characterized by less effective sorption properties compared, for example, with synthetic ion-exchange resins. However, this drawback is compensated by the good responsiveness of natural zeolite to modification processes.

To improve the sorption characteristics, a suitable low-cost modifier of natural origin–guar gumwas selected.

Guar gum is a polymeric compound classified as a polysaccharide, containing functional hydroxyl and CH_2 groups, with mannose and galactose units. It has sufficient rigidity and enhanced elasticity, is well soluble in water, exhibits good stability, and has a tendency to form structured gels [3–7].

2. Experimental part

The experiments were carried out using natural zeolite from the Shankanai deposit (Almaty, Kazakhstan) with the following mass composition: 1.38% K_2O; 0.95% Na_2O; 0.16% Fe_2O_3; 10.81% Al_2O_3; 2.32% CaO; 0.93% MgO; 65.28% SiO_2; 18.5% loss on ignition. The main sorption properties of the zeolite are as follows: static exchange capacity for cations – 0.997 mg-eq/g, static exchange capacity for anions – 0.4985 mg-eq/g, total pore volume – 0.07 cm^3/g.

The modification of natural zeolite was carried out as follows: natural zeolite with a particle size of 1–1.5 mm and guar gum were added to distilled water. The resulting mixture was stirred, after which the solid phase was separated from the liquid phase by filtration, and the obtained solid sorbent was dried.

The sorption characteristics of the sorbent are significantly influenced by the ratio of the initial components, mixing time, mixing temperature, drying temperature and time, and zeolite consumption. The influence of these factors on the modification process of natural zeolite with guar gum was studied using a one-factor-at-a-time method.

Methods for determining the parameters of the porous structure of adsorbents were applied. The main sorption characteristics were determined according to standard methods [8, 9].

3. Results and discussion

The results of studying the effect of guar gum consumption on the properties of modified zeolite, presented in Table 1, showed that with an increase in the amount of modifier (guar gum), the static exchange capacity (SEC) of the cation exchanger sharply decreases.

Table 1 – Effect of guar gum consumption on the properties of modified zeolite

Experiment number	Consumption of GKam, g	SEC,mg-eq/g		TSC, *mg-eq/g*	TPV, g/cm^3
		cation exchanger	anion exchanger		
1	0.1	*25.54*	10.9	60.57	0.3022
2	0.2	5.73	17.83	65.09	0.0384
3	0.3	6.87	26.52	69.43	0.3208
4	0.5	5.92	26.57	70.82	0.3594
5	0.7	4.89	30.21	66.85	0.7668

Thus, at a guar gum consumption of 0.2 g (Experiment 2), the static exchange capacity (SEC) of the cation exchanger decreases by 4.5 times compared to Experiment 1. The static exchange capacity of the anion exchanger increases by 2.4–2.7 times when the amount of guar gum is increased from 0.1 to 0.7 g. Increasing the amount of guar gum from 0.1 to 0.7 g leads to a 2.5-fold increase in its overall sorption capacity compared to the standard for guar gum. The change in overall sorption capacity relative to the standard reaches an extremum, with a maximum at 0.5 g of guar gum (Experiment 4).

The total pore volume (TPV) changes only slightly from Experiment 1 to 4, increasing 2.5 times at a guar gum consumption of 0.7 g. Since the sorbent is intended for the sorption of heavy metal cations, a guar gum concentration was selected at which the SEC of the cation exchanger is maximized, i.e., 0.1 g.

The study of the effect of mixing time on the properties of the sorbent (Table 2) showed that increasing the mixing time affects the static exchange capacity (SEC) of the cation and anion exchangers, the overall sorption capacity (OSC), and the TPV.

Specifically, when the mixing time is increased from 2 to 10 hours (Experiments 1–3), the SEC of the cation exchanger significantly increases–from 0.299 to 1.398 mg-eq/g, i.e., by 4.7 times. This indicates a more complete activation of the sorbent due to the extended contact time of the components. However, further increasing the mixing time to 15 hours (Experiment 4) leads to a decrease in SEC to 1.098 mg-eq/g, which may be associated with the onset of sorbent structure degradation or reduced accessibility of active sites.

The SEC of the anion exchanger changes only slightly, ranging from 14.569 to 15.293 mg-eq/g. The total sorption capacity increases from 68.217 to 73.939 mg-eq/g when the mixing time is increased up to 10 hours, after which it decreases to 66.575 mg-eq/g at 15 hours, demonstrating an extremal behavior with a maximum at 10 hours. The TPV varies slightly, from 0.8612 to 0.9387

cm^3/g. The highest value is observed at the shortest mixing time (Experiment 1), after which the volume gradually decreases. Since the sorbent is primarily used for the sorption of heavy metal cations, the optimal mixing time is 10 hours (Experiment 3), at which the maximum SEC of the cation exchanger–1.398 mg-eq/gis achieved.

Table 2 – Effect of mixture mixing time on the properties of modified zeolite

Experiment number	τ mixing, *h*	SEC,*mg-eq/g*		TSC, *mg-eq/g*	TPV, *g/cm³*
		cation exchanger	cation exchanger		
1	2	0.299	15.293	68.217	0.9387
2	5	0.469	15.054	70.389	0.9219
3	10	1.398	14.569	73.939	0.8612
4	15	1.098	14.656	66.575	0.9285

The study of the effect of mixing temperature (Table 3) on the properties of the sorbent showed that changes in mixing temperature in the range from 25°C to 75°C have little effect on the sorption characteristics of the composite sorbent. The SEC of the cation exchanger ranges from 11.88 to 13.94 mg-eq/g, and the SEC of the anion exchanger from 47.43 to 50.04 mg-eq/g. The total sorption capacity varies from 51.05 to 56.52 mg-eq/g. The total pore volume also remains stable, ranging from 0.929 to 0.9764 cm^3/g. Considering technological simplicity and economic feasibility, the mixing was carried out at room temperature (25°C) in subsequent experiments and production.

Table 3 – Effect of mixture mixing temperature on the properties of modified zeolite

Experiment number	T of mixing, °C	SEC,*mg-eq/g*		TSC, *mg-eq/g*	TPV, *g/cm³*
		cation exchanger	cation exchanger		
1	25	13.41	47.43	53.22	0.9764
2	40	12.53	50.04	51.048	0.973
3	55	13.94	47.25	56.52	0.929
4	75	11.88	48.467	54.65	0.937

The results of studying the effect of sorbent drying temperature on the properties of modified zeolite are presented in Table 4.

The data show that the drying temperature significantly affects the sorption properties of the composite sorbent. Increasing the drying temperature from 25°C to 100°C leads to an increase in the static exchange capacity of the cation exchanger from 15.87 to 18.87 mg-eq/g. The highest value is observed at 100°C (Experiment 4), indicating a positive effect of elevated drying temperature on the activation and structural stability of the sorbent. This may be associated with the removal of excess moisture and stronger fixation of guar gum within the zeolite structure.

Table 4 – Effect of sorbent drying temperature on the properties of modified zeolite

Experiment number	T Sorbent drying, °C	SEC,*mg-eq/g*		TSC, *mg-eq/g*	TPV, *g/cm³*
		cation exchanger	cation exchanger		
1	25	15.87	46.92	50.07	1.4313
2	50	15.65	48.49	49.75	1.4091
3	80	16.81	48.52	42.98	1.5394
4	100	18.87	49.51	52.19	1.5804

The SEC of the anion exchanger changes only slightly, ranging from 46.92 to 49.51 mg-eq/g, showing no pronounced dependence on the drying temperature. The total sorption capacity also increases from 50.07 to 52.19 mg-eq/g, which corresponds with the growth in the SEC of the cation exchanger. The total pore volume increases with higher temperature, reaching a maximum of 1.5804 cm^3/g at 100°C. This indicates the formation of a more porous material structure during high-temperature drying.

Thus, increasing the drying temperature to 100°C improves the sorption characteristics of the sorbent, particularly with respect to cation sorption. Therefore, a drying temperature of 100°C can be recommended for further studies and potential industrial applications.

Next, the effect of sorbent drying time on the sorption characteristics of the synthesized sorbent was studied. The results (Table 5) show that varying the drying time in the range of 0.5 to 2.5 hours has little effect on the SEC of the cation exchanger.

Table 5 – Effect of sorbent drying time on the properties of modified zeolite

Experiment number	τ sorbent drying, h	SEC,*mg-eq/g*		TSC, *mg-eq/g*	TPV, *g/cm³*
		cation exchanger	cation exchanger		
1	*0.5*	5.940	28.71	17.74	1.553
2	1	5.923	34.62	23.31	1.543
3	1.5	5.917	30.78	18.52	1.721
4	2.5	5.952	32.64	24.05	1.694

The values of the SEC for the cation exchanger vary within a very narrow range, from 5.917 to 5.952 mg-eq/g, indicating the stability of cation-exchange properties with changes in drying time.

The SEC of the anion exchanger shows more pronounced fluctuations, ranging from 28.71 to 34.62 mg-eq/g, with the maximum observed after 1 hour of drying (Experiment 2). However, after 1.5–2.5 hours, a slight decrease is observed, which may be related to partial loss of active surface area or changes in the structure of the polymer component. The TSC varies from 17.74 to 24.05 mg-eq/g, reaching a maximum after 2.5 hours (Experiment 4), indicating a slight increase in sorbent efficiency with longer drying. TheTPV ranges from 1.543 to

1.721 cm³/g and does not show a consistent dependence on drying time, with the highest value observed at 1.5 hours (Experiment 3), followed by a slight decrease.

Thus, drying time in the range of 0.5–2.5 hours does not significantly affect the cation-exchange properties, although a slight improvement in TSC is observed at longer drying times up to 2.5 hours. Nevertheless, for practical applications, considering energy consumption and the minimal difference in results, the minimum drying time of 0.5 hours is recommended.

The optimal conditions for the modification process have been determined as follows: volume of distilled water for preparing the guar gum solution – 200 mL; guar gum consumption – 0.1 g; natural zeolite consumption – 10 g; mixing time of zeolite with guar gum – 10 hours; mixing temperature – 25°C; drying temperature of the sorbent – 50°C; drying time – 2.5 hours.

As shown in Table 6, compared to natural zeolite, the modified zeolite exhibits some changes in total pore volume, iodine sorption capacity (E), and cation exchange capacity (SEC).

Table 6 – Main properties of modified and natural zeolites

TPV, g/cm^3	TSC, g/cm^3	$SEC_{cat\ exc}$, *mg-eq/g*	SEC_{anexc}, *mg-eq/g*
Modified zeolite			
1.814	35.44	14.896	42.658
Natural zeolite			
0.0235	3.67	0.997	0.4985

TheTPV and the SEC of the anion exchanger increase by 1.14 and 1.12 times, respectively. The improvement in the sorption properties of the modified zeolite is expected to enhance its sorption capacity for heavy metal cations as well.

4. Conclusion

The conditions for modifying natural zeolite with a natural polysaccharide (guar gum) using the precipitation method have been studied. The optimal synthesis conditions for the new sorbent, corresponding to high sorption characteristics, have been determined. A new sorbent has been obtained, in which the cation exchange capacity, anion exchange capacity, overall sorption capacity (TSC), and total pore volume (TPV) are 15, 85.6, 9.7, and 77 times higher, respectively, compared to natural zeolite.

Acknowledgments: This work was funded by the Committee of Science of the Ministry of Science and Higher Education of the Republic of Kazakhstan (Grant No. BR27101179, «Fundamentals of obtaining innovative, environmentally friendly, multifunctional chemical products and materials»).

Conflict of Interest: All authors declare that they have no conflict of interest.

МОДИФИКАЦИЯЛАНҒАН ЦЕОЛИТТІҢ СОРБЦИЯЛЫҚ СИПАТТАМАЛАРЫН ЗЕРТТЕУ

Сұлтанбаева Г.Ш., Қайыңбаева Р.А., Чернякова Р.М., Жүсіпбеков Ө.Ж.

Ә.Б. Бектұров атындағы Химия ғылымдары институты, Алматы, Қазақстан

Түйіндеме. *Кіріспе*. Ластанған өнеркәсіптік ағынды суларда адам денсаулығына кері әсерететін канцерогенді металдар бар. Тиімді, қолжетімді, арзан және экологиялық таза сорбенттер мен табиғи шикізатқа, атап айтқанда цеолит кенегізделген сорбциялық материалдарды пайдалана отырып, ауыр металдармен ластанған сұйық ортаны тазарту процестері саласындағы зерттеулер өзекті болып табылады. Әр түрлі кен орындарынан алынған табиғи цеолиттер минералогиялық құрамы бойынша ерекшеленеді және синтетикалық сорбенттер мен салыстырғанда тиімділігі төмен сорбциялық қасиеттерімен сипатталады. Сорбциялық сипаттамаларды жақсарту үшін арзан модификатор – гуар шайыры таңдалды. *Мақсаты.* Табиғи цеолитті гуар шайырымен тұндыру арқылы модификациялау және ең жоғары сорбциялық сипаттамаларға жету үшін оңтайлы жағдайларды анықтау. *Нәтижелер және талқылау* Гуар шайыры мөлшерінің модификацияланған цеолиттің қасиеттеріне әсерін зерттеу модификатор мөлшерінің артуымен катион алмастырғыштың статикалық алмасу сыйымдылығы (САС) күрт төмендейтінін көрсетті. Модификацияланған сорбентті алудың оңтайлы араластыру уақыты (10 сағат) анықталды, катион алмасу шайырының КАСмаксималды мәні 1398 мг-экв/г-ғажетті. Араластыру температурасының әсерін зерттеу композиттік сорбенттің сорбциялық қасиеттерінің 25°С-тан 75°С-қа дейінгі диапазонда елеусіз өзгеретінін көрсетті. Кептіру температурасын 100°С-қа дейін көтеру сорбенттің сорбциялық қасиеттерін, әсіресе сорбцияға қатысты катиондық қасиетін жақсартады. *Қорытынды*. Табиғи цеолитті табиғи полисахаридпен (гуаршайыры) тұндыру арқылы модификациялау шарттары зерттелді. Сорбентті модификациялау процесінің оңтайлы шарттары анықталды және катиондық шайырдың сорбциялық сыйымдылығы, аниондық шайырдың сорбциялық сыйымдылығы және ЖКК мәндері табиғи цеолитпен салыстырғанда сәйкесінше 15 есе, 85,6 есе, 9,7 есе және 77 есе жоғары жаңа сорбент алынды.

Түйін сөздер: табиғи цеолит, цеолит модификациясы, гуаршайыры, статикалық алмасу сыйымдылығы, жалпы кеуек көлемі, жалпы сорбциялық сыйымдылық

Сұлтанбаева ГитаШамилқызы	*Техника ғылымдары кандидаты*
ҚайыңбаеваРаушанӘлібекқызы	*Техника ғылымдары кандидаты*
ЧерняковаРаисаМихайловна	*Техника ғылымдары докторы*
Жүсіпбеков Өмірзақ Жұмасылұлы	*Техника ғылымдары докторы*

ИЗУЧЕНИЕ СОРБЦИОННЫХ ХАРАКТЕРИСТИК МОДИФИЦИРОВАННОГО ЦЕОЛИТА

Султанбаева Г.Ш., Кайынбаева Р.А., Чернякова Р.М.*, Джусипбеков У.Ж.

АО Институт химических наук им. А.Б.Бектурова, Алматы, Казахстан

Резюме. *Введение.* Загрязненные производственные стоки содержат концерогенные металлы, негативно влияющие на здоровье человека.Исследования в области процессов очистки жидких сред, загрязненных тяжелыми металлами, с использованием эффективных, доступных, недорогих и экологически чистых сорбентов и сорбционных материалов на основе природного сырья, в частности цеолитаявляются актуальными.Природные цеолиты различных месторождений различаются по своему минералогическому составу, характеризуются менее эффективными сорбционными свойствами по сравнению с синтетическими сорбентами. Для улучшения сорбционных характеристик подобран недорогой модификатор - гуаровая камедь. *Цель работы*. Модификация природного цеолита гуаровой камедью методом осаждения и определение оптимальных условий, при которых достигается максимально высокие сорбционные

характеристики. *Результаты и обсуждение.* Изучение влияние расхода гуаровой камеди на свойства модифицированного цеолита показало, что с увеличением расхода модификатора статическая обменная емкость (СОЕ) катионита резко снижается. Найдено оптимальное время перемешивания при получении модифицированного сорбента (10 часов), при котором достигается максимальное значение СОЕ катионита - 1398 мг-экв/г.Изучение влияния температуры перемешивания показало, что в диапазоне от 25°С до 75°С сорбционные характеристики композитного сорбента изменяются незначительно. А повышение температуры сушки до 100 °С приводит к улучшению сорбционных характеристик сорбента, особенно в отношении сорбции катионов. *Заключение.* Изучены условия модификации природного цеолита природным полисахаридом (гуаровой камедью) методом осаждения. Определены оптимальные условия проведения процесса модификации сорбента и получен новый сорбент, в котором сорбционная емкость по катиониту, сорбционная емкость по аниониту, ОСЕ и СОП в 15 раз, в 85.6 раз, в 9.7 раз в и 77 раз больше по сравнению с природным цеолитом.

Ключевые слова: природный цеолит, модификация цеолита, гуровая камедь, статическая обменная емкость, суммарный объем пор, общая сорбционная емкость

Гита Шамильевна Султанбаева	*Кандидат технических наук*
Раушан Алибековна Кайынбаева	*Кандидат технических наук*
Раиса Михайловна Чернякова	*Доктор технических наук, профессор*
Умирзак Жумасилович Джусипбеков	*Академик НАН РК, профессор, доктор технических наук*

References

1. Pal S., Patra A.S., Ghorai S., Sarkar A.M., Mahato V., Sarkar S., Singh R.P. Efficient and rapid adsorption characteristics of templating modified guar gum and silica nanocomposite toward removal of toxic reactive blue and Congo red dyes, *Bioresour. Technol.* **2015**. 291–299. https://doi.org/10.1016/j.biortech.2015.04.099

2. Medvedev I.F., Derevyagin S.S. *Heavy metals in ecosystems. Monograph.* Saratov: OOO «Rakurs», **2017**. 178 p. ISBN: 978-5-9758-1665-8. https://w.eruditor.one/file/2419157/

3. Osovskaya I.I., Antonova V. Effect of Acid and Enzymatic Hydrolysis of Cellulose on its Physicochemical Properties for Improved Moisture-Absorption DOI: 10.1007/s10692-025-10603-9

4. Influence of capillary-porous structure of cellulose on physicochemical properties of fibrous material. Polomarchuk D.A., Osovskaya I.I., Sevastyanova J.V., Bogolitsyn K. G., Parshina A., Bogdanovich N.I. Chemistry of plant raw material. **2025**, no. 1, pp. 351–362. DOI: 10.14258/jcprm.20250114679

5. Electronic resource: www.frontiersin.org/journals/chemistry/articles/10.3389/fchem.2024.1410876/full (accessed 21.04.2025).

6. Bobylev A.E. *Synthesis, structure, and functional properties of composite sorbents "Cationite KU-3x9-MeS [Me – Cu(II), Zn, Pb]"* / PhD dissertation, Physical Chemistry, Ural Federal University named after the first President of Russia B.N. Yeltsin, Yekaterinburg, **2016**. 160 p. https://search.rsl.ru/ru/record/01008692224

7. Shkuratov A.L. *Preparation of sorbents and membranes based on natural silicates for purification of solutions from pollutants of various nature* / PhD dissertation, Ecology (Chemistry), Far Eastern Federal University, Vladivostok, **2018**. 156 p. https://search.rsl.ru/ru/record/01009702096

8. Koganovsky A.M., Levchenko T.M., Kirichenko V.A. *Adsorption of dissolved substances.* Kyiv, **1977**. 250 p. https://search.rsl.ru/ru/record/01007677156

9. GOST 4453-74. *Powdered activated carbon for clarification.* Moscow: Standards Publishing, **1993**. 6 p.

Chemical Journal of Kazakhstan
Volume 2, Number 94(2026), 81-91 https://doi.org/10.51580/2026-2.2710-1185.16

UDC 665.64

CATALYTIC PROCESSING OF NATURAL BITUMEN FROM BITUMINOUS SANDS

Y.I. Imanbayev*, Y.A. Akkazin, Y.K. Ongarbayev, Y. Tileuberdi, A.K. Rakhimova, Y. Kanzharkhan

Institute of Combustion Problems, Almaty, Kazakhstan

**Corresponding author e-mail: erzhan.imanbayev@gmail.com*

Abstract: *Introduction.* Bituminous sands deposits are a very rich source of energy in bitumen. However, access to the main part of these reserves is difficult, and the conversion of bitumen into liquid, low-sulfur products require innovative solutions, since the properties of traditional oil and bitumen are significantly different. *Methods.* To obtain the necessary products from bituminous sands, it is first necessary to separate organic part from the bituminous sands, and only then it can be further processed. Currently, industrial bitumen production in Canada is carried out using mining technology. In this regard, Kazakhstan needs to develop domestic technology in accordance with its West Kazakhstan conditions and domestic demand. *Results and discussion.* High-temperature cracking processes of West Kazakhstan natural bitumens in the presence of mesoporous aluminosilicate, synthetic zeolite and natural zeolite catalysts have been studied. The catalysts lead to the formation of liquid products up to 92.2%, reducing the number of tar-asphaltene compounds from 52.4% to 16.3%. *Conclusion.* Natural bitumen from the Beke and Munaily Mola fields is classified as heavy oil and consists mainly n-alkanes, terpanes, and steranes. A mesoporous aluminosilicate catalyst enabled efficient catalytic cracking, giving up to 89% liquid products and increasing oil and light fraction yields. High activity is attributed to the large pore size. Cracking destroys aliphatic and polynaphthenic structures in asphaltenes, increases aromaticity, and reduces oxygen-containing compounds, while resins show increased aromaticity due to the breakdown of naphthenic rings and alkyl groups.

Key words: natural bitumen, catalysts, cracking, tar-asphaltene compounds, reaction direction

Yerzhan Imanbaiuly Imanbayev	*PhD, Associate Professor, Leading Researcher;* *E-mail: erzhan.imanbayev@gmail.com*
Yerzhan Asetovich Akkazin	*PhD, Associate Professor, Leading Researcher;* *E-mail: erzhan_akkazin@mail.ru*
Yerdos Kalimullauly Ongarbayev	*D.Sc., Professor, Head;* *E-mail: erdos.ongarbaev@kaznu.edu.kz*
Yerbol Tileuberdi	*PhD, Associate Professor, Leading Researcher;* *E-mail: er.tileuberdi@gmail.com*
Ainura Kairatovna Rakhimova	*PhD, Leading Researcher;* *E-mail: ainura_302015@mail.ru*
Yernar Kanzharkan	*Researcher; E-mail: kanzharkanyernar@gmail.com*

Citation: Imanbayev Y.I., Akkazin Y.A., Ongarbayev Y.K., Tileuberdi Y., Rakhimova A.K., Kanzharkhan Y. Catalytic processing of natural bitumen from bituminous sands. *Chem. J. Kaz.*, **2026**, 2*(94)*, 81-91. DOI: https://doi.org/10.51580/2026-2.2710-1185.16

1. Introduction

Kazakhstan's oil sector occupies a leading position in the national economy. Today, many of Kazakhstan's oil and gas fields were discovered in the 1930s and 1940s and are in the late stages of development. Most of these fields are hard-to-recover, highly viscous oils, and over 40% are sulfur and high-sulfur. Therefore, the oil and gas industry will have to increasingly focus on developing and bringing heavy, highly viscous, hard-to-recover oil fields into commercial production [1].

Direct cracking of heavy feedstocks is the simplest method technically. However, the presence of impurities in the feedstock deactivates the catalyst, promotes intensive coke formation, reduces process selectivity, and degrades the quality of the products. Pre-treatment of residual feedstock increases product yield and quality, but increases the cost of the process. Solvent-based catalytic cracking is most often used to upgrade feedstock. Deasphalting using various hydrocarbon solvents from C_3 to C_5 or their mixtures, as well as light gasolines. Less common are thermal adsorption deasphalting processes using contacts with large pores, a small surface area, and low activity. The deasphalted products and distillates obtained from these processes can be used (directly or after desulfurization) as feedstock for catalytic cracking units. These processes result in the removal of resins and asphaltenes, fairly deep demetallization , and partial desulfurization and denitrogenation, which significantly facilitates subsequent processing by catalytic processes [2-5].

The conversion of heavy crude oils into synthetic crude [6] involves mild thermal cracking of fuel oil in soaking chambers downstream of the atmospheric column. The possibility of additionally introducing physical energy into the visbreaking process in the form of acoustic cavitation is indicated. The developed technology enables the production of up to 70% synthetic crude, with a 20% increase in gasoline fractions and a 17% increase in diesel fractions compared to the original crude, and approximately 30% residue. The residual product after the thermal polycondensation unit has a density of 990-1000 kg/m^3 and, in quality, corresponds to the most liquid grades of road bitumen.

A variant of processing natural bitumen, called Donor Refined Bitumen [7], where the distillate fractions are first distilled from the bitumen, and the residue with a boiling point above 500°C is mixed with a hydrogen donor solvent. The latter is the circulating product of the process, which is pre- hydrogenated to restore the donor capacity. Hydrocracking of the mixture is carried out at a temperature of 410-460°C and a pressure of 3.5-5.5 MPa, with the degree of conversion reaching 70%. By mixing the final product with light fractions of bitumen, synthetic oil is obtained, which does not contain residual fractions. However, the use of hydrocracking as the main process for processing natural bitumen requires higher hydrogen consumption and the involvement of significant resources of natural gas or other hydrocarbon feedstock for its production.

Currently, global experience is based on approximately 20 processes for upgrading natural bitumen, deposits of which are at various stages of

development [8-10]. However, if we consider projects that have reached the industrial level, it is necessary to note that technologies traditionally used for processing heavy residues are being employed: coking, hydrogenation, and deasphalting. There is an ongoing debate regarding the optimal method for increasing the hydrogen:carbon ratio. Many researchers believe that delayed coking offers potential. The advantage of this process is the absence of hydrogen production, which significantly reduces capital investment. However, the low quality of the products in terms of sulfur and unsaturated hydrocarbon content, as well as problems with the use of low-grade coal, are increasingly limiting the use of this technology.

Natural bitumens and heavy oils are characterized by high contents of metals, N, S, and O, which create difficulties during oil refining. Concentrations of heteroatom-containing compounds in oil may be relatively low, but their impact during oil refining can be significant. The presence of these compounds in the catalytic system creates significant process limitations, causing catalytic poisoning and catalyst deactivation [11, 12]. In finished products, heteroatom-containing compounds can also cause problems, including instability during storage and discoloration. Therefore, studying the composition of high-molecular heteroorganic compounds in oil is very important.

A literature review reveals that natural bitumen from oil-bituminous rocks is an important source of hydrocarbon feedstock, and interest in it is growing annually. However, its use as a feedstock requires efficient extraction of bitumen from -bituminous sands, study of the physicochemical composition and properties, and development of processing processes. Extraction of natural bitumen from bituminous sands is dependent on the chemical composition and nature of the natural bitumen, its resin, asphaltene, and heteroatom content. Therefore, important objectives of this study include extracting natural bitumen from bituminous sands and studying the changes in high-molecular compounds during thermal processing of natural bitumen using catalytic additives. Thus, it follows from the above that cracking natural bitumen produces synthetic crude oil whose characteristics (density, viscosity, molecular weight and others) exceed those of conventional crude oils, and its processing using a conventional process flowsheet can yield a wide range of hydrocarbon components.

2. Experimental part

A distinctive feature of Kazakhstan's bituminous deposits is the outcrop of bituminous sands at the surface. In these reactivated deposits, in zones of active water exchange, light fractions have been lost, and the residual petroleum components have been exposed to various supergene factors, which have led to a heavier composition and the formation of slow-moving extra-heavy oils and solid bitumens. Bitumen deposits occur in the form of small lenses and interlayers. Visual analysis of a sample of bituminous sands reveals a rich black color with a bitumen sheen. All rock grains are coated and glued together by viscous bitumen. At a temperature of 20°C, the bituminous sands are difficult to separate into

individual pieces. When the temperature rises to 50-60°C, due to the decrease in bitumen viscosity, the sands is easily crushed with a spatula and forms a mastic-like mass. The organic part of the bituminous sands was extracted by solvent. The solvent extraction method allows to determine the exact amount of organic matter in bituminous sands and facilitates the complete extraction of the organic part. Extraction of natural bitumen from bituminous sands was carried out with chloroform.

Table 1 - Physical-chemical characteristics of natural bitumens

Indicator	Bituminous sand deposit	
	Beke	Munaily Mola
Content in bituminous sands, wt. %	10-12	16-25
Density, g/cm^3	0.99	0.99
Total sulfur content, %	1.5	1.4
Ash content, %	0.4	0.5
Coking ability, %	30	35
Viscosity at 80°C, cSt	21	26
Softening temperature, °C	20	41
Pour point, °C	18	16
Content of mechanical impurities, wt. %	0.08	0.11

Table 1 present physical and chemical characteristics of natural bitumens from two bituminous sands. Natural bitumen extracted from the Beke deposit is characterized by the following indicators: density 0.99 g/cm^3; freezing point +18°C; degree of coking 30%; ash content 0.4%; softening point +20°C. The content of natural bitumen in the sands of the Munaily Mola deposit ranges from 16 to 25% and is characterized by high values of density, viscosity, and degree of coking. Extra-heavy oils also have these characteristics.

Methodology for thermal cracking of natural bitumen

Thermal catalytic cracking of natural bitumen was conducted in a steady-state mode in 12-ml autoclave reactors. The bitumen mass loaded into the reactor was 7 g. The experiments were conducted in air, which does not significantly change the composition of the resulting products due to the small volume, at a temperature of 450°C for 60 minutes. During the experiment, the mass of the reactor without a sample and the mass of the reactor with a sample, prepared for the experiment, were recorded. After the heat treatment of natural bitumen, the yield of gaseous products was determined by the mass loss of the reactor with a sample after removing the gas products from the reactor. After collecting the liquid products, the reactor was washed with chloroform and weighed. The resulting difference between the mass of the reactor before and after the experiment was defined as coke.

Table 2 presents the characteristics of the mesoporous aluminosilicate (MP), zeolite in active hydrogen form (HY), as well as natural zeolite (NZ) catalysis. The zeolite catalyst (HY) has a high specific surface area of 874 m^2/g with a small

pore size (7.4 nm). In [12], it was shown that this catalyst increases the depth of destruction of the resinous components of heavy oil with the production of low-boiling fractions. The MP catalyst has a lower specific surface area (600 m^2/g), but its pore size is almost 7 times higher and is 50 nm. MP was used based on the assumption that it is the large pore size that will increase the depth of destruction of resins and asphaltenes without developing a coke deposition reaction. Zeolite heulandite-clinoptilolite from the Tayzhuzgen deposit (East Kazakhstan region, Tarbagatai district), activated by acid treatment and calcination, was used as a natural catalyst.

Table 2 - Characteristics of natural bitumen cracking catalysts

Catalyst	Pore size, nm	Specific surface area, m^2/g	Silicate module	Concentration of acid sites, μmol/g
MP	50	600	20	
HY	7.4	874	4.9	929
NZ	10.4	7.2		

Methodology for determining the material composition of liquid products

The organic matter composition was determined using a traditional approach: first, the asphaltene content of the sample was determined using the "cold" Golde method. The resin concentration in the resulting maltenes was then determined by adsorption. The analyzed product was applied to activated silica gel, the mixture was placed in a Soxhlet extractor, and the hydrocarbon components (oils) were sequentially eluted with n-hexane and the resins with an ethanol-benzene mixture (method 1217-2005, Institute of Petroleum Chemistry).

3. Results and discussion

Thermal degradation processes for heavy hydrocarbon feedstocks can increase the yield of low-boiling liquid products, forming coke and gas as byproducts. Cracking processes in the presence of various catalysts are of particular interest. Thermal cracking of natural bitumen produces liquid products and coke, along with a small amount of gas (Table 3). The yield of liquid cracking products from Munaily Mola bitumen was 6% higher than from Beke bitumen, while the yield of coke was lower 4.7%. Thermal processing increases the oil content, while the total amount of high-molecular-weight components in the bitumen decreases. This is likely due to increased coke formation and the breakdown of resinous components, resulting in lighter products. The data obtained indicate that the high-molecular-weight components of Munaily Mola bitumen are more readily cracked than those of Beke bitumen.

The most probable mechanism of catalytic cracking of hydrocarbons is considered to be the carbonium ion mechanism:

Catalyst + Bitumen → Coke/Catalyst + Liquid Product + Gas

Coke/catalyst + $2O_2$ → Catalyst + $2CO$ + CO_2 (regeneration)

Table 3 - Material balance of the process of thermal catalytic cracking of bitumen

Process	Content, wt . %		
	Gas	Coke	Liquid products
Natural bitumen from the Beke deposit			
Natural bitumen	0	0	100.0
Cracking	1.4	30.9	67.7
Cracking with mesoporous cat.	2.2	8.8	89.0
Cracking with synthetic zeolite	2.7	7.7	89.6
Cracking with natural zeolite	1.0	19.1	79.9
Natural bitumen from the Munaily Mola deposit			
Original bitumen	0	0	100.0
Cracking	0.2	26.2	73.6
Cracking with mesoporous cat.	1.4	7.4	91.2
Cracking with synthetic zeolite	1.6	6.2	92.2
Cracking with natural zeolite	1.2	13.4	85.4

Catalytic cracking of bitumen with a mesoporous catalyst reduces coke yield by 3.5 times for both types of bitumen. For Beke bitumen, the yield of gaseous products increases from 1.4% to 2.2%, while for Munaily Mola bitumen, the gas content increases sevenfold to 1.4% by weight. Oil content increases by more than 1.5 times compared to the initial content. This increase is due to the extensive degradation of resins, the amount of which in the cracking products decreases by more than fourfold.

The use of a synthetic zeolite (HY) catalyst also significantly slows down coke formation, with the yield of solid cracking products being 1% lower by weight compared to bitumen cracking with an MP catalyst. This catalyst allows for the significant destruction of high-molecular components of bitumen (more than 51% relative), but their content in liquid cracking products is higher than in experiments using an MP catalyst.

A natural zeolite catalyst is a catalytic additive for thermal cracking and hydrogenolysis of heavy hydrocarbons. Natural zeolite prevents secondary polymerization of the resulting low-molecular-weight fragments, is resistant to sulfur poisoning, and is capable of binding nitrogen and sulfur from the products. It is also inert to the mineral component of bituminous sands and the metals present in bitumen. At the same time, the coke and gas yields of both fields decreased by 12.2% and 11.6%, respectively, at the Beke and Munaily Mola fields, compared to thermal cracking.

Table 4 - Group composition of products of thermal catalytic cracking of natural bitumen

Process	Content, wt. %		
	Oils	Resins	Asphaltenes
Natural bitumen from the Beke deposit			
Natural bitumen	49.2	44.9	5.9
Cracking	61.3	28.3	10.4
Cracking with mesoporous cat.	77.2	13.7	9.1
Cracking with synthetic zeolite	72.8	16.8	10.4
Cracking with natural zeolite	77.0	14.4	8.6
Natural bitumen from the Munayily Mola deposit			
Natural bitumen	47.6	46.4	6.0
Cracking	83.6	13.4	3.0
Cracking with mesoporous cat.	79.7	11.1	9.2
Cracking with synthetic zeolite	75.8	13.2	11.0
Cracking with natural zeolite	61.5	27.3	11.2

Table 4 presents the results of an analysis of the component composition of the products of cracking of natural bitumen. The natural zeolite catalyst affected the material composition of natural bitumen from the Beke field, with the oil content reaching 77% and the resin content decreasing by 14.4%. For natural bitumen from the Munaily Mola field, the yield of high-molecular components was 22.1% higher than with cracking. The data obtained show that the total content of resinous-asphaltene components in the cracking products of Munaily Mola bitumen changes (compared to the composition of the initial bitumen), with the asphaltene content decreasing by 50% and the resin content by 29%. However, when processing Munaily Mola bitumen with a mesoporous catalysis, despite a significant increase in the yield of liquid cracking products and their oil content, an increase in the asphaltene component content is observed. Moreover, the oil content in the liquid cracking products of Munaily Mola bitumen is 2% higher than that of the Beke bitumen. Cracking with synthetic zeolite led to increasing the resin and asphaltene content 22% for Munaily Mola bitumen and 27% for Beke bitumen. The resin content with the natural zeolite decreased by 30% for Beke bitumen compared to the composition of the initial bitumen, and the asphaltene content increased by 2%. Munaily Mola bitumen led to increasing the oil content 14% compared to the composition of the initial bitumen.

Thus, it has been established that the use of catalysts for these objects in the cracking process increases the destruction of high-molecular-weight components (up to 50% relative). The use of mesoporous and zeolite catalysts significantly enhances the cracking process. The presence of a mesoporous structure in the synthesized aluminosilicate ensures the accessibility of its active sites located in the bulk to large molecules of petroleum feedstock (resins and asphaltenes), where they undergo destruction. Metal particles promote disproportionation and

redistribution of hydrogen from high-molecular-weight compounds to components of gasoline and diesel fractions, thereby inhibiting coke formation.

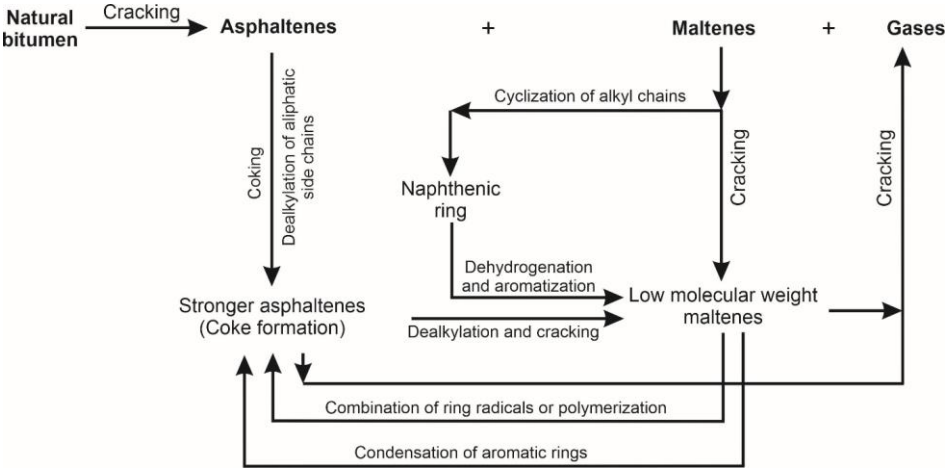

Figure 1 - Scheme of reactions of catalytic cracking of natural bitumen

Cracking at 450°C causes chemical structural changes, resulting in the formation of asphaltenes, coke, maltenes, and a small amount of gas (Figure 1). Asphaltenes in bitumen form coke, resins, and gaseous products. Coke formation occurs through dealkylation of the long aliphatic side chains of asphaltenes. The resulting strong asphaltenes, in the presence of a catalyst, form low-molecular-weight maltenes. Gaseous cracking products are then formed from the low-molecular-weight maltenes and more stable asphaltenes. Maltenes are converted at high temperatures via two reaction pathways: alkyl chain cyclization and cracking. Alkyl chain cyclization leads to the formation of an intermediate product a naphthenic ring. Naphthenic hydrocarbons then form more stable products through aromatization and dehydrogenation. As the concentration of low-molecular-weight maltenes in the system increases, the following reactions occur: radical combination (polymerization) and condensation of aromatic rings. All these reactions lead to the formation of more stable asphaltenes and then coke. Thus, thermal processing of bitumen involves primary and secondary reactions. Primary reactions during thermal cracking of bitumen mainly proceed in three directions: stable asphaltenes (coke), maltenes, and gases. Strong asphaltenes and maltenes can also undergo secondary reactions, such as dealkylation of aliphatic side chains, cyclization of alkyl chains, recombination of ring radicals or polymerization, dehydrogenation and aromatization of naphthenic rings, and condensation of aromatic rings.

4. Conclusion

The group and detailed physical-chemical composition of natural bitumen from the Beke and Munayly Mola fields shows that both hydrocarbons are heavy oils and the composition of the oils is represented by n-C_{22}-C_{25} -alkanes, aromatic hydrocarbons such as terpanes (pentacyclanes), steranes (tetracyclanes).

A mesoporous aluminosilicate catalyst was proposed for the catalytic cracking of natural bitumen from the Beke and Munaily Mola deposits. This catalyst resulted in liquid products with an 89% yield and increased oil content (77%) and light fractions. The high activity of the mesoporous catalyst is due to the large pore size (50 nm).

As a result of cracking, aliphatic and polynaphthenic structures in the asphaltene structure are destroyed, aromaticity increases, and the number of oxygen-containing structures decreases. In the resin structure, the aromaticity factor increases with the destruction of naphthenic rings and alkyl substituents.

Funding: This research has been funded by the Science Committee of the Ministry of Science and Higher Education of the Republic of Kazakhstan (Grant No. AP26100405).

Conflict of Interest: The authors declare no conflicts of interest requiring the disclosure in this paper.

МҰНАЙБИТУМДЫ ЖЫНЫСТАРДАҒЫ ТАБИҒИ БИТУМДАРДЫ КАТАЛИТИКАЛЫҚ ӨҢДЕУ

Е.И. Иманбаев, Е.Ә. Акказин, Е.К. Оңғарбаев, Е. Тілеуберді, А.К. Рахимова, Е. Қанжарқан

Жану проблемалары институты, Алматы, Қазақстан

Түйіндеме. *Кіріспе.* Мұнайбитумды жыныстар кенорындары битумға өте бай энергия көзі болып табылады. Дегенмен, бұл қорлардың негізгі бөлігіне қол жеткізу қиын, ал битумды сұйық, аз күкіртті өнімдерге айналдыру инновациялық шешімдерді қажет етеді, себебі дәстүрлі мұнай мен битумның қасиеттері айтарлықтай ерекшеленеді. *Әдістер.* Мұнайбитумды жыныстан қажетті өнімдерді алу үшін алдымен битумды жыныстан оны бөліп алу керек, содан кейін ғана оны әрі қарай өңдеуге болады. Қазіргі уақытта Канадада өнеркәсіптік битум өндірісі тау-кен технологиясын қолдану арқылы жүзеге асырылады. Осыған орай, Қазақстан өзінің Батыс Қазақстан жағдайына және ішкі сұранысқа сай отандық технологияны дамыту керек. *Нәтижелер және талқылау.* Батыс Қазақстан табиғи битумдарының мезокеуекті алюмосиликат, синтетикалық цеолит және табиғи цеолит катализаторлары қатысында жоғары температура крекинг процестері зерттелді. Катализаторлар 92,2 % дейін сұйық өнімдер түзілуіне әкеледі, шайырлы-асфальтенді қосылыстардың мөлшерін 52,4 %-дан 16,3 % дейін төмендетеді. *Қорытынды.* Беке және Мунайлы Мола кен орындарының табиғи битумдары ауыр мұнайға жатады және негізінен н-алкандарынан, терпандар мен стерандардан тұрады. Мезокеуекті алюмосиликатты катализаторды қолдану каталитикалық крекингтің тиімділігін арттырып, сұйық өнімдердің шығымын 89%-ға дейін жеткізді және жеңіл фракциялар үлесін көбейтті. Катализатордың жоғары белсенділігі ірі кеуек өлшемімен түсіндіріледі. Крекинг нәтижесінде асфальтендердегі алифатты және полинафтенді құрылымдар бұзылып, ароматтылық артады, ал оттекқұрамды қосылыстар саны азаяды; шайырларда ароматтылық нафтен сақиналары мен алкил топтарының ыдырауы есебінен өседі.

Түйінді сөздер: табиғи битум, катализаторлар, крекинг, шайырлы-асфальтенді қосылыстар, реакциялар бағыты

Ержан Иманбайұлы Иманбаев	*PhD, қауымдастырылған профессор, жетекші ғылыми қызметкер*
Ержан Әсетұлы Акказин	*х.ғ.к., қауымдастырылған профессор, жетекші ғылыми қызметкер*
Ердос Калимуллаұлы Оңғарбаев	*х.ғ.д., профессор*
Ербол Тілеуберді	*PhD, қауымдастырылған профессор, жетекші ғылыми қызметкері*
Ернар Канжаркан	*PhD, жетекші ғылыми қызметкер*
Айнура Қайратқызы Рахимова	*техника ғылымдары магистры, ғылыми қызметкер*

КАТАЛИТИЧЕСКАЯ ПЕРЕРАБОТКА ПРИРОДНЫХ БИТУМОВ НЕФТЕБИТУМИНОЗНЫХ ПОРОД

Е.И. Иманбаев, Е.А. Акказин, Е.К. Онгарбаев, Е. Тилеуберди, А.К. Рахимова, Е. Канжаркан

Институт проблем горения, Алматы, Казахстан

Резюме. *Введение.* Битумы в залежах битуминозных песчаников потенциально представляют собой очень богатый источник энергии. Вместе с тем, доступ к основной части этих запасов затруднен, и для превращения битумов в жидкие малосернистые продукты потребуются нестандартные решения, так как свойства обычной нефти и битумов существенно различаются. *Методы*. Для получения целевых продуктов из нефтебитуминозной породы сначала необходимо осуществить извлечение битумов из породы, и только после этого можно дальше перерабатывать. В настоящее время промышленная добыча битумов в Канаде ведется с применением горнотехнических методов. В связи с этим Казахстану необходимо развивать отечественные технологии, адаптированные к условиям Западного Казахстана и внутреннему спросу. *Результаты и обсуждение.* Были исследованы процессы высокотемпературного крекинга природных битумов Западного Казахстана в присутствии мезопористого алюмосиликатного, синтетического цеолитного и природного цеолитного катализаторов. Применение катализаторов обеспечило выход жидких продуктов до 92,2 % и снижение содержания смолисто-асфальтеновых соединений с 52,4 % до 16,3 %. *Заключение.* Групповой и детальный физико-химический анализ показал, что природные битумы месторождений Беке и Мунайлы Мола относятся к тяжелым нефтям и содержат н-алканы, а также ароматические углеводороды (терпаны и стераны). Для их каталитического крекинга предложен мезопористый алюмосиликатный катализатор, обеспечивающий выход жидких продуктов до 89% и повышение доли нефтяной фазы до 77% за счет увеличения легких фракций. Высокая активность катализатора обусловлена крупным размером пор. В результате крекинга разрушаются алифатические и полинафтеновые структуры асфальтенов, возрастает ароматичность и снижается содержание кислородсодержащих соединений; в смолах увеличивается ароматичность за счёт разрушения нафтеновых колец и алкильных заместителей.

Ключевые слова: природный битум, катализатор, крекинг, смолисто-асфальтеновые компоненты, направление реакции.

Ержан Иманбайұлы Иманбаев	*PhD, Ассоциированный профессор, ведущий научный сотрудник*
Ержан Әсетұлы Акказин	*к.х.н., Ассоциированный профессор, ведущий научный сотрудник*
Ердос Калимуллаұлы Оңғарбаев	*д.х.н., профессор,*
Ербол Тілеуберді	*PhD, Ассоциированный профессор, ведущий научный сотрудник*
Ернар Канжаркан	*PhD, ведущий научный сотрудник*
Айнура Қайратқызы Рахимова	*магистр технических наук, научный сотрудник*

References

1. Kuantayev N.E., Turkov O.S. Atlas of oil and gas fields of the Republic of Kazakhstan. In 2 volumes. Almaty, Kong, **2020**. (In Russian)

2. T.A. Al-Attas, S.A. Ali, M.H. Zahir, Q. Xiong, S.A. Al-Bogami, Z.O. Malaibari, S.A. Razzak, M.M. Hossain. Recent Advances in Heavy Oil Upgrading Using Dispersed Catalysts. *Energy Fuels*. **2019**. Vol. 33(9). P. 7917-7949. https://doi.org/10.1021/acs.energyfuels.9b01532

3. Ayapbergenov E., Turkpenbaeva B., Akhmetov A., Turkmenbaeva M., Akkenzheeva A., Busurmanova A., Shakirova A. Prospects and integrated technologies for processing bituminous rocks in Kazakhstan. *Combustion and plasma chemistry*. **2025**. T. 23(2). P. 193-203. (In Russian) https://doi.org/10.18321/cpc23(2)193-203

4. B. Thangaraj, Y. K. Lee. Recent progress in catalytic aquathermolysis of heavy oils. *Fuel*. Vol. 372. **2024**. 132089. https://doi.org/10.1016/j.fuel.2024.132089

5. M. Ahmadi, Z. Chen. Challenges and future of chemical assisted heavy oil recovery processes. *Advances in Colloid and Interface Science*. Vol. 275. **2020**. 102081. https://doi.org/10.1016/j.cis.2019.102081

6. L. Wang, J. Guo, C. Li, R. Xiong, X. Chen, X. Zhang. Advancements and future prospects in in-situ catalytic technology for heavy oil reservoirs in China: A review. *Fuel*. Vol. 374. **2024**. 132376. https://doi.org/10.1016/j.fuel.2024.132376

7. M.A. Suwaid, M.A. Varfolomeev, A.A. Al-Muntaser, N.I. Abdaljalil, R. Djimasbe, N. O. Rodionov, A. Zinnatullin, F.G. Vagizov. Using the oil-soluble copper-based catalysts with different organic ligands for in-situ catalytic upgrading of heavy oil. *Fuel*. Vol. 312. **2022**. 122914. https://doi.org/10.1016/j.fuel.2021.122914

8. L. Foss, N. Petrukhina, G. Kayukova, M. Amerkhanov, G. Romanov, Y. Ganeeva. Changes in hydrocarbon content of heavy oil during hydrothermal process with nickel, cobalt, and iron carboxylates. *Journal of Petroleum Science and Engineering*. Vol. 169. **2018**. P. 269-276. https://doi.org/10.1016/j.petrol.2018.04.061

9. J. Ancheyta, J. Speight. Hydroprocessing of Heavy Oils and Residua. **2007**. CRC Press Taylor & Francis Group. 376 p. https://doi.org/10.1201/9781420007435

10. Imanbayev Y., Ongarbayev Y., Tileuberdi Y., Krivtsov E., Golovko A., Mansurov Z. High temperature transformation of tar-asphaltene components of oil sand bitumen. *Journal of the Serbian Chemical Society*. **2017**. Vol. 82(9). P. 1063-1073. https://doi.org/10.2298/JSC161126069I

11. M. Seidy- Esfahlan , S. A. Tabatabaei-Nezhad, E. Khodapanah. Comprehensive review of enhanced oil recovery strategies for heavy oil and bitumen reservoirs in various countries: Global perspectives, challenges, and solutions. *Heliyon*. Vol. 10. **2024**. e37826. https://doi.org/10.1016/j.heliyon.2024.e37826

12. Sviridenko N.N. Regularities of thermal transformations of natural bitumen components: diss. ... can. chemistry sciences: 02.00.13. Tomsk, **2016**. 134 p. (In Russian)

Chemical Journal of Kazakhstan
Volume 2, Number 94(2026), 92-101 https://doi.org/10.51580/2026-2.2710-1185.17

UDC 541.128

HYDROGENATION OF TOLUENE TO METHYLCYCLOHEXANE OVER PROMOTED SKELETAL NICKEL CATALYSTS

B.Sh. Kedelbaev[1], K.M. Lakhanova[2], S.K. Turtabaev[2], S.A.Shitybaev[2]*, G.Y. Kalymbetov[1]

[1]M.Auezov South Kazakhstan Research University, Shymkent, Kazakhstan
[2]South Kazakhstan Pedagogical University named after Ozbekali Zhanibekov, Shymkent, Kazakhstan

[*]Corresponding author e-mail: shitibaev.serikbek@mail.ru

Abstract. *Introduction.* Methylcyclohexane (MCH) is a key solvent and a promising Liquid Organic Hydrogen Carrier (LOHC). The selective hydrogenation of toluene to MCH requires efficient, stable and cost-effective catalysts. Skeletal nickel (Raney Ni) is widely used but suffers from rapid deactivation. The purpose of this work is to develop multicomponent skeletal nickel catalysts modified by industrial ferroalloys (FeMo, FeTiMn, FeMn) and to study their catalytic performance in toluene hydrogenation. *Methods.* Catalysts were prepared by high-frequency induction melting of Ni-Al-ferroalloy systems, followed by leaching with 20% NaOH. Surface morphology and composition were characterized by SEM-EDXRS and BET. Kinetic experiments were carried out in a high-pressure autoclave (0.25 L) at 393–473 K and hydrogen pressures of 2.0–12.0 MPa. *Results.* The addition of 3.0 wt.% FeMo or 5.0 wt.% FeTiMn increased the hydrogenation rate by 2.2–2.5 times compared to unmodified Raney Ni. Specific surface area reached 82.1 m^2/g for Ni-Al-FeMo and 78.5 m^2/g for Ni-Al-FeTiMn. SEM-EDXRS showed uniform distribution of Fe, Mo, Ti, Mn in the nickel matrix. The reaction order was zero with respect to toluene and first with respect to H_2 (at 2-6 MPa). Apparent activation energy was 34.5 kJ/mol for Ni-Al-FeMo and 38.2 kJ/mol for Ni-Al-FeTiMn. The catalysts exhibited 99.9% selectivity to MCH and maintained >92% of initial activity after 100 h on stream. *Conclusion.* Ferroalloy-modified skeletal nickel catalysts are highly efficient, selective and stable, making them promising for industrial hydrogen storage and petrochemical applications.

Keywords: toluene, methylcyclohexane, hydrogenation, skeletal nickel, ferroalloys, kinetics, SEM-EDXRS

Kedelbaev Bakhytzhan Shilmirzaevich	*Doctor of Technical Sciences, Professor*
Lakhanova Kulzada Mergenbaevna	*Doctor of Agricultural Sciences, Professor*
Turtabayev Sarsenbek Koishabayevich	*Doctor of Technical Sciences, Professor*
Shitybayev Serikbek Altynbekovich	*Candidate of Chemical Sciences, Associate Professor*
Kalymbetov Gani Yeskermesovich	*PhD student, Senior research*

Citation: Kedelbaev B.Sh., Lakhanova K.M., Turtabaev S.K., Shitybaev S.A., Kalymbetov G.Y. Hydrogenation of toluene to methylcyclohexane over promoted skeletal nickel catalysts. *Chem. J. Kaz.*, **2026**, 2*(94)*, 92-101. DOI: https://doi.org/10.51580/2026-2.2710-1185.17

1. Introduction

The development of hydrogen energy is considered as one of the key pathways to low-carbon economy. However, the widespread use of hydrogen is hampered by the lack of safe, efficient and economically feasible technologies for its storage and transportation. Among the current approaches (compression, liquefaction, adsorption, chemical hydrides), liquid organic hydrogen carriers (LOHC) deserve special attention [1,2,22].

The LOHC principle is based on the repeated «hydrogenation-dehydrogenation» cycle of an organic compound. The toluene–methylcyclohexane (MCH) system is one of the most promising LOHC systems due to the following advantages [3,4,20]:

Parameter	Toluene	Methylcyclohexane (MCH)
Boiling point, °C	110.6	101
Mass conc., wt%	–	6.16
Density, g/cm³	0.87	0.77
Toxicity	low	extremely low

Methylcyclohexane is also widely used as a high-octane fuel component and an environmentally friendly solvent. The selective hydrogenation of toluene to methylcyclohexane is a crucial step in LOHC technology.

Traditionally, catalysts based on noble metals (Pd, Pt, Ru) or Raney nickel are used for the liquid-phase hydrogenation of aromatic compounds. Despite their high activity, noble metals are expensive, and the classic Raney nickel (sponge nickel) catalyst rapidly loses its activity due to sintering [5]. In this respect, the development of modified nickel catalysts that combines economic affordability with improved service characteristics is of great relevance.

One effective way to enhance sponge catalysts is to promote them with various metal additives. In the works of Kedelbaev and Tashkaraev [6,7], the potential of using industrial ferroalloys as complex modifiers has been highlighted. Ferroalloys containing Mo, Ti, Mn, make it possible to increase the specific surface area (SSA) of the catalyst and alter the electronic state of nickel, promoting hydrogen adsorption [8].

In recent years, highly efficient catalytic systems have been proposed for the hydrogenation of toluene, including MOF-based Ni-Co bimetallic nanoparticles [9], Ni catalysts encapsulated in zeolites [10], as well as the unique material $LaNi_5$, which combines the functions of a catalyst and a hydrogen reserve [11,21,25]. Unfortunately, these systems are difficult to scale up. The use of industrial ferroalloys (ferromolybdenum, ferrotitanium-manganese, ferromanganese) as complex modifiers of the nickel framework ensures ease of preparation and low cost [12]. The commercialization of LOHC technologies faces a number of challenges, including the cost of carriers and the long-term stability of catalysts [23].

The purpose of this work – is the development of multicomponent nickel sponge catalysts, promoted by ferroalloys (FeMo, FeTiMn, FeMn), and to

investigate their physicochemical and catalytic properties in the liquid-phase hydrogenation of toluene.

2. Experimental part

2.1 Preparation of catalysts

Starting alloys with a composition of Ni:Al = 50:50 (wt.%) containing ferroalloy additives (FeMo – ferromolybdenum grade FMo60 per GOST 4759-91, Mo content ≥60%; FeTiMn – ferrotitanium-manganese, Ti ~25%, Mn ~15%; FeMn – ferromanganese grade FeMn75 according to GOST 4755-91) were smelted in a high-frequency induction furnace (OKB-8020) in quartz crucibles at 1200-1500 °C. The amount of promoter varied from 1 to 10 wt%. The ingots were crushed to a particle size of <0.25 mm. Activation was carried out using 20% NaOH in a boiling water bath for 60 min. The catalyst was washed to pH 7 and stored in ethanol. At least three parallel samples were prepared for each composition.

2.2 Analysis methods

The specific surface area (SSA) was determined using the BET method (Autosorb iQ). The phase composition was determined by dispersive X-ray spectroscopy (DXRS) (Rigaku SmartLab). The elemental distribution was determined by SEM-EDXRS (JEOL JSM-IT200). Kinetic experiments were conducted in a batch autoclave (0.25 L) equipped with a stirrer at 393–473 K and H_2 pressures of 2.0–12.0 MPa. Sample loading: 200 mL of toluene, 0.5 g of catalyst. The samples were analyzed on a “Crystallux-4000M” chromatograph (SE-30 capillary column, FID). Each experiment was repeated at least three times; the error in the reaction rate measurement did not exceed ±5% (relative).

2.3 Properties of used catalysts

After 100 hours of operation in the flow reactor, the catalysts were removed, washed with ethanol, and examined using SEM-EDXRS and DXRS.

3. Results and discussion

3.1 Physicochemical properties of catalysts

Table 1 provides the characteristics of the studied samples. The addition of ferroalloys increases the specific surface area by 1.5-1.7 times. The catalyst with 3% FeMo has the highest SSA (82.1 m²/g). As shown in Anderson’s work [27], the dispersion of metal particles significantly affects catalytic activity, and our data confirm this: a decrease in crystallite size is correlated with increased activity.

Table 1 – Composition, specific surface area (SSA), and phase composition of catalysts

Catalyst (wt.%)	SSA m²/g (avg. ± std. dev.)	Phase composition (DXRS)
Ni-Al (50:50)	54.2 ± 1.5	Ni, $NiAl_3$, Ni_2Al_3
Ni-Al-3%FeMo	82.1 ± 2.1	Ni, Mo, Fe, NiMo
Ni-Al-5%FeTiMn	78.5 ± 2.0	Ni, Fe, MnO_x, TiO_2
Ni-Al-3%FeMn	65.4 ± 1.8	Ni, Mn, MnO_x

3.2 Catalytic activity (kinetic curves)

Fig. 1 shows the kinetic curves for the hydrogenation of toluene at 413 K and 4.0 MPa. The Ni-Al-3%FeMo catalyst turned out to be the most active, ensuring an MCH yield of 88% in 60 minutes, which is 2.5 times higher than that achieved with unmodified nickel. The Ni-Al-5%FeTiMn catalyst demonstrated a yield of 83% in 60 min.

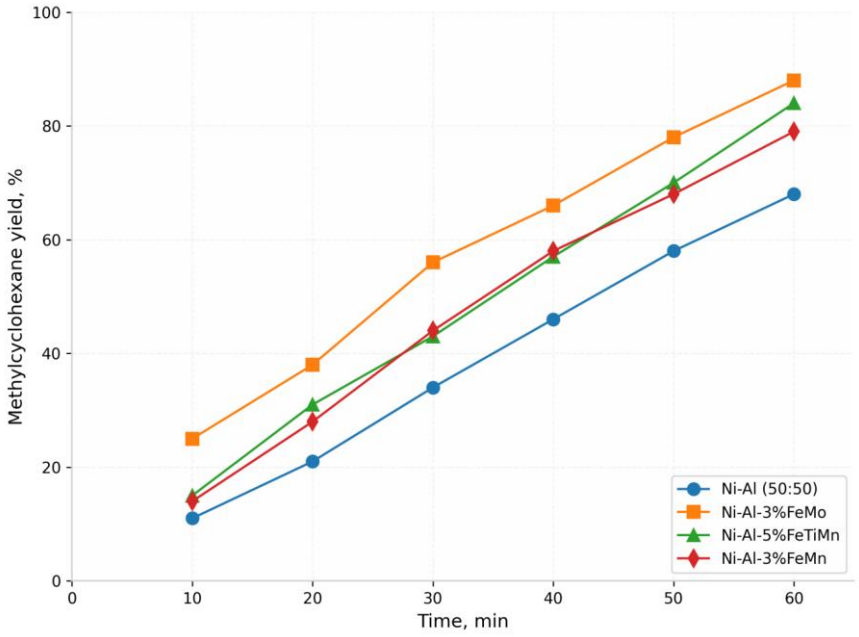

Fig. 1 - The kinetic curves for the hydrogenation of toluene (413 K, 4.0 MPa)

3.3 Kinetic trends

The rate dependence on toluene concentration (0.5–2.0 mol/L) exhibited zero-order kinetics with regards to the substrate. The rate dependence on hydrogen pressure (Fig. 2) was linear in the range of 2.0–6.0 MPa (first-order kinetics with regards to H_2). The apparent activation energy was 34.5 ± 1.2 kJ/mol for Ni-Al-3%FeMo and 38.2 ± 1.5 kJ/mol for Ni-Al-5%FeTiMn (45.0 ± 1.8 kJ/mol for Ni-Al). It confirms the promoting effect of ferroalloys. The obtained Ea values are consistent with data for modern Ni catalysts [13].

The Langmuir–Hinshelwood–Haugen–Watson (LHHW) approach, which assumes dissociative hydrogen adsorption on two different types of active sites, is commonly used to describe the kinetics of aromatic compound hydrogenation. Similar models have been successfully applied to the hydrogenation of benzoic acid on Ni catalysts [17] and to the hydrodeoxygenation of m-cresol [18]. The effect of water vapor on the hydrogenation of toluene over Ni catalysts was investigated in [19], where it was shown that even small additions of water can

alter the kinetic parameters. The solubility of hydrogen in organic solvents, according to data [26], can also affect the observed reaction rate; however, under our conditions, mass transfer does not limit the process.

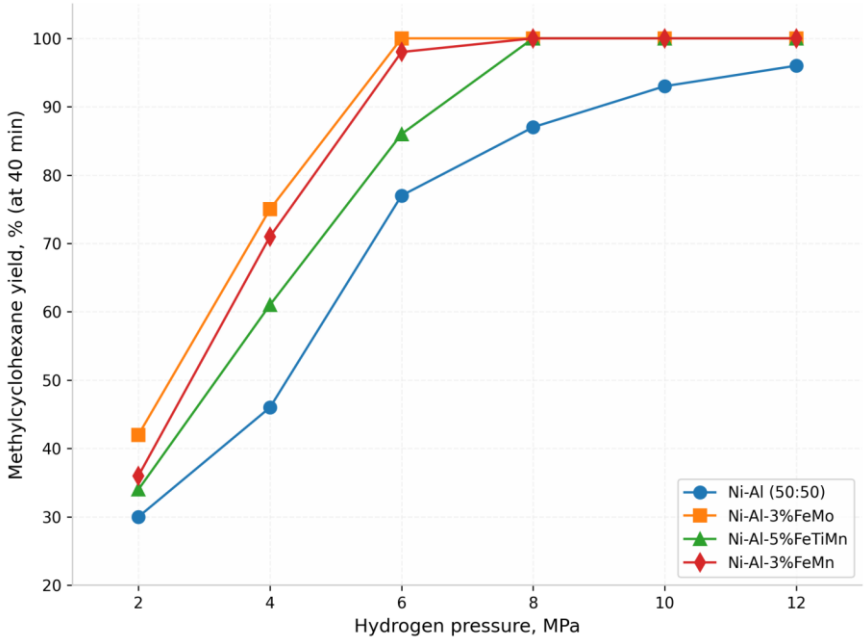

Fig. 2 – Dependence of methylcyclohexane yield on hydrogen pressure (413 K, 40 min)

3.4 Stability and selectivity

Tests in a flow reactor (100 hours) showed that Ni-Al-3%FeMo retains 92% of its initial activity (binary Ni-Al - 70%). Selectivity for MCH >99.9%. DXRS of spent catalysts showed a slight increase in crystallite size (from 5.4 to 6.1 nm for Ni-Al-3%FeMo compared to 5.4 to 8.2 nm for Ni-Al). The investigation of pressure distribution in a granular $LaNi_5$ layer [24] showed that the uniformity of particle packing is important for the long-term stability of reactors - we took this factor into account when preparing the catalyst layer.

3.5 Mechanism of Promoting Action of Ferroalloys

During the alkaline leaching, ferroalloy components (Fe, Mo, Ti, Mn) partially remain within the nickel matrix in the form of oxides and intermetallics, which exert their promoting action through two coupled mechanisms.

Electronic effect. Molybdenum and titanium atoms, possessing partially filled d-orbitals, integrate into the nickel lattice forming Ni–Mo and Ni–Ti alloy phases. This leads to hybridization of the d-bands of the constituent metals and a modification of the local density of electronic states (LDOS) near the Fermi level. The increased LDOS facilitates more efficient dissociative adsorption of

hydrogen via a reverse electron transfer from Ni to the promoter. Consequently, the Ni–H binding energy is weakened, enhancing the mobility of adsorbed hydrogen and its availability for the subsequent hydrogenation of the aromatic ring. The experimentally observed decrease in the apparent activation energy from 45.0 to 34.5-38.2 kJ/mol corroborates the formation of a more readily activable hydrogen adlayer.

Geometric effect. Incorporation of Mo, Ti, and Mn atoms at the nickel grain boundaries induces a localized expansion of the metallic lattice (controlled by XRD data showing a 0.8-1.2 % increase in the lattice parameter). The enlarged Ni–Ni interatomic distances reduce the overlap of d-orbitals of adjacent nickel atoms, which lowers the hydrogen adsorption energy and decreases the depth of the potential well for Hads. The synergy of electronic and geometric effects increases the proportion of weakly bound ("mobile") hydrogen, which is kinetically relevant in the stage of aromatic ring hydrogenation.

Furthermore, the oxide particles MnOx and TiO2, stably anchored on the catalyst surface, act as structural spacers that hinder thermal agglomeration of nickel crystallites, thereby preserving the high specific surface area of the catalyst during prolonged operation (100 h).

3.6 Comparison with commercial catalysts

Table 2 presents a comparison with commercial analogues. The developed Ni-Al-3%FeMo catalyst outperforms commercial Ni/Al_2O_3 catalysts in terms of both activity and stability and is on par with the best laboratory samples. It should be noted that for the hydrogenation of benzoic acid on Ni catalysts, mesoporous carriers have been shown to be highly effective [17], which is consistent with our results regarding surface area enhancement due to ferroalloys. The hydrogenation of N-ethylcarbazole on $LaNi_5$ [21] demonstrates an alternative approach using metal hydrides; however, our catalyst has the distinct advantage of being simple to prepare.

Table 2 – Comparison of catalytic properties

Catalyst	T, P	MCH yield per hour, %	Ea, kJ/mol	Stability (after 100 h.)
Ni-Al (50:50)	160°C, 4 MPa	68	45.0	70%
Ni-Al-3%FeMo (our version)	160°C, 4 MPa	88	34.5	92%
Ni/Al_2O_3 (commercial) [14]	180°C, 5 MPa	75	~50	85%
Ni/TiO_2 (lab.) [15]	150°C, 4 MPa	82	41.2	88%
Pt_1Co SAA [16]	180°C, 3 MPa	95	~40	95% (Pt savings)

4. Conclusion

1. Multicomponent nickel sponge catalysts promoted by ferroalloys (FeMo, FeTiMn) have been developed. The optimal compositions are Ni-Al-3%FeMo and Ni-Al-5%FeTiMn.

2. The rate of toluene hydrogenation on these catalysts is 2.2-2.5 times higher than on standard Raney nickel. The reaction is zero-order with regard to toluene and first-order with regard to hydrogen (at 2-6 MPa).

3. The apparent activation energy has been reduced to 34.5-38.2 kJ/mol.

4. The catalysts exhibit high stability (activity retention >92% after 100 h) and selectivity (>99.9%).

5. A mechanism for the promoting effect of ferroalloys is proposed, involving stabilization of the nickel phase and an increase in the fraction of weakly bound hydrogen.

6. In terms of their overall characteristics, the developed catalysts outperform commercial Ni/Al_2O_3 catalysts and are comparable to modern nanostructured systems.

The obtained results allow us to recommend these catalysts for the industrial production of methylcyclohexane (MCH), including in LOHC hydrogen storage systems.

Acknowledgments. We would like to express our sincere gratitude to the following academic institutions – the Department of Chemistry at the O. Zhanibekov South Kazakhstan Pedagogical University and the “Industrial Biotechnology” Research Laboratory at the M. Auezov South Kazakhstan Research University – for their assistance and support in this research.

This research was funded by the Science Committee of the Ministry of Science and Higher Education of the Republic of Kazakhstan, Grant No. AP32724715, “Development of a technology for the selective hydrogenation of toluene to methylcyclohexane in the presence of bifunctional nickel- and platinum-based catalysts” for the period 2026-2028.

Conflict of Interest (COI). The authors declare that they have no conflict of interest.

ПРОМОТИРЛЕНГЕН ҚАҢҚАЛЫҚ НИКЕЛЬ КАТАЛИЗАТОРЛА-РЫНДА ТОЛУОЛДЫ МЕТИЛЦИКЛОГЕКСАНҒА ГИДРЛЕУ

Б.Ш.Кедельбаев [1], К.М.Лаханова [2], С.К.Туртабаев [2], С.А.Шитыбаев [2*], Г.Калымбетов [1]

[1]М.Әуезов атындағы Оңтүстік Қазақстан зерттеу университеті, Шымкент, Қазақстан
[2]Ө.Жәнібеков атындағы Оңтүстік Қазақстан педагогикалық университеті, Шымкент, Қазақстан

Түйіндеме. *Кіріспе.* Метилциклогексан (МЦГ) сутегінің болашағы зор сұйық органикалық тасымалдаушысы (СОСТ) және негізгі еріткіші болып табылады. Толуолды МЦГ-ға селективті гидрлеу тиімді, тұрақты және экономикалық тұрғыдан тиімді катализаторларды қажет етеді. Қаңқалы никель (Реней никелі) кеңінен қолданылғанымен, ол тез дезактивациялануға бейім. Бұл жұмыстың мақсаты — өнеркәсіптік ферроқорыт-палармен (FeMo, FeTiMn, FeMn) түрлендірілген көпкомпонентті никельді қаңқалы катализаторларды әзірлеу және олардың толуолды гидрлеу процесіндегі каталитикалық қасиеттерін зерттеу. *Әдістеме.*Катализаторлар Ni-Al-ферроқорытпа жүйелерін жоғары жиілікті индукциялық балқыту, одан кейін 20%-дық NaOH ерітіндісімен шаймалау әдісімен дайындалды. Беттік морфологиясы мен элементтік құрамы ЭДС-СЭМ (энергия дисперсиялық рентгендік спектроскопиясы бар сканерлеуші электрондық микроскопия) және БЭТ

әдістерімен зерттелді. Кинетикалық тәжірибелер жоғары қысымды автоклавта (0.25 л) 393–473 К температурада және 2.0–12.0 МПа сутегі қысымында жүргізілді. *Нәтижелер*. 3.0 мас.% FeMo немесе 5.0 мас.% FeTiMn қосу гидрлеу жылдамдығын түрлендірілмеген Реней никелімен салыстырғанда 2.2–2.5 есеге арттырды. Меншікті беттік аудан Ni-Al-FeMo үшін 82.1 м²/г және Ni-Al-FeTiMn үшін 78.5 м²/г жетті. ЭДС-СЭМ деректері никель матрицасында Fe, Mo, Ti және Mn біркелкі таралуын көрсетті. Реакция реті толуол бойынша нөлінші және H_2 бойынша (2-6 МПа кезінде) бірінші екені анықталды. Көрінетін активтендіру энергиясы Ni-Al-FeMo үшін 34.5 кДж/моль және Ni-Al-FeTiMn үшін 38.2 кДж/моль құрады. Катализаторлар МЦГ-ға қатысты 99.9% деңгейінде селективтілік көрсетті және 100 сағаттық жұмыстан кейін бастапқы белсенділігінің >92%-ын сақтап қалды. *Қорытынды.* Ферроқорытпалармен түрлендірілген қаңқалы никель катализаторлары жоғары тиімділікке, селективтілікке және тұрақтылыққа ие, бұл оларды сутегіні өнеркәсіптік сақтау технологиялары мен мұнай химиясында қолдану үшін келешегі бар екенін көрсетеді.

Түйінді сөздер: толуол, метилциклогексан, гидрлеу, қаңқалы никель, ферроқорытпалар, кинетика, ЭДС-СЭМ

Кедельбаев Бахытжан Шилмирзаевич	*Техника ғылымдарының докторы, профессор*
Лаханова Кулзада Мергенбаевна	*Ауыл шаруашылық ғылымдарының докторы, профессор*
Туртабаев Сарсенбек Койшабаевич	*Техника ғылымдарының докторы, профессор*
Шитыбаев Серикбек Алтынбекович	*Химия ғылымдарының кандидаты, доцент*
Калымбетов Гани Ескермесович	*Докторант, аға ғылыми қызметкер*

ГИДРИРОВАНИЕ ТОЛУОЛА ДО МЕТИЛЦИКЛОГЕКСАНА НА ПРОМОТИРОВАННЫХ СКЕЛЕТНЫХ НИКЕЛЕВЫХ КАТАЛИЗАТОРАХ

Б.Ш.Кедельбаев [1], К.М.Лаханова [2], С.К.Туртабаев [2], С.А.Шитыбаев[2]*, Г.Е.Калымбетов [1]

[1]Южно-Казахстанский исследовательский университет им.М.Ауезова, Шымкент, Казахстан
[2]Южно-Казахстанский педагогический университет им.Ө. Жәнібеков, Шымкент, Казахстан

Резюме. *Введение.* Метилциклогексан (МЦГ) является ключевым растворителем и перспективным жидким органическим носителем водорода (ЖОНВ). Селективное гидрирование толуола в МЦГ требует эффективных, стабильных и экономически выгодных катализаторов. Скелетный никель (никель Ренея) широко применяется, однако подвержен быстрой дезактивации. Целью данной работы является разработка многокомпонентных никелевых скелетных катализаторов, модифицированных промышленными ферросплавами (FeMo, FeTiMn, FeMn), и исследование их каталитических свойств в процессе гидрирования толуола. *Методика.* Катализаторы были приготовлены методом высокочастотной индукционной плавки систем Ni-Al-ферросплав с последующим выщелачиванием 20%-ным раствором NaOH. Морфология поверхности и элементный состав исследовались методами SEM-EDXRS (scanning electron microscopy with energy-dispersive X-ray spectroscopy) и БЭТ. Кинетические эксперименты проводились в автоклаве высокого давления (0.25 л) при температуре 393-473 К и давлении водорода 2.0-12.0 МПа. *Результаты.* Добавление 3.0 мас.% FeMo или 5.0 мас.% FeTiMn увеличило скорость гидрирования в 2.2–2.5 раза по сравнению с немодифицированным никелем Ренея. Удельная площадь поверхности достигла 82.1 м²/г для Ni-Al-FeMo и 78.5 м²/г для Ni-Al-FeTiMn. Данные SEM-EDXRS показали равномерное распределение Fe, Mo, Ti и Mn в никелевой матрице. Порядок реакции оказался нулевым по толуолу и первым по H_2 (при 2–6 МПа). Кажущаяся энергия активации составила 34.5 кДж/моль для Ni-Al-FeMo и 38.2 кДж/моль для Ni-Al-FeTiMn. Катализаторы продемонстрировали селективность к МЦГ на уровне 99.9% и сохранили >92% от своей первоначальной активности после 100 часов работы. *Заключение.* Скелетные никелевые катализаторы, модифицированные ферросплавами, обладают высокой эффективностью,

селективностью и стабильностью, что делает их перспективными для применения в технологиях промышленного хранения водорода и нефтехимии.

Ключевые слова: толуол, метилциклогексан, гидрирование, скелетный никель, ферросплавы, кинетика, ЭДС-СЭМ

Кедельбаев Бахытжан Шилмирзаевич	*Доктор технических наук, профессор*
Лаханова Кулзада Мергенбаевна	*Доктор сельскохозяйственных наук, профессор*
Туртабаев Сарсенбек Койшабаевич	*Доктор технических наук, профессор*
Шитыбаев Серикбек Алтынбекович	*Кандидат химических наук, доцент*
Калымбетов Гани Ескермесович	*Докторант, старший научный сотрудник*

References

1. Zhao Y., Zhang J., Liu Y., et al. Advances in the catalytic hydrogenation of toluene to methylcyclohexane: A review of liquid organic hydrogen carriers. *Renew. Sust. Energ. Rev.*, **2022**, 156, 111956. DOI: 10.1016/j.rser.2021.111956.
2. Wang L., Chen Y., Zhang X., et al. Modelling and kinetics of the toluene/methylcyclohexane-based hydrogen storage system over Ni-supported catalysts. *Int. J. Hydrog. Energy*, **2024**, 49, 1245–1258. DOI: 10.1016/j.ijhydene.2023.11.084.
3. Niermann M., Beckendorff A., Kaltschmitt M., Bonhoff K. Liquid Organic Hydrogen Carrier (LOHC) Assessment Based on Chemical and Economic Properties. *Int. J. Hydrog. Energy*, **2019**, 44(13), 6631–6654. DOI: 10.1016/j.ijhydene.2019.01.199.
4. Daud M.U., Taddeo F., Lisi L., et al. Liquid organic hydrogen carriers (LOHC): from definitions to recent developments. *Rend. Lincei Sci. Fis. Nat.*, **2025**. DOI: 10.1007/s12210-025-01389-3.
5. Gildebrand E.I., Fasman A.B. Скелетные катализаторы в органической химии. Алма-Ата: Наука КазССР, **1982**. 136 с.
6. Tashkaraev R.A., Kedelbaev B.Sh., Sataeva Zh.I. Catalytic activity and isomerizing ability of multicomponent skeletal nickel catalysts in the hydrogenation reaction of hexene-1 and cyclopentadiene. *Physicochem. Probl. Miner. Process.*, **2024**, 60(2), 184135. DOI: 10.37190/ppmp/184135.
7. Kedelbaev B.Sh., Turtabaev S.K., Lakhanova K.M., et al. Furfural hydrating on promoted skeletal copper catalysts. *Chem. J. Kaz.*, **2025**, 90(2), 103–110. DOI: 10.51580/2025-2.2710-1185.26.
8. Modisha P.M., Ouma C.N.M., Garidzirai R., Wasserscheid P., Bessarabov D. The Prospect of Hydrogen Storage Using Liquid Organic Hydrogen Carriers. *Energy Fuels*, **2019**, 33(4), 2778–2796. DOI: 10.1021/acs.energyfuels.9b00296.
9. Deng L., Liu X., Chen C., et al. Ni–Co alloys via controlled pyrolysis of NiCo–MOF as heterogeneous hydrogenation catalysts. *New J. Chem.*, **2024**, 48(19), 8620–8630. DOI: 10.1039/D4NJ00872K.
10. Ryoo R. et al. Enhanced dispersion of Pt and Ni nanoparticles on ammonia-treated siliceous MFI zeolites for toluene hydrogenation. *Appl. Catal. A*, **2025**, 692, 120096. DOI: 10.1016/j.apcata.2024.120096.
11. Han S.J., Ramadhani S., Ha T., et al. Dual functionality of LaNi5 metal hydride as a catalyst for toluene hydrogenation. *Int. J. Hydrog. Energy*, **2025**, 167, 150891. DOI: 10.1016/j.ijhydene.2025.150891.
12. С.М.Турабджанов, Р.А.Ташкараев и Б.Ш.Кедельбаев. Гидрирование бензола на никелевых катализаторах, катализируемое ферросплавами. Теоретические основы химической инженерии Том 47,стр. 633–636 (**2013**). https://doi.org/10.1134/S0040579513050102
13. Wang J., Li P., Wang S., et al. Modelling and kinetics of the toluene/methylcyclohexane-based hydrogen storage system. *Can. J. Chem. Eng.*, **2025**. DOI: 10.1002/cjce.25608.
14. Lawal A.M., Hart A., Daly H., Hardacre C., Wood J. Kinetics of the Hydrodeoxygenation of Acetic Acid over Supported Platinum Catalyst. *Ind. Eng. Chem. Res.*, **2019**, 58(18), 7998–8008. DOI: 10.1021/acs.iecr.9b00234.
15. Liu X., Yang M., Deng Z., Dasgupta A., Guo Y. Kinetics and Mechanism of Catalytic Hydrodeoxygenation of Palmitic Acid. *Chem. Eng. J.*, **2021**, 407, 126332. DOI: 10.1016/j.cej.2020.126332.

16. Oda A., Fujita T., Yamamoto Y., Sawabe K., Satsuma A. Breaking the Structure–Activity Relationship in Toluene Hydrogenation Catalysis by Designing Heteroatom Ensembles Based on a Single-Atom Alloying Approach. *ACS Catal.*, **2023**, 13(15), 10026–10040. DOI: 10.1021/acscatal.3c02132.

17. Yusuf M., Leeke G.A., Wood J. Catalytic hydrodeoxygenation of benzoic acid as a bio-oil model compound: reaction and kinetics using nickel-supported catalysts. *Sustainable Energy Fuels*, **2024**, 8, 3347–3361. DOI: 10.1039/D4SE00589A.

18. Nie L., Resasco D.E. Kinetics and Mechanism of m-Cresol Hydrodeoxygenation on a Pt/SiO_2 Catalyst. *J. Catal.*, **2014**, 317, 22–29. DOI: 10.1016/j.jcat.2014.06.002.

19. Atsumi R., Kobayashi K., Xieli C., et al. Effects of steam on toluene hydrogenation over a Ni catalyst. *Appl. Catal. A*, **2020**, 590, 117374. DOI: 10.1016/j.apcata.2019.117374.

20. Ramadhani S., Dao Q.N., Imanuel Y., et al. Advances in Catalytic Hydrogenation of Liquid Organic Hydrogen Carriers (LOHCs) Using High-Purity and Low-Purity Hydrogen. *ChemCatChem*, **2024**, 16(24), e202401278. DOI: 10.1002/cctc.202401278.

21. Yu H., Yang X., Jiang X., et al. LaNi5.5 particles for reversible hydrogen storage in N-ethylcarbazole. *Nano Energy*, **2021**, 80, 105476. DOI: 10.1016/j.nanoen.2020.105476.

22. Preuster P., Alekseev A., Wasserscheid P. Hydrogen Storage Technologies for Future Energy Systems. *Annu. Rev. Chem. Biomol. Eng.*, **2017**, 8, 445–471. DOI: 10.1146/annurev-chembioeng-060816-101334.

23. Perreault P., Van Hoecke L., Pourfallah H., Kummamuru N.B., Boruneta C.-R., Preuster P. Critical Challenges Towards the Commercial Rollouts of a LOHC-Based H_2 Economy. *Curr. Opin. Green Sustain. Chem.*, **2023**, 41, 100836. DOI: 10.1016/j.cogsc.2023.100836.

24. Okumura M., Segawa Y., Endo N. Investigation of the internal pressure exerted by a LaNi5 bed on a vertical cylindrical vessel and its packing fraction distribution during cyclic hydrogen Ab/Desorption. *ACS Appl. Energy Mater.*, **2025**, 8, 1759–1765. DOI: 10.1021/acsaem.4c02916.

25. Wu Y., Yu H., Guo Y., et al. Promoting hydrogen absorption of liquid organic hydrogen carriers by solid metal hydrides. *J. Mater. Chem. A*, **2019**, 7, 16677–16684. DOI: 10.1039/C9TA05966K.

26. Tsuji T., Shinya Y., Hiaki T., Itoh N. Hydrogen solubility in a chemical hydrogen storage medium, aromatic hydrocarbon, cyclic hydrocarbon, and their mixture for fuel cell systems. *Fluid Phase Equilib.*, **2005**, 228–229, 499–503. DOI: 10.1016/j.fluid.2004.07.013.

27. Anderson J.R. Particle size effects in metal catalysts. *Sci. Prog.*, **1985**, 69, 461–484.

Chemical Journal of Kazakhstan
Volume 2, Number 94(2026), 102-113 https://doi.org/10.51580/2026-2.2710-1185.18

UDC 661.183.123.3

SYNTHESIS OF IONITE BASED ON EPOXY RESINS AND POLYAMINES USING NEW INITIATING SYSTEMS FOR METAL SORPTION

A.M.Rodionov*, T.K.Chalov, K.T.Serikbayeva, K.A.Sadykov, F.E.Yerbolova

JSC A.B.Bekturov Institute of Chemical Sciences, Almaty, Kazakhstan

Corresponding author e-mail: 7715819290arm@gmail.com

Abstract. Purification of drinking water, isolation of rare metals from industrial wastewater, and water treatment for a wide variety of applications are constant tasks requiring various solutions. Population growth, the development of new territories, agriculture, factories and manufacturing enterprises, all of them need clean water. Ionite is an ion–exchange resin, one of the ways to solve the described problems. Ionite is able to sort various ions from solutions, thereby purifying them or releasing valuable ions during sorption. The urgent task is to produce ionites more economically with minimal energy and material costs. The process of ionite synthesis consists in polymerization and copolymerization of various monomers, while introducing various initiators and changing the process conditions, it is possible to achieve a product with high characteristics.

The ionite was based on well-known monomers such as epoxy resins and aliphatic polyamines. The reagents used were (AGE) allylglycidyl ether, (ED-20) epoxy resin, and (PEI) polyethyleneimine. A product was synthesized from diglycidyl ether of dioxydiphenylpropane, allylglycidyl ether, and polyethylenimine using initiating systems based on potassium persulfate ($K_2S_2O_8$) and azobisisobutyronitrile (AIBN). The synthesis process and method of introducing the initiator into the reaction mass were selected. The reaction was carried out in an organic solvent medium (DMF) - dimethylformamide. These initiators have not been described in known sources in combination with specific reagents during the synthesis of the ion exchanger. Further, the properties of a weakly basic anion exchanger were investigated using various methods, gravimetric, acid-base titration, infrared spectroscopy, atomic emission spectral analysis. The study of sorption capacity was carried out on the ions of metavanadate (VO^{3-}). According to the content of vanadium - (V), in the solution before and after sorption, the sorption capacity of the ionite - (CE) in mg/g was calculated.

The resulting ionite can solve the problems of water purification and industrial wastewater treatment. It can be used for the selective extraction of non-ferrous and rare metals contained in industrial wastewater.

Keywords: ionite, ion exchange resin, sorption, initiators, epoxy resins, aliphatic polyamines, allylglycidyl ether, polyethylenimine, potassium persulfate, azobisisobutyronitrile.

Chalov Tulegen Kamenovich	*Doctor of Chemical Sciences, Professor; E-mail: chalov.45@mail.ru*
Serikbayeva Katira Turlykhanovna	*Senior Researcher; E-mail: katira_87@mail.ru*
Sadykov Kanat Amirkulovich	*Researcher; E-mail: kanat.sadykov.80@bk.ru*
Rodionov Alexey Maximovich	*Engineer; E-mail: 7715819290arm@gmail.com*
Erbolova Fatıma Yerbolkyzy	*Engineer; E-mail: yerbolovafatima@gmail.com*

Citation: Rodionov A.M., Chalov T.K., Serikbayeva K.T., Yerbolova F.E. Synthesis of ionite based on epoxy resins and polyamines using new initiating systems for metal sorption. *Chem. J. Kaz.*, **2026**, 2*(94)*, 102-113. DOI: https://doi.org/10.51580/2026-2.2710-1185.18

1. Introduction

Simple methods for producing anion exchangers based on copolymers of glycidyl methacrylate and polyamines have been studied, and their potential for extracting metal ions from aqueous solutions has been demonstrated [1, 9, 10, 22]. A comparative analysis of synthetic polyamine resins with commercial counterparts has shown their high efficiency in sorption [2]. New epoxy sorbents with amino groups for the removal of azo dyes from aqueous media [3] have been developed, as well as initiating systems for controlled radical polymerization using diazo compounds [4]. The diffusion characteristics of azo initiators and their radicals [5] have been studied, as well as the structure and application of poly(ethylene glycol)-based macroinitiators for the synthesis of cross-linked polymer structures [6]. Special attention was paid to the reproducibility of free-radical copolymerization [7], as well as to the kinetics and mechanism of the polymerization of acrylamide and methyl methacrylate in the presence of various initiators, including potassium persulfate and benzoyl derivatives [8, 14, 16]. It was found that the structural and physical-chemical properties of the resulting polymers depend on the temperature, monomer concentration, and the nature of the initiating system [13, 17, 18]. The obtained data can be used to develop thermostable and chemically stable ion exchangers with high sorption capacity for metal sorption [11, 23, 24, 25].

The aim of this study was to synthesize an ion exchanger with new initiators under new conditions and to investigate the sorption properties of the resulting product towards metal ions.

The novelty of this study lies in the use of AIBN initiators and potassium persulfate together with known starting reagents for the synthesis of an ion exchanger. The literature cited describes the use of the components separately with other reagents. Conducting a joint synthesis and studying the properties of the resulting product is an urgent task.

2. Experimental part

The initial reagents are allylglycidyl ether (AGE) with a molar mass of 114.14 g/mol, polyethyleneimine (PEI) with a molar mass of 43.04 g/mol, and epoxy resin (ED-20) with a molar mass of 60.1 g/mol. The ratio of the average molar mass of the oligomers is 1:1:1 (mol). The synthesis was carried out using equipment such as a Loip 4T-105A thermostat, as well as ISOLAB 615,10,100, and IKA eurostar 20 digital overhead mixers. AGE was introduced into a three-necked flask with a reflux condenser and heated to 80°C. ED-20 was dissolved in dimethylformamide (DMF). Next, the initiator was added at a ratio of 0.1% (mass) by weight of the reaction mass.

Ionite «A»: the initiator $K_2S_2O_8$ – potassium persulfate was introduced as a 2% aqueous solution.

Ionite "B": the initiator azobisisobutyronitrile (AIBN) was introduced as a 2% solution in DMF.

Next, PEI was added through a dropping funnel as an emulsion of a 50% aqueous PEI solution in DMF. The reaction mass was stirred until it formed a gel, making the liquid thick and viscous. Curing was carried out in furnaces at a temperature of 100 °C.

The ionite was previously washed, prepared, and converted to the OH form according to standard methods. The static exchange capacity was determined using the standard method of acid-base titration according to GOST 20255.1-89. Ionites. Methods for Determining the Static Exchange Capacity. The method of determining the moisture content of the ionite was carried out in accordance with GOST 10898.1-84, taking into account the adaptations to the specific features of the sample under study.

The sorption properties were tested on metavanadate anions (VO_3^-), and the calculation was based on the vanadium content. The starting reagent is ammonium metavanadate, NH_4VO_3. To study the dependence of the sorption capacity (1) on the concentration of the initial solution, five solutions with concentrations of 25, 50, 100, 150, and 200 mg/L were prepared over a period of 7 days. To study the dependence of the sorption capacity on the pH of the initial solution for 7 days, five solutions with a concentration of 100 mg/l were prepared, with pH values: 2, 3, 4, 5, 6, 7, acidifier – nitric acid HNO_3 0.1%, alkalizing agent - ammonia hydrate NH_4OH 0.01%. To study the dependence of the sorption capacity on the contact time of the ionite with the solution, five solutions with a concentration of 100 mg/L and a pH of 2 were prepared. The contact time was 0.5, 1, 2, 4, and 24 hours. $qe = \frac{(C_0 - C)V}{g}$ (1), $R = 100 - \left(\frac{100C}{C_0}\right)$ (2), where: qe – sorption capacity (mg/g); R – degree of extraction (%); C_0 – initial concentration of metal ions in the solution (mg/L); C – equilibrium concentration of metal ions in the solution (mg/L); V – volume of the solution (L); g – weight of the ion exchanger (g).

To study the infrared spectrum, the ionite samples were crushed and mixed with potassium bromide, then dried at 40–60 °C and cooled in an desiccator.

3. Results and their discussion

At the intermediate stage of ionite «A» synthesis, a light yellow, rather fluid gel was obtained. The finished product had a soft, rubbery texture and was insoluble in acids, alkalis, and water. After drying in an oven at 40–60 °C, the sample took the form of dark yellow-brown transparent granules. At the intermediate stage of ionite «B» synthesis, a jelly-like gel with a soft, elastic, rubber-like structure was obtained. The final product was an elastic, soft, and greasy material that was resistant to water, acids, and alkalis. After drying at 40–60 °C, the ionite looked like light brown transparent granules. The characteristics of ionites are listed in Table 1.

Table 1 - Comparison of the properties of ionites obtained using potassium persulfate and AIBN as an initiator.

	Ionite «A»	Ionite «B»
The initiator used	potassium persulfate	azobisisobutyronitrile
Molar ratio	1:1:1 - AGE: PEI: ED-20	1:1:1 - AGE: PEI: ED-20
Product yield	26.2 %	43.4 %
Curing time	70 hours	57.5 hours
Static exchange capacity	1.98 meq/g	2.54 meq/g
Ionite humidity	43.7 %.	27.1 %.
Appearance	Hard, yellowish-brown, darker, transparent, brittle	Hard, yellowish-brown, lighter, transparent, elastic

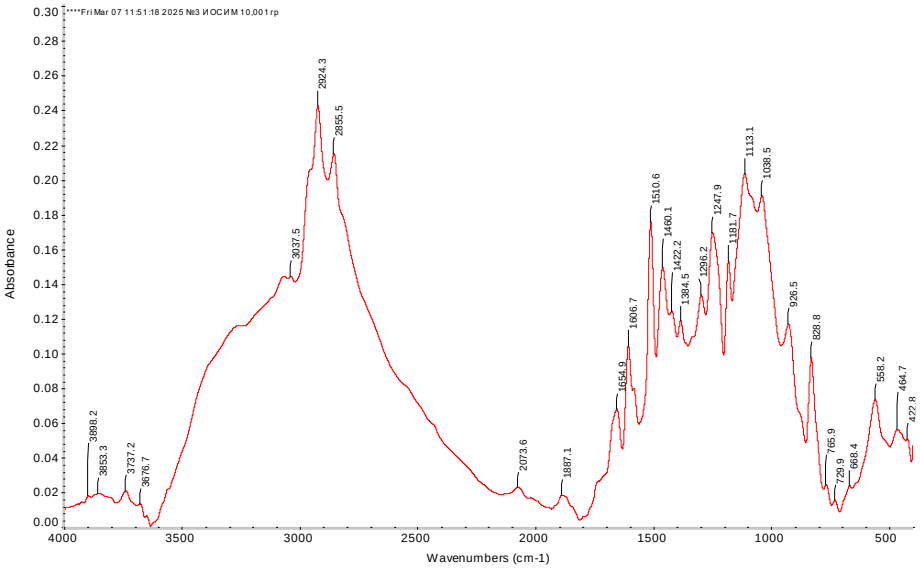

Figure 1 - IR spectrum of the «A» ionite sample

Figure 1 shows the IR spectrum of ionite «A». Figure 2 shows the IR spectrum of ionite «B». The IR spectra indicate the formation of an epoxy-amine cross-linked structure in both cases. Ion exchanger «A» is characterized by bands at 3898, 3853, 3678, 3668, and 3341 cm^{-1}, which belong to the O-H and N-H groups, as well as signals at 2937, 2924, and 2850 cm^{-1}, which correspond to the aliphatic - CH_2 fragments. The bands at 1655 and 1601 cm^{-1} are associated with the deformational vibrations of the amino groups and the aromatic framework, while the signals at 1248, 1113, and 1088 cm^{-1} indicate the CN and C-O-C bonds, i.e., the opening of the epoxy ring and the formation of a polymer network. A band around 926 cm^{-1} may indicate the presence of residual epoxy groups.

The spectrum of ion-exchange resin «B» is similar, but slightly different in the main bands. It shows bands at 3349 and 3078 cm^{-1} for the -OH, -NH-, and -NH2- groups, bands at 2925 and 2843 cm^{-1} for the -CH- fragments, and signals at 1651 and 1601 cm^{-1}. The bands at 1247 and 1112 cm^{-1} also confirm the formation of C-N and C-O-C bonds, while the band at 926 cm^{-1} is weak, which may indicate the completion of the reaction.

The difference between the spectra is no longer related to the set of functional groups, but to the way the polymer network is formed.

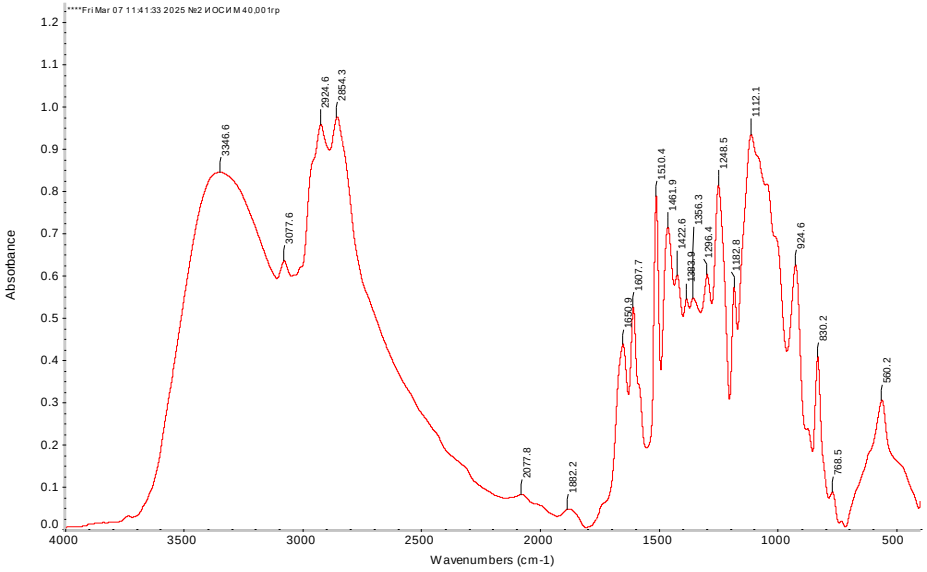

Figure 2 - IR spectrum of the «B» ionite sample

Table 2 shows the results of sorption. It has been shown that ionite «A» has higher and more stable sorption capacity values than ionite «B». In an acidic environment (pH 2.3), the maximum sorption location were observed, especially for ionite «B», but as the pH increased, its efficiency decreased significantly, while ionite «A» maintained more stable characteristics. An increase in contact time led to a regular increase in sorption capacity and degree of extraction for ionite «A», while the changes were less pronounced for ionite «B», which generally indicates a higher efficiency and stability of ionite «A» under the studied conditions. Figures 3 - 5 show the graphs of the sorption capacity as a function of concentration, pH, and time, respectively. Figure 6 shows the structural unit of the obtained ion exchange resin, where R is a branched oligomeric unit of PEI, epoxy oligomers, and oligomers of allylglycidyl ether that form a mesh structure.

Table 2 - Results of sorption of ionites «A» and «B»

Sorption depending on concentration The ionite weight is 0.05 g; T=20ºC; static sorption for 7 days in 10 ml of the initial solution.						
Initial solution (mg/L)	26.25	50.98	98.53	149	201.98	
pH of the initial solution	6.6	6.6	6.6	6.6	6.6	
Solution after sorption «A» (mg/l)	1	15.75	72.45	125.55	168.25	
Solution after sorption «B» (mg/l)	1.65	33.92	79.1	127.5	175.78	
Sorption capacity «A» (mg/g)	5.04	7.02	5.15	4.59	6.6	
Sorption capacity «B» (mg/g)	4.92	3.37	3.84	4.19	5.11	
Extraction rate «A» (%)	96.19	69.1	26.47	15.74	16.7	
Extraction rate «B» (%)	93.71	33.46	19.72	14.43	12.97	
Sorption depending on pH The ionite weight is 0.05 g; T=20ºC; static sorption for 7 days in 10 ml of the initial solution.						
Initial solution (mg/L)	99.85	104.68	101.92	102.38	103.24	99.77
pH of the initial solution	2.3	3.3	4	5.6	6.6	7.8
Solution after sorption «A» (mg/l)	37.46	57.31	71.14	73.08	72.97	64.56
Solution after sorption «B» (mg/l)	18.35	87.42	89.42	87.68	85.96	85.85
Sorption capacity «A» (mg/g)	12.4	9.36	6.12	5.77	5.92	6.97
Sorption capacity «B» (mg/g)	16.04	3.45	2.46	2.94	3.37	2.71
Extraction rate «A» (%)	62.48	45.25	30.21	28.62	29.32	35.29
Extraction rate «B» (%)	81.62	16.49	12.26	14.36	16.74	13.95
Sorption depending of time The ionite weight is 0.05 g; T=20ºC; static sorption in 10 ml of the initial solution.						
Initial solution (mg/L)	99.52	99.52	99.52	99.52	99.52	
pH of the initial solution	2.3	2.3	2.3	2.3	2.3	
Contact time (hours)	0.5	1	2	4	24	
Solution after sorption «A» (mg/l)	80.01	61.16	43.56	35.9	22.7	
Solution after sorption «B» (mg/l)	79.7	85.96	92.32	86.79	73	
Sorption capacity «A» (mg/g)	3.9	7.54	11.08	12.67	15.06	
Sorption capacity «B» (mg/g)	3.95	2.67	1.41	2.5	5.24	
Extraction rate «A» (%)	19.6	38.55	56.23	63.93	77.19	
Extraction rate «B» (%)	19.92	13.63	7.23	12.79	26.65	

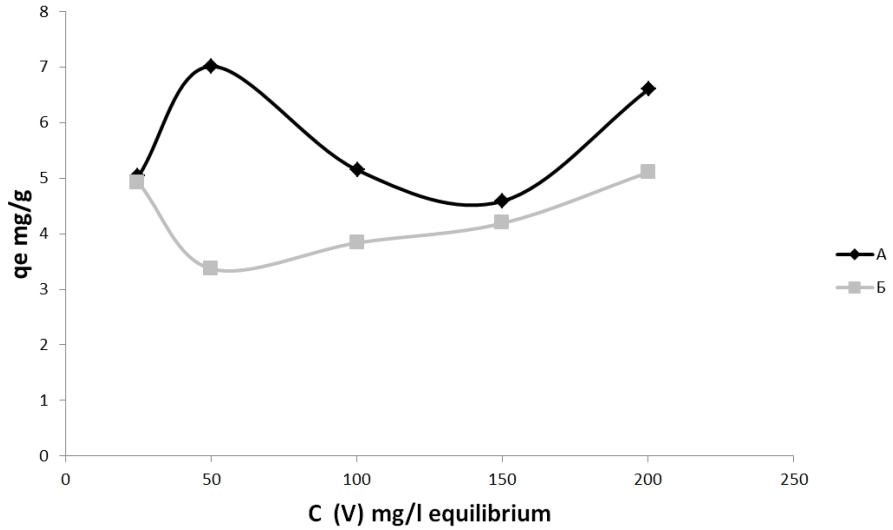

Figure 3 - Graph of the sorption capacity dependence on the concentration of the initial solution

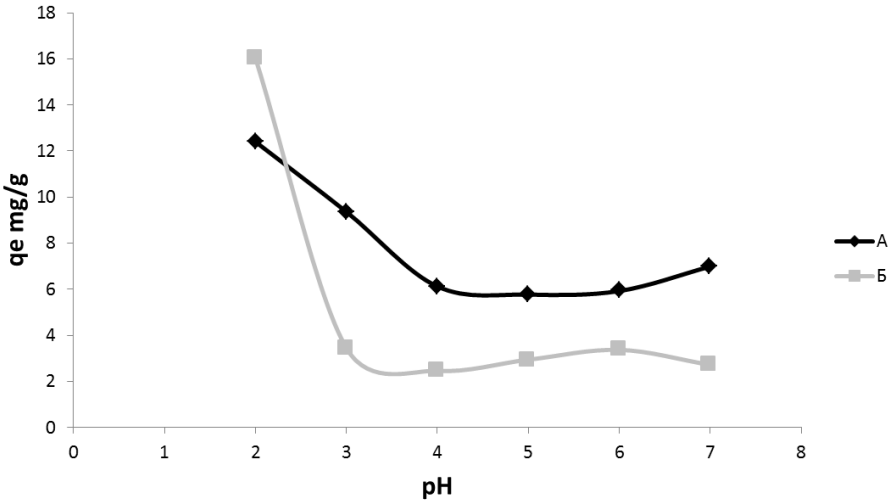

Figure 4 - Graph of the dependence of the sorption capacity on the pH of the initial solution

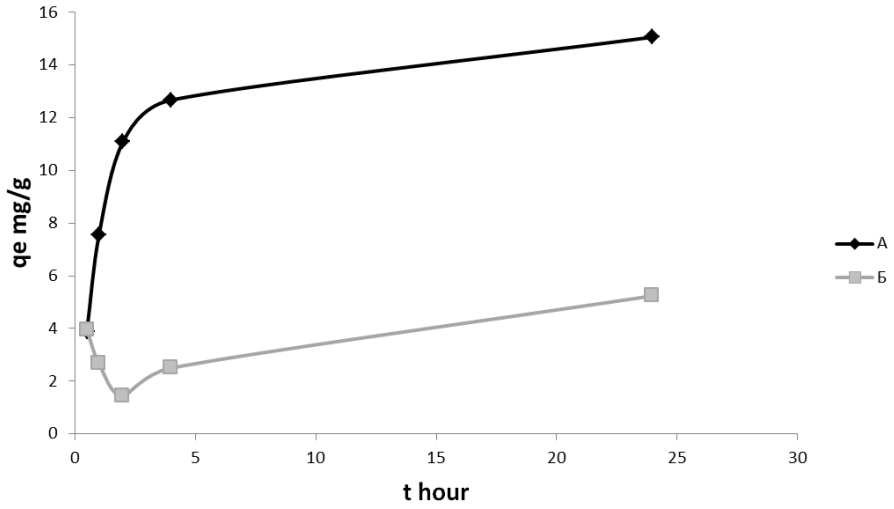

Figure 5 - Graph of the sorption capacity dependence of the sorption time

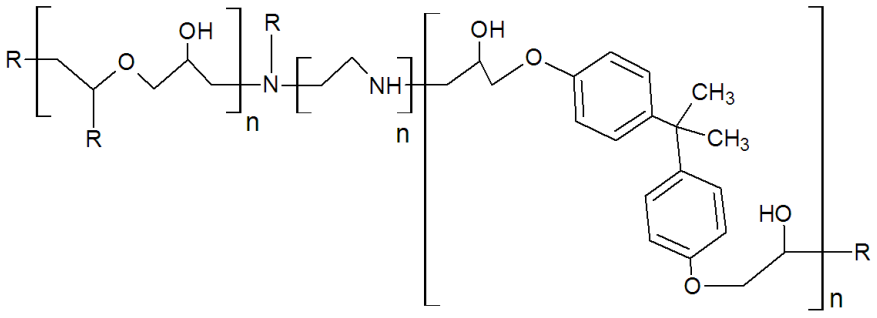

Figure 6 - Structural unit of the obtained ionite

4. Conclusion

It was possible to synthesize ionites using new initiators for this composition: potassium persulfate and AIBN. The conducted studies showed that the type of polymerization initiator significantly affects the characteristics of the obtained materials. The resulting ionites fully reflect the specific features of the synthesis conditions used and demonstrate pronounced differences in their main operational parameters.

Ionite "A" exhibited higher stability and sorption capacity, despite its higher moisture content and lower yield. The curing time was longer, which may indicate a slower polymerization process and the formation of a more developed porous structure with increased hydrophilicity. The experimental data showed that this material has stable sorption properties when interacting with metal ions. The

static exchange capacity of ionite "A" was 1.98 meq/g, and the sorption capacity was 15.06 mg/g at pH 2.3 over a long sorption time.

Ionite B with a shorter curing time and higher yield had a higher sorption capacity at low pH. The static exchange capacity of ionite B was 2.54 meq/g, and the sorption capacity was 16.04 mg/g at pH 2.3.

The results of IR spectroscopy confirmed the formation of a dense and uniform polymer matrix. The obtained results confirm the potential of the synthesized ion exchangers for use in sorption processes and further research in the field of ion exchange materials.

Funding: The work was carried out at the «A. B. Bekturov Institute of Chemical Sciences» JSC as part of the 2023-2025 targeted research funding program implemented by the Science Committee of the Ministry of Education and Science of the Republic of Kazakhstan under the BR21882220 program.

Gratitude: The authors express their gratitude to the staff of the Laboratory of Physical and Chemical Methods of Analysis and Ecology for conducting the necessary analyses.

Conflict of interest: The authors declare that there is no conflict of interest that requires disclosure in this article.

МЕТАЛДАРДЫ СОРБЦИЯЛАУ ҮШІН ЖАҢА БАСТАМАШЫЛ ЖҮЙЕЛЕРДІ ҚОЛДАНА ОТЫРЫП, ЭПОКСИДТІ ШАЙЫРЛАР МЕН ПОЛИАМИНДЕР НЕГІЗІНДЕГІ ИОНИТ СИНТЕЗІ

А.М.Родионов*, Т.К.Чалов, К.Т.Серикбаева, К.А.Садыков, Ф.Е.Ерболова

Ә.Б. Бектұров атындағы химия ғылымдары институты АҚ, Алматы, Қазақстан

Түйіндеме. Ауыз суды тазарту, өндірістік ағынды сулардан сирек металдарды бөліп алу, суды әр түрлі қолдану салаларына дайындау әр түрлі шешімдерді қажет ететін тұрақты міндеттер болып табылады. Халықтың өсуі, жердің жаңа аумақтарын игеру, ауыл шаруашылығы, зауыттар мен өндірістік кәсіпорындар, олардың барлығы таза суға мұқтаж. Ионит-ион алмасу шайыры, сипатталған мәселелерді шешудің бір жолы. Ионит ерітінділерден әртүрлі иондарды сұрыптай алады, осылайша оларды тазартады немесе сорбция процесінде құнды иондарды шығарады. Ең аз энергетикалық және материалдық шығындармен иониттерді неғұрлым экономикалық тиімді өндіру өзекті міндет болып табылады. Иониттерді синтездеу процесі әртүрлі мономерлерді полимерлеу және сополимерлеу болып табылады, ал әртүрлі бастамашыларды енгізу және процесс жағдайларын өзгерту арқылы жоғары өнімділікке қол жеткізуге болады. Иониттің негізі эпоксидті шайырлар мен алифатты полиаминдер сияқты белгілі мономерлер болды. Қолданылатын реагенттер: (АГЭ) - аллилглицид эфирі, (ЭД-20) - эпоксидті шайыр, (ПЭИ) – полиэтиленимин. Диоксидифенилпропан диглицидил эфирінен, аллилглицедил эфирінен және полиэтилениминнен калий персульфаты ($K_2S_2O_8$) және азобисизобутиронитрил - (АИБН) негізіндегі инициациялық жүйелерді қолдану арқылы өнім синтезделді. Синтез процесі және бастамашыны реакция массасына енгізу әдісі таңдалды. Реакция органикалық еріткіш (ДМФА) – диметилформамид ортасында жүргізілді. Бұл бастамашылар белгілі көздерде ионит синтезіндегі нақты реактивтермен бірге сипатталмаған. Әрі қарай әр түрлі әдістерді, гравиметриялық, қышқылдық-негіздік титрлеуді, инфрақызыл спектроскопияны, атомдық-эмиссиялық спектрлік талдауды қолдана отырып, әлсіз негізді аниониттің қасиеттері зерттелді. Сорбциялық қабілетін зерттеу метаванадат иондары (VO_3^-) бойынша жүргізілді. Ванадийдің құрамы бойынша – (V), сорбцияға дейінгі және кейінгі ерітіндіде ионитің сорбциялық сыйымдылығы - (СЕ) мг/г деп саналды. Алынған ионит су мен өндірістік ағынды суларды тазарту мәселелерін шеше алады. Өнеркәсіптік ағынды суларда кездесетін түсті және сирек металдарды селективті оқшаулау үшін қолдануға болады.

Түйінді сөздер: ионит, ион алмасу шайыры, сорбция, бастамашылар, эпоксидті шайырлар, алифатты полиаминдер, аллилглицедил эфирі, полиэтиленимин, калий персульфаты, азобисизобутиронитрил.

Чалов Тулеген Каменович	*Химия ғылымдарының докторы, профессор*
Серикбаева Катира Турлыхановна	*Аға ғылыми қызметкер*
Садыков Канат Амиркулович	*Ғылыми қызметкер*
Родионов Алексей Максимович	*Инженер*
Ерболова Фатима Ерболқызы	*Инженер*

СИНТЕЗ ИОНИТА НА ОСНОВЕ ЭПОКСИДНЫХ СМОЛ И ПОЛИАМИНОВ С ПРИМЕНЕНИЕМ НОВЫХ ИНИЦИИРУЮЩИХ СИСТЕМ ДЛЯ СОРБЦИИ МЕТАЛЛОВ

А.М.Родионов*, Т.К.Чалов, К.Т.Серикбаева, К.А.Садыков, Ф.Е.Ерболова

АО Институт химических наук имени А. Б. Бектурова, Алматы, Казахстан

Резюме. Очистка питьевой воды, выделение редких металлов из промышленных стоков, подготовка воды для самых различных областей применения являются постоянными задачами, требующие различных решений. Рост населения, освоение новых территорий земли, сельское хозяйство, заводы и производственные предприятия, все они нуждаются в чистой воде. Ионит – ионообменная смола, один из способов для решения описанных задач. Ионит способен сортировать различные ионы из растворов, тем очищая их или выделять ценные ионы в процессе сорбции. Актуальной задачей является более экономически выгодное производство ионитов с минимальными энергетическими и материальными затратами. Процесс синтеза ионитов заключается в полимеризации и сополимеризации различных мономеров, при этом вводя различные инициаторы, и меняя условия процесса можно добиться продукта с высокими характеристиками. Основой для ионита послужили известные мономеры, такие как эпоксидные смолы и алифатические полиамины. Используемые реагенты: (АГЭ) - аллилглицидиловый эфир, (ЭД-20) - эпоксидная смола, (ПЭИ) – полиэтиленимин. Был синтезирован продукт из диглицидилового эфира диоксидифенилпропана, аллилглицедилового эфира и полиэтиленимина с применением инициирующих систем на основе персульфата калия ($K_2S_2O_8$) и азобисизобутиронитрила - (АИБН). Был подобран процесс синтеза и способ введения инициатора в реакционную массу. Реакция велась в среде органического растворителя (ДМФА) – диметилформамид. Данные инициаторы не были описаны в известных источниках в сочетании с конкретными реагентами при синтезе ионита. Далее были исследованы свойства слабоосновного анионита с применением различных методов, гравиметрического, кислотно-основного титрования, инфракрасной спектроскопии, атомно-эмиссионного спектрального анализа. Исследование сорбционной способности проводилось по ионам метаванадата (VO_3^-). По содержанию ванадия - (V), в растворе до и после сорбции, считалась сорбционная емкость ионита – (СЕ) в мг/г. Полученный ионит может решить проблемы очистки воды и промышленных стоков. Может целесообразно применятся для селективного выделения цветных и редких металлов, содержащихся в промышленных стоках.

Ключевые слова: ионит, ионообменная смола, сорбция, инициаторы, эпоксидные смолы, алифатические полиамины, аллилглицедиловый эфир, полиэтиленимин, персульфат калия, азобисизобутиронитрил.

Чалов Тулеген Каменович	*Доктор химических наук, профессор*
Серикбаева Катира Турлыхановна	*Старший научный сотрудник*
Садыков Канат Амиркулович	*Научный сотрудник*
Родионов Алексей Максимович	*Инженер*
Ерболова Фатима Ерболқызы	*Инженер*

References

1. Ybraimzhanova L. Synthesis and research of ion-exchange materials based on epoxyacrylates. *The Sci. Herit.*, **2022**, № 91, P. 21-23. https://doi.org/10.5281/zenodo.6695628

2. Amphlett J. T. M., et al. Polyamine functionalised ion exchange resins: Synthesis, characterisation and uranyl uptake. *Chem. Engi. J.*, **2018**, Vol. 334. P. 1361-1370. https://doi.org/10.1016/j.cej.2017.11.040

3. Podkościelna B., Wawrzkiewicz M., Klapiszewski Ł. Synthesis, characterization and sorption ability of epoxy resin-based sorbents with amine groups. *Polymers*, **2021**, Vol. 13. № 23. P. 4139. https://doi.org/10.3390/polym13234139

4. Yamago S., Iida K., Nakajima M., Yoshida J. Practical protocols for organotellurium-mediated living radical polymerization by in situ generated initiators from AIBN and ditellurides. *Macromol.*, **2003**, Vol. 36. № 11. P. 3793-3796. https://doi.org/10.1021/ma034211a

5. Terazima M., Nogami Y., Tominaga T. Diffusion of a radical from an initiator of a free radical polymerization: a radical from AIBN. *Chem. Phys. L*. **2000**. Vol. 332. № 5-6. P. 503-507. https://doi.org/10.1016/S0009-2614(00)01298-7

6. Walz R., Bömer B., Heitz W. Monomeric and polymeric azoinitiators. *Macromol. Chem. and Phys.*, **1977**, Vol. 178. № 9. P. 2527-2534. https://doi.org/10.1002/MACP.1977.021780904

7. Marques, N., Lima, B., Silveira, R. PNIPAM-based graft copolymers prepared using potassium persulfate as free-radical initiator: synthesis reproducibility. *Coll. and Pol. Sci.*, **2016**, Vol. 294. P. 981-991. https://doi.org/10.1007/s00396-016-3854-2

8. Hunkeler D. Mechanism and kinetics of the persulfate-initiated polymerization of acrylamide. *Macromol.*, **1991**, Vol. 24. № 9. P. 2160-2171.

9. Yergozhin E. E., Chalov T. K., Kovrigina T. V. *Synthetic and Natural Ionites for Sorption Technologies*. **2018**. ISBN 978-601-332-041-0.

10. Yergozhin E. E., Chalov T. K., Iskakova R. A., Kovrigina T. V. Polyfunctional anion exchangers based on allylglycidyl ether and some polyamines. *J. of App. Chem.*, **2004**, V. 77. No. 3. Pp. 465-469.

11. Yergozhin E. E., Begenova B. E., Chalov T. K. Synthesis and study of the physical and chemical, acid-base, and complex-forming properties of ion exchangers based on glycidyl derivatives of aromatic compounds and polyamines. *J. of App. Chem.*, **2007**, Vol. 80, No. 3, pp. 473-478. https://doi.org/10.1134/S1070427207030238

12. Yergozhin E. E., Chalov T. K., Kovrigina T. V., Iskakova R. A., Nikitina A. I. Study of the Complex-Forming Ability of Anionites Based on Some Polyamines, Allyl and Epoxy Compounds. *J. of App. Chem.*, **2004**, Vol. 77, No. 10, pp. 1693-1698. https://doi.org/10.1007/s11167-005-0096-3

13. Yergozhin E. E., Mukhitdinova B. A., Chalov T. K., Iskakova R. A. Polymers based on polyglucid amines. *J. of App. Chem.*, **2005**, Vol. 78, No. 10, pp. 1716-1720. https://doi.org/10.1007/s11167-005-0587-2

14. Pirmedova T., Annadurdyeva G., Ashirov O. Ashirova B. Study of the Influence of Various Factors on the Polymerization Process and the Properties of the Resulting Polymers. *Wor. Sci.*, **2024**, Vol. 1, No. 21, pp. 280-285.

15. Pashchenko E. A. et al. Synthesis of modified epoxy oligomers with substituents based on framework compounds and study of their curing processes; Study of the curing processes of modified oligomers using ionic polymerization initiators. Study of the physical and mechanical properties of composites based on modified epoxy oligomers and SPM powders. *Rock-breaking and metal. tools-techn. and tech. of their man. and applic.*, **2014**, No. 17, pp. 379-384.

16. Zaikina A.V., Yarmukhamedova E.I., Puzin Yu.I., Monakov Yu.B. Study of the Polymerization of Methyl Methacrylate Initiated by the N, N-Dimethyl-N-Benzylamine-Benzoyl Peroxide System. *Chem. and Chem. Techn.*, **2010**, Vol. 53, No. 3, pp. 86-89.

17. Vent D.P., Savelyanov V.P., Lopatin A.G., Safin M.A. Influence of the agitator rotation speed on the dynamics of the styrene suspension polymerization reactor. *B. of the Inter. Acad. of Sys. Res. Inform., Ecol., Econom.*, **2012**, Vol. 14, No. 1, pp. 91-94.

18. Nikolaev A. V., Vorobyov I. V., Anuchin N. V. Influence of the choice of the polymerization initiator on the effectiveness of the curing of unsaturated polyester resin. *New tech. in the educ. proc. and prod*, **2019**, pp. 446-449.

19. Klenin V. I., Fedusenko I. V. *High-Molecular-Weight Compounds*. **2013**.

20. Navolokina R. A., Zilberman E. N. *Chem. of H.-Mol. Com.: Polycon. and Step-by-Step Polymer.*. **2008**.

21. Kireev V. V. *High-Molecular-Weight Compounds*. **2015**.

22. Kendi J., Nairuti R. N. Ion Exchange Processes. *Advan. Tertiary Waste. Treatment: Tech. and Meth. Cham : Sprin. Nat. Switz.*, **2026**, С. 23-39.

23. Bulenbayev M., Altaibayev B., Magomedov D., Bakrayeva A., Bekpeisov Zh. Sorption Concentration of Uranium and Vanadium from Productive Solutions of Black Shale Ores. *Complex use of min. Res.*, **2026**, Vol. 340. № 1. P. 87-94. https://doi.org/10.31643/2027/6445.09

24. Pavel Ks., Helena P., Arka L., Miroslava N., Ludek J. Co-sorption of vanadium (V) and molybdenum (VI) onto ion exchange resin with multiple hydroxyl groups. *Separ. Sci. and Tech.*, **2026**, P. 1-12.

25. Sadykov K., Bektenov N., Chalov T., Serikbayeva K., Kuznetsova Y., Yerbolova F. New anion exchangers and their sorption properties toward chromium (vi) and vanadium (v) ions. *Chem. J. of Kazakhstan*, **2025**, № 3 (91). P. 123-133. https://doi.org/10.51580/2025-3.2710-1185.41%20

Chemical Journal of Kazakhstan
Volume 2, Number 94(2026), 114-123 https://doi.org/10.51580/2026-2.2710-1185.19

UDC 547.(1+435+6+822)+549.623+631.(811+84+85)

SOFT ORGANOMODIFICATION OF BENTONITE WITH OXYPHOSPHONATE AND ITS APPLICATION AS A PROLONGED-LASTING GROWTH STIMULATOR

B.Y. Kapar,[1,2], T.Y. Zharkynbek [1,2*], B.B. Tyussyupova [2], D.M.-K. Ibraimova [2], S.M. Tazhibayeva [2], V.K. Yu [1]

[1]A.B. Bekturov Institute of Chemical Sciences JSC, Almaty, Kazakhstan
[2]Al-Farabi Kazakh National University, Almaty, Kazakhstan

[*]Corresponding author e-mail: tolganay.zharkynbek@gmail.com

Abstract. *Introduction.* Organomodified clay materials are of significant interest as functional systems for agriculture due to their ability to provide the sustained release of biologically active substances. Natural bentonite, with its high specific surface area and ion-exchange capacity, serves as an excellent matrix for the immobilization of organic growth stimulants. *The purpose* of this study is to develop a low-energy, efficient method for the soft organomodification of bentonite using a specific oxyphosphonate (Kaz-6) and to evaluate its effectiveness as a prolonged-action growth stimulator for wheat. *The proposed method* involves the pre-dispersion of bentonite in water at 40°C, followed by drying at 50°C. The prepared mineral matrix was then treated with low-concentration aqueous solutions of dimethyl(4-hydroxy-1-(2-ethoxyethyl)piperidin-4-yl)phosphonate (Kaz-6) in the concentration range of 10^{-2}–10^{-6} wt % at room temperature. The structure of the resulting composite was characterized using IR spectroscopy. It was found that the developed approach significantly reduces the process temperature and duration compared to existing analogs, while using substantially lower concentrations of the organic component. Biological trials showed that the organomodified bentonite exhibits pronounced growth-promoting activity toward wheat (varieties “Almaken” and “Zhenis”). The most significant stimulatory effect was observed at concentrations of 10^{-5}–10^{-6} wt. %, where the composite outperformed both the control group and the free (unbound) oxyphosphonate. The results indicate that the immobilization of Kaz-6 on bentonite ensures prolonged action and increased bioavailability of the active component. The developed organomineral composite can be recommended as a promising growth-promoting agent for sustainable agricultural applications.

Key words: bentonite, organomodification, oxyphosphonate, immobilization, growth stimulator, wheat, sustained release.

Kapar Bayan Yerbolkyzy	*Master student, Engineer; E-mail: kaparb13@gmail.com*
Zharkynbek Tolganay Yerkinkyzy	*Master of Engineering and Technology, Junior Researcher; E-mail: tolganay.zharkynbek@gmail.com*
Tyussyupova Bakyt Baimuratovna	*Candidate of Chemical Sciences, Associate Professor; E-mail: baimuratovna78@mail.ru*
Ibraimova Dana Mykty-Kereyevna	*Candidate of Chemical Sciences, Senior Lecturer; E-mail: dmk_82@mail.ru*
Tazhibayeva Sagdat Mederbekovna	*Doctor of Chemical Sciences, Professor; E-mail: sagdattazhibayeva2018@gmail.com*
Yu Valentina Konstantinovna	*Doctor of Chemical Sciences, Full Professor; E-mail: yu_vk@mail.ru*

Citation: Kapar B.Y., Zharkynbek T.Y., Tyussyupova B.B., Ibraimova D.M.-K., Tazhibayeva S.M., Yu V.K. Soft organomodification of bentonite with oxyphosphonate and its application as a prolonged-lasting growth stimulator. *Chem. J. Kaz.*, **2026**, *2(94)*, 114-123. DOI: https://doi.org/10.51580/2026-2.2710-1185.19

1. Introduction

Natural clay minerals, particularly bentonite, are widely used in various fields due to their high specific surface area, pronounced sorption properties, and high ion exchange capacity. These characteristics stem from the layered montmorillonite-type structure, which enables the intercalation and fixation of various organic and inorganic compounds [1].

In recent years, the use of bentonite in agriculture as a functional carrier of biologically active substances has attracted particular interest. It has been shown that the application of bentonite to soil improves its physicochemical properties, increases its water-holding capacity, and enhances the availability of nutrients to plants [2]. Furthermore, bentonite is capable of adsorbing organic compounds and ensuring their gradual release, providing a prolonged effect.

One effective approach to improving the functional properties of bentonite is its organomodification. Modern modification methods include the use of surfactants, polymers, and organic acids, which significantly alter the surface characteristics of the material and enhance its sorption activity [1,3]. However, most known approaches are characterized by high concentrations of modifying agents, elevated temperatures, and long processing times, which limits their practical application.

In this regard, a pressing task is the development of gentle and cost-effective methods for organomodification of bentonite using low concentrations of functional organic compounds. Of particular interest are oxyphosphonates , which possess high complexing capacity, hydrophilicity, and potential biological activity [4]. The introduction of phosphorus-containing groups into organomineral systems helps to enhance their coordination and adsorption properties [5].

Furthermore, modern research shows that modified bentonite compositions can improve soil fertility, stabilize organic component, and stimulate crop growth [2,6]. This area is particularly relevant for Kazakhstan due to the widespread use of bentonite clays and the need to increase crop yields in arid climates [7].

Previous studies have demonstrated that organomodified clay materials serve as effective carriers for agrochemicals and controlled-release systems, minimizing the loss of active substances and improving their utilization efficiency [8–10].

In particular, it has been shown that the intercalation of organic molecules into the interlayer space of montmorillonite promotes the formation of stable hybrid structures with controlled desorption kinetics [11].

Modern research also demonstrates that functionalization of the bentonite surface with phosphorus-containing compounds increases its affinity for biologically active molecules and improves their retention in the soil system [12,13]. An important factor is the use of low concentrations of modifying agents, which helps avoid aggregation and preserve the active surface of the mineral [14].

In addition, the use of nanostructured organo-mineral compositions is considered as a promising direction in agrochemistry, aimed at creating environmentally friendly and resource-saving technologies [15–17].

The aim of this work is to develop a method for obtaining organomodified bentonite using Kaz-6 under mild conditions, as well as to study its growth-stimulating activity in relation to wheat.

2. Experimental part

Materials

Natural bentonite from the Tagan deposit (Kazakhstan) was used in the study. Before use, the bentonite was pre-treated (dispersed and dried). Dimethyl(4-hydroxy-1-(2-ethoxyethyl)piperidin-4-yl)phosphonate (Kaz-6) was prepared previously by a known method and used as a modifying agent [18]. Distilled water was used to prepare the solutions. All reagents were used without further purification.

Preparation of organomodified bentonite

Bentonite was pre-treated as follows: the original bentonite was dispersed in distilled water at 40°C until a homogeneous suspension was obtained. The resulting suspension was dried at 50°C for 3 hours, after which the dried material was ground to a powder.

Organomodification was carried out by treating prepared bentonite with Kaz-6 aqueous solutions with various concentrations (10^{-2}–10^{-6} wt. %). For this, 1 g of bentonite was mixed with 50 mL of the modifier solution and kept at room temperature for 40 minutes with occasional stirring.

After completion of the process, the mixture was filtered and the resulting solid product was dried at 50°C for 2 hours. As a result, organomodified bentonite was obtained in powder form.

IR spectroscopy

The IR spectra were recorded in the 4000–400 cm^{-1} range using a Nicolet 5700 IR spectrometer, using thin-films.

Spectral analysis was performed to confirm the immobilization of the organic component on the bentonite surface. Particular attention was paid to the bands corresponding to the stretching vibrations of the P=O (≈1230–1250 cm^{-1}), P–O–C (≈1000–1050 cm^{-1}) groups, as well as O–H and N–H bonds.

Biological testing

The growth-promoting activity of organomodified bentonite was studied on the seeds of the “Almaken” and “Zhenis” wheat varieties. The experiments were conducted under laboratory conditions at Al-Farabi Kazakh National University at an average temperature of 22 ± 2 °C and a relative humidity of 50 ± 5%.

The seeds were treated with suspensions of organomodified bentonite containing Kaz-6 at concentrations of 10^{-2}–10^{-6} wt. %. Distilled water and solutions of free phosphonate at appropriate concentrations were used as controls.

The growth-stimulating effect was assessed based on shoot length on days 2 and 14. A series of parallel experiments (n = 3–5) were conducted for each treatment, and the results were expressed as mean values.

3. Results and Discussion

A comparative analysis of the developed method is presented in Table 1. Compared to the method described in [19], the proposed approach is characterized by a simpler process flow. Direct immobilization of organic oxyphosphonate on a mineral matrix eliminates the need for suspension preparation, multiple washings, and centrifugation. This results in reduced synthesis time and reduced reagent consumption while maintaining the effectiveness of the modification.

Table 1 – Comparison of conditions for obtaining organomodified bentonite (developed method and prototype)

Concentration of Organic Component, wt.%	Temperature, °C				Time, h			
	Soaking	Drying (pre-treatment)	Aging	Drying	Soaking	Drying (pre-treatment)	Aging	Drying
Dimethyl (4-hydroxy-1-(2-ethoxyethyl)piperidin-4-yl) phosphonate								
10^{-2}	40	50	Room temp.	50	12	3	2/3 (40 min)	2
10^{-3}	40	50	Room temp.	50	12	3	2/3 (40 min)	2
10^{-4}	40	50	Room temp.	50	12	3	2/3 (40 min)	2
10^{-5}	40	50	Room temp.	50	12	3	2/3 (40 min)	2
10^{-6}	40	50	Room temp.	50	12	3	2/3 (40 min)	2
Aminoacetic acid (prototype)								
5.0-5.5	–	110	Room temp.	70	24	6	24	4

Specifically, the processing temperature was reduced from 110 to 50°C, and the holding time was reduced from 24 hours to 40 minutes. Furthermore, the total duration of the preparation and modification stages was more than halved.

A significant advantage of the developed approach is the use of significantly lower concentrations of the organic component (10^{-2}–10^{-6} wt. %), whereas the prototype uses concentrations of approximately 5 wt. %. Reducing the modifier concentration not only reduces the cost of the process but also promotes a more uniform distribution of organic matter on the bentonite surface.

The IR spectra of organomodified bentonite demonstrate the appearance and/or strengthening of bands characteristic of the oxyphosphonate fragment (Table 2). In particular, bands of the P=O group stretching vibrations are observed in the region of ~1200 cm^{-1} and the characteristic P–O–C bands appear as prominent peaks at 1150–1030 cm^{-1}. Simultaneously, changes are recorded in the region of broad O–H bands (≈3200–3600 cm^{-1}), indicating the interaction of the organic component with the hydroxyl groups of the clay mineral surface.

The strong retention of Kaz-6 in the bentonite matrix is likely due to the formation of hydrogen and coordination interactions between the phosphonate groups of the modifier and the active sites of the clay mineral. Although specific

studies of desorption kinetics, binding strength, and the effect of pH on the release of the active component were not conducted in this study, the results of 14-day biological tests indicate the prolonged action of the composite and the effective retention of the modifier in the mineral matrix. A detailed study of the release kinetics and pH-dependent behavior of the system is of significant practical interest and will be the subject of further research.

The results of biological tests are presented in Figure 1. The obtained data indicate a pronounced growth-stimulating activity of organomodified bentonite.

Compared to the control (H_2O), a significant increase in shoot length was observed on both the 2nd and 14th days. The most pronounced effect was achieved at concentrations of 10^{-5}–10^{-6} wt. %, where seedling length exceeded control values by an average of 20–40%.

It is important to note that organomodified bentonite exhibits higher activity compared to free oxyphosphonate in similar concentrations. This confirms the effectiveness of immobilization of the active substance on the mineral matrix (Figure 2).

Table 2 – IR spectra data of bentonite, oxyphosphonate and obtained composite

Functional group	Bentonite, cm^{-1}	Oxyphosphonate, cm^{-1}	Composite, cm^{-1}
ν O–H	3628, 3438	3269	3631, 3442, 3347
ν C–H_{alkyl}	2922, 2853	2957, 2931, 2878, 2822, 2773	2977, 2756
ν P=O	–	1225	~1200 (overlaps with Si–O)
ν P–O–C / P–O	–	1150–1030	1150–1030 (overlaps with Si–O)
ν Si–O	~1008	–	~1009
ν Al–OH	916	–	916
δ CH_2 и CH_3	–	1500–1300 (intense)	1500–1300 (weak)
δ Si–O–Al	754, 694	–	768, 700
δ P–O, Si–O, Al–O	541, 469	565, 492, 429	519, 489, 424

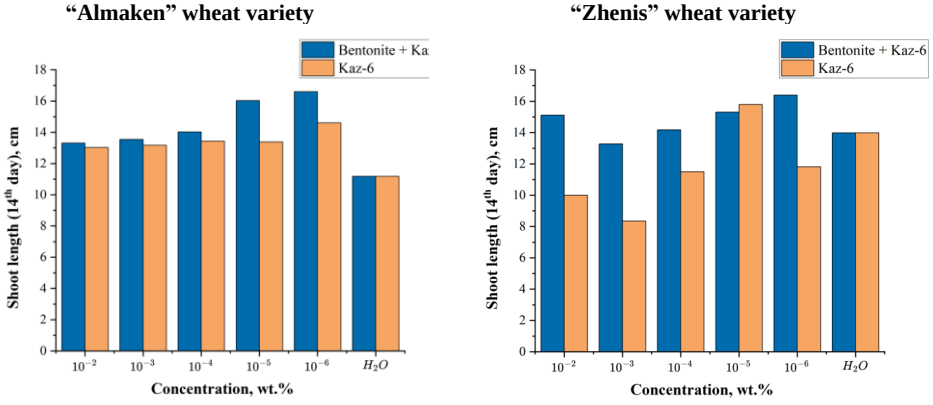

Figure 1 – The effect of organomodified bentonite on the growth of wheat seedlings of the "Almaken" and "Zhenis" varieties.

An important aspect of using the developed organomineral complexes is assessing their environmental safety and phytotoxicity. During a 14-day observation period, no signs of growth inhibition, chlorosis, or necrotic changes were detected in seedlings of the "Almaken" and "Zhenis" wheat varieties at concentrations ranging from 10^{-2} to 10^{-6} wt.%. Active development of the root system and aboveground parts of the plants indicates the absence of phytotoxic effects and confirms the high biocompatibility of the Kaz-6-bentonite composite at the concentrations studied.

Visual observation of the experimental samples on the 11th day (Figure 3) correlates with the quantitative morphometric data. Wheat seedlings of the "Almaken" and "Zhenis" varieties treated with the bentonite-Kaz-6 composite at a concentration of 10^{-6} wt. % show visibly more robust development of the vegetative mass compared to both the distilled water control (H_2O) and the free oxyphosphonate.

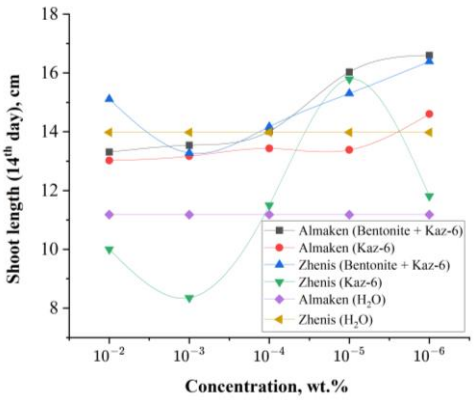

Figure 2 – Dependence of sprout length on modifier concentration

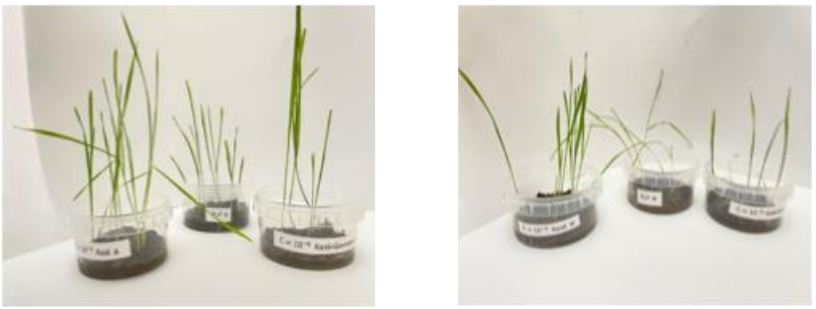

"Almaken" wheat variety **"Zhenis" wheat variety**

Figure 3 – Visual observation of the experimental shoots on the 11th day

The results obtained allow us to propose a probable mechanism for the formation of organomodified bentonite and its biological activity. Immobilization of oxyphosphonate on the bentonite surface is apparently achieved through:

- coordination interaction between the phosphoryl group (P=O) and surface hydroxyl (Si–OH) of bentonite;
- hydrogen bonds involving O–H and N–H groups;
- possible ion adsorption in the interlayer spaces of montmorillonite.

This interaction leads to the formation of a stable organomineral system in which the oxyphosphonate is fixed on the surface and in the interlayer space of bentonite.

Unlike the free compound, immobilized oxyphosphonate is released gradually, providing a prolonged effect. This explains the higher effectiveness of organomodified bentonite at low concentrations (10^{-5}–10^{-6} wt. %).

Additionally, bentonite acts as a carrier, improving the distribution of the active ingredient and promoting its retention in the plant root zone. The combination of the mineral's sorption properties and the biological activity of the oxyphosphonate results in a synergistic effect.

4. Conclusion

In this study, we developed an effective method for the mild organomodification of bentonite using Kaz-6 as a modifying agent. It was demonstrated that the proposed approach allows the process to be carried out under mild conditions (40–50 °C) with a significant reduction in processing time compared to known methods.

It was established that the use of low concentrations of oxyphosphonate (10^{-2}–10^{-6} wt. %) ensures effective immobilization of the organic component on the bentonite surface. IR spectroscopy data confirm the formation of an organomineral system due to the interaction of phosphorus-containing functional groups with the active sites of the clay mineral.

Biological testing results showed that the resulting organomodified bentonite exhibits pronounced growth-promoting activity against the “Almaken” and “Zhenis” wheat varieties. The greatest effect is observed at low modifier concentrations (10^{-5}–10^{-6} wt. %), indicating a prolonged action and increased efficiency of the active substance.

It was found that immobilization of oxyphosphonate on bentonite provides higher biological activity compared to the free compound, which is associated with its gradual release and more uniform distribution in the system.

Thus, the proposed organomodified bentonite is a promising functional material combining the properties of a mineral carrier and a biologically active component. The practical significance of this work lies in the possibility of creating effective, prolonged-release growth-promoting preparations with reduced active ingredient consumption and a simplified production technology. The developed approach can be used to create new agrochemical compositions adapted to the conditions of arid regions, including Kazakhstan.

Funding: This research has been funded by the Science Committee of the Ministry of Science and Higher Education of the Republic of Kazakhstan (BR27101179).

Conflict of interests: The authors declare that there are no conflicts of interests between the authors to disclose in this article.

БЕНТОНИТТІ ОКСИФОСФОНАТПЕН ЖҰМСАҚ ОРГАНОМОДИФИКАЦИЯЛАУ ЖӘНЕ ОНЫ ҰЗАҚ УАҚЫТ ӘСЕР ЕТЕТІН ӨСУ ЫНТАЛАНДЫРҒЫШЫ РЕТІНДЕ ҚОЛДАНУ

Б.Е.Капар[1,2], Т.Е.Жарқынбек [1,2*], Б.Б.Тюсюпова [2], Д.М.-К.Ибраимова [2], С.М.Тажибаева [2], В.К.Ю [1]

[1] Ә.Б. Бектұров атындағы Химия ғылымдары институты АҚ, Алматы, Қазақстан
[2]Әл-Фараби атындағы Қазақ ұлттық университеті, Алматы, Қазақстан

Түйіндеме. *Кіріспе.* Органомодификацияланған сазды материалдар биологиялық белсенді заттардың бақыланатын бөлінуін қамтамасыз ету қабілетіне байланысты ауыл шаруашылығына арналған функционалды жүйелер ретінде үлкен қызығушылық тудырады. Жоғары меншікті беттік ауданы мен ион алмасу қабілеті бар табиғи бентонит органикалық өсу ынталандырғышын иммобилизациялау үшін тамаша матрица болып табылады. *Бұл жұмыстың мақсаты* – ерекше оксифосфонатты (Каз-6) қолдана отырып, бентонитті жұмсақ органомодификациялаудың энергия тиімді әдісін жасау және оның бидайдың өсу ынталандырғышы ретіндегі тиімділігін бағалау. *Ұсынылған әдіс* бентонитті 40 °C температурада суда алдын ала диспергирлеуді, содан кейін 50 °C температурада кептіруді қамтиды. Дайындалған минералды матрица бөлме температурасында 10^{-2}–10^{-6} мас. % концентрация ауқымында диметил(4-гидрокси-1-(2-этоксиэтил)пиперидин-4-ил)фосфонаттың (Каз-6) сулы ерітінділерімен өңделді. Алынған композиттің құрылымы ИҚ-спектроскопия әдісімен сипатталды. Әзірленген тәсіл органикалық компоненттің айтарлықтай төмен концентрациясын қолдана отырып, белгілі аналогтармен салыстырғанда процестің температурасы мен ұзақтығын айтарлықтай төмендетуге мүмкіндік беретіні анықталды. Биологиялық сынақтар органомодификацияланған бентониттің бидайға («Алмакен» және «Жеңіс» сорттары) қатысты айқын өсуді ынталандырушы белсенділікті көрсететінін дәлелдеді. Ең жоғары тиімділік 10^{-5}–10^{-6} мас. % концентрациясында байқалды, мұнда композит бақылау тобынан және еркін оксифосфонаттан асып түсті. Нәтижелер Каз-6-ны бентонитке иммобилизациялау белсенді компоненттің ұзақ әсер етуін және жоғары биожетімділігін қамтамасыз ететінін көрсетеді. Әзірленген органоминералды композит ауыл шаруашылығын тұрақты дамыту үшін перспективалы өсу стимуляторы ретінде ұсынылуы мүмкін.

Түйін сөздер: бентонит, органомодификация, оксифосфонат, иммобилизация, өсу ынталандырғышы, бидай, біртіндеп босату.

Капар Баян Ерболқызы	*Магистрант, Инженер*
Жарқынбек Толғанай Еркінқызы	*Техника және технология магистрі, кіші ғылыми қызметкер*
Тюсюпова Бахыт Баймуратовна	*Химия ғылымдарының кандидаты, қауымдастырылған профессор*
Ибраимова Дана Мыкты-Кереевна	*Химия ғылымдарының кандидаты, аға оқытушы*
Тажибаева Сагдат Медербековна	*Химия ғылымдарының докторы, профессор*
Ю Валентина Константиновна	*Химия ғылымдарының докторы, профессор*

МЯГКАЯ ОРГАНОМОДИФИКАЦИЯ БЕНТОНИТА ОКСИФОСФОНАТОМ И ЕГО ПРИМЕНЕНИЕ КАК ПРОЛОНГИРОВАННОГО РОСТСТИМУЛЯТОРА

Б.Е.Капар,[1,2], Т.Е.Жарқынбек [1,2*], Б.Б.Тюсюпова [2], Д.М.-К.Ибраимова [2], С.М.Тажибаева [2], В.К.Ю [1]

[1]АО Институт химических наук им. А.Б. Бектурова, Алматы, Казахстан
[2]Казахский национальный университет им. аль-Фараби, Алматы, Казахстан

Резюме. *Введение.* Органомодифицированные глинистые материалы представляют значительный интерес как функциональные системы для сельского хозяйства благодаря их способности к контролируемому высвобождению биологически активных веществ. Природный бентонит, обладающий высокой удельной поверхностью и ионообменной емкостью, является отличной матрицей для иммобилизации органических стимуляторов роста. *Целью* данной работы является разработка энергоэффективного метода мягкой органомодификации бентонита с использованием специфического оксифосфоната (Каз-6) и оценка его эффективности в качестве стимулятора роста пшеницы пролонгированного действия. *Предложенный метод* включает предварительное диспергирование бентонита в воде при 40°C с последующей сушкой при 50°C. Подготовленную минеральную матрицу обрабатывали водными растворами диметил(4-гидрокси-1-(2-этоксиэтил)пиперидин-4-ил)фосфоната (Каз-6) в диапазоне концентраций 10^{-2}–10^{-6} мас. % при комнатной температуре. Структура полученного композита охарактеризована методом ИК-спектроскопии. Установлено, что разработанный подход позволяет существенно снизить температуру и продолжительность процесса по сравнению с известными аналогами при использовании значительно меньших концентраций органического компонента. Биологические испытания показали, что органомодифицированный бентонит проявляет выраженную ростстимулирующую активность по отношению к пшенице (сорта «Алмакен» и «Женис»). Наиболее значимый эффект наблюдался при концентрациях 10^{-5}–10^{-6} мас. %, где композит превзошел показатели контроля и свободного оксифосфоната. Результаты указывают на то, что иммобилизация Каз-6 на бентоните обеспечивает пролонгированное действие и повышенную биодоступность активного компонента. Разработанный органоминеральный композит может быть рекомендован как перспективный стимулятор роста для устойчивого развития сельского хозяйства.

Ключевые слова: бентонит, органомодификация, оксифосфонат, иммобилизация, стимулятор роста, пшеница, пролонгированное высвобождение.

Капар Баян Ерболқызы	*Магистрант, инженер*
Жарқынбек Толганай Еркінқызы	*Магистр техники и технологии, младший научный сотрудник*
Тюсюпова Бахыт Ибраимова	*Кандидат химических наук, ассоциированный профессор*
Дана Мыкты-Кереевна Баймуратовна	*Кандидат химических наук, старший преподаватель*
Тажибаева Сагдат Медербековна	*Доктор химических наук, профессор*
Ю Валентина Константиновна	*Доктор химических наук, профессор*

References

1. Borah D., Nath H., Saikia H. Modification of bentonite clay and its applications: A review. *Rev. Inorg. Chem.*, **2021**, *42*, No. 3, 3123–142. DOI: 10.1515/revic-2021-0030
2. Datta R., Holatko J., Latal O., Hammerschmiedt T., Elbl J., Pecina V., Kintl A., Balakova L., Radziemska M., Baltazar T., Skarpa P., Danish S., Zafar-ul-Hye M., Vyhnanek T., Brtnicky M. Bentonite-Based Organic Amendment Enriches Microbial Activity in Agricultural Soils. *Land*, **2020**, *9*, No. 8, 258. DOI: 10.3390/land9080258
3. Guégan R. Organoclay applications and limits in the environment. *C.r., Chim.*, **2019**, *22*, No. 2–3, 132–141. DOI: 10.1016/j.clay.2021.106336

4. Yu V.K., Praliyev K.D. *1-(2-ethoxyethyl)-4-(dimethoxyphosphoryl)-4-hydroxypiperidine, obladayushii stimuliruyushei rost rastenii aktivnost'yu* [1-(2-ethoxyethyl)-4-(dimethoxyphosphoryl)-4-hydroxypiperidine, which possesses plant growth stimulating activity] Provisional patent RK, No. 5011, **1997**. https://kz.patents.su/0-pp5011-1-2-etoksietil-4-dimetoksifosforil-4-gidroksipiperidin-obladayushhijj-stimuliruyushhejj-rost-rastenijj-aktivnostyu.html (accessed on 2 April 2026).

5. Spohn M. Preferential adsorption of nitrogen- and phosphorus-containing organic compounds to minerals in soils: A review. *Soil Biol. Biochem.*, **2024**, *194*, 109428. DOI: 10.1016/j.soilbio.2024.109428

6. Shen Y., Jiao S., Ma Z., Lin H., Gao W., Chen J. Humic acid-modified bentonite composite material enhances urea-nitrogen use efficiency. *Chemosphere*, **2020**, *255*, 126976. DOI: 10.1016/j.chemosphere.2020.126976

7. Montayeva N.S., Montayev S.A., Montayeva A.S. Studies of Montmorillonitic (Bentonite) Clay of Western Kazakhstan as a Therapeutic Mineral Feed Additive for Animals and Poultry. *Agric. Res.*, **2023**, *12*, 226–231. DOI: 10.1007/s40003-022-00634-7

8. Zheng Q.H., Yu A.B., Lu G.Q., Paul D.R. Clay-Based Polymer Nanocomposites: Research and Commercial Development. *J. Nanosci. Nanotechnol.*, **2005**, *5*, No. 10. 1574–1592. DOI: 10.1166/jnn.2005.411

9. Teng B.K.G. Chapter 7 - Polymer–Clay Nanocomposites. *Dev. Clay Sci.*, **2012**, *4*, 201–241. DOI: 10.1016/B978-0-444-53354-8.00007-4

10. Undabeytia T., Shuai U., Nir S., Rubin B. Applications of Chemically Modified Clay Minerals and Clays to Water Purification and Slow Release Formulations of Herbicides. *Minerals*, **2021**, *11*, No. 1, 9. DOI: 10.3390/min11010009

11. Bergaya F., Lagaly G. Intercalation chemistry of layerd minerals. *Layered Mineral Structures and their Application in Advanced Technologies*, **2021**, *11*. DOI: 10.1180/EMU-notes.11

12. Verma Y., Datta S.C., Mandzhieva S.S., Jatav S.S., Perelomov L., Burachevskaya, Rajput V.D. Release Behavior of Phosphorus from Bentonite Clay-Polymer Composites with Varying Cross-Linker Levels, and Neutralization Degree. *Eurasian Soil Sc.*, **2023**, *56*, S214–S226. DOI: 10.1134/S1064229323601476

13. Wei L., Millo A., Xing W., Zhao L., Zhang W., Zhang L. Simultaneous adsorption of phosphate and phosphonate by zirconium-modified biotite: implications for reverse osmosis concentrate treatment. *Desalination*, **2025**, *614*, 119144. DOI: 10.1016/j.desal.2025.119144

14. Leiva W., Toro N., Robles P., Quezada G.R., Salazar I., Flores-Badillo J., Jeldres R.I. Rheology Modifying Reagents for Clay-Rich Mineral Suspensions: A Review. *Polymers*, **2025**, *17*, No. 17, 2427. DOI: 10.3390/polym17172427

15. Mridha D., Lamsal B., Antonangelo J.A Nanotechnology in agriculture: Innovations for sustainability and greenhouse gas mitigation-A review. *Sci. Total Environ.*, **2025**, *995*, 180065. DOI: 10.1016/j.scitotenv.2025.180065

16. Pagano M., Lunetta E., Belli F., Mocarli G., Cocozza C., Cacciotti I. Advancements in Agricultural Nanotechnology: An Updated Review. *Plants*, **2025**, *14*, No. 18, 2939. DOI: 10.3390/plants14182939

17. DeRosa M.C., Monreal C., Schnitzer M., Walsh R., Sultan Y. Nanotechnology in fertilizers. *Nat. Nanotechnol.*, **2010**, *5*, 91. DOI: 10.1038/nnano.2010.2

18. Kystaubayeva N.U., Zharkynbek T.Y., Durap F., Yu V.K., Aydemir M., Merik N., Zazybin A.G., Ten A.Y., Rafikova K.S., Binbay N.E., Çelik Ö. Synthesis, and characterization of palladium(II) and platinum(II) complexes with α -hydroxy[1-(2-ethoxyethyl) piperidin-4-yl]phosphonate and use of the palladium(II) complex as pre-catalyst in Suzu -ki- Miyaura cross-coupling reactions. *J. Mol. Struct*., **2022**, *1270*, 133912. DOI: 10.1016/j.molstruc.2022.133912

19. Bortnikov S.V., Gorenkova G.A., Golubkov V.A., Vorozhtsov E.P. *Sposob polucheniya poroshkoobraznogo gidrofil'nogo rganobentonita* [Method for obtaining powdered hydrophilic organobentonite] Patent RF, No. 2754533, **2021**. https://new.fips.ru/iiss/document.xhtml?faces-redirect=true&id=ad1096cb70810c78f5d8bbee2dd3375f (accessed on 19 March 2026).

Chemical Journal of Kazakhstan
Volume 2, Number 94(2026), 124-135 https://doi.org/10.51580/2026-2.2710-1185.20

UDC 547.447

PHYTOTOXICITY OF THE BIOLOGICALLY ACTIVE COMPOUNDS LIBRARY CONSISTING OF O-*para*-TOLUOYL-β-(MORPHOLIN-1-YL)PROPIOMIDOXIME SALTS AND 5-ARYL-3-β-(PIPERIDIN-1-YL)ETHYL-1,2,4-OXADIAZOLES

L.A. Kayukova[1*], A.K. Tursunova[2], A.M. Duysenali[3], A. Yerlanuly[1], A.B. Sartoyeva[1], A.A. Sardar[2], Sh.M. Turbekova[2]

[1]JSC «A.B. Bekturov Institute of Chemical Sciences», Almaty, Kazakhstan
[2]Zh. Zhiembaev Kazakh Research Institute of Plant Protection and Quarantine, Almaty, Kazakhstan
[3]Abai Kazakh National Pedagogical University, Almaty, Kazakhstan

[*]Corresponding author e-mail: lkayukova@mail.ru

Abstract. *Introduction.* Agrochemical use increases environmental and health risks, making phytotoxicity studies essential. Amidoximes and 1,2,4-oxadiazoles are exogenous sources of NO, which can reduce abiotic stress and the phytotoxicity of agrochemicals; nevertheless, their phytotoxic profile has been poorly studied. *Goals and objectives.* To assess phytotoxicity of water-soluble compounds: O-*para*-toluoyl-β-(morpholin-1-yl)propioamidoxime salts (hydrochloride, oxalate, citrate) and three 5-aryl-3-β-(piperidin-1-yl)ethyl-1,2,4-oxadiazoles (aryl: *para*-MeC_6H_4, *para*-BrC_6H_4, *meta*-ClC_6H_4). *Methods.* Compounds were synthesized via improved multi-step synthesis. Phytotoxicity was tested on *Lactuca sativa* L. root and stem lengths at 100, 500, 1000 μg/ml. *Results.* Phytotoxicity depended on concentration and organ; roots were more sensitive. The highest phytotoxic effect was observed for *para*-bromo-oxadiazole with phytotoxicity from 57-67% at 500-1000 μg/ml 33-72%, followed by *meta*-chloro-oxadiazole with phytotoxicity from 33-72% at 100-1000 μg/ml. A growth-stimulating effect of amidoxime chloride and oxalate on stem growth is noted. Moderate toxicity was seen for hydrochloride salt and *para*-methyl oxadiazole. Citrate salt exhibited minimal phytotoxicity, comparable to control. *Conclusion.* The studied compounds showed different degrees of phytotoxicity depending on concentration and plant organ; roots were more sensitive with increasing concentration. Phytotoxicity is maximum for oxadiazoles with halogen substituents (*para*-bromo, *meta*-chloro), moderate/minimal for *para*-methyl oxadiazole and amidoxime hydrochloride and citrate. Shoot growth was stimulated by amidoxime hydrochloride and oxalate.

Key words: phytotoxic effects, root and shoot length of *Lactuca sativa* L., biological activity, O-*para*-toluoyl-β-(morpholin-1-yl)propioamidoxime salts, 5-aryl-3-β-(piperidin-1-yl)ethyl-1,2,4-oxadiazoles

Kayukova Lyudmila Alexandrovna	*Doctor of Chemical Sciences, Professor, Chief Researcher; E-mail: lkayukova@mail.ru*
Tursunova Alnura Kairatovna	*Master of Technical Sciences, Head of the Laboratory; E-mail: alnura_89.12.12@mail.ru*
Duysenali Aidana Macsutovna	*Al-Farabi Kazakh National University PhD student, Junior researcher; E-mail: duisenali-a@mail.ru*

Citation: Kayukova L.A., Tursunova A.K., Duysenali A.M., Yerlanuly A., Sartoyeva A.B., Sardar A.A., Turbekova Sh.M. Phytotoxicity of the biologically active compounds library consisting of O-*para*-toluoyl-β-(morpholin-1-yl)propiomidoxime salts and 5-aryl-3-β-(piperidin-yl)ethyl-1,2,4-oxadiazoles. *Chem. J. Kaz.*, **2026**, 2*(94)*, 124-135. (In Russ.). DOI: https://doi.org/10.51580/2026-2.2710-1185.20

Erlanuly Azamat	*Abai Kazakh National Pedagogical University PhD student; E-mail: azaraze8575@mail.ru*
Sartoyeva Aruzhan Bakhtiyerkuzu	*Bachelor, engineer; E-mail: aruzhansartaeva01@gmail.com*
Sardar Aizhan Anarbekkyzy	*Master of Natural Sciences, Senior Researcher; E-mail: aizhan.888sardar@gmail.com*
Turbekova Shyryn Meirambekovna	*Master of Natural Sciences, Senior Researcher; E-mail: shyrynka_turbekova@mail.ru*

ФИТОТОКСИЧНОСТЬ БИБЛИОТЕКИ БИОЛОГИЧЕСКИ АКТИВНЫХ СОЕДИНЕНИЙ, СОСТОЯЩЕЙ ИЗ СОЛЕЙ О-*пара*-ТОЛУОИЛ-β-(МОРФОЛИН-1-ИЛ)ПРОПИОАМИДОКСИМА И 5-АРИЛ-3-β-(ПИПЕРИДИН-1-ИЛ)ЭТИЛ-1,2,4-ОКСАДИАЗОЛОВ

Л.А. Каюкова[1*], А.К. Турсунова[2], А.М. Дүйсенәлі[3], А. Ерланұлы[1], А.Б. Сартоева[1], А.А. Сардар[2], Ш.М. Турбекова[2]

[1]АО Институт химических наук им. А.Б. Бектурова, Алматы, Казахстан
[2]ТОО Казахский научно-исследовательский институт защиты и карантина растений им. Ж. Жиембаева, Алматы, Казахстан
[3]Казахский национальный педагогический университет им. Абая, Алматы, Казахстан

Аннотация. *Введение.* Использование агрохимикатов увеличивает экологические и медицинские риски, что делает исследования фитотоксичности крайне важными. Амидоксимы и 1,2,4-оксадиазолы являются экзогенными источниками NO, который может снижать абиотический стресс и фитотоксичность агрохимикатов; однако их фитотоксический профиль изучен ограниченно. *Цели и задачи.* Оценить фитотоксичность водорастворимых соединений: солей О-*пара*-толуоил-β-(морфолин-1-ил)пропиоамидоксима (гидрохлорид, оксалат, цитрат) и трех 5-арил-3-β-(пиперидин-1-ил)этил-1,2,4-оксадиазолов (арил: *пара*-MeC_6H_4, *пара*-BrC_6H_4, *мета*-ClC_6H_4). *Методы*. Соединения были синтезированы с помощью усовершенствованного многоступенчатого синтеза. Фитотоксичность тестировали на корнях и стеблях *Lactuca sativa* L. при концентрациях 100, 500, 1000 мкг/мл. *Результаты.* Фитотоксичность зависела от концентрации и органа растения; корни оказались более чувствительными. Наибольший фитотоксический эффект наблюдался у *пара*-бром-оксадиазола с фитотоксичностью от 57–67 % при 500–1000 мкг/мл 33-72%, за которым следовал *мета*-хлор-оксадиазол с фитотоксичностью от 33-72% при 100-1000 мкг/мл. Отмечено стимулирующее рост действие хлорида и оксалата амидоксима на рост стебля. Умеренная токсичность наблюдалась у гидрохлорида и *пара*-метил-оксадиазола. Цитратная соль О-*пара*-толуоил-β-(морфолин-1-ил)пропиоамидоксима проявляла минимальную фитотоксичность, сопоставимую с контролем. *Выводы.* Изученные соединения показали различную степень фитотоксичности в зависимости от концентрации и органа растения; корни были более чувствительны с увеличением концентрации. Фитотоксичность максимальна для оксадиазолов с галогенными заместителями (*пара*-бром, *мета*-хлор), умеренная/минимальная для *пара*-метил-оксадиазола, а также для гидрохлорида и цитрата амидоксима. Рост стебля стимулировался гидрохлоридом и оксалатом амидоксимома.

Ключевые слова: фитотоксическое действие, длина корня и стебля *Lactuca sativa L.*, биологическая активность, основание и соли О-*пара*-толуоил-β-(морфолин-1-ил)пропиоамидоксима, 5-арил-3-β-(пиперидин-1-ил)этил-1,2,4-оксадиазолы

Каюкова Людмила Александровна	*Доктор химических наук, профессор, главный научный сотрудник*
Турсунова Альнура Кайратовна	*Магистр технических наук, заведующий лабораторией*
Дүйсенәлі Айдана Мақсұтқызы	*PhD докторант, младший научный сотрудник*
Ерланұлы Азамат	*PhD докторант, инженер*

Сартоева Аружан Бахтиёрқизи	*Бакалавр, инженер*
Сардар Айжан Анарбекқызы	*Магистр естественных наук, старший научный сотрудник*
Турбекова Шырын Мейрамбековна	*Магистр естественных наук, старший научный сотрудник*

1. Введение

Использование агрохимикатов в сельском хозяйстве для борьбы с заболеваниями растений приобрело решающее значение. Однако широкое использование этих соединений вызывает обеспокоенность из-за вредного воздействия таких веществ на окружающую среду и здоровье человека [1].

Общие фитотоксические эффекты включают изменение метаболизма растений, замедление роста или гибель растений [2].

Гербициды также могут вызывать фитотоксичность у сельскохозяйственных культур, если применяются неправильно, на неподходящей стадии роста или в избыточном количестве Фитотоксическое воздействие гербицидов является важным предметом изучения в области экотоксикологии [3].

Амидоксимы интенсивно изучаются как потенциальные лекарственные средства, пролекарства, фунгицидные или бактерицидные вещества [4].

Принято считать, что амидоксимы, продукты их О-алкилирования, О-ацилирования, а также 1,2,4-оксадиазолы очень реакционноспособны и используются в качестве пролекарств амидина [4,5,6]. Амидоксимы представляют собой окисленную химическую форму амидинов; они обладают хорошей растворимостью в воде. Концепция пролекарств основана на том факте, что пролекарства под действием фермента mARC подвергаются биотрансформации в биологически активную форму амидина [6]. В этом случае, в зависимости от количества стадий гидролиза производных амидоксима под действием эстераз, можно говорить о вторичных и третичных пролекарствах [7].

Амидиновый фрагмент присутствует в гуанидиновой цепи L-аргинина - жизненно важной аминокислоты, синтезируемой в организме человека в почках и печени. Важным метаболическим путем L-аргинина является его биотрансформация в оксид азота [8]. Оксид азота (NO) — это молекула, которая вызвала значительный интерес во многих научных дисциплинах, таких как медицина, биохимия, физиология и генетика. Благодаря своему широкому распространению и разнообразным характеристикам, он выполняет широкий спектр сложных биологических функций как у животных, так и у растений [9].

Оксид азота образуется различными биохимическими путями. В растениях существуют два основных альтернативных процесса: восстановительный путь, включающий превращение нитрита в NO, и окислительный путь, связанный с окислением молекул, содержащих аминогруппы [10]. Ключевыми экзогенными источниками оксида азота

являются амидоксимная группа, а также амидиновые, оксимные и нитрогруппы [11].

Оксид азота служит важной сигнальной молекулой с многочисленными физиологическими и биохимическими функциями. Он играет роль в запуске различных внутриклеточных процессов, связанных с управлением абиотическим стрессом, включая защитные реакции против активных форм кислорода (АФК) в неблагоприятных условиях окружающей среды. Абиотический стресс относится к негативному воздействию стрессовых факторов на рост растений и защитные механизмы, включая гербициды, затопление, тяжелые металлы, интенсивный свет, засоление, УФ-излучение, засуху, экстремальные температуры, озон и другие [12,13].

Фитотоксический профиль амидоксимов и 1,2,4-оксадиазолов изучен ограниченно.

Нами выполнено исследование фитотоксических свойств библиотеки производных β-аминопропиоамидоксимов (**1**–**6**) с ранее установленными структурами и биологической активностью (рисунок 1):

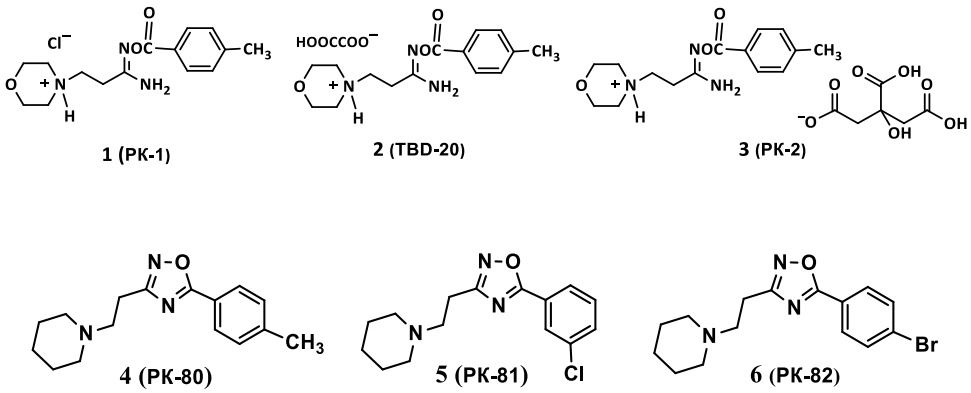

Рисунок 1 – Структуры и шифры исследованных солей О-пара-толуоил-β-(морфолин-1-ил)пропиоамидоксима: гидрохлорид (1), оксалат (2), цитрат (3) [14] и 5-арил-3-β-(пиперидин-1-ил)этил-1,2,4-оксадиазолов [арил: пара-MeC_6H_4 (4), мета-ClC_6H_4 (5), пара-BrC_6H_4 (6)] [15].

Установлено, что библиотека соединений (**1**–**6**) обладает ценными биологическими активностями: высокой противотуберкулезной на микобактериях человеческого вида *M. tuberculosis* и бычьего вида *M. bovis* [16], высокой противомикробной и противогрибковой активностью на стандартной панели микроорганизмов *Staphylococcus aureus, Bacillus subtilis, Escherichia coli, Pseudomonas aeruginosa, Candida albicans* [17,18]. В этой работе библиотека соединений (**1**–**6**) была исследована на *in vivo* фитотоксичность на семенах модельной культуры салата (*Lactuca sativa* L.).

2. Результаты

2.1 Синтез и строение

Указанные биологически активные соединения были синтезированы трех, четырехстадийным синтезом с использованием усовершенствованного метода получения исходных β-аминопропиоамидоксимов [19]. Метод заключался во взаимодействии вторичного гетероциклического амина и акрилонитрила в абсолютированном этаноле при комнатной температуре с последующим добавлением основания гидроксиламина при мольном соотношении гетероциклический амин:гидроксиламин 1:1,2 при комнатной температуре. Это позволяет повысить выход целевых β-аминопропиоамидоксимов и сократить время процесса за счет получегния готового продукта без примесей неорганической соли NaCl. На последующих стадиях библиотека изучаемых соединений **1**–**6** синтезирована с использованием методов, описанных в [14,15].

2.2 Испытания на фитотоксичность

На основании проведенных опытов установлено, что исследуемые соединения проявляют разную степень фитотоксичности в зависимости от концентрации и органа растения, причем корневая система *Lactuca sativa* L. оказалась более чувствительной, чем стебель. При этом для двух соединений **1** (**РК-1**) и **2** (**РК-2**) на стебле отмечен ростстимулирующий эффект в 23,5-35,3% и 35,3-41,2% в концентрациях 100–1000 мкг/мл и 100–500 мкг/мл, соответственно. Одновременно при указанных концентрациях происходило ингибирование роста корня на 37,8–45,9% и 43,2–51,4% (таблица, рисунок 2). В остальных случаях у соединений **4**–**6** не отмечено ростстимулирующего эффекта.

Максимальный ингибирующий эффект зафиксирован у соединения 5 (**РК-81**), при котором сокращение длины корней составляло около 33% уже при 100 мкг/мл и достигало 72% при концентрациях 500–1000 мкг/мл, тогда как длина стеблей оставалась на уровне контроля.

Высокую фитотоксичность также проявило соединение **6** (**РК-82**) (подавление корней на 57–67 % при 500–1000 мкг/мл), причем во всех случаях влияние на стебли было минимальным. Соединения **4** (**РК-80**) и **1** (**РК-1**) характеризовались умеренной фитотоксичностью, уменьшая длину корней на 30–40 % при высоких дозах. Соединение **3** (**TBD-20**), продемонстрировало низкую фитотоксичность во всем диапазоне концентраций.

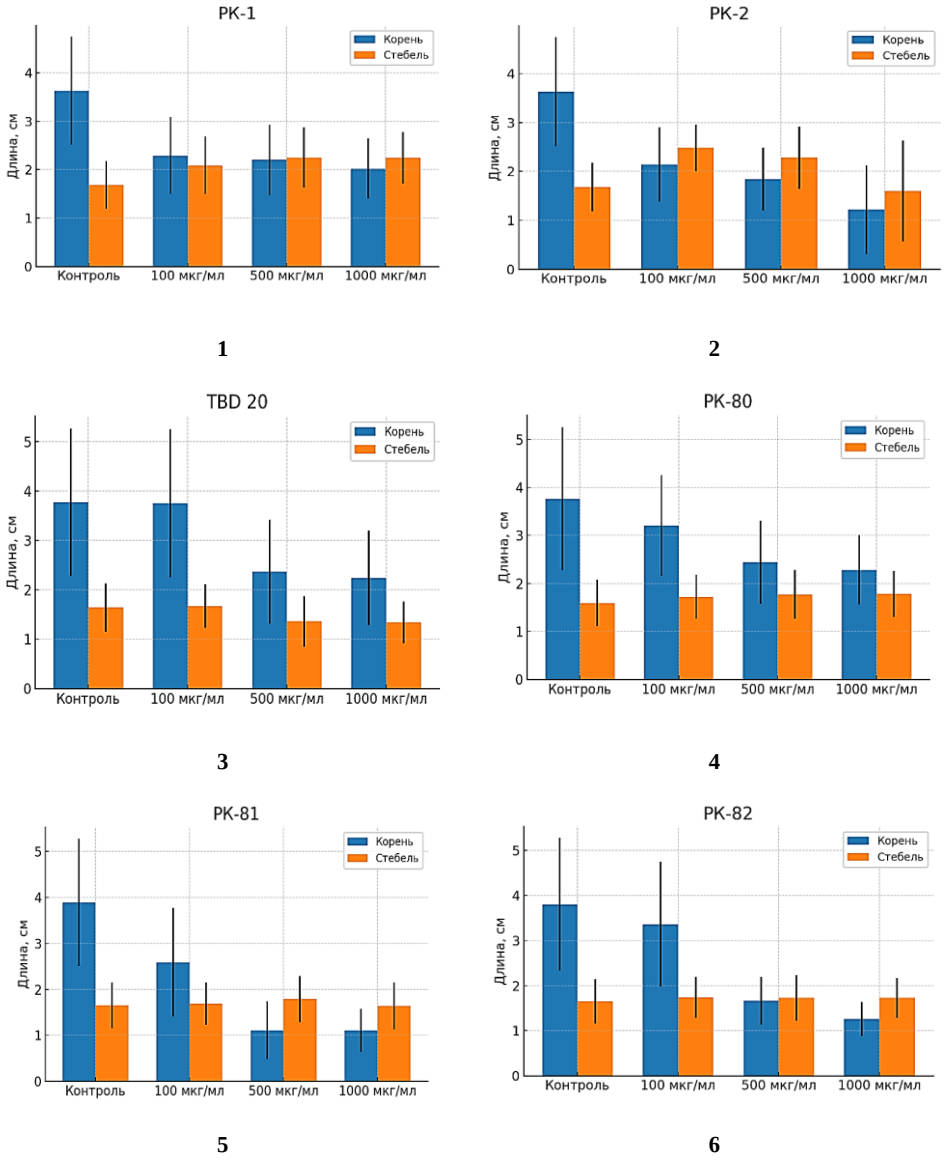

Рисунок 2 – Сравнительный анализ влияния испытуемых производных β-аминопропиоамидоксимов (**1**–**6**) и их концентрации на ростовые показатели корней и стеблей листьев салата *Lactuca sativa* L

3. Экспериментальная часть

3.1 Синтез производных β-аминопропиоамидоксимов

Синтез β-(морфолин-1-ил)пропиоамидоксима. К 20 г (0,23 молей) морфолина в 50 мл абсолютированного этанола добавляют 12,2 г (0,23 молей) акрилонитрила в 10 мл абсолютированного этанола, перемешивают

при комнатной температуре 5 ч, добавляют 9,11 г (0,276 молей) гидроксиамина в 10 мл абсолютированного этанола. Реакционную смесь перемешивают при к.т. в течение 37 ч, упаривают досуха, продукт перекристаллизовывают из изопропанола с выделением β-(морфолин-1-ил)пропиоамидоксима с выходом 28,8 г (72%) [19].

Синтез β-(пиперидин-1-ил) пропиоамидоксима с выходом 82% выполнен по этому методу.

Последующие стадии получения соединений **1**–**3** на основе β-(морфолин-1-ил)пропиоамидоксима описаны в работе [14] и соединений **4**–**6** на основе β-(пиперидин-1-ил)пропиоамидоксима представлены в статье [16].

Биологический скрининг проводился для хроматографически чистых образцов **1**–**6**, имеющих одно пятно на пластинках ТСХ.

Физико-химические характеристики и спектральные данные [ИК- и ЯМР (^{1}H и ^{13}C) спектры] соединений **1**–**6** воспроизводят ранее полученные значения.

3.2 Оценка фитотоксичности химических соединений на проростках салата *Lactuca sativa* L.

Лабораторные эксперименты по определению фитотоксичности соединений **1**–**6** проведены на модельной культуре *Lactuca sativa* L. с оценкой их влияния на морфометрические параметры растений: длину корневой системы и длину стебля, при трех уровнях концентраций действующего вещества (100, 500 и 1000 мкг/мл).

Оценка фитотоксичности образцов проводилась на семенах модельной культуры салата *Lactuca sativa* L. Выполнено 4 повтора на вариант – образец каждого соединения по 25 штук семян на повтор; семена предварительно стерилизовали (70% этанол 1 минуту, 1% NaOCl 5 минут при пятикратной промывке стерильной дистиллированной водой. Затем проводили обработку растворами исследуемых соединений **1 (РК-1), 2** (**РК-2**), **3** (**TBD-20**), **4** (**РК-80**), **5** (**РК-81**) **6** (**РК-82**) в концентрациях 100, 500 и 1000 мкг/мл (контроль - вода) путем замачивания при 22 °С в течение 30 мин с последующей подсушкой и проращиванием на увлажненной стерильной фильтровальной бумаге в чашках Петри при 22 ± 2 °С и фотопериоде 16/8 ч. На 4-е сутки измеряли длину корневой системы и побега у всех нормальных проростков, результаты выражали как среднее ± стандартное отклонение.

Таблица – Влияние испытуемых производных β-аминопропиоамидоксимов (**1**–**6**) и их концентраций на ростовые показатели корней и стеблей листьев салата *Lactuca sativa* L

Концентрация	Корень	Стебель
РК-1		
Контроль	3.7 ± 0.9^{a}	1.7 ± 0.4^{b}
100 мкг/мл	2.3 ± 0.3^{b}	2.1 ± 0.3^{a}
500 мкг/мл	2.2 ± 0.5^{b}	2.3 ± 0.4^{a}
1000 мкг/мл	2.0 ± 0.6^{b}	2.3 ± 0.3^{a}
РК-2		
Контроль	3.7 ± 0.9^{a}	1.5 ± 0.4^{b}
100 мкг/мл	2.1 ± 0.7^{b}	2.4 ± 0.3^{a}
500 мкг/мл	1.8 ± 0.4^{bc}	2.3 ± 0.5^{a}
1000 мкг/мл	1.2 ± 0.7^{c}	1.6 ± 0.9^{b}
TBD-20		
Контроль	3.8 ± 1.1^{a}	1.7 ± 0.4^{a}
100 мкг/мл	3.8 ± 1.1^{a}	1.7 ± 0.3^{a}
500 мкг/мл	2.4 ± 0.6^{b}	1.4 ± 0.3^{b}
1000 мкг/мл	2.2 ± 0.6^{b}	1.4 ± 0.2^{b}
РК-80		
Контроль	3.8 ± 1.1^{a}	1.6 ± 0.4^{a}
100 мкг/мл	3.2 ± 0.9^{ab}	1.7 ± 0.3^{a}
500 мкг/мл	2.4 ± 0.7^{b}	1.8 ± 0.3^{a}
1000 мкг/мл	2.3 ± 0.6^{b}	1.8 ± 0.3^{a}
РК-81		
Контроль	3.9 ± 1.1^{a}	1.6 ± 0.4^{a}
100 мкг/мл	2.6 ± 0.7^{b}	1.7 ± 0.4^{a}
500 мкг/мл	1.1 ± 0.5^{c}	1.8 ± 0.3^{a}
1000 мкг/мл	1.1 ± 0.3^{c}	1.6 ± 0.3^{a}
РК-82		
Контроль	3.8 ± 1.2^{a}	1.7 ± 0.4^{a}
100 мкг/мл	3.3 ± 1.2^{ab}	1.8 ± 0.3^{a}
500 мкг/мл	1.7 ± 0.3^{c}	1.8 ± 0.3^{a}
1000 мкг/мл	1.3 ± 0.2^{c}	1.7 ± 0.3^{a}

Примечание – Данные представлены как среднее ± стандартное отклонение (Mean ± SD, n = 100). Статистическую обработку данных проводили с использованием программного обеспечения IBM SPSS Statistics v.26.0 (IBM Corp., Armonk, NY, USA).
Для оценки различий между вариантами использовали однофакторный дисперсионный анализ (ANOVA) с последующим множественным сравнением средних по критерию Тьюки (Tukey HSD) при уровне значимости $p < 0.05$. Различные буквенные индексы в пределах одного варианта указывают на статистически значимые различия между концентрациями. Средние значения, обозначенные одинаковыми буквами, статистически не различаются, тогда как значения с различными буквами отличаются достоверно. Комбинированные индексы (например, «^{ab}») указывают на перекрытие статистических групп. Сравнение проводилось отдельно для каждого варианта.

4. Заключение

Исследованные соединения показали различную степень фитотоксичности в зависимости от концентрации и органа растения, при этом корневая система *Lactuca sativa* L. оказалась более чувствительной. Степень фитотоксичности возрастала с увеличением концентрации химических соединений; фитотоксичность зависит от структуры

исследуемых соединений и достигает максимума для 1,2,4-оксадиазолов с галогенными заместителями (*пара*-бром- и *мета*-хлор) в арильном кольце; умеренная и минимальная фитотоксичность характерна для 1,2,4-оксадиазола с *пара*-CH_3 группой, а также для гидрохлорида и цитрата О-*пара*-толуоил-β-(морфолин-1-ил)пропиоамидоксима. Два соединения – гидрохлорид и оксалат амидоксима проявили ростстимулирующий эффект на стебле салата *Lactuca sativa* L.

Полученные результаты формируют основу для дальнейшего изучения взаимосвязи “структура-фитотоксичность» и отбора соединений с приемлемым фитотоксическим профилем для последующих биологических исследований».

Финансирование: Работа выполнена по программе целевого финансирования научных исследований на 2025–2026 гг., осуществляемого Комитетом науки Министерства науки и образования Республики Казахстан, по программе BR27101179.

Конфликт интересов: Авторы заявляют об отсутствии конфликта интересов, требующего раскрытия в данной статье.

О-*пара*-ТОЛОУИЛ-β-(МОРФОЛИН-1-YL)ПРОПИОМИДОКСИМ ЖӘНЕ 5-АРИЛ-3-β-(ПИПЕРИДИН-1-YL)ЭТИЛ-1,2,4-ОКСАДИАЗОЛДАР ТҰЗДАРЫН ҚАМТИТЫН БИОЛОГИЯЛЫҚ БЕЛСЕНДІ ҚОСЫЛЫСТАР КІТАПХАНАСЫНЫҢ ФИТОТОКСИКАЛЫҚ ӘСЕРІ

Л.А. Каюкова[1*], А.К. Турсунова[2], А.М. Дүйсенәл[3], А. Ерланұлы[1], А.Б. Сартоева[1], А.А. Сардар[2], Ш.М. Турбекова[2]

[1]А.Б. Бектуров атындағы химия ғылымдары институты АҚ, Алматы, Қазақстан
[2]ЖШС Ж. Жиембаев атындағы Қазақ өсімдіктерді қорғау және карантин ғылыми-зерттеу институты, Алматы, Қазақстан
[3]Абай атындағы Қазақ ұлттық педагогикалық университеті, Алматы, Казахстан

Түйіндеме. *Кіріспе.* Агрохимикаттарды қолдану қоршаған ортаға және денсаулыққа қауіп төндіреді, бұл фитоуыттылықты зерттеуді өте маңызды етеді. *Мақсаттар мен міндеттер*. Суда еритін қосылыстардың: О-*пара*-толуоил-β-(морфолин-1-ил)пропиоамидоксим тұздарының (гидрохлорид, оксалат, цитрат) және үш 5-арил-3-β-(пиперидин-1-ил)этил-1,2,4-оксадиазолдардың (арил: *пара*-MeC_6H_4, *пара*-BrC_6H_4, *мета*-ClC_6H_4) фитоуыттылығын бағалау. *Әдістер*. Қосылыстар жақсартылған көп сатылы синтезді қолдану арқылы синтезделді. Фитоуыттылық *Lactuca sativa* L. тамырлары мен сабақтарында 100, 500, 1000 мкг/мл концентрациясында сыналды. *Нәтижелер*. Фитоуыттылық концентрацияға және өсімдік мүшесіне байланысты болды; тамырлар сезімтал болды. Ең жоғары фитоуытты әсер *пара*-бромо-оксадиазол үшін 500-1000 мкг/мл 33-72% фитоуыттылығымен 57-67% аралығында байқалды, одан кейін 100-1000 мкг/мл кезінде фитоуыттылығымен 33-72% аралығында *мета*-хлор-оксадиазол байқалды. Амидоксим хлориді мен оксалаттың сабақтың өсуіне өсуді ынталандырушы әсері байқалды. Гидрохлорид пен *пара*-метилоксадиазолда орташа уыттылық байқалды. О-*пара*-Толуоил-β-(морфолин-1-ил)пропиоамидоксимнің цитрат тұзы бақылау тобымен салыстыруға болатын минималды фитотоксикалықты көрсетті. *Қорытынды*. Зерттелген қосылыстар концентрация мен өсімдік мүшесіне байланысты әртүрлі фитотоксикалық дәрежелерді көрсетті; тамырлар концентрацияның жоғарылауымен сезімтал болды. Фитотоксикалық әсер галоген алмастырғыштары (*пара*-бром, *мета*-хлор) бар оксадиазолдар үшін ең жоғары, *пара*-метилоксадиазол үшін орташа/минималды, сондай-ақ амидоксим гидрохлориді мен цитрат үшін орташа/минималды. Сабақтың өсуі амидоксим гидрохлориді мен оксалатпен ынталандырылды.

Түйін сөздер: фитотоксикалық әсер, *Lactuca sativa* L. тамыры мен сабағының ұзындығы, биологиялық белсенділігі, О-*пара*-толуоил-β-(морфолин-1-ил)пропиоамидоксимнің негізі және тұздары, 5-арил-3-β-(пиперидин-1-ил)этил-1,2,4-оксадиазолдар

Каюкова Людмила Александровна	*Химия ғылымдарының докторы, профессор, бас ғылыми қызметкер*
Турсунова Альнура Кайратқызы	*Техника ғылымдарының магистрі, зертхана меңгерушісі*
Дүйсенәлі Айдана Мақсұтқызы	*PhD докторант, кіші ғылыми қызметкер*
Ерланұлы Азамат	*PhD докторант*
Сартоева Аружан Бахтиёрқизи	*Бакалавр, инженер*
Сардар Айжан Анарбекқызы	*Жаратылыстану ғылымдарының магистрі, аға ғылыми қызметкер*
Турбекова Шырын Мейрамбекқызы	*Жаратылыстану ғылымдарының магистрі, аға ғылыми қызметкер*

References

1. Hasanuzzaman M., Mohsin S.M., Bhuyan M.B., Bhuiyan T.F., Anee T.I., Masud A.A., Nahar K. Phytotoxicity, environmental and health hazards of herbicides: challenges and ways forward, *Agrochemicals Detection, Treatment and Remediation*, Elsevier, **2020**, pp. 55–99, doi:10.1016/b978-0-08-103017-2.00003-9

2. Barbaś P., Pietraszko M., Pszczółkowski P., Skiba D., Sawicka B. Assessing Phytotoxic Effects of Herbicides and Their Impact on Potato Cultivars in Agricultural and Environmental Contexts. *Agronomy*, **2023**, *14*, 85, DOI:10.3390/agronomy14010085

3. Gruss I., Bączek P., Ćwieląg-Piasecka I., Jędrzejewski S., Magiera-Dulewicz J., Twardowska K. Assessing the ecotoxicological effects of pesticides on non-target plant species. *Environ. Monit. Assess.*, **2025**, *197*, 1047. DOI: 10.1007/s10661-025-14532-2

4. Baykov S.V., Semenov A.V., Tarasenko M.V., Boyarskiy V.P. Application of amidoximes for the heterocycles synthesis. *Tetrahedron Lett.*, **2020**, *61*, 152403. DOI: 10.1016/j.tetlet.2020.152403.

5. *Ovdiichuk O.V., Hordiyenko O.V. Amidoximes and their masked derivatives as prodrugs of amidines – arginine mimetics.* J. Org. Phar. Chem., ***2016***, 14(1(53)), *36-45. DOI: 10.24959/ophcj.16.878*

6. Clement B., Struwe M.A. The History of mARC. *Molecules*, **2023**, *28*, 4713. DOI: 10.3390/ molecules28124713

7. Hetrick K.J., Raines R.T. Assessing and utilizing esterase specificity in antimicrobial prodrug development. *Methods Enzym.*, **2022**, *664*, 199–220. DOI: 10.1016/bs.mie.2021.11.008

8. Pedrazini M.C., Martinez E.F., dos Santos V.A.B., Groppo F.C. L-arginine: its role in human physiology, in some diseases and mainly in viral multiplication as a narrative literature review. *Futur. J. Pharm. Sci*., **2024**, *10*, 99. DOI: 10.1186/s43094-024-00673-7

9. Andrabi S.M., Sharma N.S., Karan A., Shahriar S.M.S., Cordon B., Ma B., Xie J.

Nitric Oxide: Physiological Functions, Delivery, and Biomedical Applications. *Adv. Sci.* (Weinh). **2023**, *10(30),* e2303259. DOI: 10.1002/advs.202303259

10. Kolupaev Y.E., Shkliarevskyi M.A., Pyshchalenko M.A., Dmitriev A.P. Nitric oxide: functional interaction with phytohormones and applications in crop production. *Agriculture and Forestry*. **2024**, *70(1)*, 379-411. DOI: 10.17707/AgricultForest.70.1.24

11. Sahyoun T., Arrault A., Schneider R. Amidoximes and Oximes: Synthesis, Structure, and Their Key Role as NO Donors. *Molecules*, **2019**, *24*, 2470. DOI: 10.3390/molecules24132470

12. Wojtaszek P., Rybczyński J., Grzesiak S., Niemirowicz-Szczytt K., Marszałkowski G. The role of nitric oxide in plant growth regulation and responses to abiotic stresses. *Acta Physiol. Plant.,* **2004**, *26(4),* 459-472. DOI: 10.1007/s11738-004-0039-2

13. Singh K., Shukla I., Tiwari A.K., Azmi L. Physiological, Biochemical, and Molecular Mechanism of Nitric Oxide-Mediated Abiotic Stress Tolerance // In: Aftab, T., Hakeem, K.R. (eds) Plant Growth Regulators. Springer, Cham., **2021**. https://doi.org/10.1007/978-3-030-61153-8_11

14. Kayukova L.A., Baitursynova G.P., Praliev K.D., Kemelbekov U.S. Pharmacologically acceptable chemical forms of O-para-toluoyl-β-morpholinopropioamidoxime. *Chem. J. Kaz.*, **2012**, № 3, 69–76. (In Russ.).

15. Kayukova L.A., Praliev K.D., Zhumadildaeva I.S. Cyclization of O-benzoyl-β-piperidinopropionamidoximes to form 5-phenyl-3-(β-piperidino)ethyl-1,2,4-oxadiazoles. *Russ. Chem. Bull.*, **2002**, *51*, 2100–2105. DOI: 10.1023/A:1021628430346

16. Kayukova L., Bismilda V., Turgenbayev K., Uzakova A., Baitursynova G., Jussipbekov U., Mukanova M., Chingissova L., Dyussembayeva G., Borsynbayeva A., Yerlanuly A., Auyezov A. β-Aminopropioamidoximes derivatives as potential antitubercular agents against anthropozoonotic infections caused by Mycobacterium tuberculosis and Mycobacterium bovis, *Vet. World*, **2025**, *18(3)*, 731–745. DOI: 10.14202/vetworld.2025.731-745

17. Patent KZ for Utility Model No. 8787. *Primenenie oksalata O-para-toluoil-(β-morfolin-1-il)propioamidoksima v kachestve soedineniya s antibakterial`noj i protivogribkovoj aktivnost`yu* [Use of O-para-toluoyl-(β-morpholin-1-yl)propioamidoxime oxalate as a compound with antibacterial and antifungal activity]. Kayukova L.A., Erlanuly A., Sartoeva A.B., Seidakhmetova R.B., **2024**.

18. Kayukova L.A., Seydakhmetova R.B., Duisenali A.M., Yerlanuly A., Sartoyeva A.B. Search for effective drugs against pathogenic flora in the series of O-para-toluoyl-β-(morpholin-1-yl)propiomidoxime and 5-aryl-3-β-(piperidine-1-yl)ethyl-1,2,4-oxadiazoles derivatives. *Chem. J. Kaz.*, **2025**, *1(89)*, 129–139. (In Russ.). DOI: https://doi.org/10.51580/2025-1.2710-1185.13

19. Notification of Patent KZ for Utility Model issuance for application No. 2026/0772.2 dated 04.07.2026. *Sposob polucheniya β-(morfolin-1-il)propioamidoksima* [Method for producing β-(morpholine-1-yl)propioamidoxime], Kayukova L.A., Duisenali A.M., Yerlanuly A., Sartoyeva A.B., **2026**.

Список использованных источников

1. Hasanuzzaman M., Mohsin S.M., Bhuyan M.B., Bhuiyan T.F., Anee T.I., Masud A.A., Nahar K. Phytotoxicity, environmental and health hazards of herbicides: challenges and ways forward, *Agrochemicals Detection, Treatment and Remediation*, Elsevier, **2020**, pp. 55–99, doi:10.1016/b978-0-08-103017-2.00003-9

2. Barbaś P., Pietraszko M., Pszczółkowski P., Skiba D., Sawicka B. Assessing Phytotoxic Effects of Herbicides and Their Impact on Potato Cultivars in Agricultural and Environmental Contexts. *Agronomy*, **2023**, *14*, 85, DOI:10.3390/agronomy14010085

3. Gruss I., Bączek P., Ćwieląg-Piasecka I., Jędrzejewski S., Magiera-Dulewicz J., Twardowska K. Assessing the ecotoxicological effects of pesticides on non-target plant species. *Environ. Monit. Assess.*, **2025**, *197*, 1047. DOI: 10.1007/s10661-025-14532-2

4. Baykov S.V., Semenov A.V., Tarasenko M.V., Boyarskiy V.P. Application of amidoximes for the heterocycles synthesis. *Tetrahedron Lett.*, **2020**, *61*, 152403. DOI: 10.1016/j.tetlet.2020.152403.

5. *Ovdiichuk O.V., Hordiyenko O.V. Amidoximes and their masked derivatives as prodrugs of amidines – arginine mimetics.* J. Org. Phar. Chem., ***2016***, 14(1(53)), *36-45. DOI: 10.24959/ophcj.16.878*

6. Clement B., Struwe M.A. The History of mARC. *Molecules*, **2023**, *28*, 4713. DOI: 10.3390/molecules28124713

7. Hetrick K.J., Raines R.T. Assessing and utilizing esterase specificity in antimicrobial prodrug development. *Methods Enzym.*, **2022**, *664*, 199–220. DOI: 10.1016/bs.mie.2021.11.008

8. Pedrazini M.C., Martinez E.F., dos Santos V.A.B., Groppo F.C. L-arginine: its role in human physiology, in some diseases and mainly in viral multiplication as a narrative literature review. *Futur. J. Pharm. Sci*., **2024**, *10*, 99. DOI: 10.1186/s43094-024-00673-7

9. Andrabi S.M., Sharma N.S., Karan A., Shahriar S.M.S., Cordon B., Ma B., Xie J.

Nitric Oxide: Physiological Functions, Delivery, and Biomedical Applications. *Adv. Sci.* (Weinh). **2023**, *10(30)*, e2303259. DOI: 10.1002/advs.202303259

10. Kolupaev Y.E., Shkliarevskyi M.A., Pyshchalenko M.A., Dmitriev A.P. Nitric oxide: functional interaction with phytohormones and applications in crop production. *Agriculture and Forestry*. **2024**, *70(1)*, 379-411. DOI: 10.17707/AgricultForest.70.1.24

11. Sahyoun T., Arrault A., Schneider R. Amidoximes and Oximes: Synthesis, Structure, and Their Key Role as NO Donors. *Molecules*, **2019**, *24*, 2470. DOI: 10.3390/molecules24132470

12. Wojtaszek P., Rybczyński J., Grzesiak S., Niemirowicz-Szczytt K., Marszałkowski G. The role of nitric oxide in plant growth regulation and responses to abiotic stresses. *Acta Physiol. Plant.*, **2004**, *26(4)*, 459-472. DOI: 10.1007/s11738-004-0039-2

13. Singh K., Shukla I., Tiwari A.K., Azmi L. Physiological, Biochemical, and Molecular Mechanism of Nitric Oxide-Mediated Abiotic Stress Tolerance // In: Aftab, T., Hakeem, K.R. (eds) Plant Growth Regulators. Springer, Cham., **2021**. https://doi.org/10.1007/978-3-030-61153-8_11

14. Kayukova L.A., Baitursynova G.P., Praliev K.D., Kemelbekov U.S. Pharmacologically acceptable chemical forms of O-para-toluoyl-β-morpholinopropioamidoxime. *Chem. J. Kaz.*, **2012**, № 3, 69–76. (In Russ.).

15. Каюкова Л.А., Пралиев К.Д., Жумадильдаева И.С. О-Бензоил-β-пиперидинопропиоамидоксимы и их дегидратация до 3-(β-пиперидино)этил-5-фенил-1,2,4-оксадиазолов. *Изв. АН. Сер. хим.*, **2002**, *51*, 1945–1949.

16. Kayukova L., Bismilda V., Turgenbayev K., Uzakova A., Baitursynova G., Jussipbekov U., Mukanova M., Chingissova L., Dyussembayeva G., Borsynbayeva A., Yerlanuly A., Auyezov A. β-Aminopropioamidoximes derivatives as potential antitubercular agents against anthropozoonotic infections caused by Mycobacterium tuberculosis and Mycobacterium bovis, *Vet. World*, **2025**,*18(3)*, 731–745. DOI: 10.14202/vetworld.2025.731-745

17. Патент РК на полезную модель № 8787. *Применение оксалата О-пара-толуоил-(β-морфолин-1-ил)пропиоамидоксима в качестве соединения с антибактериальной и противогрибковой активностью.* Каюкова Л.А., Ерланулы А., Сартоева А.Б., Сейдахметова Р.Б., **2024**.

18. Kayukova L.A., Seydakhmetova R.B., Duisenali A.M., Yerlanuly A., Sartoyeva A.B. Search for effective drugs against pathogenic flora in the series of O-para-toluoyl-β-(morpholin-1-yl)propiomidoxime and 5-aryl-3-β-(piperidine-1-yl)ethyl-1,2,4-oxadiazoles derivatives. *Chem. J. Kaz.*, **2025**, *1(89)*, 129–139. (In Russ.). DOI: https://doi.org/10.51580/2025-1.2710-1185.13

19. Уведомление о выдаче патента KZ на полезную модель по заявке № 2026/0772.2 от 07.04.2026. *Способ получения β-(морфолин-1-ил)пропиоамидоксима,* Каюкова Л.А., Дүйсенәлі А.М., Ерланулы А., Сартоева А.Б., **2026**.

Chemical Journal of Kazakhstan
Volume 2, Number 94(2026), 136-147 https://doi.org/10.51580/2026-2.2710-1185.21

UDC 547.89+615.31+615.211

BENZOYLATED BISPIDONE: SYNTHESIS AND INVESTIGATION OF BIOLOGICAL EFFECTS

A.E. Malmakova [1*], T.K. Iskakova [2], K.D. Praliyev [1], O.T. Seilkhanov [3], K.B. Otegulova [1], M.K. Amirkulova [4,5], Ye.M. Satbayeva [4], D.M. Kadyrova [4]

[1] A.B. Bekturov Institute of Chemical Sciences, Almaty, Kazakhstan
[2] Kazakh National Research Technical University named after K. I. Satbayev, Almaty, Kazakhstan
[3] Sh. Ualikhanov Kokshetau University, Kokshetau, Kazakhstan
[4] Department of Pharmacology, Asfendiyarov Kazakh National Medical University/School of General Medicine, Almaty, Kazakhstan
[5] National Centre for Expertise of Medicines and Medical Devices, Astana, Kazakhstan

**Corresponding author e-mail: malmakova@mail.ru*

Abstract. *Introduction.* Local anaesthetics work by blocking voltage-gated sodium channels, which causes a temporary loss of sensation, a property used in many medical procedures. While novocaine, lidocaine, and trimecaine are effective, they have drawbacks such as short duration, possible toxicity, and tolerability problems. This study set out to create a complex of benzoylated 3-(3-butoxypropyl)-7-cyclopropanemethyl-substituted bispidone with β-cyclodextrin (LAC-5) and to compare its local anaesthetic effects with medicals using standard preclinical tests. LAC-5 was synthesised using Mannich condensation, oximation, *O*-benzoylation, and β-cyclodextrin complexation. Its structure was confirmed by methods such as infrared and nuclear magnetic resonance spectroscopies. Tests showed that LAC-5 has strong local anaesthetic effects, performing better than trimecaine, lidocaine, and novocaine in both infiltration and conduction anaesthesia models. In infiltration anaesthesia, LAC-5 achieved the maximum measurable depth of anaesthesia (index 36.0) at a 0.25% concentration, with a duration of complete anaesthesia of 56.66 min and a total duration of action of 76.66 min, exceeding the reference medications by up to 5.66- and 2.6-fold, respectively ($p < 0.001$). In conduction anaesthesia, LAC-5 produced a total duration of action of 160.0 ± 4.7 min, surpassing reference medications. Based on the results obtained, LAC-5 is recommended for comprehensive preclinical pharmacological evaluation, including assessment of acute toxicity, safety profile, and mechanism of action.

Keywords: benzoylated bispidone; β-cyclodextrin complex; biological activity; infiltration anaesthesia; conduction anaesthesia.

Malmakova Aigul Erbosynovna	*PhD, associated professor; E-mail: malmakova@mail.ru*
Iskakova Tynyshtyk Kadyrovna	*Doctor of chemical sciences, professor; E-mail: t.iskakova@satbayev.university*
Praliyev Kaldybay Dzhailovovich	*Doctor of chemical sciences, professor; E-mail: praliyevkd@mail.ru*
Seilkhanov Olzhas Tulegenovich	*Master of Natural Sciences; E-mail: seilkhanov@mail.ru*

Citation: Malmakova A.E., Iskakova T.K., Praliyev K.D., Seilkhanov O.T., Otegulova K.B., Amirkulova M.K., Satbayeva Ye.M., Kadyrova D.M. Benzoylated bispidone: Synthesis and investigation of biological effects. *Chem. J. Kaz.*, **2026**, 2*(94)*, 136-147. DOI: https://doi.org/10.51580/2026-2.2710-1185.21

Otegulova Kamila Babazhankyzy	*Master's degree; E-mail: otegulova00@mail.ru*
Amirkulova Marzhan Kuliashovna	*Expert; E-mail: m.amirkulova@dari.kz*
Satbayeva Yelmira Maratovna	*Candidate of medicinal sciences, professor; E-mail: satbaeva.e@kaznmu.kz*
Kadyrova Diliara Moldashevna	*Candidate of medicinal sciences, professor; E-mail: kadyrova.d@kaznmu.kz*

1. Introduction

Local anaesthetics are widely used in surgery, dentistry, and many other medical procedures worldwide. Local anaesthetics work by temporarily stopping nerve signals. They do this by blocking voltage-gated sodium channels in nerve cell membranes. After crossing the nerve membrane, the non-ionised form of the anaesthetic enters the axon, picks up a proton inside the cell, and then attaches to sodium channels. This blocks sodium from entering the cell and stops action potentials from starting or spreading. As a result, sensory signals like pain do not reach the central nervous system, so you temporarily lose sensation [1,2]. After cocaine was isolated in the late XIX century and synthetic options like procaine (Novocaine), lidocaine, and bupivacaine were developed, researchers have continued to look for new local anaesthetics that work better, act faster, last longer, and have fewer side effects [3].

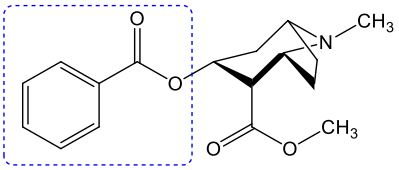

Lead compound (A)
Cocaine, 1884

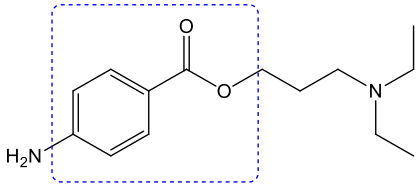

Lead compound (B)
Novocaine, 1905

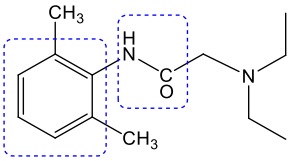

Lead compound (C)
Lidocaine. 1948

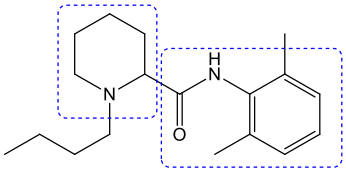

Lead compound (D)
Bupivacaine, 1963

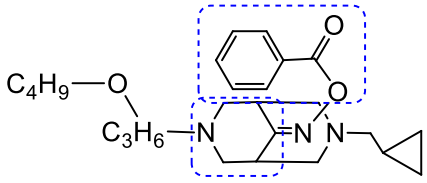

Target compound
Benzoylated 3-(3-butoxypropyl)-7-cyclopropanemethyl substituted bispidone

Amino amides and amino esters are the two basic types of local anaesthetics. In contrast to amino esters, which have an ester connection between the intermediate chain and the aromatic end, amino amides contain an amide link. Amino amides and amino esters are different in several ways. While amino amides are broken down in the liver, amino esters are broken down in plasma by pseudocholinesterase. While amino amides are quite stable in solution, amino esters are unstable. Compared to amino amides, amino esters are far more prone to trigger allergic hypersensitivity reactions (Table 1) [4].

Table 1 - Comparison of the pharmacological characteristics of representative local anaesthetics

Class	**Local anaesthetics**	**Duration of action**	Metabolism	**Stability**	**Clinical use**
Ester group	Novocaine	Short	Hydrolysed in plasma by pseudocholinesterases	Less stable in solution	Limited use today; infiltration anaesthesia and diagnostic procedures
Amide type	Lidocaine	Intermediate	Primarily metabolised in the liver by cytochrome P450 enzymes	More chemically stable	Most widely used for infiltration, nerve block, epidural, spinal, and topical anaesthesia.
	Bupivacaine	Long	Metabolised primarily in the liver		Long-duration regional anaesthesia, epidural anaesthesia, peripheral nerve blocks, and postoperative pain management

Despite the current medications being clinically effective, problems such as cardiotoxicity, neurotoxicity, and allergic reactions continue to drive the search for new chemical entities with improved safety profiles [5]. Since 2008, human exposures with less severe consequences have dropped by 2.48% annually, whereas those with more severe consequences (moderate, major, or death) have increased by 4.44% annually since 2000. Approximately 3200 single exposures to additional or unknown local and/or topical anaesthetics and 1410 single exposures to lidocaine were recorded in the US in 2017. Additionally, 197 lidocaine exposures had a minor effect, 71 had a moderate outcome, 13 had a serious event, and one fatality was documented [6].

Azaheterocyclic systems are of considerable value in the development of new local anaesthetics owing to their structural rigidity, favourable lipophilicity,

and resemblance to naturally occurring alkaloids. Among these, 3,7-diazabicyclo[3.3.1]nonan-9-one (bispidone) is readily accessible synthetically and amenable to structural modification at both nitrogen atoms. Bispidone derivatives have been reported to exhibit antiarrhythmic, analgesic, and antimicrobial activities, and certain compounds of this class have been shown to interact with voltage-gated sodium channels - the primary molecular targets of local anaesthetics [7-13].

Adding a benzoyloxy group to bispidone can change its electronic properties and stability. These changes are important for how local anaesthetics work. Adding a benzoyloxy group can make the compound more lipophilic and create an ester bond that can be broken down in the body, releasing the original oxime [14-16].

In this study, we synthesised an oxime ether derivative of bispidone by reacting a bicyclic ketone precursor with hydroxylamine, followed by benzoylation. By combining the rigid bispidone structure with the *O*-benzoyloxime group and changing the substituents on the nitrogen atoms, we were able to study how these changes affect anaesthetic strength. The results help to understand bispidone-based compounds better and support the design of better local anaesthetics.

2. Experimental part

Chemical experimental part

Al_2O_3 with second-degree activity was used in TLC to monitor reaction progress and in column chromatography for purification. IR spectra were recorded using an FT-IR spectrometer Nicolet 5700, and NMR spectra were recorded using a JEOL JNM-ECA 400 spectrometer using $CDCl_3$ at frequencies of 399.78. Dry solvents and an inert gas environment were used for oxygen- or moisture-sensitive syntheses.

Benzoylated 3-(3-butoxypropyl)-7-cyclopropanemethyl substituted bispidone was synthesised using a method previously reported [17,18].

3-(3-Butoxypropyl)-7-cyclopropanemethyl substituted bispidone (2), pale yellow oil; 92%. Calculated for $C_{18}H_{32}N_2O_2$: C 70.09; H 10.46; N 9.08. Found: C 70.16; H 10.42. IR (KBr) (ν_{max}/ cm^{-1}): 1734 (C=O), 1114 (C–O–C). ^{13}C NMR ($CDCl_3$, δ, ppm): 46.9 ($C_{1,5}$), 58.3, 58.7 ($C_{2,4,6,8}$), 215.4 (C_9).

Oxime of 3-(3-butoxypropyl)-7-cyclopropanemethyl substituted bispidone (3), pale yellow oil; 85%. Calculated for $C_{18}H_{33}N_3O_2$: C 66.83; H 10.28; N 12.99. Found: C 70.01; H 10.20 IR (KBr) (ν_{max}/ cm^{-1}): 3133 (OH), 1670 (C=N). ^{13}C NMR ($CDCl_3$, δ, ppm): 30.7, 32.1 ($C_{1,5}$), 56.4, 56.3, 58.6, 58.1 ($C_{2,4,6,8}$), 161.2 (C_9).

Benzoylated 3-(3-butoxypropyl)-7-cyclopropanemethyl substituted bispidone (4), pale yellow oil; 69%. Calculated for $C_{25}H_{37}N_3O_3$: C 70.22; H 8.72; N 9.83. Found: C 70.17; H 8.65. IR (KBr) (ν_{max}/ cm^{-1}): 1742 (C=O), 1641 (C=N).

β-Cyclodextrin complex of benzoylated 3-(3-butoxypropyl)-7-cyclopropanemethyl substituted bispidone (5), cream-colored amorphous powder. Calculated for $C_{67}H_{107}N_3O_{38}$: C 51.50; H 6.90; N 2.69. Found: C 51.89; H 6.83.

Biological activity study

The β-cyclodextrin complex of benzoylated 3-(3-butoxypropyl)-7-cyclopropanemethyl substituted bispidone (5), designated as LAC-5, was evaluated for its local anaesthetic activity. Data were compared with those of the reference drugs trimecaine, lidocaine, and novocaine. Results are summarised in Tables 2 and 3.

Infiltration anaesthetic activity

Infiltration anaesthetic activity was evaluated in male guinea pigs (200-250 g) using the Bülbring-Wade method. Following shaving of the animals' backs, 0.2 mL of isotonic solutions of the test compound and medications were injected into 4 sites arranged in a 3-cm square.

Each concentration was tested for local anaesthetic activity 6-8 times. Sensitivity was assessed by pressing a blunted injection needle 6 consecutive times at intervals of 3 to 4 sec. This process was repeated every five minutes for thirty minutes.

The anaesthesia index, which was computed as the average of 6 studies and had a maximum possible value of 36, was used to measure the depth of anaesthesia. The reference medications trimecaine, lidocaine, and novocaine at comparable concentrations were used to compare the test compound's action.

Conduction anaesthetic activity

Using basic screening techniques suggested by the Guidelines for Experimental Preclinical Studies of New Pharmacological Substances and the Pharmacological Committee of the Republic of Kazakhstan, local anaesthetic activity under conduction anaesthesia was assessed [19,20].

The tail-flick method was used to examine the activity of the test chemical and the comparative medicines in rats.

The following criteria were used to compare the chemical with the reference medications:

- Duration of complete anaesthesia induced;
- Total duration of action.

Non-anesthetised outbred white rats of both sexes were used, with 6 animals in each experimental and control group. One per cent aqueous solutions of the compounds were tested.

Statistical analysis

Data are presented as mean ± standard error of the mean (M±m). Statistical analysis was performed using Student's t-test. Differences were considered

statistically significant at $p < 0.05$. Data processing was carried out using GraphPad Prism 9.0 (GraphPad Software, USA).

Results and Discussion

The starting compound, benzoylated 3-(3-butoxypropyl)-7-cyclopropanemethyl substituted bispidone (2), was synthesised through a one-pot Mannich condensation of 1-(3-butoxypropyl)piperidin-4-one (1), paraformaldehyde, and cyclopropanemethylamine in acidified acetic acid-methanol solution, achieving a yield of 92%.

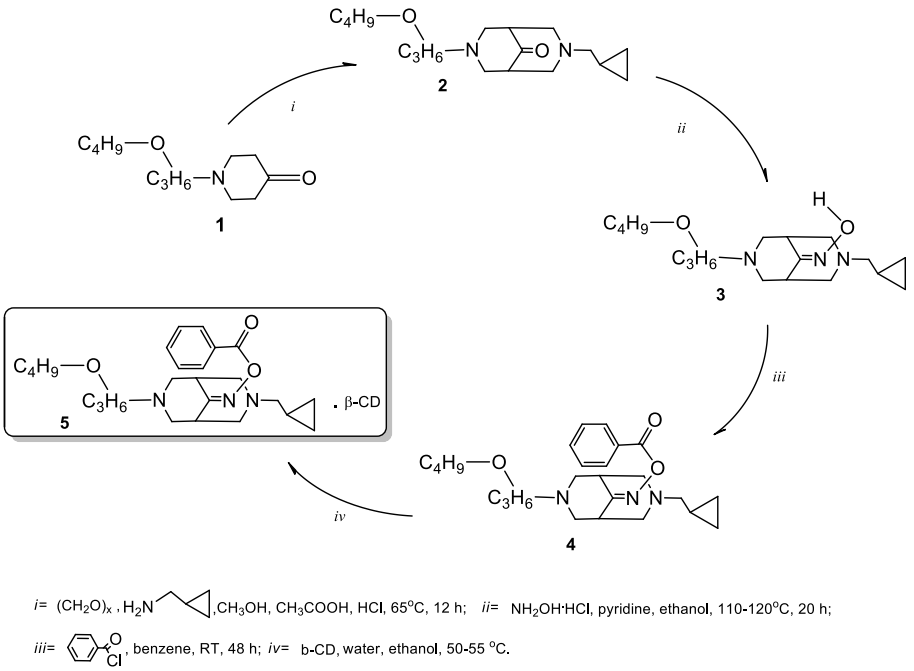

The reaction of 3-(3-butoxypropyl)-7-cyclopropanemethyl substituted bispidone (2) with hydroxylamine hydrochloride yielded the corresponding oxime (3), which was then acylated with benzoyl chloride to obtain the *O*-benzoyl derivative (4). The β-cyclodextrin complex (5) was synthesised by combining the *O*-benzoyloxime (4) with an equimolar amount of β-cyclodextrin. The structures and identities of these compounds were verified using elemental analysis, TLC, IR spectroscopy, and NMR spectroscopy. The IR spectrum of compound ***2*** showed a band at 1734 cm^{-1}, corresponding to the C=O stretching vibration of a ketone carbonyl within the bispidone ring. A band at 1114 cm^{-1}, assigned to C–O–C stretching, confirmed the presence of the butoxy ether group and further supported the proposed structure. In the ^{13}C NMR spectrum, C1 and C5 signals appeared at 46.9 ppm, which was attributed to the diazabicyclic core. In comparison, the cluster of resonances at 58.3 and 58.7 ppm accounted for the

methylene carbons C_2, C_4, C_6, and C_8 within the bispidone framework. A signal of an aliphatic ketone carbonyl C_9 appeared at 215.4 ppm, providing unambiguous evidence for the formation of a new ketone. In the oxime IR spectrum, a broad absorption at 3133 cm^{-1} was characteristic of the O–H stretch belonging to the newly introduced hydroxyl group. Meanwhile, the strong carbonyl band at 1734 cm^{-1} that had defined compound ***2*** was completely absent — replaced by a new band at 1670 cm^{-1}, right where C=N stretching would be expected. This pattern of disappearance and emergence provided straightforward, unambiguous evidence for oxime formation.

The ^{13}C NMR data C_1 and C_5 resonated at 30.7 and 32.1 ppm, shifted noticeably upfield from their positions in compound ***2*** - a natural consequence of the change in electronic environment when a ketone gives way to an oxime. The methylene carbons C_2, C_4, C_6, and C_8 in the bicyclic ring were identified at 56.3, 56.4, 58.1, and 58.6 ppm, respectively. The clinching evidence, though, came from the carbonyl region: the ketone signal at 215.4 ppm had disappeared without a trace, and in its place stood a new resonance at 161.2 ppm - exactly where an oxime carbon (C=N) is known to appear. Altogether, the spectroscopic data made a compelling case that compound ***2*** had been cleanly and successfully transformed into oxime ***3***.

The IR spectrum of compound ***4*** was fully consistent with the successful *O*-benzoylation of oxime ***3***. The broad O–H stretching band at 3133 cm^{-1}, clearly seen in compound ***3***, was no longer present in compound ***4***, which indicates that the hydroxyl group of the oxime was acylated. A new signal at 1742 cm^{-1} was assigned to the C=O stretching of the aryl ester group. The C=N stretching band shifted from 1670 cm^{-1} in oxime (3) to 1641 cm^{-1} in benzoylated bispidone (4). This shift is due to the change in electron density at the C=N bond after *O*-benzoylation. The fact that this band remained confirmed that the oxime group remained intact. These spectral results support the structure of compound ***4*** as the O-benzoylated oxime derivative.

According to the data presented in Table 1, compound LAC-5 demonstrated a pronounced local anaesthetic effect, with an anaesthesia index of 35.6.

6 animals were used for each concentration test. The average response values collected over 30 minutes were used to calculate the anaesthesia index. LAC-5 reached the highest level of anaesthesia that this method can measure, with an anaesthesia index of 36 (Table 2).

At a 0.25% concentration, it was statistically more potent than all reference medications, showing 1.1 times the activity of trimecaine, 1.55 times that of lidocaine, and 1.44 times that of novocaine.

Table 2 - Efficacy of LAC-5 and medications in infiltration anaesthesia

Compound / Reference Drug	0.25%					
	Anesthesia Index M±m		Complete Anaesthesia Duration, min		Total Duration of Action, min	
LAC-5	36.0±0	p_1<0.001 p_2<0.001 p_3<0.001	56.66±1.05	p_1<0.001 p_2<0.001 p_3<0.001	76.66±1.05	p_1<0.001 p_2<0.001 p_3<0.001
Trimecaine	33.6±0.33		20,0±1.7		38.3±1.05	
Lidocaine	23.1±0.9		14.2±0.8		30.8±0.8	
Novocaine	25.0±1.0		10.0±1.2		29.1±1.5	

Note: p_1, compared with trimecaine; p_2, compared with lidocaine; p_3, compared with novocaine.

Comparison of duration parameters, including both the duration of complete anaesthesia and the total duration of action, showed that the compound outperformed the reference medications in these parameters.

The duration of complete anaesthesia induced by LAC-5 was 56.66 minutes, which was 2.83, 3.9, and 5.66 times longer than that of each medication, respectively. The total duration of the LAC-5 effect was 76.66 minutes. In comparison, the total anaesthesia duration for the reference medications was shorter: 38.3 minutes for trimecaine, 30.8 minutes for lidocaine, and 29.1 minutes for novocaine. Thus, the effect of LAC-5 was 2.0-, 2.4-, and 2.6-fold longer than that of the comparison medications, respectively.

The results of the conduction anaesthesia study for LAC-5 are presented in Table 3.

Table 3 - Activity of LAC-5 and medications in conduction anesthesia

Compound / Reference Drug	Duration of Action, min	
LAC-5	160.0±4.7	p_1 <0.02 p_2 <0.01 p_3 <0.001
Trimecaine	56.9±12.8	
Lidocaine	90.8±18.4	
Novocaine	42.3±13.6	

Note: p_1, compared with trimecaine; p_2, compared with lidocaine; p_3, compared with novocaine.

LAC-5 provided anaesthesia for 160 minutes, lasting 2.8, 1.8, and 3.8 times longer than the comparison medications. LAC-5 demonstrated a pronounced effect in infiltration anaesthesia, exceeding the performance of all reference medications across all measured parameters. Consequently, LAC-5 is recommended for further comprehensive pharmacological evaluation.

Conclusion

A study of LAC-5 showed that this compound has strong local anaesthetic effects that are better than those of the commonly used medications trimecaine, lidocaine, and novocaine. For infiltration anaesthesia, LAC-5 reached the

maximum depth of anaesthesia (index 36.0 ± 0) at a concentration of 0.25%, outperforming all reference medications. The complete anaesthesia lasted 56.66 minutes, which is 2.83, 3.9, and 5.66 times longer than the medications, respectively. The total duration of action was 76.66 minutes, 2.0 to 2.6 times longer than the reference medications ($p < 0.001$ for all comparisons). In conduction anaesthesia, LAC-5 provided anaesthesia for 160 minutes. All these differences were statistically significant.

Overall, these results show that LAC-5 is a very effective local anaesthetic, with greater strength and a much longer duration of action than those of medications currently in use.

Funding: The Science Committee of the Ministry of Science and Higher Education of the Republic of Kazakhstan funded this research (Grant No. AP26198287).

Conflict of interest: The authors report no conflicts of interest related to this article.

БЕНЗОИЛДЕНГЕН БИСПИДОН: СИНТЕЗІ ЖӘНЕ БИОЛОГИЯЛЫҚ ӘСЕРІН ЗЕРТТЕУ

Малмакова А.Е.[1]*, Искакова Т.К.[2], Пралиев Қ.Д.[1], Сейілханов О.Т.[3], Өтегұлова К.Б.[1], Әмірқұлова М.Қ.[4,5], Сатбаева Е.М.[4], Қадырова Д.М.[4]

[1] Ә.Б. Бектұров атындағы Химия ғылымдары институты, Алматы, Қазақстан
[2] Қ.И. Сәтбаев атындағы Қазақ ұлттық зерттеу техникалық университеті, Алматы, Қазақстан
[3] Ш. Уәлиханов атындағы Көкшетау университеті, Көкшетау, Қазақстан
[4] С.Ж. Асфендияров атындағы Қазақ ұлттық медицина университеті / Жалпы медицина мектебі, фармакология кафедрасы, Алматы, Қазақстан
[5] Дәрілік заттар мен медициналық бұйымдарды сараптау ұлттық орталығы, Астана, Қазақстан

Түйіндеме. *Кіріспе.* Жергілікті анестетиктер кернеуге тәуелді натрий арналарының белсенділігін қайтымды түрде бөгеп, хирургияда, стоматологияда және медициналық тәжірибедегі әртүрлі процедураларда қажетті сезімталдықтың уақытша жойылуын қамтамасыз етеді. Новокаин, лидокаин және тримекаиннің тиімділігіне қарамастан, олардың әсер ету ұзақтығы, уыттылығы және көтере алуға байланысты шектеулері анағұрлым жетілдірілген препараттарды іздеуді талап етеді. *Зерттеудің мақсаты* – бензоилденген 3-(3-бутоксипропил)-7-циклопропанметил орынбасқан биспидонның β-циклодекстриндік кешенін (LAC-5) синтездеу және оның жергілікті анестезиялық белсенділігін стандартты клиникаға дейінгі скрининг әдістерін пайдалана отырып, салыстырмалы препараттар - тримекаин, лидокаин және новокаинмен салыстыру. *Нәтижелер және талқылау.* LAC-5 Манних реакциясы, оксимдеу, *О*-бензоилдеу және β-циклодекстринмен кешен түзу арқылы синтезделді; барлық қосылыстардың құрылымы инфрақызыл және ядролық магниттік резананс спектроскопия зерттеу әдістері расталды. *Қорытынды.* Биологиялық бағалау нәтижелері LAC-5-тің инфильтрациялық және өткізгіштік анестезия модельдерінде клиникалық тәжірибеде қолданылатын салыстырмалы препараттар - тримекаин, лидокаин және новокаиннен жоғары айқын жергілікті анестезиялық қасиеттерге ие екенін көрсетті. Инфильтрациялық анестезия кезінде LAC-5 0.25 % концентрацияда анестезияның ең жоғары өлшенетін тереңдігіне (индекс 36.0 ± 0) жетіп, толық анестезия ұзақтығы 56.66 мин және жалпы әсер ету ұзақтығы 76.66 мин болды, бұл көрсеткіштер салыстырмалы препараттардан сәйкесінше 5.66 және 2.6 есеге дейін жоғары болды ($p < 0.001$). Өткізгіштік анестезия жағдайында LAC-5 жалпы әсер ету ұзақтығы салыстыру препараттарынан асып түсіп 160.0 ± 4.7 мин құрады. Алынған нәтижелер негізінде LAC-5 қосылысы жедел уыттылықты, қауіпсіздік бейінін және әсер ету механизмін бағалауды қамтитын кешенді клиникаға дейінгі фармакологиялық зерттеулерге ұсынылады.

Түйінді сөздер: бензоилденген биспидон; β-циклодекстрин кешені; биологиялық белсенділік; инфильтрациялық анестезия; өткізгіштік анестезия.

Малмакова Айгүл Ербосынқызы	*PhD, қауымдастырылған профессор*
Искакова Тыныштық Қадірқызы	*Химия ғылымдарының докторы, профессор*
Пірәлиев Қалдыбай Жайлауұлы	*Химия ғылымдарының докторы, профессор*
Сейілханов Олжас Төлегенұлы	*Жаратылыстану ғылымдары магистрі*
Өтегұлова Камила Бабажанқызы	*Магистр*
Әміркұлова Маржан Құлашқызы	*Сарапшы*
Сатпаева Эльмира Маратқызы	*Медицина ғылымдарының кандидаты, професссор*
Қадырова Диляра Молдашқызы	*Медицина ғылымдарының кандидаты, професссор*

БЕНЗОИЛИРОВАННЫЙ БИСПИДОН: СИНТЕЗ И ИССЛЕДОВАНИЕ БИОЛОГИЧЕСКИХ ЭФФЕКТОВ

А.Е.Малмакова [1*], Т.К.Искакова [2], К.Д.Пралиев [1], О.Т.Сеилханов [3], К.Б.Отегулова [1], М.К.Амиркулова [4,5], Е.М.Сатбаева [4], Д.М.Кадырова [4]

[1] Институт химических наук имени А.Б. Бектурова, Алматы, Казахстан
[2]Казахский национальный исследовательский технический университет имени К.И. Сатпаева, Алматы, Казахстан
[3]Кокшетауский университет имени Ш. Уалиханова, Кокшетау, Казахстан
[4]Кафедра фармакологии, Казахский национальный медицинский университет имени С.Д. Асфендиярова / Школа общей медицины, Алматы, Казахстан
[5]Национальный центр экспертизы лекарственных средств и медицинских изделий, Астана, Казахстан

Резюме. *Введение.* Местные анестетики обратимо блокируют потенциалзависимые натриевые каналы, вызывая временную потерю чувствительности, необходимую в хирургии, стоматологии и других медицинских процедурах. Несмотря на эффективность новокаина, лидокаина и тримекаина, их ограничения, связанные с продолжительностью действия, токсичностью и переносимостью, обусловливают необходимость поиска более совершенных препаратов. *Цель исследования* синтезировать β-циклодекстриновый комплекс бензоилированного 3-(3-бутоксипропил)-7-циклопропанметил замещенного бисидона (LAC-5) и оценить его местноанестезирующую активность в сравнении с препаратами с использованием стандартных методов доклинического скрининга. *Результаты и обсуждение.* LAC-5 был получен посредством реакции Манниха, оксимирования, *О*-бензоилирования и комплексообразования с β-циклодекстрином; структуры полученных производных подтверждены методами инфракрасной и ядерной магнитно-резонансной спектроскопии. *Заключение.* Биологическая оценка показала, что LAC-5 обладает выраженными местноанестезирующими свойствами, превосходящими клинически применяемые препараты сравнения - тримекаин, лидокаин и новокаин - как в моделях инфильтрационной, так и проводниковой анестезии. При инфильтрационной анестезии LAC-5 достиг максимальной измеряемой глубины анестезии (индекс 36.0 ± 0) при концентрации 0.25 %, при длительности полной анестезии 56.66 мин и общей продолжительности действия 76.66 мин, превышая показатели препаратов сравнения соответственно до 5.66 и 2.6 раза ($p < 0.001$). В условиях проводниковой анестезии LAC-5 обеспечивал общую продолжительность действия 160.0 ± 4.7 мин, превосходя препараты сравнения. На основании полученных результатов LAC-5 рекомендуется для углублённого доклинического фармакологического исследования, включая оценку острой токсичности, профиля безопасности и механизма действия.

Ключевые слова: бензоилированный биспидон; β-циклодекстриновый комплекс; биологическая активность; инфильтрационная анестезия; проводниковая анестезия.

Малмакова Айгул Ербосыновна	*PhD, ассоциированный профессор*
Искакова Тыныштык Кадыровна	*Доктор химических наук, профессор*
Пралиев Калдыбай Джайлович	*Доктор химических наук, профессор*
Сейлханов Олжас Тулегенович	*Магистр естественных наук*
Отегулова Камила Бабажанкызы	*Магистр*
Амиркулова Маржан Куляшовна	*Эксперт*
Сатпаева Эльмира Маратовна	*Кандидат медицинских наук, профессор*
Кадырова Диляра Молдашевна	*Кандидат медицинских наук, профессор*

References

1. Fozzard H.A., Sheets M.F., Hanck D.A. The sodium channel as a target for local anaesthetic medications. *Front. Pharmacol.* **2011**, 2, 68, 1-6. https://doi.org/10.3389/fphar.2011.00068
2. Elajnaf T., Baptista-Hon D.T., Hales T.G. Potent inactivation-dependent inhibition of adult and neonatal NaV1.5 channels by lidocaine and levobupivacaine. *Anesth. Analg.* **2018**, 127, 650-660. https://doi.org/10.1213/ANE.0000000000003597
3. Cherobin A.C.F.P., Tavares G.T. Safety of local anesthetics. *Anais Brasileiros De Dermatologia*, **2020**, 95(1), 82-90. https://doi.org/10.1016/j.abd.2019.09.025
4. Becker D.E., Reed K.L. Local anesthetics: review of pharmacological considerations. *Anesthesia Prog*ress, **2012**, 59(2), 90-101. https://doi.org/10.2344/0003-3006-59.2.90
5. Camargo-Ayala L., Prent-Peñaloza L., Bedoya M., Gutiérrez M., González W. Rational design, synthesis, and in-silico evaluation of homologous local anesthetic compounds as TASK-1 channel blockers. *Chemistry Proceedings*, **2020**, 3(1), 8416. https://doi.org/10.3390/ecsoc-24-08416
6. Gummin D.D., Mowry J.B., Beuhler M.C., Spyker D.A., Rivers L.J., Feldman R., DesLauriers, C. 2023 Annual Report of the National Poison Data System® (NPDS) from America's Poison Centers®: 41st Annual Report. *Clinical Toxicology*, **2024**, 62(12), 793-1027. https://doi.org/10.1080/15563650.2024.2412423
7. Tomassoli I., Gündisch D. Bispidine as a privileged scaffold. *Curr. Top. Med. Chem.* **2016**, 16(11), 1314-1342. https://doi.org/10.2174/1568026615666150915111434
8. Kopp I., Cieslik P., Anger K., Josephy T., Neupert L., Velmurugan G., Gast M., Wadepohl H., Brühlmann S.A., Walther M., Kopka K., Bachmann M., Stephan H., Kubeil M., Comba P. Bispidine chelators for radiopharmaceutical applications with lanthanide, actinide, and main group metal ions. *Inorg. Chem*. **2023**, 62(50), 20754-20768. https://doi.org/10.1021/acs.inorgchem.3c02340 nih
9. Gillet R., Roux A., Brandel J., Huclier-Markai S., Camerel F., Jeannin O., Nonat A.M., Charbonnière L.J. A bispidol chelator with a phosphonate pendant arm: synthesis, Cu(II) complexation, and ^{64}Cu labeling. *Inorg. Chem*. **2017**, 56(19), 11738-11752. https://doi.org/10.1021/acs.inorgchem.7b01731
10. Haridas V., Rajgokul K.S., Sadanandan S., Agrawal T., Sharvani V., Gopalakrishna M.V.S., Bijesh M.B., Kumawat K.L., Basu A., Medigeshi G.R. Bispidine–amino acid conjugates act as a novel scaffold for the design of antivirals that block Japanese Encephalitis Virus replication. *PLoS Negl. Trop. Dis*. **2013**, 7(1), e2005. https://doi.org/10.1371/journal.pntd.0002005
11. Bleher K., Cieslik P.A., Comba P. Bispidine coordination chemistry. *Dalton Trans*. **2025**, 54, 4405–4431. https://doi.org/10.1039/D5DT00050E
12. Comba P., Grimm L., Orvig C., Rück K., Wadepohl H. Synthesis and coordination chemistry of hexadentate picolinic acid based bispidine ligands. *Inorg. Chem*. **2016**, 55(24), 12531-12543. https://doi.org/10.1021/acs.inorgchem.6b01787
13. Sy M., Ndiaye D., da Silva I., Lacerda S., Charbonnière L.J., Tóth É., Nonat A.M. $^{55/52}Mn^{2+}$ complexes with a bispidine-phosphonate ligand: high kinetic inertness for imaging applications. *Inorg. Chem*. **2022**, 61(34), 13421-13432. https://doi.org/10.1021/acs.inorgchem.2c01681
14. Mello de Souza M., Rodriguez Gini A.L., Alves Moura J., Scarim C.B., Man Chin C., Leandro dos Santos J. Promedication approach as a strategy to enhance medication permeability. *Pharmaceuticals*, **2025**, 18(3), 297. https://doi.org/10.3390/pharmaceutics18030297

15. Kosmalski T., Kupczyk D., Baumgart S., Paprocka R., Studzińska R. A review of biologically active oxime ethers. *Molecules*, **2023**, 28, 5041, 1-31. https://doi.org/10.3390/molecules28135041

16. Chandran N., Bose K., Thekkantavida A.C., Thomas R.R., Anirudhan K., Bindra S., Sura S., Hasan H.A., Kumar S., Rangarajan T.M., Al-Sehemi A.G., Gahtori P., Kim H., Mathew B. Oxime derivatives: a valid pharmacophore in medicinal chemistry. *ChemistrySelect*, **2024**, 9(27), e202401726. https://doi.org/10.1002/slct.202401726

17. Praliev D., Iskakova T.K., Baktybaeva L.K., Malmakova A.E. Synthesis and myelostimulatory activity of a number of 3,7-diazabicyclo[3.3.1]nonan-9-one derivatives. *Pharmaceutical Chemistry Journal*, **2015**, 49(5), 292-295. https://doi.org/10.1007/s11094-015-1272-2 (Russian Original Vol. 49, No. 5, May, 2015)

18. Malmakova A.E., Yu V.K., Praliyev K.D., Kaldybayeva A.B., Amirkulova M.K. Synthesis, structure, and biological activity of novel bispidine derivatives. *International Journal of Applied Pharmaceutics*, **2021**, 13(1), 69-74. https://doi.org/10.22159/ijap.2021.v13s1.Y1013

19. Ministry of Health of the Republic of Kazakhstan. Rules for Conducting Preclinical (Non-Clinical) Studies and Requirements for Preclinical Bases for Assessing the Biological Effect of Medical Devices. Order No. RK ДСМ-255/2020 of December 11, 2020. Almaty, Kazakhstan: Ministry of Health of the Republic of Kazakhstan; 2020.

20. Engalycheva G.N., Syubaev R.D., Goryachev D.V. Quality standards of preclinical pharmacological studies. *The Bulletin of the Scientific Centre for Expert Evaluation of Medicinal Products*, **2019**, 9(4), 248-255. (In Russ.) https://doi.org/10.30895/1991-2919-2019-9-4-248-255

Chemical Journal of Kazakhstan
Volume 2, Number 94(2026), 148-157 https://doi.org/10.51580/2026-2.2710-1185.22

UDC 54.061+54.062

DETERMINATION OF THE COMPONENT COMPOSITION OF A SERIES OF CALCIUM-CONTAINING DEPOSITS AND TECHNOLOGICAL RECOMMENDATIONS FOR THEIR UTILIZATION

A.A. Yespenbetov[1], E.A. Tusupkaliyev[1], Zh.N. Kainarbayeva[1], A.Zh. Baizak[1], Z.K. Maymekov[2], A.Zh. Abyurov[1]

[1]Institute of Chemical Sciences after A.B. Bekturov, Almaty, Kazakhstan
[2] Kyrgyz State Technical University named after I. Razzakov, Bishkek, Kyrgyzstan

[*]Corresponding author e-mail: asyespenbet@gmail.com

Abstract. A comprehensive analysis of samples of calcium-containing mineral raw materials from deposits in Russia (Bryansk), Kazakhstan (Beineu, Shetpe, Zhanakorgan), and Uzbekistan (Fergana) was carried out to assess their suitability as precursors of calcium oxide used in technologies for the remediation of oil-contaminated soils. The study employed methods of X-ray phase analysis (XRD), elemental analysis, and infrared spectroscopy (FTIR). By the XRD method, the phase composition of the samples was established and their semi-quantitative evaluation was performed. Based on the obtained data, the samples were classified into three groups: 1) calcium oxide–hydroxide (Bryansk, Beineu, Fergana), characterized by a high content of CaO (76.1-92.5%) and $Ca(OH)_2$ (7.5–19.0%); 2) calcium hydroxide (Zhanakorgan), representing almost pure $Ca(OH)_2$ (99.6%); 3) carbonate (Shetpe), consisting of calcite $CaCO_3$ (>98%). FTIR results confirmed the presence of the identified phases. Elemental analysis showed high purity of most samples in terms of calcium (>52% CaO in normalized form). The sample from Bryansk contains an increased amount of silica ($SiO_2 \approx 4\%$). Technological recommendations for the use of the raw materials are proposed. The Beineu-1 and Beineu-2 samples, containing 92.5% and 81.0% CaO, respectively, were identified as the most promising raw materials for the energy-efficient production of active CaO.

Keywords: calcium-containing raw materials, X-ray diffraction, infrared spectroscopy, elemental analysis, classification, oil-contaminated soils

Yespenbetov Assylbek Alimbekovich	*Doctor of Chemical Sciences; E-mail: asyespenbet@gmail.com*
Tusupkaliyev Ersin Adietovich	*Candidate of Chemical Sciences; E-mail: t_ersin@mail.ru*
Kainarbayeva Zhaniya Nurbekovna	*Master; E-mail: zhaniya.kn@gmail.com*
Bayzak Assel Zheniskyzy	*Master; E-mail:asel6.03.78@mail.ru*
Maymekov Zarlyk Kaparovich	*Doctor of technical sciences, professor; E-mail: zarlyk.maymekov@manas.edu.kg*
Abyurov Arman Zhumagalievich	*Doctor PhD*

Citation: Yespenbetov A.A., Tusupkaliyev E.A., Kainarbayeva Zh.N., Baizak A.Zh., Maymekov Z.K., Abyurov Zh.A. Determination of the component composition of a series of calcium-containing deposits and technological recommendations for their utilization. *Chem. J. Kaz.*, **2026**, 2*(94)*, 148-157. DOI: https://doi.org/10.51580/2026-2.2710-1185.22

Introduction

This work is devoted to the analysis of raw material sources of calcium-containing materials used for the production of calcium oxide, which is applied in technologies for the remediation of oil-contaminated soils. Calcium oxide (CaO, quicklime) is a highly reactive reagent widely used in metallurgy, construction, the chemical industry, and environmental applications [1, 2]. In particular, in remediation technologies for oil-contaminated soils, CaO is used for the stabilization of hydrocarbons, adjustment of the pH of the medium, and immobilization of heavy metals [3, 4]. The efficiency of these processes directly depends on the reactivity of CaO, which is determined by its purity, particle size (dispersion), and structure. These characteristics, in turn, are defined by the composition of the initial mineral raw materials and the conditions of their processing. Despite the abundance of deposits of carbonate and other calcium-containing rocks, their composition can vary significantly depending on geological conditions. The presence of associated phases (calcium hydroxide, dolomite, silicate and clay minerals) and chemical impurities (compounds of Mg, Fe, Si, and Al) significantly affects both the technology of calcium oxide production and its final properties [5–9]. Therefore, systematic research and comparative evaluation of the component composition of raw materials from various sources represent a relevant scientific and practical task.

Samples from Bryansk (Russian Federation), as well as from deposits in Kazakhstan (Beineu, Shetpe, Zhanakorgan) and Uzbekistan (Fergana), were investigated. The main research method is semi-quantitative X-ray phase analysis (XRD), supplemented by the results of elemental analysis and IR spectroscopy.

The aim of the work is to determine the component composition of the studied samples and to classify them based on the obtained data for further use in industrial purposes:

1. Bryansk, Russian Federation (sample 1)
2. Beineu, quarry 1 (sample 2)
3. Beineu, quarry 2 (sample 3)
4. Shetpe, quarry 1 (sample 4)
5. Shetpe, quarry 2 (sample 5)
6. Zhanakorgan (sample 6)
7. Fergana, Uzbekistan (sample 7)

Experimental part

Sampling and sample preparation were carried out in accordance with methods [10, 11].

1. X-ray phase analysis was carried out according to the standard method [12] using a powder diffractometer DW-XRD-27mini ($Cu_{K\alpha}$ radiation, voltage — 40 kV, current — 40 mA, graphite monochromator). Scanning was performed in θ–2θ mode in the angular range of 2θ from 5° to 120°.

2. The analysis of the content of major elements (Ca, Mg, Fe, Al, Si, K, Na, Ba, Mn in oxide forms) in solid samples was carried out using an inductively

coupled plasma atomic emission spectrometer (ICP-OES) Thermo Scientific iCAP PRO XP Duo (Germany), in accordance with the measurement methodology for solid objects.

3. IR spectra were recorded on a Fourier spectrometer Nicolet 5700 in the range of 400–4000 cm^{-1}. The spectra were recorded using OMNIC software. Samples were prepared in the form of pellets with KBr. Before analysis, the samples were dried at 110°C to remove adsorbed moisture.

Results and discussion

Figures 1–7 show the X-ray diffraction patterns of the studied samples. Table 1 presents the data on their component composition.

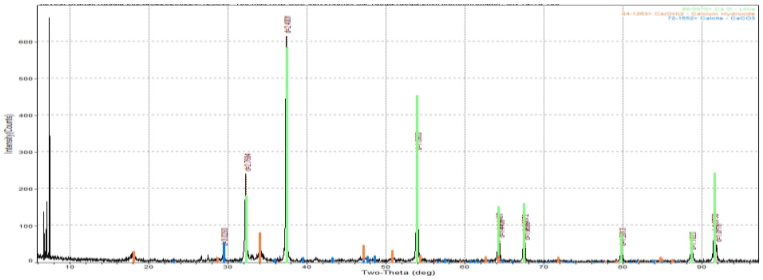

Figure 1 — X-ray diffraction pattern of sample 1

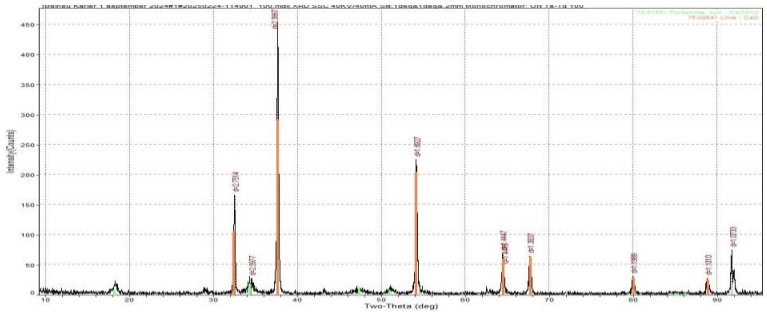

Figure 2 — X-ray diffraction pattern of sample 2

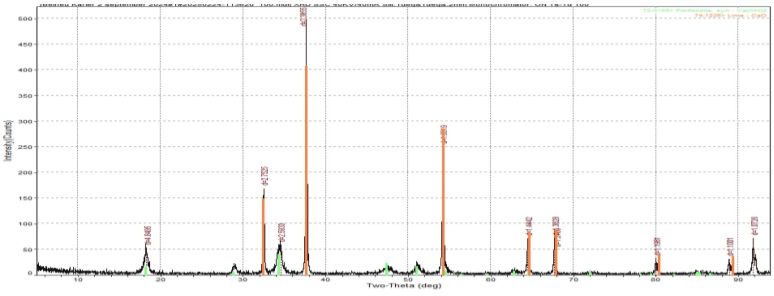

Figure 3 — X-ray diffraction pattern of sample 3

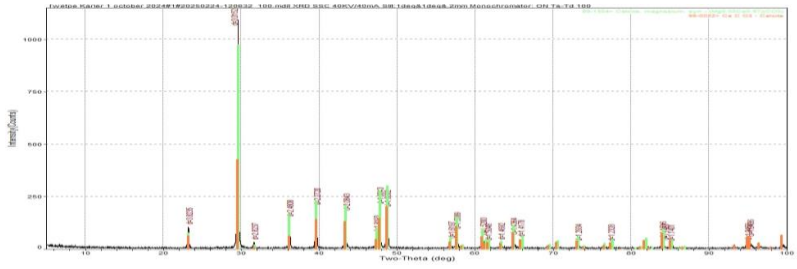

Figure 4 — X-ray diffraction pattern of sample 4

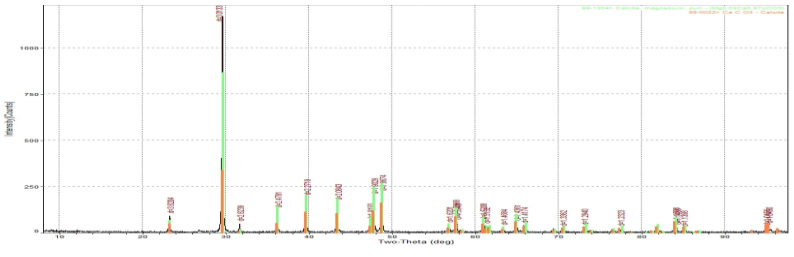

Figure 5 — X-ray diffraction pattern of sample 5

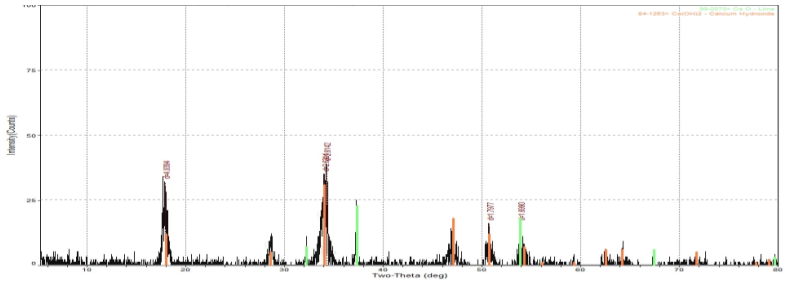

Figure 6 — X-ray diffraction pattern of sample 6

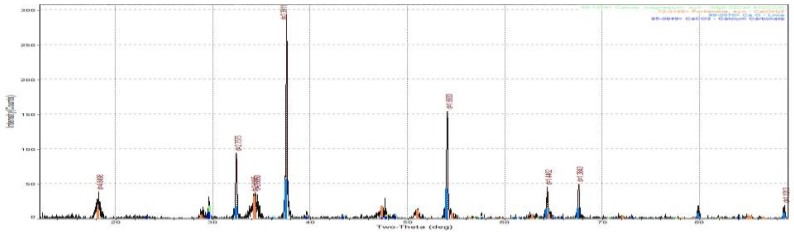

Figure 7 — X-ray diffraction pattern of sample 7

Table 1 — Data of semi-quantitative analysis by X-ray phase analysis (XRD) of the studied samples, %

Sample ID	CaO	$Ca(OH)_2$	Magnesian calcite*	$CaCO_3$
1. Bryansk, RF	78.8	16.9	-	4.3
2. Beineu, quarry 1	92.5	7.5	-	-
3. Beineu, quarry 2	81.0	19.0	-	-
4. Shetpe, quarry 1	-	-	99.9	0.1
5. Shetpe, quarry 2	-	-	98.7	1.3
6. Zhanakorgan	0.4	99.6	-	-
7. Fergana, Uzbekistan	76.1	19.1	1.5	3.3

* $Mg_{0,03}Ca_{0,97}(CO_3)$

Based on the analysis of the component composition of calcium-containing samples from various deposits in Russia, Kazakhstan, and Uzbekistan, three main groups can be identified:

1. Calcium oxide–hydroxide group. This group includes samples containing calcium oxide and calcium hydroxide (samples 1–3 and 7). It should be noted that samples 1 and 7 also contain carbonates and are generally similar in composition. In samples 2 and 3 (Beineu, quarries 1 and 2, respectively), only calcium oxide and calcium hydroxide are observed. At the same time, sample 2 shows the highest relative content of calcium oxide.

2. Calcium hydroxide group. The sample from Zhanakorgan is characterized by an exclusively high content of calcium hydroxide ($Ca(OH)_2$ — 99.6%).

3. Calcite group. The samples from Shetpe (quarries 1 and 2) consist entirely of calcite.

Table 2 presents the data on the elemental composition of the selected major elements (normalized compositions). Normalized compositions allow you to compare the relative content of elements to each other in different samples. The content of the remaining elements is below the limits of their detection.

Table 2 — Elemental analysis of selected elements in oxide form, %

	Sample ID	Al_2O_3	BaO	CaO	Fe_2O_3	K_2O	MgO	MnO	Na_2O	SO_4^{2-}	SiO_2
1	Bryansk, RF	1.2100	0.0071	70.8	1.22	0.676	0.207	0.0457	0.496	0.481	4.04
2	Beineu, quarry 1	<0.014	0.0017	77.2	0.124	0.585	0.087	0.00230	0.247	1.43	0.0863
3	Beineu, quarry 2	<0.014	0.0039	80.3	0.126	0.997	0.362	0.00322	0.430	1.61	<0.7
4	Shetpe, quarry 1	<0.014	0.0009	66.0	0.260	0.973	0.0263	0.0255	0.468	1.13	0.245
5	Shetpe, quarry 2	<0.014	0.0009	52.4	0.204	0.592	0.0425	0.0287	0.291	0.500	0.222
6	Zhanakorgan	0.36	0.007	66.4	0.12	0.035	0.65	0.013	<0.02	<0.4	2.2
7	Fergana, Uzbekistan	<0.014	0.0012	67.2	0.0403	0.650	0.294	0.00354	0.251	2.73	<0.5

Figure 8 shows the IR spectra of the studied samples. Table 3 presents the positions of the absorption bands in their IR spectra.

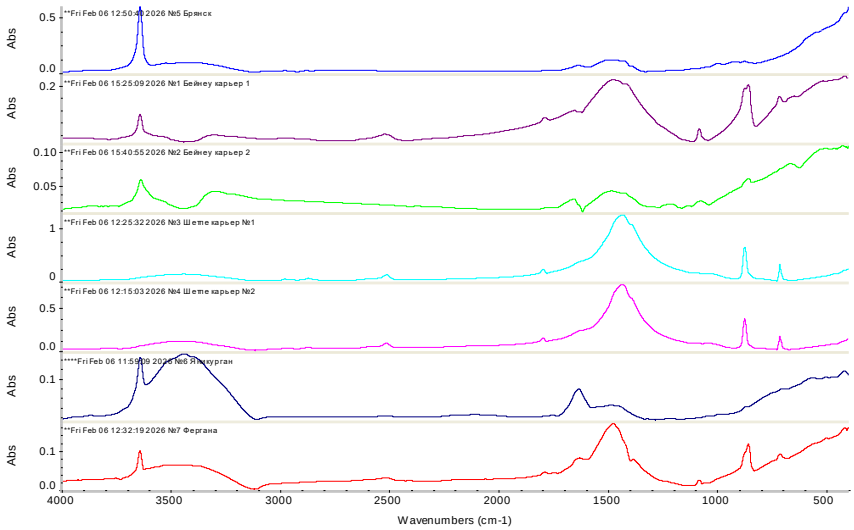

Figure 8 - IR spectra of the studied samples

Table 3 — Absorption frequencies of the studied samples

Sample ID						
Bryansk, RF	Beineu, quarry 1	Beineu, quarry 2	Shetpe, quarry 1	Shetpe, quarry 2	Zhanakorgan	Fergana, Uzbekistan
Wavenumbers, cm^{-1}						
3642.7	3643.1	3639.3	-	-	3642.0	3643.4
3439.1	3303.4	3299.8	-	3448.5	3441.0	-
-	-	-	2981.2	2971.0	-	-
-	-	-	2873.0	2873.3	-	-
-	2521.5	-	2514.3	2514.5	-	-
-	1789.2	-	1798.0	1798.1	-	1786.2
1630.7	1652.1	1654.0	-	-	1633.9	1624.7
1480.0	1475.1	1480.3	-	-	1491.7	1476.0
-	-	-	1434.4	1434.0		
-	-	-	-	-	1377.3	1380.9
-	-	1214.0	-	-	-	-
-	-	1137.0	-	-	-	1076.9
997.7	-	-	-	-	-	-
918.5	-	-	-	-	-	-
874.5	858.3	858.0	874.6	875.3	-	858.8
-	716.0		712.6	712.8	-	719.0
-	-	665.3	-	-	-	-
-	-	429.7	-	-	-	-

In samples 1–3 and 6–7, narrow and intense absorption bands in the 3640–3650 cm^{-1} region are observed, corresponding to the stretching vibrations of

hydroxyl groups. These bands indicate the presence of free or weakly bonded OH groups, characteristic of pure calcium hydroxide ($Ca(OH)_2$), and suggest the absence of hydrogen bonding. Deformation vibrations of OH groups are also present in the same samples (around 1640 cm^{-1}).

The absorption bands observed in the 3000–3450 cm^{-1} region are attributed to O–H bonds associated with groups participating in hydrogen bonding. For the Shetpe quarry samples (4 and 5), absorption bands in the 2870–2980 cm^{-1} region are observed, which are characteristic of hydrocarbons, i.e., indicating the presence of organic impurities. In addition, the spectra of the Shetpe samples (4 and 5) are dominated by intense carbonate-ion bands: the asymmetric stretching vibration ν_3 in the 1420–1460 cm^{-1} region, as well as deformation out-of-plane ν_2 (~870 cm^{-1}) and in-plane ν_4 (~710 cm^{-1}) vibrations.

The IR spectroscopy data are actually fully consistent with the conclusions of XRD regarding the component composition:

- Bryansk (1): The IR spectrum shows the presence of OH groups (moderate), CO_3^{2-} (weak), and water. XRD confirms a mixed composition with a predominance of CaO.
- Beineu-1 (2) and Beineu-2 (3): The IR spectra exhibit strong OH group bands, while CO_3^{2-} bands are weak or absent.
- Shetpe-1 (4) and Shetpe-2 (5): The IR spectra are characterized by absorption bands of carbonate groups. XRD confirms an almost pure calcite composition.
- Zhanakorgan (6): The IR spectrum shows intense OH group bands characteristic of calcium hydroxide, with no CO_3^{2-} group bands detected.
- Fergana (7): The IR spectrum, similar to that of Bryansk, shows the presence of OH groups (moderate), carbonate groups (moderate), and water, confirming the XRD data indicating a mixed composition containing CaO, $Ca(OH)_2$, and calcite.

Technological aspects (recommendations) of raw material utilization

The performed analysis made it possible to classify the investigated calcium-containing deposits according to their component composition and to determine their suitability for the production of calcium oxide.

1. Raw materials of the Calcium oxide–hydroxide group are the most preferable for obtaining highly active CaO. Samples Beineu-1 and Beineu-2 are particularly notable, requiring minimal energy input for activation (dehydroxylation at ~500–600 °C). Samples Bryansk and Fergana are also promising; however, the presence of impurities (SiO_2, Fe_2O_3, Mg) requires control of their influence on the process and the properties of the final product.
2. Raw materials of the calcium hydroxide group (Zhanakorgan) are easily converted to CaO under low-temperature calcination. The key risk is a high tendency toward recarbonation during storage, which necessitates airtight packaging.

3. Raw materials of the carbonate group (Shetpe) represent a classical but the most energy-intensive feedstock for lime production, requiring high-temperature decarbonation (850–1000 °C).

Overall, the results of the study provide valuable information for selecting optimal raw materials and developing technological regimes for calcium oxide production for various industrial applications, including the treatment of oil-contaminated soils. Further research may include determining the purity of the obtained CaO and its reactivity.

Conclusion

1. A comparative study of calcium-containing mineral raw materials from seven deposits was carried out using a combination of methods (XRD, IR spectroscopy, and elemental analysis). Fundamental differences in their phase composition were established.
2. A classification of the raw materials into three groups was proposed: calcium oxide–hydroxide, calcium hydroxide, and carbonate groups.
3. The most promising raw material for the energy-efficient production of highly active calcium oxide is limestone from the Beineu deposit (Quarry 1 and Quarry 2), which is characterized by the highest CaO contents (92.5% and 81.0%, respectively) and the lowest concentrations of inert impurities.
4. The raw material from the Zhanakorgan deposit (almost pure $Ca(OH)_2$) requires low-temperature treatment but special storage conditions.
5. The sample from Bryansk, despite its high CaO content, contains significant amounts of SiO_2 and Fe_2O_3, which must be taken into account when developing its processing technology.
6. The obtained results provide a scientific basis for selecting optimal raw materials and thermal activation regimes for the production of calcium oxide for environmental remediation technologies.

Funding: This research has been funded by the Science Committee of the Ministry of Science and Higher Education of the Republic of Kazakhstan (BR27101179).

Conflict of interests: The authors declare that there are no conflicts of interests between the authors to disclose in this article.

КАЛЬЦИЙҚҰРАМДЫ БІРҚАТАР КЕН ОРЫНДАРЫНЫҢ КОМПОНЕНТТІК ҚҰРАМЫН АНЫҚТАУ ЖӘНЕ ОЛАРДЫ ПАЙДАЛАНУ БОЙЫНША ТЕХНОЛОГИЯЛЫҚ ҰСЫНЫСТАР

А.А. Еспенбетов[1], Е.А. Тусупкалиев[1], Ж.Н. Кайнарбаева[1], Ә.Ж. Байзақ[1], З.К. Маймеков[2], А.Ж. Абюров[1]

[1] А.Б. Бектуров атындағы химиялық ғылымдар институты, Алматы, Қазақстан
[2] И. Разаков атындағы Қырғыз мемлекеттік техникалық университеті, Бішкек, Қырғызстан

Түйіндеме. Мұнаймен ластанған топырақтарды ремедиациялау технологияларында қолданылатын кальций оксидінің прекурсорлары ретінде кальцийқұрамды минералдық шикізаттың жарамдылығын бағалау мақсатында Ресей (Брянск), Қазақстан (Бейнеу, Шетпе, Жаңақорған) және

Өзбекстан (Ферғана) кен орындарының үлгілеріне кешенді зерттеу жүргізілді. Зерттеу әдістері ретінде рентгенфазалық талдау (РФА), элементтік талдау және инфрақызыл Фурье-спектроскопия қолданылды. РФА әдісі арқылы үлгілердің доминантты фазалық құрамы анықталып, жартылай сандық бағалау жүргізілді. Алынған нәтижелер негізінде үлгілер үш топқа жіктелді: 1) кальций-оксид-гидроксидтік топ (Брянск, Бейнеу, Ферғана), CaO мөлшері 76.1-92.5% және $Ca(OH)_2$ 7.5–19.0% құрайтын үлгілер; 2) кальций-гидроксидтік топ (Жаңақорған), іс жүзінде таза $Ca(OH)_2$ (99,6%); 3) карбонаттық топ (Шетпе), негізінен кальциттен $CaCO_3$ (>98%) тұратын үлгілер. ИҚ-спектроскопия нәтижелері анықталған фазаларды растады. Элементтік талдау үлгілердің басым бөлігінде кальцийдің жоғары тазалығын көрсетті (>95% CaO, нормаланған). Брянск үлгісінде SiO_2 мөлшерінің жоғары екені анықталды (~4%). Зерттеу нәтижелері негізінде шикізатты тиімді пайдалану бойынша технологиялық ұсынымдар берілді. Энергия тиімділігі тұрғысынан белсенді CaO алу үшін Бейнеу-1 және Бейнеу-2 үлгілері (сәйкесінше 92.5 және 81.0 % CaO) ең перспективті деп танылды.

Түйінді сөздер: кальцийқұрамды шикізат, кальций оксиді, рентгенофазалық талдау, ИҚ-спектроскопия, элементтік талдау, жіктеу, мұнаймен ластанған топырақтар

Еспенбетов Асылбек Алимбекович	*доктор химических наук*
Тусупкалиев Ерсин Адиетович	*кандидат технических наук*
Кайнарбаева Жания Нурбековна	*магистр*
Байзақ Әсел Жеңісқызы	*магистр*
Маймеков Зарлык Капарович	*техника ғылымдарының докторы, профессор*
Абюров Арман Жумабаевич	*PhD-докторант*

ОПРЕДЕЛЕНИЕ КОМПОНЕНТНОГО СОСТАВА РЯДА КАЛЬЦИЙ СОДЕРЖАЩИХ МЕСТОРОЖДЕНИЙ И ТЕХНОЛОГИЧЕСКИЕ РЕКОМЕНДАЦИИ ПО ИХ ИСПОЛЬЗОВАНИЮ

А.А. Еспенбетов[1], Е.А. Тусупкалиев[1], Ж.Н. Кайнарбаева[1], Ә.Ж. Байзақ[1], З.К. Маймеков[2], А.Ж. Абюров[1]

[1]АО Институт химических наук имени А.Б. Бектурова, Алматы, Казахстан
[2]Кыргызский государственный технический университет им. И. Разакова, Бишкек, Кыргызстан

Аннотация. Проведен комплексный анализ образцов кальцийсодержащегоминерального сырья из месторождений России (Брянск), Казахстана (Бейнеу, Шетпе, Жанакорган) и Узбекистана (Фергана) для оценки их пригодности в качестве прекурсоров оксида кальция, используемого в технологиях ремедиации нефтезагрязненных грунтов. В работе применены методы рентгенофазового (РФА), элементного анализа и инфракрасной спектроскопии (ИК-Фурье). Методом РФА установлен фазовый состав образцов и выполнена их полуколичественная оценка. На основе полученных данных предложена классификация образцов на три группы: 1) кальциево-оксидно-гидроксидная (Брянск, Бейнеу, Фергана), характеризующаяся высоким содержанием CaO (76.1-92.5%) и $Ca(OH)_2$ (7.5–19.0%); 2) кальциево-гидроксидная (Жанакоган), представляющая собой практически чистый $Ca(OH)_2$ (99.6%); 3) карбонатная (Шетпе), состоящая из кальцита $CaCO_3$ (>98%). Данные ИК-спектроскопии подтвердили наличие идентифицированных фаз. Элементный анализ показал высокую чистоту большинства образцов по кальцию (>95% CaO в нормированном виде). Образец из Брянска содержит повышенное количество кремнезема ($SiO_2 \approx$ 4%). Предложены технологические рекомендации по использованию сырья. Наиболее перспективным для энергоэффективного получения активного CaO признан образцы Бейнеу-1 и Бейнеу-2 (92.5 и 81.0 % CaO соответственно).

Ключевые слова: кальцийсодержащее сырье, оксид кальция, рентгенофазовый анализ, ИК-спектроскопия, элементный анализ, классификация, нефтезагрязненные грунты

Еспенбетов Асылбек Алимбекович	*химия ғылымдарының докторы*
Тусупкалиев Ерсин Адиетович	*химия ғылымдарының кандидаты*
Кайнарбаева Жания Нурбековна	*магистр*
Байзақ Әсел Жеңісқызы	*магистр*
Маймеков Зарлык Капарович	*техника ғылымдарының докторы, профессор*
Абюров Арман Жумабаевич	*PhD-докторант*

References

1. Boynton R.S. Chemistry and technology of lime and limestone, 2nd Ed. N.Y.: John Wiley and Sons, **1980**, 520 p.

https://archive.org/details/chemistrytechnol0000unse_u0w0/page/n5/mode/2up (accessed on 05 May 2026).

2. Oates J.A.H. Lime and limestone: chemistry and technology, production and uses. Weinheim: Wiley-VCH, **1998**, 472 p. DOI: https://doi.org/10.1002/9783527612024

3. Voronov A.V., Sidorov V.A. Application of calcium oxide for the remediation of oil-contaminated soils. *Ecology and Industry of Russia*, **2015**, *19, No. 9*, 52–55. (In Russ.).

4. Reginald B. K., Josiah M. A., Ikechukwu O., Victoria E., ThankGod D. D. Stabilisation/Solidification and Bioaugmentation Treatment of Petroleum Drill Cuttings. *Applied Geochemistry*, **2016**, *71*, 1–12. DOI: https://doi.org/10.1016/j.apgeochem.2016.05.010

5. Mokhov A.A., Batrakova M.S. Effect of impurities on the reactivity of calcium oxide. *Journal of Applied Chemistry*, **2010**, *83, No. 4*, 543–548. (In Russ.).

6. Samylina V.S., Maslenitsyn L.S. Carbonate rocks as raw materials for the chemical industry. Moscow: Khimiya, **1985**, 300 p. (In Russ.).

7. Shand M.A. The Chemistry and Technology of Magnesia. Hoboken: John Wiley and Sons, **2006**, 266 p. https://www.wiley-vch.de/de/fachgebiete/ingenieurwesen/the-chemistry-and-technology-of-magnesia-978-0-471-65603-6?utm_source=chatgpt.com (accessed on 05 May 2026).

8. Mehvish Bilal, Ammar Mohammed Alshammari, Aaqib Ali. Binder-Based Remediation of Heavy Metal Contaminated Soils: A Review of Solidification/Stabilization Methods. *Knowledge-based Engineering and Sciences*, **2023**, *4*, 17–34.

DOI: https://doi.org/10.51526/kbes.2023.4.3.17-34

9. Ochepo J. and Joseph V. Effect of Oil Contamination on Lime Stabilized Soil. *Jordan Journal of Civil Engineering*, **2014**, *8*, 88-96. DOI:https://doi.org/10.14525/jjce.8.1.2632

10. GOST EN 1482-2-2013 – Fertilizers and liming materials. Sampling and sample preparation. Moscow: Standartinform, **2014**.

https://meganorm.ru/Data2/1/4293774/4293774341.pdf (accessed on 05 May 2026).

11. GOST 22688-2018 – Building lime. Test methods. Moscow: Standartinform, **2018**.

https://meganorm.ru/Data2/1/4293734/4293734170.htm (accessed on 05 May 2026).

12. ASTM C1271-99 - Standard Test Method for X-ray Spectrometric Analysis of Lime and Limestone, USA, **2020**. https://webstore.ansi.org/standards/astm/astmc127199 (accessed on 05 May 2026).

Chemical Journal of Kazakhstan
Volume 2, Number 94(2026), 158-167 https://doi.org/10.51580/2026-2.2710-1185.23

UDC 54.057

SYNTHESIS AND PHYSICOCHEMICAL CHARACTERIZATION OF CHITOSAN–SiO_2-BASED COMPOSITES

S.N.Saryuisin[1,2*], E.T. Talgatov[1], Zh.K. Korganbaeva[2], E.A. Tusupkaliyev[3], Zh.N. Kainarbayeva[3]

[1] JSC D.V. Sokolskiy Institute of Fuel, Catalysis and Electrochemistry, Almaty, Kazakhstan
[2]Abai Kazakh National Pedagogical University, Almaty, Kazakhstan
[3] Institute of Chemical Sciences after A.B. Bekturov, Almaty, Kazakhstan

[*]Corresponding author e-mail: Saryuisin.sn@gmail.com

Abstract. *Introduction.* Composites based on chitosan are of particular interest owing to their biodegradability, environmental safety, and strong affinity for metal ions. Immobilization of chitosan on an inorganic support such as silica can be used as a method to improve physicochemical properties of hybrid materials such as their thermal stability and mechanical strength. *Objectives.* The main purpose of this work was preparation of chitosan–SiO_2 composites with different chitosan loadings and determination of their physicochemical properties. *Methods.* Composite chitosan–SiO_2 with 5, 10, and 20 wt.% content of chitosan was synthesized via adsorption immobilization followed by alkaline precipitation. Physical characteristics of obtained materials were studied using methods such as thermo gravimetric analysis (TGA), nitrogen adsorption–desorption analysis (BET), and scanning electron microscopy (SEM). *Results and discussion.* In our study, we showed that alkaline precipitation greatly increased the efficiency of adsorption and immobilization of chitosan, giving immobilization yields of 93-100%. From thermo gravimetric analysis, it was found that content of organic substances in the materials is gradually increased by increasing chitosan loading. According to the classification of the IUPAC, the isotherm is classified as type IV isotherms with H3 hysteresis loop characteristic for mesoporous materials. Scanning electron microscopy revealed heterogeneous and relatively rough surface morphology. *Conclusion.* Obtained composite materials have developed mesoporous structure, high thermal stability, and good immobilization of chitosan, which allows to consider them as prospective sorbents for heavy metal ion elimination from aqueous solutions.

Keywords: chitosan, silicon dioxide, composite materials, adsorption immobilization, mesoporous materials

Saryuisin Saniya Nurbekkyzy	*PhD doctoral student; E-mail: Saryuisin.sn@gmail.com*
Talgatov Eldar Talgatovich	*PhD, Professor acting; E-mail: e.talgatov@ifce.kz*
Korganbayeva Zhanar Kozhamberdykyzy	*Candidate of chemical sciences, Professor acting; E-mail: korganbaeva.zhan@mail.ru*
Tusupkaliyev Ersin Adietovich	*Candidate of Chemical Sciences; E-mail: t_ersin@mail.ru*
Kainarbayeva Zhaniya Nurbekovna	*Master; E-mail: zhaniya.kn@gmail.com*

Citation: Saryuisin S.N., Korganbaeva Zh.K., Talgatov E.T., Tusupkaliyev E.A., Kainarbayeva Zh.N. Synthesis and physicochemical characterization of chitosan– SiO_2-based composites. *Chem. J. Kaz.*, **2026**, 2*(94)*, 158-167. DOI: https://doi.org/10.51580/2026-2.2710-1185.23

Introduction

Heavy metal pollution in our water systems is still a big environmental challenge [1, 2]. That's mainly because these metal ions are toxic, stick around for a long time, and can build up in living organisms. Among the various pollutants, nickel (Ni(II)) and cobalt (Co(II)) are commonly found in industrial wastewater from electroplating, mining, metallurgy, and chemical processes [3]. High levels of these metals can lead to serious environmental and health issues, which is why there's a strong interest in developing efficient and eco-friendly materials to remove them [4].

One of the best ways to tackle this problem is through adsorption, as it's a straightforward and cost-effective method to extract heavy metal ions from water. Because of its simplicity and efficiency, there's been a growing focus on biopolymer-based adsorbents lately, thanks to their low toxicity, biodegradability, and easy availability [5, 6].

Chitosan stands out as a highly promising natural polymer for adsorption due to its amino and hydroxyl groups that can effectively bond with metal ions [7]. But there are some drawbacks; pure chitosan lacks mechanical stability and doesn't hold up well in acidic environments, which limits its use [8]. To overcome this, researchers have started to combine chitosan with inorganic materials like SiO_2 to enhance its structural integrity, surface characteristics, and overall adsorption capabilities.

Mesoporous silica is a great choice for support because it has a high surface area, a well-developed porous structure, and surface silanol groups, making it ideal for immobilizing polymers [9]. By combining chitosan with SiO_2, it’s possible to create hybrid materials that have improved physical and adsorption properties.

Therefore, the aim of this work was to prepare chitosan–SiO_2 composites with different polymer contents and investigate their physicochemical properties using thermogravimetric analysis, nitrogen adsorption–desorption analysis and scanning electron microscopy.

Experimental part

Materials and reagents

Silicon dioxide (SiO_2) and chitosan (degree of deacetylation ≥75%, derived from shrimp shells) were used as the main reagents and purchased from Sigma-Aldrich (Germany). Hydrochloric acid (HCl) and sodium hydroxide (NaOH) were used in the experiments. All chemicals and reagents were of analytical grade and used without further purification.

Preparation of chitosan–SiO_2 composites

A 1% chitosan solution was prepared by dissolving 1.0 g of chitosan in 100 ml of 1% hydrochloric acid solution (Figure 1a). The working HCl solution was prepared by diluting 2.34 ml of concentrated HCl with distilled water to a final volume of 100 ml. Dissolution was carried out at room temperature under magnetic stirring until complete polymer dissolution.

Chit/SiO_2 composites containing 5, 10, and 20 wt.% of chitosan were prepared by adsorption immobilization from solution. For this purpose, 1.0 g of SiO_2 was dispersed in 34.7, 28.9, and 15 mL of distilled water, respectively, and stirred for 10–15 min at room temperature. Then, 5.3, 11.1, and 25 ml of 1% chitosan solution were added to the suspensions (Figure 1b). In all cases, the total volume of the system was adjusted to 40 ml. The resulting suspensions were stirred for 1 h, after which the pH was adjusted to 7.5 using NaOH solution in order to decrease the protonation degree of chitosan amino groups and enhance its adsorption onto the SiO_2 surface (Figure 1c). The mixtures were then additionally stirred for 2 h. The systems were left at room temperature for 12 h to reach adsorption equilibrium (Figure 1d). The solid phase was separated by filtration, washed with distilled water until neutral pH, and dried at room temperature to constant weight (Figure 1e). The filtrates were collected and analyzed by viscometry.

Thus, SiO_2 composite samples modified with different chitosan contents were obtained and further used for physicochemical characterization and adsorption studies.

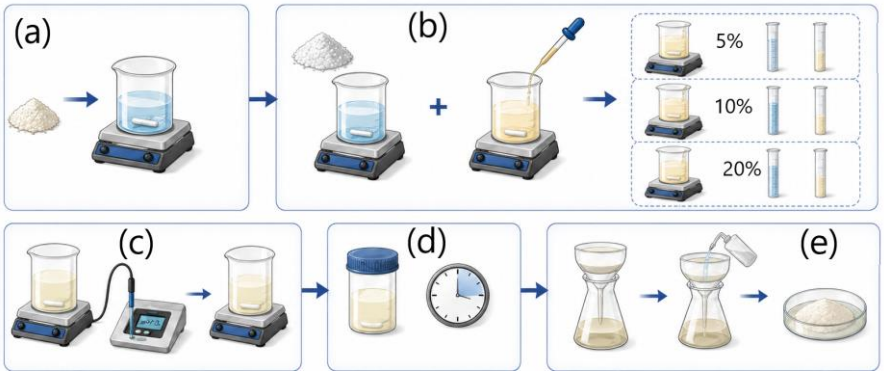

Figure 1 –Experimental procedure for the preparation of chitosan–SiO_2 composites

Results and discussion

The chitosan-SiO_2 composites containing 5, 10, and 20 wt.% of chitosan were synthesized via the adsorption immobilization method. The extent of polymer adsorption on the surface of the matrix was calculated based on the remaining amount of the polymer in the mother liquor after adsorption. The measurement of mother liquor viscosity allowed estimating the remaining chitosan amount based on the previously constructed calibration curve.

Quantitative data of chitosan adsorption in Chit/SiO_2 composites, fabricated both in the absence and in the presence of an alkaline precipitation, are presented in Table 1. It has been established that the synthesis method significantly affects the effectiveness of the composite formation. In the samples synthesized without

precipitation, the adsorption degree stayed comparatively low at 28–30%, regardless of the increasing initial chitosan content. This can be caused by low interaction strength between chitosan macromolecules and the silica surface at acidic pH due to the repulsion forces acting between molecules [10]. Consequently, only a low number of polymer molecules are adsorbed, and hence, the content of chitosan in composites becomes low. This is associated with protonation of amino groups (- NH_3^+) preventing their interaction with silica silanol groups (Si-OH) [11].

However, in the samples prepared through an additional alkaline precipitation, a considerable increase in adsorption degree up to 93–100% was observed. It means that nearly all initial chitosan is adsorbed and immobilized on the silica surface. It is connected with the shift in the pH value towards neutral and the corresponding deprotonation of amino groups ($-NH_3^+ \rightarrow -NH_2$). As a result, interaction between polymer and silica becomes more intensive.

Therefore, the polymer content in the obtained composites was significantly higher than in precipitate-free samples and reached the level of 4.7, 10, and 20 wt.% according to the initial loading.

Table 1 – The results of the assessment of chitosan content in Chit /SiO_2 composites

m(Chit) in the Initial Solution, mg	m(Chit) in Solution after Sorption, mg	m(Chit) Adsorbed, mg	Adsorption Degree, %	Chit Content, %
Chit/SiO_2 without precipitation				
53	38.0	15.0	28	1.4
111	79.2	31.8	29	2.9
250	175.0	75.0	30	6.0
Chit/SiO_2 with precipitation (by NaOH)				
53	4.0	49.0	93	4.7
111	0.0	111.0	100	10.0
250	0.0	250.0	100	20.0

The thermal behavior of pure chitosan and Chit/SiO_2 composites with different polymer contents was investigated using TG–DTA analysis (Figure 2). Pure chitosan exhibited significant thermal degradation accompanied by a total mass loss of approximately 66.9%. The initial weight loss below 150–180℃ was associated with the removal of physically adsorbed and bound water molecules. The main decomposition stage started at approximately 292.5℃ and corresponded to degradation of the chitosan polymer backbone, including decomposition of saccharide and amino-containing groups. In comparison, the Chit/SiO_2 composites demonstrated considerably higher thermal stability due to the presence of the inorganic silica matrix. All composites showed gradual mass loss with increasing temperature while preserving the characteristic thermal decomposition behavior of immobilized chitosan. The first weight-loss stage below 200℃ was mainly related to desorption of adsorbed water and partial

dehydroxylation of silanol groups. The corresponding mass losses were approximately 5.01%, 5.07%, and 5.18% for 5%, 10%, and 20% Chit/SiO_2 composites, respectively. The second decomposition stage observed in the range of approximately 250–400℃ was attributed to thermal degradation of the immobilized chitosan phase. The mass loss in this region increased with increasing polymer content and reached 3.38%, 3.89%, and 7.85% for 5%, 10%, and 20% Chit/SiO_2 composites, respectively. The total mass losses for the composites were 11.86%, 14.54%, and 18.56%, respectively. The progressive increase in mass loss with increasing chitosan loading confirms the successful incorporation of chitosan into the SiO_2 matrix and the formation of hybrid organic–inorganic composites. As one can see, the experimental data agree well with literature sources [12].

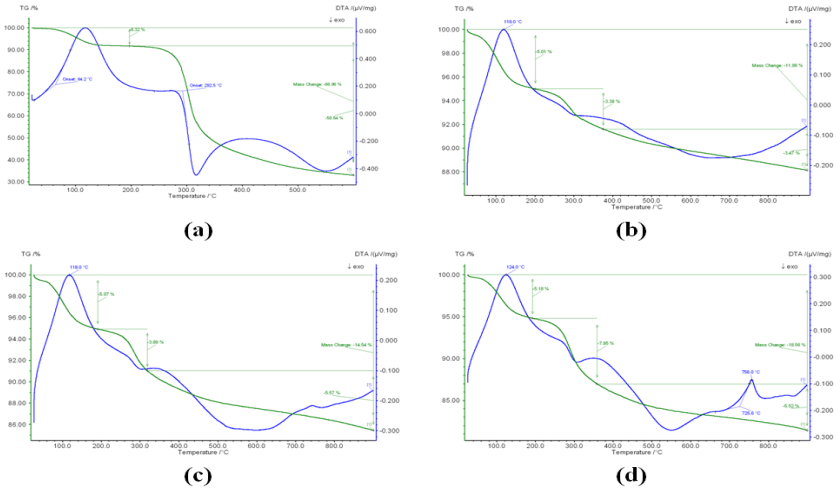

Figure 2 – TGA and DTA of (a) chitosan (b) 5% Chit/SiO_2 (c) 10% Chit/SiO_2 (d) 20% Chit/SiO_2

The probable process of the interaction of chitosan with the SiO_2 surface is depicted in Figure 3. At an acidic pH value, chitosan dissolves owing to the protonation of amino groups with the generation of $–NH_3^+$ groups. During the neutralization reaction with NaOH and the further increase in pH value up to 7.5, the deprotonation of amino groups occurs partially, enhancing the capability of chitosan macromolecules to bind with the SiO_2 surface. The binding of chitosan molecules with silica is governed mainly by hydrogen bonds and physical adsorption.

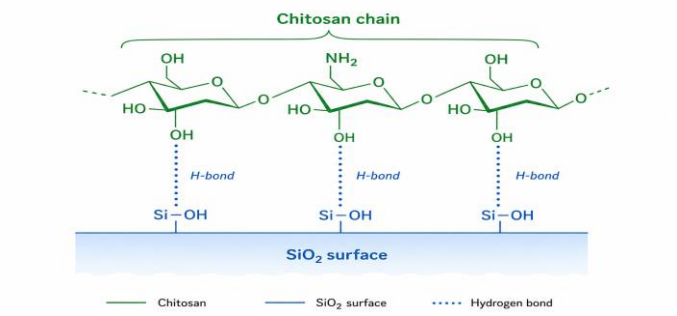

Figure 3 – Schematic illustration of the interaction between chitosan chains and the SiO_2 surface via hydrogen bonding

Figure 4 shows the adsorption-desorption isotherms and the pore size distribution for SiO_2, chitosan, and 10% Chit/SiO_2. Based on the classification of adsorption isotherms by IUPAC, the isotherms are classified as type IV adsorption isotherms with the existence of hysteresis loops of H3 type [13]. Silica is characterized by the mesoporous structure with a high value of nitrogen adsorption in the whole range of relative pressures. A hysteresis loop at medium and high relative pressure indicates capillary condensation inside mesopores. Additionally, the pore-size distribution proves the prevalence of mesopores with uniform pore structure [14].

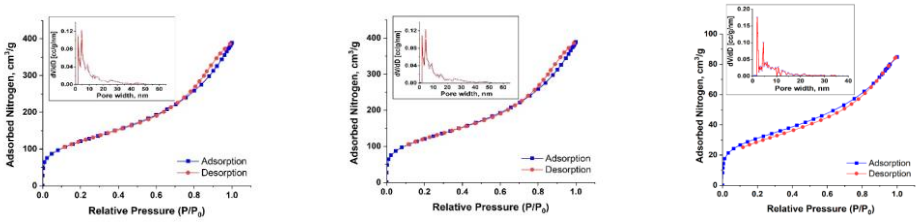

(a) (b) (c)

Figure 4 - N_2 -adsorption−desorption isotherm plots of (a) SiO_2 (b) Chitosan (c) 10%Chitosan-SiO_2 composite. The insets show the corresponding pore-size distribution

A much lower amount of nitrogen absorption by the chitosan sample indicates poor development of the porous structure and low specific surface area. The 10% Chit/SiO_2 composite still preserves mesoporous character of silica; however, the volume of nitrogen adsorption decreased after the immobilization process. It occurs due to the blockage of silica pores with chitosan macromolecules. Nevertheless, preservation of isotherms of type IV indicates that silica mesoporous structure has not been destroyed completely. The analysis of experimental results confirms the successful immobilization of chitosan molecules to the surface of silica without a complete breakdown of its porous structure.

Morphology of the surface of 10% Chit/SiO_2 composite was studied using scanning electron microscopy and the corresponding micrograph is provided in Figure 5. Composite material demonstrates heterogeneity and rather rough surface morphology featuring clusters of agglomerated particles. As compared to pure silica described in the literature sources, the surface morphology became less uniform as a result of chitosan immobilization, which indicates that the polymer layer was formed on the surface of silica nanoparticles [15]. Formation of clusters can be attributed to possible interaction of chitosan molecules and silica nanoparticles during the immobilization step. Moreover, no big crystallites or phase separation was noticed, which means that chitosan molecules are homogeneously distributed in the composite material. Surface morphology and porosity of the developed composite material are beneficial for adsorption, because they provide a lot of active sites for ion adsorption.

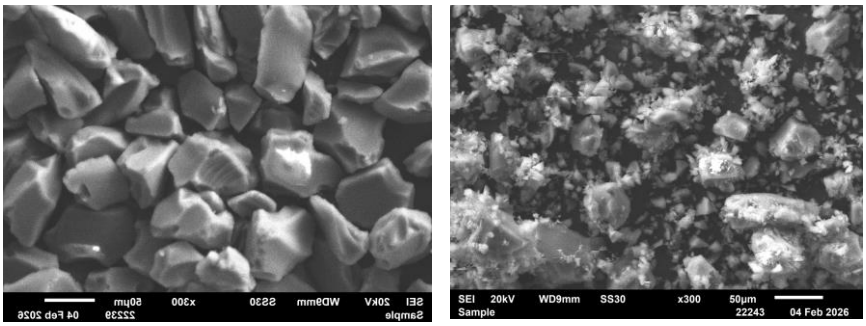

(a) (b)

Figure 5 - SEM micrograph of the (a) SiO_2 (b) 10%Chitosan-SiO_2

Conclusion

Successful synthesis of the Chitosan-SiO_2 composites at different polymer loadings was realized through the method of adsorption immobilization from solution and alkaline precipitation. Obtained results proved the important role of pH regulation with sodium hydroxide during immobilization process, providing maximum chitosan adsorption efficiency up to 93-100%. It was found via thermogravimetric analysis that the introduction of chitosan into silica resulted in gradual rise of material's organic content. The nitrogen adsorption-desorption isotherms proved the formation of mesoporous structure in the resulting composites with the typical type IV adsorption behavior and hysteresis loop H3 according to the International Union of Pure and Applied Chemistry classification. Moreover, results of BET analysis confirmed the presence of partially filled pores, proving that specific surface area and total pore volume decreased at an increase in the polymer content in composite composition. In conclusion, obtained results proved that synthesized Chitosan-SiO_2 composites are prospective hybrid materials for their further use as adsorbents for selective removal of heavy metals ions from aqueous solutions.

Conflict of interests: The authors declare that there are no conflicts of interests between the authors to disclose in this article.

ХИТОЗАН– SiO_2 НЕГІЗІНДЕГІ КОМПОЗИТТЕРДІ СИНТЕЗДЕУ ЖӘНЕ ОЛАРДЫҢ ФИЗИКА-ХИМИЯЛЫҚ СИПАТТАМАЛАРЫ

С.Н. Сарыүйсін[1,2]*, Э.Т. Талғатов[1], Ж.Қ. Қорғанбаева[2], Е.А. Тусупкалиев[3], Ж.Н. Қайнарбаева[3]

[1] Д.В. Сокольский атындағы Жанармай, катализ және электрохимия институты АҚ, Алматы, Қазақстан
[2] Абай атындағы Қазақ Ұлттық Университеті, Алматы, Қазақсатан
[3]Ә.Б. Бектұров атындағы Химия ғылымдары институты АҚ, Алматы, Қазақстан

Түйіндеме: *Кіріспе.* Хитозан негізіндегі композиттік материалдар соңғы жылдары биологиялық ыдырағыштығы, экологиялық қауіпсіздігі және металл иондарын тиімді байланыстыру қабілетінің арқасында зерттеушілердің үлкен қызығушылығын тудырып отыр. Осындай материалдардың қасиеттерін жақсартудың тиімді тәсілдерінің бірі – хитозанды бейорганикалық тасымалдағыштардың, әсіресе диоксид кремнийдің бетіне иммобилизациялау болып табылады. SiO_2 қолдану алынған гибридті жүйелердің механикалық беріктігі мен термиялық тұрақтылығын арттыруға, сондай-ақ олардың пайдалану сипаттамаларын жақсартуға мүмкіндік береді. *Зерттеудің мақсаты.* Құрамындағы хитозан мөлшері әртүрлі хитозан–SiO_2 композиттерін синтездеу және олардың физика-химиялық қасиеттерін зерттеу болды. *Әдістемесі.* Құрамында 5, 10 және 20 масс.% хитозан бар композиттер ерітіндіден адсорбциялық иммобилизациялау және кейінгі сілтілік тұндыру әдісі арқылы алынды. Алынған материалдардың қасиеттерін зерттеу үшін термогравиметриялық талдау (ТГА), азоттың төмен температурадағы адсорбциясы (БЭТ) және сканерлеуші электрондық микроскопия (СЭМ) әдістері қолданылды. *Нәтижелер және талқылау.* Зерттеу нәтижелері сілтілік тұндыру процесі хитозанның SiO_2 бетіне бекітілу тиімділігін едәуір арттыратынын көрсетті, бұл жағдайда иммобилизация дәрежесі 93–100% аралығында болды. Термогравиметриялық талдау нәтижелері композит құрамындағы хитозан мөлшері артқан сайын органикалық бөліктің де біртіндеп көбейетінін дәлелдеді. IUPAC классификациясына сәйкес алынған изотермалар H3 гистерезис ілмегі бар IV типке жатады, бұл материалдардың мезокеуекті құрылымға ие екенін көрсетеді. СЭМ арқылы жүргізілген талдау композиттердің беті біркелкі емес және салыстырмалы түрде кедір-бұдырлы морфологиямен сипатталатынын көрсетті. *Қорытынды.* Осылайша, синтезделген хитозан–SiO_2 композиттері дамыған мезокеуекті құрылымымен, жоғары термиялық тұрақтылығымен және полимердің тиімді иммобилизациялануымен ерекшеленеді. Мұндай қасиеттер олардың ауыр металл иондарын сулы ерітінділерден бөліп алуға арналған перспективті сорбенттер ретінде қолданылуына мүмкіндік береді.

Түйінді сөздер: хитозан, кремний диоксиді, композиттік материалдар, адсорбциялық иммобилизация, мезокеуекті материалдар

Сарыүйсін Сәния Нурбекқызы	*PhD докторант*
Талғатов Эльдар Талгатович	*PhD доктор, қауымдастырылған профессор*
Қорғанбаева Жанар Қожамбердіқызы	*химия ғылымдарының кандидаты, қауымдастырылған профессор*
Тусупкалиев Ерсин Адиетович	*химия ғылымдарының кандидаты*
Кайнарбаева Жания Нурбековна	*магистр*

СИНТЕЗ И ФИЗИКО-ХИМИЧЕСКАЯ ХАРАКТЕРИСТИКА КОМПОЗИТОВ НА ОСНОВЕ ХИТОЗАНА И SiO_2

С.Н. Сарыүйсін[1,2]*, Э.Т. Талгатов[1], Ж.Қ. Қорганбаева[2], Е.А. Тусупкалиев[3], Ж.Н. Қайнарбаева[3]

[1] АО «Институт топлива, катализа и электрохимии им. Д.В.Сокольского», Алматы, Казахстан [2]Казахский национальный педагогический университет имени Абая», Алматы, Казахстан

[3] АО «Институт химических наук имени А.Б. Бектурова», Алматы, Казахстан

Резюме. *Введение.* Композиты на основе хитозана в последние годы привлекают значительное внимание благодаря сочетанию биоразлагаемости, экологической безопасности и способности эффективно связывать ионы металлов. Одним из подходов к улучшению свойств таких материалов является иммобилизация хитозана на поверхности неорганических носителей, в частности диоксида кремния. Использование SiO_2 позволяет повысить механическую прочность и термическую устойчивость получаемых гибридных систем, а также улучшить их эксплуатационные характеристики. *Целью данной работы* являлось получение композитов хитозан–SiO_2 с различным содержанием полимера и исследование их физико-химических свойств. *Методика.* Синтез композитов с содержанием хитозана 5, 10 и 20 масс.% проводили методом адсорбционной иммобилизации из раствора с последующим щелочным осаждением. Для характеристики полученных материалов использовали методы термогравиметрического анализа (ТГА), низкотемпературной адсорбции азота (БЭТ) и сканирующей электронной микроскопии (СЭМ). *Результаты и обсуждения.* Результаты исследования показали, что проведение щелочного осаждения существенно повышает эффективность закрепления хитозана на поверхности SiO_2, обеспечивая степень иммобилизации в пределах 93–100%. Данные термогравиметрического анализа свидетельствуют о постепенном увеличении содержания органической составляющей при повышении доли хитозана в составе композитов. Согласно классификации IUPAC, полученные изотермы относятся к IV типу и характеризуются наличием петли гистерезиса H3, что указывает на мезопористую структуру материалов. Анализ поверхности методом СЭМ показал, что композиты обладают неоднородной и сравнительно шероховатой морфологией поверхности. *Заключение.* Таким образом, синтезированные композиты хитозан–SiO_2 характеризуются развитой мезопористой структурой, высокой термической стабильностью и эффективной иммобилизацией полимера. Совокупность полученных свойств позволяет рассматривать данные материалы как перспективные сорбенты для извлечения ионов тяжелых металлов из водных растворов.

Ключевые слова: хитозан, диоксид кремния, композиционные материалы, адсорбционная иммобилизация, мезопористые материалы

Сарыүйсін Сәния Нурбекқызы	*PhD докторант*
Талгатов Эльдар Талгатович	*кандидат химических наук, ассоц. профессор*
Қорганбаева Жанар Қожамбердіқызы	*кандидат химических наук*
Тусупкалиев Ерсин Адиетович	*магистр*
Кайнарбаева Жания Нурбековна	*магистр*

References

1. Saravanan P., Saravanan V., Rajeshkannan R., Arnica G., Rajasimman M., Baskar G., Pugazhendhi A. Comprehensive review on toxic heavy metals in the aquatic system: sources, identification, treatment strategies, and health risk assessment. *Environmental Research*, **2024**, Vol. 258, P. 119440. https://doi.org/10.1016/j.envres.2024.119440.

2. Chowdhury S., Mazumder M.A.J., Al-Attas O., Husain T. Heavy metals in drinking water: Occurrences, implications, and future needs in developing countries. *Science of The Total Environment*, **2016**, Vol. 569–570, P. 476–488. https://doi.org/10.1016/j.scitotenv.2016.06.166.

3. Liu X., Guo H., Zhang X., Zhang S., Cao X., Lou Z., Zhang W., Chen Z. Modeling the transport behavior of Pb(II), Ni(II) and Cd(II) in the complex heavy metal pollution site under the influence of coexisting ions. *Process Safety and Environmental Protection*, **2022**, Vol. 162, P. 211–218. https://doi.org/10.1016/j.psep.2022.04.016.

4. Chen J., Ji C., Liu J., Zhang J. Preparation of PMDA@CS/PVA composite membranes and their sorption for Cu(II), Co(II), and Ni(II) in water: Experimental and statistical physics exploration. *Desalination and Water Treatment*, **2025**, Vol. 324, P. 101513.
https://doi.org/10.1016/j.dwt.2025.101513.

5. Wang J., Wang C., Zhang Q. Efficient extraction and recovery of Co(II) and Ni(II) from spent ChCl-EG deep eutectic solvent via solvent extraction: A mechanism and performance study. *Journal of Environmental Chemical Engineering*, **2025**, Vol. 13, No 3, P. 116671.
https://doi.org/10.1016/j.jece.2025.116671.

6. Ghasemzadeh H., Shidrang S., Vanashi A.K. Nanocomposite magnetic hydrogel based on κ-carrageenan and acrylic acid for the removal of Cd(II), Co(II), Cu(II), and Ni(II); Efficient adsorption enhanced by activated carbon and magnetic nanoparticles. *International Journal of Biological Macromolecules*, **2025**, Vol. 292, P. 139164.
https://doi.org/10.1016/j.ijbiomac.2024.139164.

7. Zeng H., Ma G., Zheng X., Lin D., Zhang J., Li D. Preparation, application and regeneration of chitosan composite adsorbents for arsenic removal: A review from a sustainable perspective. *International Journal of Biological Macromolecules*, **2025**, Vol. 330, Part 3, P. 148156. https://doi.org/10.1016/j.ijbiomac.2025.148156.

8. Raees A., Hassan F., Awwad N.S., Ibrahium H.A., Mir S., Rafiq M., Mukhtiar A., Batoo K.M. Chitosan derivatives for wastewater treatment: Magnetically active chitosan for toxic metal removal. *Journal of Industrial and Engineering Chemistry*, **2026**.
https://doi.org/10.1016/j.jiec.2026.03.021

9. Gou K., Wang Y., Xie L., Guo X., Guo Y., Ke J., Wu L., Li S., Li H. Synthesis, structural properties, biosafety and applications of chiral mesoporous silica nanostructures. *Chemical Engineering Journal*, **2021**, Vol. 421, Part 2, P. 127862.
https://doi.org/10.1016/j.cej.2020.127862.

10. Oliveira F.C., Barros-Timmons A., Lopes-da-Silva J.A. Preparation and characterization of chitosan/SiO_2 composite films. *Journal of Nanoscience and Nanotechnology*, **2010**, Vol. 10, No. 4, P. 2816–2825. https://doi.org/10.1166/jnn.2010.1442.

11. Wang J., Ma R., Gu P. Chitosan modified silicon dioxide composites for the capture of graphene oxide. *Journal of Physics and Chemistry of Solids*, **2020,** Vol. 147, P. 109629. https://doi.org/10.1016/j.jpcs.2020.109629.

12. Zhong T., Xia M., Yao Z., Han C. Chitosan/Silica Nanocomposite Preparation from Shrimp Shell and Its Adsorption Performance for Methylene Blue. *Sustainability*, **2023**, Vol. 15, No. 1, P. 47. https://doi.org/10.3390/su15010047.

13. Abebe B., Murthy H.C. Ananda, Zereffa E. Summary on adsorption and photocatalysis for pollutant remediation: Mini review. *Journal of Encapsulation and Adsorption Sciences*, **2018**, Vol. 8, P. 225–255. https://doi.org/10.4236/jeas.2018.84012.

14. Sang H., Mao C., Wu Y., Wei Y. Study on the effect of gamma-ray irradiation on the adsorption of Tc and Re by a silica-based pyridine resin. *Toxics*, **2022**, Vol. 10, P. 638.
https://doi.org/10.3390/toxics10110638.

15. Mehmood Y., Ullah Khan I., Shahzad Y., Khalid S., Asghar S., Irfan M., Asif M., Khalid I., Yousaf A., Hussain T. Facile synthesis of mesoporous silica nanoparticles using modified sol-gel method: Optimization and in vitro cytotoxicity studies. *Pakistan Journal of Pharmaceutical Sciences*, **2019**, Vol. 32, P. 1805–1812. https://pubmed.ncbi.nlm.nih.gov/31680076/

Chemical Journal of Kazakhstan
Volume 2, Number 94(2026), 168-180 https://doi.org/10.51580/2026-2.2710-1185.24

UDC 615.074:543.422.3

VALIDATION OF THE METHOD FOR DETERMINING THE CONCENTRATION OF IODIDE IONS IN DIFFERENT DOSAGE FORMS BY UV SPECTROPHOTOMETRY

R. Karzhaubayeva*, S. Turganbay, Zh. Taganov, Z. Ashimkhanova, G. Baigaipova, A. Kurmanaliyeva

JSC Scientific Centre for Anti-infectious Drugs, Almaty, Kazakhstan

**Corresponding author e-mail: karzhaubayeva@mail.ru*

Abstract. This article is devoted to the validation of an analytical method for the determination of iodide ions in various dosage forms using UV spectrophotometry. This method is an important part of analytical chemistry and drug quality control systems, in which the sensitivity, specificity, and reproducibility of the method are crucial. The relevance of the study is determined by the need for accurate and reliable quantitative determination of iodide ions in pharmaceutical substances and finished drug products. Validation was conducted in accordance with the requirements of the International Council for Harmonisation of Technical Requirements for Pharmaceuticals for Human Use (ICH Q2(R1)/Q2(R2)). The aim of this study was to determine the validation characteristics of a method for the quantitative determination of iodide ions in dosage forms using UV spectrophotometry. Results and discussion. The following parameters were evaluated: specificity, linearity, working range, accuracy, repeatability, within-laboratory precision, and solution stability. The working range was found to be from 20 to 240 mg/L, and the correlation coefficient was 0.9998. The method demonstrated high sensitivity and compliance with international requirements. Conclusion. The results obtained confirm the linearity of the method across the studied range of iodide ion concentrations. High sensitivity and a high degree of linearity ($R^2 = 0.9998$) were demonstrated. The developed method is suitable for its intended purpose and can be successfully applied in the analysis of iodine-containing medicinal products. The method has practical significance for pharmaceutical quality control systems.

Key words: iodide ions, UV spectrophotometry, method validation, ICH Q2, pharmaceutical analysis.

Karzhaubayeva Roza Askarovna	*Candidate of Technical Sciences; Email: karzhaubayeva@mail.ru*
Turganbay Seitzhan	*PhD; Email: turganbay.s@gmail.com*
Taganov Zhasur Ibragimovich	*Master of Technical Sciences; Email: taganovjasur@mail.ru*
Ashimkhanova Zauresh Saidakhmetovna	*Senior Researcher; Email: A_zauresh.72@mail.ru*
Baigaipova Gulshat Kuanbekovna	*Senior Researcher; Email: baigaipovag@mail.ru*
Kurmanaliyeva Assel Rakhimovna	*Master of Technical Sciences, Senior Researcher; Email: wasilek.07@mail.ru*

Citation: Karzhaubayeva R., Turganbay S., Taganov Zh., Ashimkhanova Z., Baigaipova G., Kurmanaliyeva A. Validation of the method for determining the concentration of iodide ions in different dosage forms by UV spectrophotometry. *Chem. J. Kaz.*, **2026**, 2*(94)*, 168-180. DOI: https://doi.org/10.51580/2026-2.2710-1185.24

Introduction

In accordance with the requirements of international regulatory documents, analytical methods used for the quality control of medicinal products are subject to mandatory validation. The main requirements for the validation of analytical procedures are set out in the International Council for Harmonisation (ICH Q2(R1)/Q2(R2)) guideline, which defines parameters such as trueness, accuracy, specificity, linearity, range, limit of detection, limit of quantification and robustness of the method [1]. The validation of analytical methods is an essential step in ensuring the reliability of analytical results and confirming the suitability of the method for practical application in pharmaceutical quality control [2].

UV spectrophotometry is one of the most widely used analytical methods in analytical and pharmaceutical chemistry. The method is characterised by high sensitivity, ease of use, rapid analysis and relatively low equipment costs, making it a convenient tool for routine quality control of medicinal products [3]. UV spectrophotometric methods are widely used for the quantitative determination of active substances and inorganic ions in various dosage forms [4].

Iodide ions are widely used in pharmaceutical practice and are found in various medicinal products, including ophthalmic solutions, antiseptics and other dosage forms. Consequently, the development and validation of reliable analytical methods for the quantitative determination of iodide ions is a pressing task in pharmaceutical analysis.

Various methods for the determination of iodide ions have been described in the literature, including titrimetric methods, ion chromatography, electrochemical methods and spectrophotometric methods of analysis [5–7]. However, UV-spectrophotometric methods remain attractive due to their high analytical sensitivity, the availability of equipment and the possibility of rapid analysis [8–10].

The UV spectrophotometry method is based on measuring the absorption of ultraviolet (200–400 nm) and visible (400–800 nm) radiation by the molecules of a substance. Quantitative determination is carried out in accordance with the Beer-Lambert law, which establishes a linear relationship between the optical density of the solution and the concentration of the substance being analysed. Thanks to these characteristics, the method is widely used in the quality control of medicinal products, the verification of the authenticity of preparations, and the quantitative analysis of active substances.

The aim of this study is to validate an analytical method for determining the concentration of iodide ions in various pharmaceutical formulations using UV spectrophotometry in accordance with the requirements of the ICH international guidelines.

During the validation, the following characteristics were investigated: trueness, precision, repeatability, intra-laboratory accuracy, specificity, linearity, working range and robustness of the method when analysing iodide ion solutions.

Experimental section

Objects of Study

The objects of study included the iodide ion standard reference material (SRM 9426-2009, Saint Petersburg, Russian Federation), the FS-1 medicinal product after complete reduction of molecular iodine to iodide ions using formaldehyde, purified water, a 0.05% dextrin solution, and a 1% formaldehyde solution. These materials were used for validation of the analytical method and for the assessment of specificity, linearity, accuracy, precision, and robustness.

Instrumentation and Analytical Conditions

Validation was performed using a Lambda-35 UV spectrophotometer equipped with a diode-array detector. The analysis was carried out under the following conditions:

- wavelength: 226 nm;
- quartz cuvettes with an optical path length of 10.0 mm.

The instrument was operated in accordance with the user manual and standard operating procedure SOP-EQ-035 “Operation of the Lambda-35 Spectrophotometer” [11,12].

Iodide ion standard reference material (SRM 9426-2009) was used as the reference standard. Validation solutions were prepared within the concentration range of 0–200 mg/L.

Validation Procedure

Method validation was performed in accordance with the standard operating procedure SOP-GE-004 “Validation of Analytical Methods” [13] and the requirements of ICH guideline Q2(R1)/Q2(R2) [1].

The following validation characteristics were evaluated: accuracy, repeatability, intra-laboratory precision, specificity, linearity, working range, and robustness.

For the validation study:

- a reference standard solution containing 200 mg/L of iodide ions was prepared by diluting 5 mL of SRM 9426-2009 solution to 25 mL in a volumetric flask according to the manufacturer's instructions;
- iodide ion validation solutions with concentrations of 2, 20, 50, 100, and 200 mg/L were prepared;
- the FS-1 medicinal product was subjected to complete reduction of molecular iodine to iodide ions using formaldehyde;
- purified water, 0.05% dextrin solution, and 1% formaldehyde solution were used as blank matrices;
- the absorbance of the 200 mg/L reference standard solution and validation solutions was measured in ten replicates by different analysts on different days;
- the absorbance of the FS-1 medicinal product and blank matrices was measured in triplicate;
- mean values and standard deviations were calculated;

- the working range of the analytical method was established based on the validation results.

Results and Discussion

Accuracy

The "accuracy" parameter of the analytical method was determined by measuring the optical density of a standard solution with a concentration of 200 ppm of iodide ions. The concentration was calculated based on the measured optical density using the specific optical density, which is the tangent of the slope of the calibration line in the concentration range of 2–200 ppm.

The acceptance criterion for the "accuracy" parameter was a deviation of the calculated concentration from the true value not exceeding ± 3 % for a concentration of 200 mg/l.

Table 1 – Accuracy assessment results

No.	Concentration C, mg/l
1	200.1665
2	200.0588
3	200.1175
4	200.1273
5	200.284
6	200.1371
7	200.0784
8	200.0196
9	200.2742
10	200.2547
Average value	200.1518
True value	200.00
Accuracy	0.1518 (0.076%)

The data presented in Table 1 show that the systematic error of the method is 0.1518 mg/l or 0.076 %. The results obtained satisfy the established acceptance criteria, as they fall within the limits specified in validation plan VP-PCM-015 " Determination of iodide ions in various dosage forms using UV spectrophotometry" [14].

Repeatability

The "repeatability" parameter was determined in a similar manner by measuring a solution of iodide ions (GSO) at a concentration of 200 mg/l ten times. To assess repeatability, optical density data obtained for validation solutions with concentrations of 20, 50, 100 and 200 ppm of iodide ions were used. The concentration of iodide ions was calculated automatically using UV WinLab software, version 5.1.4 (Perkin Elmer, 2004). The mean value and standard deviation for individual determinations were calculated using the validated Excel spreadsheet CS-PCM-002 or according to formula (1):

$$СКО = \sqrt{\sum_{i=1}^{n} \frac{(x_i - \underline{x})^2}{(n-1)}}$$

where: x_i – individual measurement;
$\underline{x}$ – mean value;
n – sample size.

In accordance with the requirements of the verification methodology and ICH Q2 (R1) (CPMP/ICH/381/95), the acceptability criterion for repeatability is characterised by a standard deviation value, which must not exceed ±3 %. The results of the determination of the 'repeatability' parameter are given in Table 2.

Table 2 – Results of the repeatability assessment

No.	20.0 ppm	50.0 ppm	100.0 ppm	200.0 ppm
1	0.2212	0.5109	1.0385	2.0437
2	0.2218	0.5111	1.0388	2.0426
3	0.2221	0.5111	1.0391	2.0432
4	0.2222	0.511	1.0393	2.0433
5	0.2222	0.5111	1.0395	2.0449
6	0.2223	0.5111	1.0397	2.0434
7	0.2224	0.511	1.0396	2.0428
8	0.2223	0.511	1.0398	2.0422
9	0.2224	0.5111	1.0398	2.0448
10	0.2224	0.5112	1.0396	2.0446
Average value	0.2221	0.5111	1.0394	2.0436
Standard deviation	0.0004 (0.18%)	0.0001 (0.02%)	0.0004 (0.04%)	0.0009 (0.04%)

As can be seen from the data in Table 2, the standard deviation values for all concentrations studied are significantly lower than the established acceptability criterion. Thus, the method demonstrates high repeatability and complies with the requirements of validation plan VP-PCM-015 "Determination of iodide ions in various dosage forms using UV spectrophotometry".

Intra-laboratory precision

The "intra-laboratory precision" parameter was determined in a manner similar to the "repeatability" parameter; however, the measurements were carried out on a different day by a different operator using UV WinLab software version 5.1.4 (Perkin Elmer, 2004).

The acceptance criteria were based on the standard deviation (SD) of optical density, which should not exceed ±4%.

The results of the "intra-laboratory precision" assessment are shown in Table 3.

Table 3 – Results of the intra-laboratory precision assessment

No.	**20.0 ppm**	**50.0 ppm**	**100.0 ppm**	**200.0 ppm**
1	0.2087	0.5278	1.0496	2.0533
2	0.2087	0.5275	1.0499	2.0539
3	0.2085	0.5274	1.0497	2.0525
4	0.2038	0.5276	1.0495	2.0529
5	0.2039	0.5277	1.0492	2.0524
6	0.204	0.5276	1.0493	2.0518
7	0.2042	0.5277	1.0491	2.0536
8	0.2042	0.5276	1.0491	2.0513
9	0.2043	0.5273	1.0488	2.0532
10	0.2042	0.5274	1.0491	2.0515
Average value	0.2055	0.5276	1.0493	2.0526
Standard Deviation	0.0022 (1.07%)	0.0002 (0.04%)	0.0003 (0.03%)	0.0009 (0.04%)

The data in Table 3 show that the obtained standard deviation values fall within the established acceptability criteria. Consequently, the method demonstrates satisfactory intra-laboratory precision

The joint statistical analysis of the measurement results obtained by two operators on different days is presented in Table 4.

Table 4 – Precision assessment results over two days

Parameter	20.0 ppm	50.0 ppm	100.0 ppm	200.0 ppm
Average value	0.2147	0.5193	1.0443	2.0481
Standard deviation	4.0%	1.6%	0.5%	0.2%

The obtained results show that the acceptance criteria for the intralaboratory precision parameters are met for all the concentrations studied.

Specificity

The “specificity” parameter was determined by analysing in three replicates of purified water, a 0.05% dextrin solution, a 1% formaldehyde solution, and an FS-1 solution after complete reduction of elemental iodine to iodide ions by formaldehyde in an alkaline medium.

Acceptance criteria:

1. The optical density of purified water, the dextrin solution and the formaldehyde solution at a wavelength of 226 nm must be less than 0.02 units of optical density.

2. The concentration of total iodine in the FS-1 solution must not differ from the specified value by more than ±10%.

The results of the specificity determination are presented in Table 5.

Table 5 – Optical density of various matrices and the FS-1 solution at 226 nm

No.	Water	FS-1	Dextrin	Formaldehyde
1	0.0006	0.9520	0.005	0.000
2	0.0007	0.9519	0.005	0.000
3	0.0008	0.9515	0.006	0.000
Average Value	0.0007	0.9518	0.0053	0.000
Standard Deviation	0.0001	0.0003	0.0006	0.000

As can be seen from Table 5, the optical density values of purified water, a 0.05% dextrin solution and a 1% formaldehyde solution are 0.0007, 0.0053 and 0.000 respectively, which is significantly lower than the established criterion (0.02). Consequently, there is no influence of matrix components on the measurement results.

According to the specifications, the FS-1 solution contains 8.2 g/l of iodine and 12.1 g/l of potassium iodide. A concentration of 12.1 g/l of potassium iodide corresponds to 9.26 g/l of iodide ions (12.1 × 127/166). After complete reduction of elemental iodine to iodide ions, the total concentration of iodide ions in the FS-1 solution is 17.46 g/l.

The FS-1 sample under investigation was diluted 200-fold (0.5 ml to 100 ml). Thus, the calculated concentration of iodide ions in the analysed solution is 0.0873 g/l or 87.3 mg/l.

The measured optical density of the sample solution was 0.9518, which corresponds to an iodide ion concentration of 93.2 mg/l, calculated from the calibration curve (0.9518/0.01021). The difference between the calculated and experimental values does not exceed 10%, which satisfies the established acceptability criterion. Thus, the results obtained confirm the specificity of the developed method.

Linearity

To assess the “linearity” parameter, data obtained from the repeatability study (Table 2) were used, as well as the results of measurements of a standard solution with a concentration of 2 mg/l and purified water. The experimental data were processed and the calibration curve plotted using Origin software.

Based on the data obtained, the parameters of the linear equation and the correlation coefficient were calculated. The tangent of the slope of the calibration line corresponds to the specific optical density of the compound under investigation.

Acceptance criterion: the correlation coefficient (R) must be greater than 0.99. The optical density values used to assess linearity are given in Tables 2 and 6.

Table 6 – Optical density measurement results for linearity assessment (concentrations of 2 and 0 ppm)

No.	Solution with a concentration of 2 mg/l	Purified water
1	0.0161	0.0006
2	0.0163	0.0007
3	0.0164	0.0008
4	0.0166	
5	0.0165	
6	0.0166	
7	0.0168	
8	0.0167	
9	0.0168	
10	0.0171	
Average value	0.0166	0.0007
SD	0.0003 (1.7%)	0.0001

Using Origin software, a graph was plotted showing the dependence of optical density on the concentration of iodide ions in the range 0–200 ppm (Figure 1).

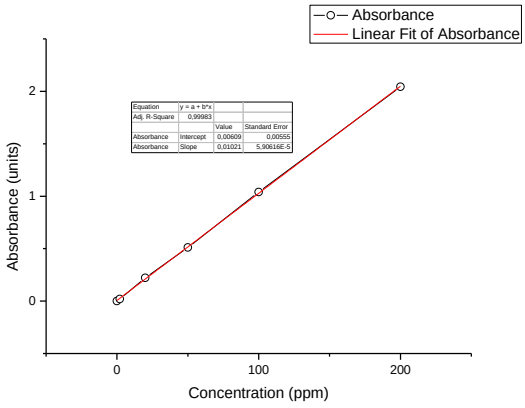

Figure 1 – Dependence of optical density on the concentration of iodide ions in the range 0–200 ppm

The calculated parameters of the linear equation are as follows:

$$Y = a + bx$$

where: a = 0.0061 – the y-intercept;
b = 0.0102 – the tangent of the slope of the calibration line.

The correlation coefficient is R = 0.99983, which exceeds the established acceptability criterion. Thus, the results obtained confirm the linearity of the method across the entire concentration range studied.

Working range

The “operating range” parameter was determined based on linearity data within the experimentally verified concentration range of 0–200 ppm. The permissible range extension is 20%.

Acceptability criterion: the error in determining optical density within the working range must not exceed ±5%.

The results used to determine the working range are presented in Tables 2, 3 and 6.

The baseline noise when measuring purified water is approximately 0.0006 units of optical density. Theoretically, the limit of quantification can start at a level of 0.006 optical density units. However, the optical density of a 0.05% dextrin solution at a wavelength of 226 nm is 0.006 units, which makes an additional contribution to the signal of the solutions being analysed.

At a concentration of 2 ppm, the optical density of the solution is approximately 0.017, which leads to a relative error exceeding 30%. At the same time, for a solution with a concentration of 20 ppm, the optical density is approximately 0.205 and the error contribution of 0.006 corresponds toncentration of iodide ions in various dosage forms using UV spectrophotometry.

Robustness

The “robustness” parameter was assessed by measuring the concentration of the same solutions after storage under ambient conditions for 24 hours. The measurements were carried out by a different operator using a different cuvette. The data presented in Tables 2 and 3 were used for the analysis.

Acceptance criterion: the difference between the mean optical density values within the working range, obtained on different days by different operators, must not exceed 4%. The results obtained are presented in Table 7.

Table 7 – Optical density data extracted from Tables 2 and 3

Parameter	**20 ppm**	**50 ppm**	**100 ppm**	**200 ppm**
Average value (day 1)	0.2221	0.5111	1.0394	2.0436
Standard deviation	0.0004	0.0001	0.0004	0.0009
Average value (day 2)	0.2055	0.5276	1.0493	2.0526
Standard deviation	0.0022	0.0002	0.0003	0.0009
Difference	0.0166	0.0165	0.0099	0.0090
Difference, %	7.5	3.1	0.9	0.4

The data in Table 7 show that the acceptability criterion is met for the range 50–200 mg/l. The differences in mean values for solutions with concentrations of 50, 100 and 200 mg/l are 3.1%, 0.9% and 0.4% respectively.

For the solution with a concentration of 20 mg/l, the difference is 7.5%, which exceeds the established criterion. This indicates that diluted solutions are less stable; consequently, it is recommended that they be analysed on the day of preparation. The summarised results of the validation are presented in Table 8.

Table 8 – Results of the validation of the method for determining the concentration of iodide ions in various dosage forms using UV spectrophotometry

Parameter	**20 ppm**	**50 ppm**	**100 ppm**	**200 ppm**
Accuracy, %	-	-	-	0.08
Repeatability, %	0.18	0.02	0.04	0.04
Intra-laboratory precision, %	4.0	1.6	0.5	0.2
Linearity	R = 0.9998			
Operating range	20–240 ppm			
Stability	Stable			
Specificity	Specific			

The results of the validation are presented in detail in the validation report VR-PCM-015 [15], as well as in papers devoted to the practical aspects of analytical method validation [16–17]. This article examines the key parameters of analytical method validation: accuracy, repeatability, intra-laboratory precision, linearity, working range, specificity and robustness. The results obtained confirm the practical applicability of the developed method.

The method developed and validated is successfully used for the quantitative determination of iodide ions in medicinal substances and preparations developed at the Scientific Centre.

Conclusion

During the study, the analytical method TP-SA-015 ‘Determination of the concentration of iodide ions in various dosage forms by UV spectrophotometry’ [18], in accordance with the requirements of the international ICH Q2(R1)/Q2(R2) guideline and the company’s internal standard operating procedures.

The results obtained showed that the developed method possesses the necessary validation characteristics and meets the established acceptability criteria. The method demonstrates high accuracy and reproducibility of results, as confirmed by low standard deviation values in the assessment of repeatability and intra-laboratory precision. It has been shown that the method exhibits a high degree of linearity within the concentration range under investigation, with a correlation coefficient of $R^2 = 0.9998$.

It has been established that the working range of the method lies within the interval 20–240 mg/L, which ensures the possibility of reliable quantitative determination of iodide ions in the analysed samples. The studies conducted also confirmed the specificity of the method with respect to the matrix components of dosage forms and its resistance to changes in analytical conditions.

The results obtained confirm the suitability of the UV spectrophotometry method for the quantitative determination of iodide ions in drug substances and finished medicinal products. The developed and validated method can be recommended for use in the quality control system for iodine-containing

medicinal products, as well as in the analytical practice of pharmaceutical laboratories.

Funding: under programme BR24992760 2024–2026 'Development of an antimicrobial potentiator for antibiotic combinations, for the effective treatment of diseases caused by bacteria with multiple drug resistance'.

Conflict of interest: there is no conflict of interest between the authors in this work.

ВАЛИДАЦИЯ МЕТОДИКИ ОПРЕДЕЛЕНИЯ КОНЦЕНТРАЦИИ ИОДИД ИОНОВ В РАЗНЫХ ЛЕКАРСТВЕННЫХ ФОРМАХ МЕТОДОМ УФ-СПЕКТРОФОТОМЕТРИИ

Р.А. Каржаубаева*, С. Турганбай, Ж.И. Таганов, З.С. Ашимханова, Г.К. Баигаипова, А.Р. Курманалиева

АО Научный центр протовоинфекционных препаратов, Алматы, Казахстан

Резюме. Статья посвящена валидации аналитической методики определения иодид ионов в различных лекарственных формах методом УФ-спектрофотометрии. Данное направление является важной частью аналитической химии и системы контроля качества лекарственных средств, в которой чувствительность, специфичность и воспроизводимость метода имеют решающее значение. Актуальность исследования обусловлена необходимостью точного и достоверного количественного определения иодид-ионов в субстанциях и готовых лекарственных препаратах. Валидация проводилась в соответствии с требованиями International Council for Harmonisation of Technical Requirements for Pharmaceuticals for Human Use (ICH Q2(R1)/Q2(R2)). *Целью работы* являлось определение валидационных характеристик методики количественного определения иодид-ионов в лекарственных формах методом УФ-спектрофотометрии. *Результаты и обсуждение.* В ходе исследования были оценены следующие параметры: специфичность, линейность, рабочий диапазон, правильность, повторяемость, внутрилабораторная точность и стабильность растворов. Установлено, что рабочий диапазон - от 20 до 240 мг/л, коэффициент корреляции - 0,9998. Метод продемонстрировал высокую чувствительность и соответствие международным требованиям. *Заключение*. Полученные результаты подтверждают линейность методики в исследуемом диапазоне концентраций иодид-ионов. Доказаны высокая чувствительность метода и высокая степень линейности (R^2 = 0.9998). Разработанная методика соответствует своему назначению и может успешно применяться при анализе иодсодержащих лекарственных препаратов. Метод имеет практическую значимость для системы контроля качества фармацевтической продукции.

Ключевые слова: иодид ионы, УФ-спектрофотометрия, метод валидации, ICH Q2, фармацевтический анализ.

Каржаубаева Роза Аскаровна	*Кандидат технических наук*
Тұрганбай Сейтжан	*PhD*
Таганов Жасур Ибрагимович	*Магистр технических наук*
Ашимханова Зауреш Сайдахметовна	*Старший научный сотрудник*
Баигаипова Гулшат Куанбековна	*Старший научный сотрудник*
Курманалиева Асель Рахимовна	*Магистр технических наук*

ӘРТҮРЛІ ДӘРІЛІК ФОРМАЛАРДАҒЫ ИОДИД ИОНДАРЫНЫҢ КОНЦЕНТРАЦИЯСЫН УФ-СПЕКТРОФОТОМЕТРИЯ ӘДІСІМЕН АНЫҚТАУ ӘДІСТЕМЕСІН ВАЛИДАЦИЯЛАУ

Р.А. Каржаубаева*, С. Тұрғанбай, Ж.Таганов, З.С. Ашимханова, Г.К. Баигаипова, А.Р. Курманалиева

Инфекцияға қарсы препараттар ғылыми орталығы АҚ, Алматы, Казахстан

Түйіндеме. Мақалада әртүрлі дәрілік формалардағы иодид иондарының мөлшерін ультракүлгін спектрофотометрия (УФ-спектрофотометрия) әдісімен анықтауға арналған аналитикалық әдістемені валидациялау мәселелері қарастырылған. Бұл бағыт аналитикалық химияның және дәрілік заттардың сапасын бақылау жүйесінің маңызды бөлігі болып табылады, мұнда әдістің сезімталдығы, спецификалығы және қайталанғыштығы шешуші рөл атқарады. Зерттеудің өзектілігі субстанциялар мен дайын дәрілік препараттардағы иодид иондарын дәл әрі сенімді сандық анықтаудың қажеттілігімен негізделген. Валидация жұмыстары International Council for Harmonisation of Technical Requirements for Pharmaceuticals for Human Use (ICH Q2(R1)/Q2(R2)) талаптарына сәйкес жүргізілді. *Зерттеудің мақсаты* – дәрілік формалардағы иодид иондарын УФ-спектрофотометрия әдісі арқылы сандық анықтау әдістемесінің валидациялық сипаттамаларын анықтау. *Нәтижелер және талқылау.* Зерттеу барысында келесі параметрлер бағаланды: спецификалық, сызықтылық, жұмыс диапазоны, дұрыстық, қайталанғыштық, зертханаішілік дәлдік, сандық анықтау шегі және ерітінділердің тұрақтылығы. Анықтау нәтижесінде сандық анықтау шегі 20 мг/л құрайтыны, жұмыс диапазоны 20–240 мг/л аралығында екені, корреляция коэффициенті 0,9998-ге тең екені анықталды. Әдіс жоғары сезімталдықты (2,6 мг/л) және халықаралық талаптарға сәйкестігін көрсетті. *Қорытынды.* Алынған нәтижелер зерттелген концентрациялар диапазонында иодид иондары үшін әдістеменің сызықтылығын растайды. Әдістің жоғары сезімталдығы және жоғары сызықтылық дәрежесі (R^2 = 0,9998) дәлелденді. Әзірленген әдістеме өз мақсатына толық сәйкес келеді және иод құрамды дәрілік препараттарды талдауда тиімді қолданылуы мүмкін. Бұл әдіс фармацевтикалық өнімдердің сапасын бақылау жүйесі үшін практикалық маңызға ие.

Түйін сөздер: йодид иондары, УФ-спектрофотометрия, әдіс валидациясы, ICH Q2, фармацевтикалық талдау

Қаржаубаева Роза Асқаровна	*Техника ғылымдарының кандидаты*
Тұрғанбай Сейтжан	*PhD*
Жасур Таганов	*Техника ғылымдарының магистрі*
Ашимханова Зауреш Сайдахметовна	*Аға ғылыми қызметкер*
Баигаипова Гулшат Куанбековна	*Аға ғылыми қызметкер*
Курманалиева Асель Рахимовна	*Техника ғылымдарының магистрі*

References

1. ICH Q2(R1). Validation of Analytical Procedures: Text and Methodology. International Council for Harmonisation. **2005**. 16 pp. URL: https://pharmadvisor.ru/document/tr3569/

2. Boulanger B., Dewé W., Gilbert A., Govaerts B., Maumy M. Risk management for analytical methods based on the total error concept: Conciliating the objectives of the pre-study and in-study validation phases. Chemom. Intell. Lab. Syst., **2007**, Vol. 86, No. 2, 198–207. DOI: https://doi.org/10.1016/j.chemolab.2006.06.008

3. Skoog D.A., Holler F.J., Crouch S.R. Principles of Instrumental Analysis. 6th ed. Cengage Learning, **2014.**

4. Rahman H., Haque S.M. Development and Validation of Chromatographic and Spectrophotometric Methods for the Quantitation of Rufinamide in Pharmaceutical Preparations. Turk. J. Pharm. Sci., **2022,** Vol. 19, No. 3, 267–272. DOI: https://doi.org/10.4274/tjps.galenos.2021.37043

5. Sycz J., Duda-Madej A., Szumny A. A Rapid Method for the Determination of Potassium Iodide in Pharmaceutical Formulations using Chromatographic Techniques. Applied Sci., **2025**, Vol. 15, No. 23, 12795. DOI: https://doi.org/10.3390/app152312795

6. Mendham J., Denney R., Barnes J., Thomas M. Vogel's Textbook of Quantitative Chemical Analysis. Pearson Education, **2000.**

7. Harris D.C. Quantitative Chemical Analysis. 9th ed. W.H. Freeman and Company, **2016.**

8. Christian G.D., Dasgupta P.K., Schug K.A. Analytical Chemistry. 7th ed. Wiley, **2014.**

9. Oday J., Hadi H., Hashim P., Richardson S., Iles A., Pamme N. Development and validation of spectrophotometric method and paper-based microfluidic devices for the quantitative determination of Amoxicillin in pure form and pharmaceutical formulations. Heliyon, **2024**, Vol. 10, No. 3. DOI: https://doi.org/10.1016/j.heliyon.2024.e24968

10. Uncu L., Evtodienco V., Mazur K., Donici E. Validation of the spectrophotometric method for the dosing of some combined capsule. The Moldovan Medical Journal, **2021**, Vol. 64, No. 4, P. 10–16. DOI: https://doi.org/10.52418/moldovan-med-j.64-4.21.02.

11. Karzhaubaeva R.A. Methodological procedure "Recording UV-Vis spectra of aqueous solutions". **2026**, ed. 7, 9 pp.

12. Karzhaubaeva R.A. Working with the Lambda-35 UV-Vis spectrophotometer. **2026**, Vol. 8, 10 pp.

13. Sabitov A.N. Validation of analytical methods. **2013**, Vol. 3, 28 pp.

14. European Pharmacopoeia. 7th ed. – Strasbourg: European Union. **2011**, Vol. 1, pp. 40–41.

15. Magnusson B. and Örnemark U. Eurachem Guide: The Fitness for Purpose of Analytical Methods – A Laboratory Guide to Method Validation and Related Topics. **2014**, www.eurachem.org.

16. Shelyudyakov Yu.L. Validation plan "Determination of iodide ion concentration in various dosage forms using UV spectrophotometry". **2015**, ed. 1, 16 pp.

17. Shelyudyakov, Yu.L. Validation report: "Determination of iodide ion concentration in various pharmaceutical forms using UV spectrophotometry". **2015**, 1st ed., 18 pp.

18. Karzhaubaeva R.A. Methodological procedure "Determination of iodide ion concentration in various dosage forms using UV spectrophotometry". **2026**, ed. 4, 11 pp.

19. Aladysheva Zh.I., Belyaev V.V., Beregovykh V. Practical aspects of work on the validation of analytical methods. Pharmacy. **2008**, No. 7, 9–14.

МАЗМҰНЫ

СОДЕРЖАНИЕ

CONTENTS

Правила оформления статей в журнале
«ХИМИЧЕСКИЙ ЖУРНАЛ КАЗАХСТАНА»

1. ОБЩИЕ ПОЛОЖЕНИЯ

Журнал «Химический журнал Казахстана» (ISSN 1813-1107, eISSN 2710-1185) выпускается ордена Трудового Красного Знамени АО «Институтом химических наук им. А.Б. Бектурова» 4 раза в год и публикует работы по широкому кругу фундаментальных, прикладных и инновационных исследований в области химии и химической технологии.

Языки публикации: казахский, русский, английский. Журнал индексируется Казахстанской библиометрической системой и включен в Перечень изданий, рекомендуемых Комитетом по контролю в сфере образования и науки Министерства образования и науки Республики Казахстан для публикации основных результатов научной деятельности.

Издание имеет следующие рубрики:

1. Обзорные статьи до 20 печатных страниц
2. Оригинальные статьи (до 8–10 печатных страниц)
3. Краткие сообщения (до 4–5 печатных страниц)

2. ПРЕДСТАВЛЕНИЕ СТАТЕЙ

Редакция принимает статьи от казахстанских и зарубежных авторов. В целях популяризации Журнала, редакционной коллегией приветствуется прием статей на английском языке.

Для регистрации и публикации статьи материал статьи представляется в редакцию через систему электронной подачи статьи на сайте Журнала (https://www.chemjournal.kz/) в комплекте со следующими документами:

1. Электронная версия статьи в форматах Word и PDF со встроенными в текст таблицами, схемами, рисунками (файл должен быть назван по фамилии первого автора на английском языке).

2. Сопроводительное письмо, адресованное в Редакцию Химического журнала Казахстана от организации, в которой данное исследование выполнено, с утверждением, что материал рукописи нигде не публиковался, не находится на рассмотрении для опубликования в других журналах и в материалах статьи отсутствуют секретные данные. В сопроводительном письме указываются сведения об авторе для корреспонденции: Фамилия, имя и отчество автора, служебный адрес с указанием почтового индекса, адрес электронной почты, телефон и ORCID.

3. Все статьи, опубликованные в Химическом журнале Казахстана (ISSN 1813-1107, eISSN 2710-1185) публикуются в открытом доступе. Чтобы обеспечить свободный доступ читателям и покрыть расходы на экспертную оценку, редактирование, поддержание сайта журнала, долгосрочное архивирование и ведение журнала, взимается плата за обработку статьи. Правила оплаты за опубликование принятой к печати статьи находятся в отдельном документе на сайте Журнала «Оплата за опубликование».

4. Статье присваивается регистрационный номер, который сообщается авторам в течение недели после получения указанного перечня документов; на этот номер необходимо ссылаться при переписке.

5. Принятым к печати статьям присваивается цифровой идентификатор (DigitalObjectIdentifier – DOI).

6. Учитывая невозможность проводить статьи на казахском языке через систему антиплагиат, будут учитываться формулировки рецензентов и решение издательской коллегии.

7. Статьи должны быть оформлены согласно шаблону, который можно скачать в разделе «Отправка материалов» на сайте Химического Журнала Казахстана.

3. СТРУКТУРА ПУБЛИКАЦИЙ

3.1. В начале **обзоров, оригинальных статей и кратких сообщений** на первой строке указывается номер по Универсальной десятичной классификации (УДК или UDC), соответствующий заявленной теме. Дается прописными буквами в верхнем левом углу. Также на первой строке справа прописными буквами полужирным шрифом № 14 указывается название журнала **ХИМИЧЕСКИЙ ЖУРНАЛ КАЗАХСТАНА (ҚАЗАҚСТАННЫҢ ХИМИЯ ЖУРНАЛЫ, CHEMICAL JOURNAL OF KAZAKHSTAN)**, год, номер.

3.2. Далее через строку приводится международный стандартный сериальный номер журнала (ISSN 1813-1107, eISSN 2710-1185) и на следующей строке слева приводится DOI: который будет иметь значение после принятия статьи к печати.

3.3. Далее, после отступа строки указывается **заглавие статьи** прописными буквами, шрифт № 14 – полужирный, выравнивание текста по центру. Название должно максимально полно и точно описывать содержание статьи, включать ключевые слова, отражающие направление и/или основной результат исследования, но в то же время быть коротким и ясным и не содержать сокращений.

3.4. Далее, после отступа строки, указываются **инициалы и фамилии автора(-ов)** строчными буквами, шрифт № 12 полужирный, курсив, выравнивание текста по центру. Фамилия автора, с которым следует вести переписку, должна быть отмечена звездочкой (*): ***С.С. Сатаева*, А.М. Джубаналиева.***

3.5. Через строку шрифтом № 12, строчными буквами, курсивом с выравниванием текста по центру следуют **наименование(я) организации(й)** с указанием части названия организации, которая относится к понятию юридического лица (в английском тексте необходимо указывать официально принятый перевод названия), город, страна. В английском варианте адресные сведения должны быть представлены на английском языке, в т.ч. город и страна.

Строки с фамилиями авторов и названиями организаций содержат надстрочные индексы (после фамилии и перед названием организации), указывающие на место работы авторов.

На следующей строке курсивным начертанием, шрифт № 12, с выравниванием текста по центру указывается электронный адрес для переписки.

3.6. **Резюме (Abstract, Түйіндеме)** состоит из краткого текста (не менее 150–250 слов, шрифт № 12) на языке статьи. **Abstract** публикуется в международных базах, данных в отрыве от основного текста. Резюме должно быть автономным, все вводимые обозначения и сокращения необходимо расшифровать здесь же.

Приветствуется структурированное резюме, повторяющее структуру статьи и включающее: *введение, цели и задачи, методы, результаты и обсуждение, заключение (выводы)*. В то же время, цели и задачи описываются, если они не ясны из заглавия статьи, методы следует описывать, если они отличаются новизной. В резюме включаются новые результаты, имеющие долгосрочное значение, важные

открытия, опровергающие существующие теории, а также данные, имеющие практическое значение. Следует использовать техническую (специальную) терминологию вашей дисциплины.

Резюме дается без абзацного отступа строчными буквами; оно не должно содержать номера соединений, экспериментальные данные и ссылки на литературу. **Резюме** только одно – в начале текста.

3.7. Далее на языке статьи без абзацного отступа строчными буквами шрифтом № 12, выравнивание текста по левому краю приводятся **ключевые слова** (от 5 до 10 шт.), обеспечивающие наиболее полное раскрытие содержания статьи.

3.8. В **кратких сообщениях** приводится резюме (150–200 слов), ключевые слова, но деления на разделы не требуется. Дается текст краткого сообщения на одном из трех языков с выполнением требований к УДК, названию статьи, перечню авторов, наименований организаций, в которых они работают, указанию автора для переписки. В тексте краткого сообщения приводятся конкретные **существенно новые результаты, требующие закрепления приоритета** с необходимыми экспериментальными подробностями. Затем следуют: информация о финансировании, благодарности, сведения о конфликте интересов, информация об авторах и список литературы.

3.9. Статья начинается с **введения**, в котором формулируется цель и необходимость проведения исследования, кратко освещается состояние вопроса со ссылками на наиболее значимые публикации с избеганием ссылок на устаревшие результаты. Излагаются открытия, сделанные в ходе данного исследования. Указывается структура статьи.

3.10. **Экспериментальная часть** содержит описание хода и результатов эксперимента, характеристику полученных соединений. В начале экспериментальной части приводятся названия приборов, на которых зарегистрированы физико-химические характеристики веществ и указываются условия измерения; также указываются либо источники использованных нетривиальных реагентов (например, «коммерческие препараты, название фирмы»), либо даются ссылки на методики их получения.

Каждый параграф экспериментальной части, описывающий получение конкретного соединения, должен содержать его полное наименование по номенклатуре ИЮПАК и его порядковый номер в статье. В методиках обязательно указывать количества реагентов в мольных и массовых единицах (для катализаторов – массу и мольные проценты), объемы растворителей. Методика эксперимента излагается в *прошедшем* времени.

Для известных веществ, синтезированных опубликованным ранее методом, необходимо привести ссылку на литературные данные. Для известных веществ, полученных новыми или модифицированными методами, должны быть представлены их физические и спектральные характеристики, использованные для подтверждения идентичности структуры, метод синтеза и ссылка на литературные данные.

Для всех впервые синтезированных соединений необходимо привести доказательства приписываемого им строения и данные, позволяющие судить об их индивидуальности и степени чистоты. В частности, должны быть представлены данные элементного анализа или масс-спектры высокого разрешения, ИК спектры и спектры ЯМР ^{1}H и ^{13}C.

Данные рентгеноструктурного анализа представляются в виде **рисунков и таблиц**. Все **новые соединения**, данные РСА которых приводятся в статье, должны быть **зарегистрированы в Кембриджской базе структурных данных** и иметь соответствующие **CCDC номера**.

Если, по мнению рецензента или редактора, новые соединения не были удовлетворительно охарактеризованы, статья не будет принята к печати.

Пример методики: *3-(2-Amino-6-methylpyridino)-3-carbonyl-3,4-dihydrocoumarin **(12)***.To the alcoholic solution of 2.18 g (0.01 mol) of 3-carbethoxycoumarin, 1.08 g (0.01 mol) of 2-amino-6-methylpyridine was added with stirring. The mixture was boiled for 10 h. The solution was cooled, the precipitate was filtered. Then it was washed with cold EtOH. After the drying and recrystallization of the residue from i-PrOH yield of the product ***12*** was 2.05 g (63%), mp 226–228 °C, Rf 0.82 (1/2, EtOAc/hexane as eluent). Calculated, %: C 68.56; H 4.32; N 9.99 for $C_{16}H_{12}N_2O_3$. Found, %: C 68.41; H 4.22; N 9.83. *Spectral data.*

Внимание! В статьях, посвященных синтезу новых соединений, допускается размещение **экспериментальной части** за разделом **Результаты и обсуждение**.

3.11. В разделе **Результаты и обсуждение**, который является наиболее важным, следует обсудить и объяснить полученные в работе **результаты**, проанализировать особенности синтеза, продемонстрировать и указать возможные ограничения. Провести сравнение полученных результатов с опубликованными ранее. Все новые соединения должны быть полностью охарактеризованы соответствующими спектральными и другими физико-химическими данными. В тексте обобщаются и разъясняются только те спектральные данные, которые используются для подтверждения структуры полученных соединений. Перечисление одних и тех же данных в тексте, таблицах и на рисунках не допускается. Для новых методов синтеза желательно обсудить механизм реакции. Для обобщения данных необходимо использовать понятные рисунки и таблицы. Представленные данные должны поддаваться интерпретации.

При обсуждении результатов следует придерживаться официальной терминологии IUPAC. Результаты рекомендуется излагать в прошедшем времени.

Обсуждение не должно повторять описание результатов исследования. В тексте должны быть использованы общепринятые в научной литературе сокращения. Нестандартные сокращения должны быть расшифрованы после первого появления в тексте. Единицы измерений должны быть указаны в Международной системе СИ.

3.12. Затем рекомендуется сформулировать **заключение**, в котором указать основные достижения, представленные в статье, и основной вывод, содержащий ответ на вопрос, поставленный во вводной части статьи, а также возможность использования материала статьи в фундаментальных или прикладных исследованиях.

3.13. Приводится информация о **финансировании** исследований.

3.14. Выражается **благодарность** тем, кто помог вам в подготовке вашей работы.

3.15. В рукописи должно быть заявлено о том, имеется ли **конфликт интересов**

3.16. В **информации об авторах** указываются: ученая степень, звание, должность, e-mail, ORCID.

3.17. Статья заканчивается **списком литературы** со ссылками на русском (или казахском) языке и ссылками на языке оригинала. Ссылки на литературные источники в тексте приводятся порядковыми арабскими цифрами в квадратных скобках по мере упоминания. Каждая ссылка должна содержать только одну литературную цитату. Список литературы должен быть представлен наиболее свежими и актуальными источниками без излишнего самоцитирования(не более 20 процентов). Для статей желателен список из не менее 10 ссылок со строками доступа в интернете.

3.18. Обязательна **информация об авторах**. В ней указываются: ученая степень, звание, должность, e-mail, ORCID, **фамилия, имя, отчество** полностью на трех языках.

Информация об авторах:

Джусипбеков Умирзак Жумасилович – АО «Институт химических наук им. А.Б. Бектурова», заведующий лабораторией химии солей и удобрений, член-корреспондент Национальной академии наук Республики Казахстан, профессор; e-mail:jussipbekov@mail.ru, ORCID: https://orcid.org/0000-0002-2354-9878 .

Нургалиева Гульзипа Орынтаевна – доктор химических наук, АО «Институт химических наук им. А.Б. Бектурова», Алматы, Республика Казахстан, e-mail: n_gulzipa@mail.ru , ORCID: https://orcid.org/0000-0003-2659-3361 .

Баяхметова Замира Кенесбековна – кандидат химических наук, ведущий научный сотрудник, АО «Институт химических наук им. А.Б. Бектурова», Алматы, Республика Казахстан, e-mail: zamirabkz@mail.ru , ORCID: https://orcid.org / 0000-0001-7261-2215.

Information about authors:

Zhusipbekov Umerzak Zhumasilovich – JSC «A.B. Bekturov Institute of Chemical Sciences», Head of the Laboratory of Chemistry of Salts and Fertilizers, Corresponding Member of the National Academy of Sciences of the Republic of Kazakhstan, Professor; e-mail:jussipbekov@mail.ru, ORCID ID: https://orcid.org/0000-0002-2354-9878.

Nurgaliyeva Gulzipa Oryntayevna – Doctor of chemical sciences, JSC «A.B. Bekturov Institute of Chemical Sciences», Almaty, Republic of Kazakhstan, e-mail: n_gulzipa@mail.ru, ORCID ID: https://orcid.org/0000-0003-2659-3361.

Baiakhmetova Zamira Kenesbekovna – Candidate of chemical sciences, leading researcher, JSC «A.B. Bekturov Institute of Chemical Sciences», Almaty, Republic of Kazakhstan, e-mail: zamirabkz@mail.ru, ORCID ID: https://orcid.org/ 0000-0001-7261-2215.

Авторлар туралы ақпарат:

Жүсіпбеков Өмірзақ Жұмасылұлы - "Ә.Б. Бектұров атындағы химия ғылымдары институты" АҚ, тұздар және тыңайтқыштар химиясы зертханасының меңгерушісі, Қазақстан Республикасы Ұлттық Ғылым академиясының корреспондент-мүшесі, профессор; e-mail:jussipbekov@mail.ru, ORCID ID: https://orcid.org/0000-0002-2354-9878 .

Нұрғалиева Гүлзипа Орынтайқызы - химия ғылымдарының докторы, "Ә.Б. Бектұров атындағы химия ғылымдары институты" АҚ, Алматы, Қазақстан Республикасы, e-mail: n_gulzipa@mail.ru . ORCID ID: https://orcid.org/0000-0003-2659-3361 .

Баяхметова Замира Кеңесбекқызы - химия ғылымдарының кандидаты, жетекші ғылыми қызметкер, "Ә.Б. Бектұров атындағы химия ғылымдары институты" АҚ,

Алматы, Қазақстан Республикасы, e-mail: zamirabkz@mail.ru . ORCID ID: https://orcid.org / 0000-0001-7261-2215.

Список цитируемой литературы оформляется в соответствии с нижеприведенными образцами библиографических описаний (4.8.).

3.19. В конце статьи после списка литературы *дополнительно* приводится перевод **Резюме** на казахский (**Түйіндеме**) и на английский языки (**Abstract**). Слово **Резюме** (**Abstract**, **Түйіндеме**) дается по центру. На следующей строке с выравниванием по левому краю прописными буквами полужирным шрифтом № 12 приводится название статьи. Через строку без абзацного отступа курсивом, полужирным шрифтом № 11 даются инициалы и фамилии авторов.

На следующей строке без абзацного отступа курсивом, строчными буквами, шрифтом № 11 приводятся места работы авторов с надстрочными индексами (после фамилии и перед названием организации), указывающие на место работы авторов. Затем через строку с абзацного отступа с выравниванием текста по ширине идет текст резюме, набранный строчным шрифтом № 12.

Далее через строку с абзацным отступом строчными буквами шрифтом № 12, с выравниванием текста по ширине приводятся **ключевые слова** (от 5 до 10 шт.), обеспечивающие наиболее полное раскрытие содержания статьи.

3.20. Для статей, подаваемых на языке, отличном от английского (на казахском или русском языке), в конце статьи находится английский блок (**Abstract, Information about authors, References**).

3.21. Все страницы рукописи следует пронумеровать.

4. ТРЕБОВАНИЯ К ОФОРМЛЕНИЮ РУКОПИСЕЙ

4.1. Объем статьи, включая аннотацию и список литературы: до 8–10 страниц. Обзорные статьи могут быть до 20 страниц. Статья должна быть напечатана на одной стороне листа А4 шрифтом Times New Roman, размер кегля 14 пт; межстрочный интервал – одинарный и полями: верхнее – 2.0 см, нижнее – 2.0 см, левое – 3.0 см, правое – 1.5 см; расстановка переносов не допускается; абзацный отступ – 1.0 см; форматирование – по ширине. Должен быть использован текстовый редактор *Microsoft Word for Windows*, в виде *doc*-файла, версия 7.0 и более поздние.

Для краткости и наглядности обсуждения соединения, упоминаемые более одного раза, следует нумеровать **арабскими** цифрами в сочетании со строчными **латинскими** буквами (для обозначения соединений с переменным заместителем). При упоминании полного названия соединения шифр дается в скобках.

Стереохимические символы и приставки, характеризующие структурные особенности или положение заместителя в молекуле, следует набирать курсивом (*italic*): (*R*)-энантиомер, *трет*-бутил, *пара*-ксилол. Вместо громоздких названий неорганических и часто употребляемых органических соединений следует давать их формулы: NaBr, TsOH вместо бромид натрия и толуолсульфоновая кислота. При использовании терминов и обозначений, не имеющих широкого применения в литературе, их значения поясняются в тексте при первом употреблении: например, полиэтилентерефталат (ПЭТФ).

Для изображения структурных формул химических соединений необходимо использовать редактор химических формул **ChemDrawUltra**. Все надписи на схемах приводятся на английском языке. В схеме необходимо указывать все условия реакций: над стрелкой – реагенты, катализаторы, растворители, под

стрелкой – температура, время, выход. Если условия реакций сильно загружают схему, их можно перенести в конец схемы, расшифровывая буквенными индексами, например, *i*: HCl, H_2O, 80 °C, 5h. Такой же буквенный индекс должен быть указан над стрелкой соответствующей реакции.

4.2. Уравнения, схемы, таблицы, рисунки и ссылки на литературу нумеруются в порядке их упоминания в тексте и *должны быть вставлены в текст статьи* после первого упоминания. Таблицы и рисунки должны сопровождаться подписью; заголовки к схемам даются при необходимости.

4.3. По возможности следует готовить **рисунки** с помощью компьютера. Однотипные кривые должны быть выполнены в одинаковом масштабе на одном рисунке. Кривые на рисунках нумеруются арабскими цифрами, которые расшифровываются в подписях к рисункам. Для всех **рисунков** необходимо представить графические файлы в формате *jpeg* с минимальным разрешением 300 dpi. Надписи на рисунках должны быть на английском языке и по возможности заменены цифрами, расшифровка которых дается в подписи к рисунку.

Одиночные прямые, как правило, не приводят, а заменяют уравнением линии регрессии. Пересечение осей координат следует располагать в левом углу рисунка, стрелки на концах осей не ставятся, линии, ограничивающие поле рисунка не приводятся, масштабная сетка не наносится. Малоинформативные рисунки, не обсуждаемые в статье спектры, вольтамперограммы и другие зависимости не публикуются. **Рисунки спектров не должны быть выполнены от руки**. Все рисунки должны иметь нумерацию арабскими цифрами (если рисунок не один). Слово «Рисунок» и наименование помещают после пояснительных данных и располагают следующим образом: Рисунок 1 – Детали прибора.

4.4. Каждая **таблица** должна иметь тематический заголовок и порядковый арабский номер (без знака №), на который дается ссылка в тексте (таблица 1). Название таблицы располагается над таблицей слева без абзацного отступа в одну строку с ее номером через тире без точки после названия. Графы в таблице должны иметь краткие заголовки, отражающие параметры, численные значения которых приведены в таблице; они пишутся в именительном падеже единственного числа с прописной буквы и через запятую сопровождаются соответствующими единицами измерения (в сокращенной форме). Рисунки или структурные формулы в графах таблиц не допускаются. Пропуски в графах при отсутствии данных обозначают тремя точками, при отсутствии явления – знаком «тире». Примечания к таблицам индексируются арабскими цифрами и помещаются в границах таблицы под материалом таблицы. Слово «Примечание» следует печатать с прописной буквы с абзаца. Если примечание одно, то после слова «Примечание» ставится тире и примечание печатается с прописной буквы. Несколько примечаний нумеруют по порядку арабскими цифрами без проставления точки и печатают с абзаца. В таблицах используют тот же шрифт, что и в тексте статьи; допускается уменьшенный (не менее № 10 шрифт TimesNewRoman).

4.5. При выборе единиц измерения рекомендуется придерживаться системы СИ: г, мг, м, см, мкм (микрометр, микрон); нм (нанометр, миллимикрон); пм (пикометр); Е (ангстрем); с (секунда); мин, ч (час), Гц (герц); МГц (мегагерц); Э (эрстед); Гс (гаусс); В (вольт); эВ (электронвольт); А (ампер); Ом, Па (паскаль); МПа (мегапаскаль); гПа (гектопаскаль); Дж (джоуль); К (кельвин), °С (градус Цельсия); Д (Дебай).

В десятичных дробях целая часть отделяется от дробной не запятой, а точкой.

Используются следующие сокращения: т.кип. и т.пл. (точки кипения и плавления) – перед цифрами; конц. (концентрированный перед формулой соединения); М – молекулярная масса); моль, кал, ккал, н. (нормальный), М. (молярный); концентрация растворов обозначается (г/см^3, г/л, моль/л).

Для всех впервые синтезированных соединений обязательны данные элементного анализа либо масс-спектры высокого разрешения.

В *брутто-формулах* элементы располагаются в следующем порядке: С, Н и далее согласно латинскому алфавиту. Формулы молекулярных соединений и ониевых солей даются через точку (например, $C_5H_5N.HCl$). Пример записи констант и данных элементного анализа: т.кип. 78°С (100 мм рт. ст.), т.пл. 50°С (EtOH), d_4^{20}0.9809, n^{20}1.5256; Найдено, %: С 59.06; Н 7.05; I 21.00; N 8.01. $C_aH_bI_cN_dO_e$. Вычислено, %: С 59.02; Н 7.01; I 21.20; N 8.22.

ИК и УФ спектры. В экспериментальной части для ИК и УФ спектров должны быть указаны характеристические частоты полос, длины волн максимумов поглощения, коэффициенты экстинции (или их логарифмы) и условия, при которых записан спектр.

Примеры записи: ИК спектр (тонкий слой), ν, см$^{-1}$: 1650 (C=N), 3200–3440 (O–H). УФ спектр (EtOH), λ_{max}, нм (lgε): 242 (4.55), 380 (4.22).

Спектры ЯМР ^{1}Н и ^{13}С. Должны быть указаны рабочая частота прибора, использованный стандарт и растворитель. Протоны в составе сложных групп, к которым относится сигнал, следует подчеркнуть снизу – 3.17–3.55 (4Н, м, $N(CH_2CH_3)_2$); для положения заместителей использовать обозначения 3-CH_3; для обозначения положения атомов – С-3, N-4 и т.д. Если какой-нибудь сигнал в спектре описывается как дублет, триплет или дублет дублетов и т.п. (а не синглет или мультиплет), необходимо привести соответствующие КССВ. Если проведены дополнительные исследования для установления строения или пространственных взаимодействий атомов, должны быть указаны использованные двумерные методы. В описании спектров ЯМР ^{13}С отнесение конкретного сигнала к конкретному атому углерода приводится только тогда, когда определение проведено на основе двумерных экспериментов.

Примеры записи:

Спектр ЯМР^{1}Н (400 МГц, $CDCl_3$), δ, м. д. (*J*, Гц): 0.97 (3Н, т, *J*= 7.0, CH_3); 3.91 (2Н, к,
J= 7.0, $COOCH^2$); 4.46 (2Н, д, *J*= 6.1, NCH_2); 7.10–7.55 (6Н, м, Н-6,7,8, $NHCH_2C_6H_5$); 7.80 (1Н,
с, HAr); 7.97 (1Н, с, Н-5'); 8.13 (1Н, д. д, *J*= 8.2, *J*= 2.3, Н-5); 11.13 (1Н, с, NH).

Спектр ЯМР^{13}С (100 МГц, ДМСО-d_6), δ, м. д. (*J*, Гц): 36.3 (CH_2CH_3); 48.5 (С-5); 62.3
(CH_2CH_3); 123.0(CAr); 125.8 (д, $^2J_{CF}$ = 26.1, С-3',5' Ar); 128.9 (CPh); 134.4 (С-5a); 168.3 (С=О).

Масс-спектры приводятся в виде числовых значений *m/z* и относительных значений ионного тока. Необходимо указывать метод и энергию ионизации, массовые числа характеристических ионов, их интенсивность по отношению к основному иону и по возможности их генезис. В случае химической ионизации при описании прибора необходимо указать газ-реагент. В масс-спектрах высокого разрешения найденные и вычисленные значения *m/z* приводятся с четырьмя

десятичными знаками; если найденное значение *m/z* соответствует не молекулярному иону, брутто-формула и вычисленное значение *m/z* также приводится для того же иона.

Пример записи данных масс-спектра: Масс-спектр (ЭУ, 70 эВ), *m/z* ($I_{отн}$, %): 386 $[M]^+$ (36),368 $[M–H_2O]^+$ (100), 353 $[M–H2O–CH3]^+$ (23).

Масс-спектр (ХИ, 200 эВ), *m/z* ($I_{отн}$, %): 387 $[M+H]^+$(100), 369 $[M+H–H_2O]^+$ (23).

Пример записи данных масс-спектра высокого разрешения:

Найдено, *m/z*: 282.1819 $[M+Na]^+$. $C_{17}H_{25}NNaO$.

Вычислено, *m/z*: 282.1828.

4.6. **Данные рентгеноструктурного исследования** следует предоставлять в виде рисунка молекулы с пронумерованными атомами, например, C(1), N(3) (по возможности в представлении атомов эллипсо и дамитепловых колебаний). Полные кристаллографические данные, таблицы координат атомов, длин связей и валентных углов, температурные факторы в журнале не публикуются, а депонируются в Кембриджском банке структурных данных (в статье указывается регистрационный номер депонента).

4.7. По требованиям международных баз данных Scopus, Clarivate Analytics, Springer Nature при оценке публикаций на языках, отличных от английского, библиографические списки должны даваться не только на языке оригинала, но и на латинице (романским алфавитом). Поэтому авторы статей, подаваемых на русском и казахском языке, должны предоставлять список литературы в двух вариантах: *один на языке оригинала* (**Список литературы**), а другой — в *романском алфавите* (**References**). Последний список входит в английский блок, который расположен в конце статьи.

Если в списке есть ссылки на иностранные публикации, они полностью повторяются в списке **References**. При цитировании русскоязычного журнала, переводимого за рубежом, в русскоязычной версии Списка литературы необходимо привести полную ссылку на русскоязычную версию, а в **References** – на международную.

Список источников в **References** должен быть написан только на романском алфавите- латинице (при этом он должен оставаться полным аналогом Списка литературы, в котором источники были представлены на оригинальном языке опубликования).

Для написания ссылок на русскоязычные источники (и источники на иных, не использующих романский алфавит, языках) следует использовать ОФИЦИАЛЬНЫЙ ПЕРЕВОД и ТРАНСЛИТЕРАЦИЮ (см. Требования к переводу и транслитерации).

В **References** требуется следующая структура библиографической ссылки из русскоязычных источников: авторы (транслитерация), перевод названия статьи или книги на английский язык, название источника (транслитерация – для тех изданий, которые не имеют установленного редакцией английского названия), выходные данные в цифровом формате, указание на язык статьи в скобках (in Russian или in Kazakh).Транслитерацию можно выполнить на сайте http://www.translit.ru.

Условные сокращения названий русскоязычных журналов и справочников приводятся в соответствии с сокращениями, принятыми в «Реферативном журнале Химия». англоязычных и других иностранных журналов – в соответствии с сокращениями, рекомендуемыми издательством «Springer and Business Media»:

http://chemister.ru/Chemie/journal-abbreviations.htm. Для статей на русском и казахском языках название журнала «Химический Журнал Казахстана» следует сокращать: «*Хим. Журн. Каз*.» и «*Қаз. Хим. Журн*.» соответственно, а для статей на английском языке: «Chem. J. Kaz.». Приводятся фамилии и инициалы **всех авторов** (сокращения и *др*. и *et al* не допускаются).

В Списке литературы и в **References** все работы перечисляются **В ПОРЯДКЕ ЦИТИРОВАНИЯ**, а **НЕ** в алфавитном порядке.

DOI. Во всех случаях, когда у цитируемого материала есть цифровой идентификатор, его необходимо указывать в самом конце описания источника. Проверять наличие doi у источника следует на сайте http://search.crossref.org или https://www.citethisforme.com.

Для формирования списка литературы (всех без исключения ссылок) в Журнале принят библиографический стандарт без использования разделителя «//»:

Author A.A., Author B.B., Author C.C. Title of article. Title of Journal, **2005**, 10, No. 2, 49–53.

Для казахско- или русскоязычного источника:

Author A.A., Author B.B., Author C.C. Title of article. Title of Journal, **2005**, 10, No. 2, 49– 53. (In Kazakh or In Russian).

Ниже приведены образцы оформления различных видов документов, которых необходимо придерживаться авторам при оформлении романского списка **References**.

Описание статьи из журналов:

Zagurenko A.G., Korotovskikh V.A., Kolesnikov A.A., Timinov A.V., Kardymov D.V. Technical and economical optimization of hydrofracturing design. Neftyanoe khozyaistvo. Oil Industry, **2008**, No. 11, 54–57. (In Russian).

Описание статьи с DOI:

Zhang Z., Zhu D. Experimental Research on the localized electrochemical micromachining. *Rus. J. Electrochem.*, **2008**, 44, No. 8, 926–930. doi: 10.1134/S1023193508080077.

Описание Интернет-ресурса:

Kondrat'ev V.B. *Global'naya farmatsevticheskaya promyshlennost'* [The global pharmaceutical industry]. Available at: http://perspektivy.info/rus/ekob/globalnaja_farmacevticheskaja_promyshlennost_2011-07-18.html (Accessed 23.06.2013).

или

APA Style (2011). Available at: http://www.apastyle.org/apa-style-help.aspx (accessed 5 February 2011).

или

Pravila Tsitirovaniya Istochnikov (Rules for the Citing of Sources) Available at: http://www.scribd.com/doc/1034528/ (Accessed 7 February 2011).

Описание статьи из электронного журнала:

Swaminatan V., Lepkoswka-White E., Pao B.P. Browsers or buyers in cyberspace? An investigation of electronic factors influencing electronic exchange. Journal of Computer-Mediated Communication, **1999**, 5, No. 2. Available at: http://www.ascusc.org/jcmc/vol.5/issue2/(Accessed 24 April 2011).

Описание статьи из продолжающегося издания (сборника трудов)

Astakhov M.V., Tagantsev T.V. Eksperimental'noe issledovanie prochnost soedinenii «stal'- kompozit» [Experimental study of the strength of joints «steel-

composite»]. Trudy MGTU
«*Matematicheskoe modelirovanie slozhnykh tekhnicheskikh sistem*» [Proc. Of the Bauman MSTU
«Mathematic Modeling of the Complex Technical Systems»], **2006**, No. 593, 125–130.

Описание материалов конференций:

Usmanov T.S., GusmanovA.A., MullagalinI.Z., MuhametshinaR.Ju., ChervyakovaA.N., SveshnikovA.V. Featuresof the design of the field development with the use of hydraulic fracturing. *Trudy 6 Mezhdunarodnogo Simpoziuma «Novye resurso sberegayushchie tekhnologii nedropol'zovaniya i povysheniya neftegazootdachi»* [Proc. 6th Int. Symp. «New energy saving subsoil technjologies and the increasing of the oil and gas impact»]. Moscow, **2007**, 267–272. (In Russ.)

Нежелательно оставлять одно переводное название конференции (в случае если нет переведенного на английский язык названия конференции), так как оно при попытке кем- либо найти эти материалы, идентифицируется с большим трудом.

Описание книги (монографии, сборника):

Nenashev M.F. *Poslednee pravitel'stvo SSSR* [Last government of the USSR]. Moscow, Krom Publ., **1993**, 221 p.

Описание переводной книги:

Timoshenko S.P., Young D.H., Weaver W. *Vibration problems in engineering*. 4thed. New York, Wiley, 1974.521 p. (Russ. ed.: Timoshenko S.P., Iang D.Kh., Uiver U. *Kolebaniia v inzhenernom dele*. Moscow, Mashinostroenie Publ., **1985**. 472 p.).

Brooking A., Jones P., Cox F. *Expert systems. Principles and cases studies*. Chapman and Hall, 1984. 231 p. (Russ. ed.: Bruking A., Dzhons P., Koks F. *Ekspertnye sistemy. Printsipy raboty i primery*. Moscow, Radioisviaz' Publ., **1987**. 224 p.).

Описание диссертации или автореферата диссертации:

Grigor'ev Yu. A. *Razrabotka nauchnykh osnov proektirovaniia arkhitektury raspredelennykh sistem obrabotki dannykh. Diss. Dokt. Tekhn. Nauk* [Development of scientific bases of architectural design of distributed data processing systems. Dr. tech. sci. diss.]. Moscow, Bauman MSTU Publ., **1996**. 243 p.

Описание ГОСТа:

GOST *8.596.5–2005*. *Metodikavypolneniia izmerenii. Izmerenie raskhoda I kolichestva zhidkostei I gazov s pomoshch'iu standartnykh suzhaiushchikh ustroistv* [State Standard 8.586.5 – 2005. Method of measurement. Measurement of flow rate and volume of liquids and gases by means of orifice devices]. Moscow, Standartinform Publ., **2007**. 10 p.

или

State Standard 8.586.5 – 2005. Method of measurement. Measurement of flow rate and volume of liquids and gases by means of orifice devices. Moscow, Standartinform Publ., **2007**. 10 p. (In Russian).

Описание патента:

Patent RU 228590. *Sposob orientirovaniia po krenu letatel'nogo apparata s opticheskoi golovkoi samonavedeniia* [The way to orient on the roll of aircraft with optical homing head]., Palkin M.V., Ivanov N.M., Gusev B.B., Petrov R.H., **2006**.

4.9. **Пример англоязычного блока для представления статьи, написанной на языке, отличном от английского:**

Abstract

DETERMINATION OF THE HAZARD CLASS OF OIL-CONTAMINATED AND NEUTRALIZIED SOIL

Zhusipbekov U.Zh.[1], Nurgaliyeva G.O.[1*], Baiakhmetova Z.K.[1], Aizvert L.G.[2]

[1]JSC «A.B. Bekturov Institute of Chemical Sciences», Almaty, Kazakhstan

[2]Scientific and practical center of sanitary-epidemiological examination and monitoring of the Ministry of Health of the Republic of Kazakhstan Almaty, Kazakhstan

E-mail: n_gulzipa@mail.ru

Introduction. Pollution by oil has a negative effect on chemical, physical, agrophysical, agrochemical and biological properties of soils. Sorption methods of cleaning the soil with the help of humic preparations from oil pollution are of great importance. *The purpose* of this work is to study the composition and properties of the contaminated and neutralized soil, the determination of the toxicity indexes of all components of oil waste, the calculation of the hazard class of waste according to their toxic-ecological parameters. *Methodology*. Samples of the contaminated and neutralized soil were treated with the use of humate-based energy-accumulating substances. The metal content in the contaminated soil was determined by spectrometry using an AA 240 instrument using the method of decomposing the sample with a mixture of nitric, hydrofluoric and perchloric acids until the sample was completely opened. *Results and discussion*. Fractional composition of oil products of all samples is stable: the content of complex acetylene hydrocarbons is ~ 70.0% of the total mass of oil products, the content of resins and paraffin-naphthenic group of hydrocarbons is 27.3%, the content of bitumens is 2.6%. In the neutralized soil, paraffin-naphthenic fractions, resins, bitumens and asphalteneswere mainly found; complex acetylene hydrocarbons are not present. *Conclusion*. It has been established that the contaminated soil belongs to the substances of the 3rd hazard class. Neutralized soil became less toxic and according to the total toxicity index, it was classified as hazard class 4 (low hazard). Neutralized soil can be used as construction and road materials, at the improvement of boreholes and at land reclamation.

Keywords: oil, contaminated soil, neutralized soil, humate-based energy storage substance, toxicity, radioactivity, hazard class.

References

1. Evdokimova G.A., Gershenkop A.Sh.,Mozgova N.P., Myazin V.A., Fokina N.V. Soils and waste water purification from oil products using combined methods under the North conditions. *J. Environ. Sci.*, **2012**, *47*, No. 12, 1733–1738, https://doi.org/10.1080/10934529.2012.689188

2. Badrul I. Petroleum sludge, its treatment and disposal: a review. *Int. J. Chem. Sci.*, **2015**, *13*, No. 4, 1584–1602. https://www.tsijournals.com/articles/petroleum-sludge-its-treatment- and-disposal--a-review.pdf (accessed on 2 April 2021).

3. Krzhizh L., Reznik D. Technology of cleaning the geological environment from oil pollution. *Jekologija proizvodstva*, **2007**, No. 10, 54. (in Russ.). https://www.ripublication.com/ijaer18/ijaerv13n7_44.pdf (accessed on 2 April 2021).

4. Nocentini M., Pinelli D., Fava F. Bioremediation of soil contaminated by hydrocarbon mixtures: the residual concentration problem. *Chemosphere*, **2000**, No. 41, 1115–1123, https://doi.org/10.1016/S0045-6535(00)00057-6

5. Cerqueira V.S., Peralba M.C.R., Camargo F.A.O., Bento F.M. Comparison of bioremediation strategies for soil impacted with petrochemical oily sludge. *International Biodeterioration & Biodegradation*, **2014**, *95*, 338–345, https://doi.org/10.1016/j.ibiod.2014.08.015

54. Zemnuhova L.A., Shkorina E.D., Filippova I.A. The study of the sorption properties of rice husk and buckwheat in relation to petroleum products. *Himija rastitel'nogo syr'ja*, **2005**, No. 2, 51–(in Russ.). http://journal.asu.ru/cw/article/view/1659 (accessed on 2 April 2021).

8. Mokrousova M.A., Glushankova I.S. Remediation of drill cuttings and oil-contaminated soils using humic preparations. *Transport. Transportnye Sooruzhenija. Jekologija*, **2015**, No. 2, 57–72. (in Russ.). https://www.dissercat.com/content/razrabotka-nauchnykh-osnov-primeneniya-guminovykh-veshchestv-dlya-likvidatsii-posledstvii (accessed on 2 April 2021).

9. Teas Ch., Kalligeros S., Zanikos F., Stournas S. Investigation of the effectiveness of absorbent materials in oil spill clean up. *Desalination*, **2001**, No. 140, 259–264. http://www.desline.com/proceedings/140.shtml (accessed on 2 April 2021).

10. Ivanov A.A., Judina N.V., Mal'ceva E. V., Matis E.Ja. Investigation of the biostimulating and detoxifying properties of humic acids of different origin under conditions of oil-contaminated soil. *Himija rastitel'nogo syr'ja*, **2007**, No. 1, 99–103. (in Russ.). http://journal.asu.ru/cw/issue/view/6 (accessed on 2 April 2021).

11. Dzhusipbekov U.Zh., Nurgalieva G.O., Kuttumbetov M.A., Zhumasil E., Dujsenbaj D., Sulejmenova O.Ja. Pilot-industrial tests of the processing of oil-contaminated soil. *Chem. J. Kazakhstan*, **2015**, No. 3, 234–240. http://www.chemjournal.kz/images/pdf/2019/01/2019-1-2.pdf (accessed on 2 April 2021).

12. Patent RU 2486166. *Sposob obezvrezhivanija neftezagrjaznennyh gruntov, sposob obezvrezhivanija otrabotannyh burovyh shlamov* [The method of disposal of oil-contaminated soils, the method of disposal of waste drill cuttings]. Kumi V.V., **2013**. http://www.freepatent.ru/patents/2491266 (accessed on 2 April 2021).

13. Kozlova, E.N., Stepanov, A.L. & Lysak, L.V. The influence of bacterial-humus preparations on the biological activity of soils polluted with oil products and heavy metals. *Eurasian Soil Sc.*, **2015**, *48*, 400–409. https://doi.org/10.1134/S1064229315020052.

Ғылыми жарияланымның этикасы

«Қазақстанның химиялық журналы» (бұдан әрі – Журнал) баспасының алқасы мен бас редакторы «Жариялану этикасы жөніндегі комитет – (Committee on Publication Ethics – COPE)» (http://publicationethics.org/about),«Еуропалық ғылыми редакторлардың қауымдастығы » (European Association of Science Editors – EASE) (http://www.ease.org.uk) және Ғылыми жарияаным этикасының комитетінде (http://publicet.org/code/) қабылданылған халықаралық талаптарды ұстанады.

Баспа қызметіндегі әдепке сай емес іс - әрекеттерді (плагиат, жалған ақпарат және т.б.) болдырмауға және ғылыми жарияланымдардың жоғары сапасын қамтамасыз ету үшін, қол жеткізген ғылыми нәтижелерді жұртшылыққа жариялау мақсатында редакция алқасы, авторлар, рецензенттер, сондай-ақ баспа үдерісіне қатысатын мекемелер этикалық нормалар мен ережелерді сақтауға міндетті және олардың бұзылмауына барлық шараларды пайдалануы тиіс. Осы үдеріске қатысушылардың барлығының ғылыми жарияланымдар этикасының ережелерін сақтауы, авторлардың зияткерлік меншік объектілеріне құқықтарын қамтамасыз етуге, жарияланымдар сапасын арттыруға және авторлық құқықпен қорғалған материалдарды жеке тұлғалардың мүддесі үшін пайдалану мүмкіндігін жоюға көмектеседі.

Редакцияға жіберілген барлық ғылыми мақалалар міндетті түрде екі жақты құпия сараптамаға жіберіледі. Журналдың редакциялық алқасы мақаланың журнал тақырыбына және талаптарына сәйкестігін анықтайды, журналға тіркеу үшін оны алдын ала саралауға журналдың жауапты хатшысына жібереді. Ол қолжазбаның ғылыми құндылығын анықтап, мақала тақырыбына жақын ғылыми мамандықтары бар екі тәуелсіз сарапшыны анықтайды. Мақалаларды редакциялық алқа және редакциялық алқа мүшелері, сондай-ақ басқа елдерден шақырылған рецензенттер сараптайды. Мақаланы сараптау үшін рецензенттерді таңдау туралы шешімді бас редактор қабылдайды. Сараптау мерзімі 2-4 апта және рецензент өтініші бойынша оны 2 аптаға ұзартуға болады.

Редакция мен рецензент қарауға жіберілген жарияланбаған материалдардың құпиялылығына кепілдік береді. Жариялау туралы шешім журналдың редакциялық алқасы тексергеннен кейін қабылданады. Қажет болған жағдайда (редактор(лар) және/немесе рецензент(лер) тарапынан ескертулердің болуы) қолжазба авторларға қосымша түзетулерге жіберіледі, содан кейін ол қайта қаралады. Этика нормалары бұзылған жағдайда, мақаланы жариялаудан бас тарту құқығын Редакция өзіне қалдырады. Жауапты редактор мақалада плагиат деп есептеуге жеткілікті ақпарат болған жағдайда оны жариялауға рұқсат бермейді.

Авторлар редакцияға жіберілген материалдардың жаңа, бұрын жарияланбаған және түпнұсқа екендігіне кепілдік береді. Авторлар ғылыми нәтижелердің сенімділігі мен маңыздылығына, сондай-ақ ғылыми этика қағидаттарының сақталуына, атап айтқанда, ғылыми этиканы бұзылмауына (ғылыми деректерді қолдан жасау, зерттеу деректерін бұрмалауға әкелетін бұрмалау, плагиат және жалған бірлескен авторлық, қайталау, басқа адамдардың нәтижелерін иемдену және т.б.)тікелей жауапты.

Мақаланы редакцияға беру авторлардың мақаланы (түпнұсқада немесе басқа тілдерге немесе тілден аудармада) басқа журналға(ларға) жібермегенін және бұл материалдың бұрын жарияланбағанын білдіреді. Олай болмаған жағдайда мақала

авторларға «Авторлық құқықты бұзғаны үшін мақаланы жарияламау» деген шешіммен қайтарылады. Басқа автордың туындысының 10 пайыздан астамын, оның авторлығын және дереккөзге сілтемелерді көрсетпей сөзбе-сөз көшіруге жол берілмейді. Алынған үзінділер немесе мәлімдемелер автор мен дереккөзді міндетті түрде көрсете отырып ресімделуі керек. Шамадан тыс өзге материалдарды пайдалану, сондай-ақ кез келген нысандағы плагиат, соның ішінде дәйексіз дәйексөздер, басқа адамдардың зерттеулерінің нәтижелерін иемдену этикаға жатпайды және қабылданбайды. Зерттеу барысына қатынасқан барлық тұлғалардың үлесін мойындау қажет және мақалада зерттеуді жүргізуде маңызды болған жұмыстарға сілтемелер берілуі керек. Бірлескен авторлар арасында зерттеуге қатыспаған адамдарды көрсетуге жол берілмейді.

Автор(лар) жұмыстарында қателіктер байқалса, бұл туралы дереу редакторға хабарлап, түзету туралы ұсыныс беруі тиіс.

Қолжазбаны басып шығарудан бас тарту туралы шешім рецензенттердің ұсыныстарын ескере отырып, редакция алқасының отырысында қабылданады. Редакциялық алқаның шешімімен жариялауға ұсынылмаған мақала қайта қарауға қабылданбайды. Жариялаудан бас тарту туралы хабарлама авторға электрондық пошта арқылы жіберіледі.

Журналдың редакциялық алқасы мақаланы жариялауға рұқсат беру туралы шешім қабылдағаннан кейін редакциялық алқа бұл туралы авторға хабарлайды және жариялау шарттарын көрсетеді. Мақалаға берілген пікірлердің түпнұсқасы Журнал редакциясында 3 жыл сақталынады.

Этика научных публикаций

Редакционная коллегия и главный редактор научного журнала «Химический журнал Казахстана» (далее – Журнал) придерживаются принятых международных стандартов «Комитета этики по публикациям» (Committee on Publication Ethics – COPE) (http://publicationethics.org/about),, **«Европейской ассоциации научных редакторов»** (European Association of Science Editors – EASE) (http://www.ease.org.uk) и «**Комитета по этике научных публикаций**» (http://publicet.org/code/)..

Во избежание недобросовестной практики в публикационной деятельности (плагиат, изложение недостоверных сведений и др.) и в целях обеспечения высокого качества научных публикаций, признания общественностью, полученных автором научных результатов, члены редакционного совета, авторы, рецензенты, а также учреждения, участвующие в издательском процессе, обязаны соблюдать этические стандарты, нормы и правила и принимать все меры для предотвращения их нарушений. Соблюдение правил этики научных публикаций всеми участниками этого процесса способствует обеспечению прав авторов на интеллектуальную собственность, повышению качества издания и исключению возможности неправомерного использования авторских материалов в интересах отдельных лиц.

Все научные статьи, поступившие в редакцию, подлежат обязательному двойному слепому рецензированию. Редакция Журнала устанавливает соответствие статьи профилю Журнала, требованиям к оформлению и направляет ее на первое рассмотрение ответственному секретарю Журнала, который определяет научную ценность рукописи и назначает двух независимых рецензентов – специалистов, имеющих наиболее близкие к теме статьи научные специализации. Рецензирование статей осуществляется членами редакционного совета и редакционной коллегии, а также приглашенными рецензентами других стран. Решение о выборе того или иного рецензента для проведения экспертизы статьи принимает главный редактор. Срок рецензирования составляет 2-4 недели, но по просьбе рецензента он может быть продлен, но не более чем на 2 недели.

Редакция и рецензент гарантируют сохранение конфиденциальности неопубликованных материалов присланных на рассмотрение работ. Решение о публикации принимается редакционной коллегией Журнала после рецензирования. В случае необходимости (наличие замечаний редактора(-ов) и /или рецензента(-ов)) рукопись направляется авторам на доработку, после чего она повторно рецензируется. Редакция оставляет за собой право отклонить публикацию статьи в случае нарушения правил этики. Ответственный редактор не должен допускать к публикации информацию, если имеется достаточно оснований полагать, что она является плагиатом.

Авторы гарантируют, что представленные в редакцию материалы являются новыми, ранее неопубликованными и оригинальными. Авторы несут ответственность за достоверность и значимость научных результатов, а также соблюдение принципов научной этики, в частности, недопущение фактов нарушения научной этики (фабрикация научных данных, фальсификация, ведущая к искажению исследовательских данных, плагиат и ложное соавторство, дублирование, присвоение чужих результатов и др.)

Направление статьи в редакцию означает, что авторы не передавали статью (в оригинале или в переводе на другие языки или с других языков) в другой(-ие) журнал(ы) и что этот материал не был ранее опубликован. В противном случае статья немедленно возвращается авторам с формулировкой «Отклонить статью за нарушение авторских прав». Не допускается дословное копирование более 10 процентов работы другого автора без указания его авторства и ссылок на источник. Заимствованные фрагменты или утверждения должны быть оформлены с обязательным указанием автора и первоисточника. Чрезмерные заимствования, а также плагиат в любой форме, включая неоформленные цитаты, перефразирование или присвоение прав на результаты чужих исследований, неэтичны и неприемлемы. Необходимо признавать вклад всех лиц, так или иначе повлиявших на ход исследования, в частности, в статье должны быть представлены ссылки на работы, которые имели значение при проведении исследования. Среди соавторов недопустимо указывать лиц, не участвовавших в исследовании.

Если автором(-ами) обнаружена ошибка в работе, необходимо срочно уведомить редактора и вместе принять решение об исправлении.

Решение об отказе в публикации рукописи принимается на заседании редакционной коллегии с учетом рекомендаций рецензентов. Статья, не рекомендованная решением редакционной коллегии к публикации, к повторному рассмотрению не принимается. Сообщение об отказе в публикации направляется автору по электронной почте.

После принятия редколлегией Журнала решения о допуске статьи к публикации редакция информирует об этом автора и указывает сроки публикации. Оригиналы рецензий хранятся в редакции Журнала в течение 3 лет.

Scientific Publication Ethics

The Editorial Board and Editor-in-Chief of the scientific journal the "Chemical Journal of Kazakhstan" (hereinafter referred to as the Journal) adhere to the accepted international standards of the "Committee on Publication Ethics" (Committee on Publication Ethics – COPE) (http://publicationethics.org/about)**, the "European Association of Science Editors"** (European Association of Science Editors – EASE) (http://www.ease.org.uk) **and the "Committee on Scientific Publication Ethics"** (http://publicet.org/code/).

To avoid unfair practices in the publishing activities (plagiarism, false information, etc.) and in order to ensure the high quality of the scientific publications and public recognition of the scientific results, obtained by the author, the members of the Editorial Board, authors, reviewers, as well as institutions, involved in the publishing process, are obliged to comply with ethical standards, rules and regulations, and take all measures to prevent their violation. The compliance with the rules of the scientific publication ethics by all process participants contributes to ensuring the rights of authors to intellectual property, improving the quality of the publication and excluding the possibility of misuse of the copyrighted materials in the interests of the individuals.

All scientific articles submitted to the editors are subject to mandatory double-blind peer reviewing. The Editorial Board of the Journal determines the compliance of the article with the specificity of the Journal, the registration requirements and sends it for the first reviewing to the Executive Secretary of the Journal, who determines the scientific value of the manuscript and appoints two independent reviewers – the specialists with the scientific specializations closest to the topic of the article. The articles are reviewed by the members of the Editorial Board and the Editorial Staff, as well as the invited reviewers from the other countries. The decision to choose one or another reviewer for reviewing the article is made by the Editor-in-Chief. The reviewing period is 2-4 weeks, though at the request of the reviewer, it can be extended, but no more than for 2 weeks.

The editors and the reviewer guarantee the confidentiality of the unpublished materials submitted for reviewing. The decision to publish is made by the Editorial Board of the Journal after reviewing. If necessary (the presence of comments by the editor(s) and/or reviewer(s)) the manuscript is sent to the authors for revision, after which it is re-reviewed. The editors reserve the right to reject from the publication of the article in case of violation of the rules of ethics. The Executive Editor should not allow the information to be published if there is sufficient reason to believe that it is plagiarism.

The authors guarantee that the materials, submitted to the editors are new, previously unpublished and original. The authors are responsible for the reliability and significance of the scientific results, as well as compliance with the principles of scientific ethics, in particular, the prevention of violations of scientific ethics (fabrication of the scientific data, falsification leading to distortion of the research data, plagiarism and false co-authorship, duplication, appropriation of other people's results, etc.).

The submission of an article to the editor means that the authors did not submit the article (in the original or translated into or from the other languages) to the other Journal(s), and that this material was not previously published. Otherwise, the article is immediately returned to the authors with the wording "Reject the article for the copyright infringement." The word-for-word copying of more than 10 percent of the work of another author is not allowed without indicating his authorship and references to the source. The borrowed fragments or statements should be drawn-up with the obligatory

indication of the author and source. Excessive borrowing, as well as plagiarism in any form, including inaccurate quotations, paraphrasing, or appropriation of the rights to the results of the other people's research, is unethical and unacceptable. It is necessary to recognize the contribution of all persons, who in one way or another influenced the course of the research, in particular, the article should provide links to the works, which were important in the research conduction. Among the co-authors, it is unacceptable to indicate persons, who did not participate in the research.

If the author(s) finds an error in the work, it is necessary to immediately notify the editor thereof, and together decide on the correction.

The decision to refuse from the publication of the manuscript is made at a Meeting of the Editorial Board, taking into account the recommendations of the reviewers. An article, which is not recommended by the decision of the Editorial Board for the publication, is not accepted for re-consideration. A notice of the refusal to publish is sent to the author by e-mail.

After the Editorial Board of the Journal makes a decision on the admission of the article for the publication, the Editorial Board informs the author thereof, and specifies the terms of the publication. The original reviews are kept in the Editorial Office of the Journal for 3 years.

Технический редактор: *Ж.Б.Узакова*

Подписано в печать 26.06.2026г.
Формат 70x100 $^{1}/_{16}$. 12.68. п.л. Бумага офсетная. Тираж 300.

Типография ИП «Тойходжаев Н.О.»
г.Алматы, Алмалинский район, ул. Нурмакова, 26/195 кв. 49
e-mail: iparuna@yandex.ru